Flavor Physics: Neutrinoproduction of Resonances and Semileptonic $B \to K, K^* \bar{l} l$ Decays

Dissertation

zur Erlangung des Grades eines

Doktors der Naturwissenschaften

des Fachbereiches Physik

der Technischen Universität Dortmund

technische universität
dortmund

vorgelegt von

Giorgi Piranishvili

August 2008

Abstract

The goal of this research is the precise investigations of the processes which are helpful to test the physics of the Standard Model and beyond it. We concentrate on the flavor sector of the theory which is still one of the sticking point in high energy physics. At the same time flavor physics possesses a rich phenomenology which makes it one of the hot topics in the current theoretical and experimental investigations.

In this thesis we present the studies of several processes of particle physics taking place at the energy scale of $\mathcal{O}\,(\mathrm{GeV})$, namely neutrino interactions with nucleons and semileptonic B meson decays.

For the neutrino scattering on nucleons with neutrino energies of about one GeV, we determine the form factors of the nucleon-resonance transition with the help of the recent electroproduction data. We extend the analysis to the second resonance region, where in addition to the resonance $P_{33}(1232)$, also $D_{13}(1520)$, $P_{11}(1440)$ and $S_{11}(1535)$ resonances contribute. Using the updated form factor fit we calculate the differential and total cross sections for the resonance production by neutrinos.

A detailed analysis of angular distributions is done for the exclusive decays $B \to K, K^*\bar{l}l$. The calculations are performed in the large recoil region using the QCD factorization formalism. We give the Standard Model predictions for the coefficients of angular distribution of $B \to K\bar{l}l$ decays, namely F_H^l and A_{FB}^l. The predicted values are remarkable for their vanishing values in the Standard Model and small theoretical uncertainties. The sensitivity of these coefficients to New Physics is studied in a model-independent way.

In the case of the decay $B \to K^*(\to K\pi)\bar{l}l$ we investigate eight CP asymmetries in the Standard Model and Beyond. Three of them are T-odd and five T-even CP asymmetries. In the Standard Model, where the CP violation comes from the CKM matrix, we predict the values of the CP asymmetries to be of $\mathcal{O}\,(10^{-3})$. We also show that the current experimental bounds allow the T-odd asymmetries to be of $\mathcal{O}\,(1)$, whereas the values of the T-even asymmetries can be of $\mathcal{O}\,(0.1)$ in the presence of New Physics.

Zusammenfassung

In dieser Arbeit präsentieren wir die Studien einiger ausgewählter Prozesse der Teilchenphysik, die an der Energieskala von $\mathcal{O}\,(\mathrm{GeV})$ stattfinden, erstens die Wechselwirkung zwischen Neutrinos und Nukleonen und zweitens semileptonische Zerfälle der B-Mesonen.

Im Falle der Streuung von Neutrinos an Nukleonen im Energiebereich von ca. 1 GeV, bestimmen wir die Formfaktoren der Nukleon-Resonanz-Übergänge mit Hilfe neuester Elektron-Nukleon Streuungs-Daten. Unsere Analyse beinhaltet außer der $P_{33}(1232)$ Resonanz auch die $D_{13}(1520)$, $P_{11}(1440)$, $S_{11}(1535)$ Resonanzen. Unter Verwendung dieser aktualisierten Formfaktoren berechnen wir den differentiellen und gesamten Wirkungsquerschnitt für die Erzeugung von Resonanzen in der Neutrino-Nukleon Streuung.

Im Falle der semileptonischen B-Mesonzerfälle werden Winkelverteilungen des Spektrums für die exklusiven Zerfälle $B \to K, K^* \bar{l} l$ detailliert diskutiert. Die Rechnung beschränkt sich auf kleine invariante Massen des Dileptonsystemes im Rahmen des Formalismus der QCD Faktorisierung. Wir bestimmen die Standardmodell Vorhersage der Koeffizienten der Winkelverteilung F_H^l und A_{FB}^l des Zerfalles $B \to K \bar{l} l$. Diese Observablen zeichnen sich durch ihre verschwindend kleinen Standardmodellwerte und kleinen Unsicherheiten aus. Desweiteren wird die Sensitivität dieser Koeffizienten auf Signale Neuer Physik in modellunabhängiger Art und Weise studiert. Für die Zerfälle $B \to K^*(\to K\pi)\bar{l} l$ untersuchen wir acht CP Asymmetrien im Standardmodell und darüber hinaus. Drei von ihnen sind T-ungerade und fünf T-gerade CP Asymmetrien. Im Standardmodell ist die Ursache der CP Verletzung die CKM Matrix und die CP Asymmetrien verschwindend klein im Bereich $\mathcal{O}\,(10^{-3})$. Wir zeigen außerdem, dass die gegenwärtigen experimentellen Daten keine wesentlichen Einschränkungen darstellen und folglich die T-ungeraden Asymmetrien im Falle Neuer Physik im Bereich $\mathcal{O}\,(1)$ sein können. Die Sensitivität der T-geraden Asymmetrien auf Signale Neuer Physik ist etwas kleiner, diese können im Bereich $\mathcal{O}\,(0.1)$ liegen.

Contents

Introduction

The developments of the last 50 years in particle physics give the hope that the description of the nature can be arranged in terms of several fundamental principles. The Standard Model (SM) [1, 2, 3], the model describing electromagnetic, weak and strong interactions, is such an attempt. With the help of the quantum field theory and the principle of local gauge invariance the SM explains successfully the wide range of particle physics phenomena up to distances of $\mathcal{O}\left(10^{-18}\,\mathrm{m}\right)$, which has been confirmed by a large number of accelerator experiments.

In spite of its success one believes that the SM is not complete. The reason is a number of unanswered questions raised in the theory. Namely, there is a number of parameters in the theory whose values are unnaturally remote from each other, more than one would expect. For example, there is a large difference, about seventeen orders of magnitude, between the electroweak scale and the Planck scale. Similarly, it is unclear why the spectrum of matter particles in the SM is so different. The mass of the top quark exceeds the mass of one of the neutrinos by eleven orders of magnitude. This problem is probably correlated with the question: "Where do masses of the particles come from?". We also do not know why there are only three generations of particles. Although, the direct experimental constraints still do not rule out an additional fourth generation [4, 5]. The neutrinos are massless in the SM, whereas the oscillation experiments confirmed that neutrinos have masses. Another problem is related to the fact that our Universe is observed to have an excess of matter over antimatter. It would be impossible to achieve it without the existence of CP violating processes during the evolution of the Universe [6]. Thus, it generates the need to have CP violation in the theory. Unfortunately, the amount of CP violation in the SM is not enough to explain quantitatively the asymmetry between matter and antimatter. Thus, these shortcomings and inconsistencies motivate us to think about the existence of physics beyond the SM, i.e., New Physics (NP). We hope that the dedicated experiments at the Large Hadron Collider (LHC) will shed light on some of these questions.

The most part of this manuscript is devoted to various phenomenological aspects of flavor physics. In the SM the matter particles (fermions) appear in three generations. Flavor physics describes the interactions responsible for the transitions between different generations. There are two sectors of flavor physics: quark and

lepton flavor physics. These two parts are often discussed separately in spite of many similarities. However, the belief in the Grand Unified Theories (GUT) unifying quarks and leptons makes us expect that quark and lepton flavor physics have same origins. Concerning the SM, the following question raises: "What is the source of such generation (flavor) changing interactions in the SM?". The fermions in the SM take part in the gauge (coupling to gauge boson) and Yukawa interactions (coupling to scalar boson). Yukawa terms are unconstrained in generation space which leads to flavor violation transitions. In the SM Yukawa couplings are just free parameters which should be extracted from experiment. Going beyond the SM one introduces some flavor (family) symmetry which is spontaneously broken by the vacuum expectation value of some scalar filed called $flavon$. Further, by constructing non-renormalizable theory valid below some scale we can introduce interactions describing the SM fields plus the flavon in such way that for the low energies they lead to Yukawa couplings.

Why is flavor physics so interesting to investigate? The processes of flavor physics have a potential to test the SM and even predict its extensions. There are some examples from the past when new particles were predicted before their direct observations in accelerator experiments. One of such examples is the measured value of Kaon mass difference which led to a successful prediction of charm quark mass before it was discovered. Therefore, if NP appears at or below the TeV scale, predicted by some SM extensions, NP particles can contribute either at tree or loop level, depending on NP flavor structure, to some low energy obsevables. Again, the discrepancy between experimental and theoretical estimates of those flavor physics observables can be a signal of the physics beyond the SM.

The other problem related to flavor physics is a need of new sources of CP violation. In the SM there is only one CP violating phase originated from the quark flavor mixing, which, as we said above, is not enough to produce matter-antymatter asymmetry of the Universe. Measuring CP sensitive observables in flavor changing processes can provide evidence of additional sources of CP violation.

On the other hand lepton flavor physics is also very important. The measurements of neutrino mass differences and mixing in the oscillation experiments gave the first experimental result being inconsistent with the SM. In the SM leptons, i.e., electron, muon and tau, obtain their masses through the Yukawa terms, whereas neutrinos stay massless. To construct Yukawa-like terms for neutrinos one adds heavy right-handed singlets to the theory which leads to Dirac neutrino masses. Another possibility is to introduce a triplet Higgs scalar coupled only to left-handed neutrinos. Such terms would generate Majorana neutrino masses (more on neutrino masses see [7]). In the both cases there is a problem with unnaturally small Yukawa

couplings needed to tune with the experimental neutrino mass scale of $\mathcal{O}(0.1\,\mathrm{eV})$. This problem can be solved with a help of *seesaw* mechanism. In this framework small neutrino masses are naturally generated by the ratio of two mass scales, i.e., square of SM Higgs scalar scale of $\mathcal{O}(100\,\mathrm{GeV})$ over the scale of heavy right-handed singlet of order GUT or Placnk scales $\gtrsim \mathcal{O}(10^{16}\,\mathrm{GeV})$.

This thesis is split into two parts. The first part is dedicated to the process of the resonance production in neutrino scattering on nucleons. The current and future experiments on neutrino oscillations, like K2K, MiniBoone, MINOS, JHF, provide the evidence of non-vanishing neutrino masses. Since the neutrinos are massless in the SM, the observations of the neutrino masses in oscillation experiments call for an extension of the SM. For the accurate measurements of the oscillation parameters, i.e., constrains on NP, one needs precise knowledge of neutrino-nucleon scattering cross sections. For the low neutrino energies, $E_\nu \simeq 1\,\mathrm{GeV}$ the resonance production reactions give significant contribution to the total cross section. For this purpose we study these reactions in detail and present the results in the publication:

- O. Lalakulich, E. A. Paschos, G. Piranishvili, "Resonance production by neutrinos: The Second resonance region.", Phys.Rev.D74:014009,2006.

Cross section of these processes depend on the nucleon-resonance form factors. The underlying fundamental theory of such nucleon-resonance transitions is quantum chromodynamics (QCD). However, in the non-pertubative regime QCD calculations are not currently practicable due to their complexity. Therefore one has to investigate nucleon-resonance transitions with a help of phenomenological approaches and experimental data. We update the form factors of nucleon-resonance transition for the $P_{33}(1232)$ resonance and give fits of form factors for higher resonances $D_{13}(1520)$, $P_{11}(1440)$ and $S_{11}(1535)$. The extraction of the vector form factors is possible due to the new data on electron-nucleon scattering from JLAB and the Mainz accelerators, whereas for the axial form factors we adopted the concept of *partially conserved axial-vector currents* (PCAC). We present these investigations in Chapter 2, where we show the detailed extraction of the form factors. Using the newly fitted form factors we calculate differential and total cross sections as functions of kinematic parameters.

The second part of the thesis is dedicated to quark flavor physics. In the last decade, experimental investigations done at B-factories put forward our knowledge on the quark-flavor sector of the SM. The major part of these researches are devoted to the B-meson system. At SLAC (BaBar detector) and KEK (Belle detector), e^+e^- collision experiments are able to produce $\Upsilon(S4)$ resonances decaying subsequently in B-mesons, e.g., $B^+(u\bar{b})$, $B^-(\bar{u}b)$, $B^0(d\bar{b})$ and $\bar{B}^0(\bar{d}b)$. Furthermore , Tevatron (Fermilab) with the help of detectors CDF and D0 gives a possibility to study the

phenomenology of B_s and B_c mesons. Thanks to the LHCb experiment, further and more profound investigations concerning B-physics will be performed at the LHC. The phenomenology of B-physics gives a huge possibility to understand the flavor structure of the SM better. Due to improved measurements of various observables one is able to constrain NP being a source of additional flavor and CP violations. On the other side the theoretical predictions still suffer from large "hadronic" uncertainties due to the complex nature of the strong interactions. Therefore, various strategies are elaborated by constructing observables being free of hadronic uncertainties.

Here we study the semileptonic $B \to K, K^* \bar{l} l$ decays. These decays belong to the flavor changing neutral current (FCNC) processes and appear only at loop level in the SM, which makes them very sensitive to NP. Since these decays are loop induced and suppressed in the SM, NP particles contributing either through loops or at tree level can enhance the magnitudes of the observables. Therefore the goal of the research is to elaborate such observables of $B \to K, K^* \bar{l} l$ decays which would have precise SM values. Thank to multi-partical final states of $B \to K \bar{l} l$ and $B \to K^*(\to K\pi)\bar{l} l$ decays one can investigate normalized angular distributions offering a number of useful obsevables to study NP.

For the case of $B \to K \bar{l} l$ decays we study several observables which are sensitive to lepton flavor changing NP. We also give some examples of NP models which might manifest themselves in $B \to K \bar{l} l$ decays. To study additional sources of CP violation we apply the angular distribution of $B \to K^*(\to K\pi)\bar{l} l$ having richer final structure due to the subsequent decay $K^* \to K\pi$. It allows to have nine coefficients in the angular distribution. With the help of these coefficients one can construct eight CP asymmetries, three T-odd CP-odd and five T-even CP-odd asymmetries (T is a transformation changing the sign of all particle momenta and spins). All asymmetries are doubly Cabibbo-suppressed in the SM and are of $\mathcal{O}(10^{-3})$ which makes them very attractive probes of NP sources of CP violation. They can be additionally suppressed due to the smallness of strong phases generated by quark loops. In this case the T-odd CP asymmetries are especially remarkable exhibiting maximal CP violation in the limit when strong phases vanish. In Chapter 3 we present the investigations of those observables and the results, published in:

- C. Bobeth, G. Hiller, G. Piranishvili, "Angular distributions of $B \to K \bar{l} l$ decays", JHEP 0712:040, 2007.

- C. Bobeth, G. Hiller, G. Piranishvili, " CP Asymmetries in $\bar{B} \to \bar{K}^*(\to \bar{K}\pi)\bar{l} l$ and Untagged $\bar{B}_s, B_s \to \phi(\to K^+K^-)\bar{l} l$ Decays at NLO", JHEP 0807:106, 2008.

The plan of this thesis is the following. In Chapter 1 we overview flavor and CP violation in the SM and consider the various symmetries of the quark sector. Here we also make an introduction into the concept of effective Hamiltonians. Chapter 2 is devoted to the topic of neutrino production of resonances, giving the detailed analysis of the second resonance region. The analysis of angular distributions of $B \to K, K^* \bar{l} l$ decays is given in Chapter 3 where we discuss various number of observables in the SM and beyond. Appendices A and B contain formulae and technical details relevant for the calculations.

1 Basics

1.1 Flavor in the Standard Model

The SM of particle physics contains in the matter sector three generations of elementary particles which are split into two parts

Leptons

$$\begin{pmatrix} \nu_e \\ e \end{pmatrix}_L , \begin{pmatrix} \nu_\mu \\ \mu \end{pmatrix}_L , \begin{pmatrix} \nu_\tau \\ \tau \end{pmatrix}_L , \; e_R, \; \mu_R, \; \tau_R \tag{1.1}$$

and

Quarks

$$\begin{pmatrix} u \\ d \end{pmatrix}_L , \begin{pmatrix} c \\ s \end{pmatrix}_L , \begin{pmatrix} t \\ b \end{pmatrix}_L , \; u_R, \; d_R, \; c_R, \; s_R, \; t_R, \; b_R, \tag{1.2}$$

where the indices L, R stand for the transformation property of the field under the $SU(2)_L$ gauge group, i.e., doublet and singlet, respectively. One introduces a quantum number, i.e., $e, \nu_e, u, d...$, which distinguishes different particles, and calls it $flavor$. Therefore, in the SM we have twelve kinds of flavor. However, in the SM, flavor is not a conserved quantum number. Due to the gauge group structure, i.e. $SU(2)_L$, the flavor transitions are allowed within a particular doublet only.

Further flavor transitions are induced after spontaneous symmetry breaking (SSB) $SU(2)_L \times U(1)_Y \to U(1)_{QED}$ [8, 9, 10]. Due to SSB the quarks and leptons obtain their masses by the Yukawa interactions with the so-called Higgs field

$$\begin{pmatrix} H^+ \\ H^0 \end{pmatrix}, \tag{1.3}$$

whose neutral component receives a non-vanishing vacuum expectation value. The neutrinos stay massless due to the absence of right-handed neutrino singlets under $SU(2)_L$ which was based on phenomenological grounds before the discovery of neutrino oscillations. Thus, the SM by itself does not predict a mechanism of neutrino mass generation which requires an extension in this regard. However, in view of neutrino oscillation experiments neutrinos are massive. The recent oscillation results and mechanisms of neutrino mass generation are reviewed in [11, 7, 12]. After SSB the flavor-violating effects manifest themselves in the SM in terms of fermion

masses. CP-violation appears in the modified structure of the charged-current (CC) interactions which reads in terms of the mass eigenstates

$$\mathcal{L}_{\rm int}^{CC} = -\frac{g}{\sqrt{2}} \left(\begin{array}{ccc} \bar{u}_L & \bar{c}_L & \bar{t}_L \end{array} \right) \gamma^\mu V_{\rm CKM} \left(\begin{array}{c} d_L \\ s_L \\ b_L \end{array} \right) W_\mu^\dagger + \text{h.c.}, \tag{1.4}$$

where g is the gauge coupling corresponding to the $SU(2)_L$ gauge group and W_μ corresponds to the charged W-boson. $V_{\rm CKM}$ is the Cabibbo-Kobayashi-Maskawa (CKM) 3×3 matrix [13, 14] presenting the strength of charged-current interactions. The appearance of such a matrix is due to the fact that after SSB the mass matrices of quarks and leptons in terms of the gauge eigenstates are in general non-diagonal in the SM. However, such a matrix does not appear in the CC-interaction of leptons with neutrinos due to the absence of right-handed neutrino singlets in the SM. Then the diagonalization of mass matrices leads to the non-diagonal structure in generation space of $V_{\rm CKM}$ in the charged-current interaction.

On the other side, neutral-current interactions (NC), i.e., corresponding to the photon A and $Z-$bosons, stay diagonal in generation and flavor space preventing the theory from the existence of FCNC processes at the tree level. The Lagrangian for those interactions reads as

$$\mathcal{L}_{\rm int}^{NC} = -\frac{g}{\cos\theta_W} \sum_i (\bar{\psi}_{iL} \gamma^\mu I_3 \psi_{iL} - Q_i \sin^2\theta_W \bar{\psi}_i \gamma^\mu \psi_i) Z_\mu - e Q_i \sum_i \bar{\psi}_i \gamma^\mu \psi_i A_\mu, \tag{1.5}$$

where i is the flavor index and $I_3 = +1/2$ for neutrinos and up-type quarks and $I_3 = -1/2$ for charged leptons and down-type quarks. Here Q_i presents the electric charges of the fermions ψ_i in units of the electron charge. θ_W is the angle corresponding to electoweak mixing. The absence of flavor changing transitions in (1.5) is a prediction of the SM.

Being the characteristic quantity for flavor physics of the SM, $V_{\rm CKM}$ will be considered closer. $V_{\rm CKM}$ is a complex unitary (3×3) matrix with 9 real parameters. However, the freedom of phase redefinitions of the quark fields leaves only four real parameters in the case of three generations. $V_{\rm CKM}$ can be parametrized in different ways leading to the same physical consequences, i.e., physics is independent of the particular choice. Particularly, in Euler parametrization those parameters are three angles and one complex phase, which is the only source of CP-violation in the SM. A possible Euler parametrization is the so-called "Standard Parametrization" [15], defining $V_{\rm CKM}$ as

$$\left(\begin{array}{ccc} c_{12}c_{13} & s_{12}c_{13} & s_{13}e^{-i\delta_{13}} \\ -s_{12}c_{23} - c_{12}s_{23}s_{13}e^{i\delta_{13}} & c_{12}c_{23} - s_{12}s_{23}s_{13}e^{i\delta_{13}} & s_{23}c_{13} \\ s_{12}s_{23} - c_{12}c_{23}s_{13}e^{i\delta_{13}} & -c_{12}s_{23} - s_{12}c_{23}s_{13}e^{i\delta_{13}} & c_{23}c_{13} \end{array} \right) \tag{1.6}$$

where $s_{ij} \equiv \sin\theta_{ij}$ and $c_{ij} \equiv \cos\theta_{ij}$. The advantage of this parametrization is that if one of the mixing angles, e.g., θ_{ij}, becomes zero then the corresponding mixing between the two generations i and j vanishes.

Another useful parametrization of $V_{\rm CKM}$, widely used in phenomenological analysis, was introduced by L.Wolfenstein [16]. The experimental data shows a strong hierarchy between non-diagonal matrix elements of $V_{\rm CKM}$, namely, the farther off-diagonal an element is the more suppressed it is. This hierarchy can be approximately written as

$$s_{12} \approx 0.22 \gg s_{23} \approx \mathcal{O}\left(10^{-2}\right) \gg s_{13} \approx \mathcal{O}\left(10^{-3}\right). \tag{1.7}$$

Applying this to the Standard parametrization we define mixing angles as

$$s_{12} = \lambda, \quad s_{23} = A\lambda^2, \quad s_{13}e^{-i\delta_{13}} = A\lambda^3(\rho + i\eta), \tag{1.8}$$

and expand (1.6) in the so-called Cabibbo-angle λ. Keeping terms up to $\mathcal{O}\left(\lambda^6\right)$ one obtains the following expression for the CKM matrix

$$V_{\rm CKM} = \begin{pmatrix} 1-\frac{1}{2}\lambda^2-\frac{1}{8}\lambda^4 & \lambda & A\lambda^3(\rho-i\eta) \\ -\lambda+\frac{1}{2}A^2\lambda^5[1-2(\rho+i\eta)] & 1-\frac{1}{2}\lambda^2-\frac{1}{8}\lambda^4(1+4A^2) & A\lambda^2 \\ A\lambda^3[1-(\bar{\rho}+i\bar{\eta})] & -A\lambda^2-A\lambda^4(\rho+i\eta)+\frac{1}{2}A\lambda^4 & 1-\frac{1}{2}A^2\lambda^4 \end{pmatrix} + \mathcal{O}\left(\lambda^6\right) \tag{1.9}$$

where $\bar{\rho} = \rho(1-\lambda^2/2)$ and $\bar{\eta} = \eta(1-\lambda^2/2)$. In spite of its approximative character, the CKM matrix remains unitary in the Wolfenstein parametrization up to negligible higher order terms. The useful consequence of this parametrization is that the matrix element V_{ub}, which contains the CP-violating phase, is exact, i.e., does not receive power corrections in λ. Since the different parametrizations of the CKM matrix are just different reformulations of the same mechanism, the most convenient version can be chosen depending on the particular phenomenological or experimental studies.

Thus, this simple framework appears to be very effective in studies of flavor and CP-violating processes. On the other hand this picture as a whole can be tested experimentally. For this purpose one uses the so-called Unitarity Triangle (UT). As we already discussed, the CKM matrix is unitary

$$V_{\rm CKM}^\dagger V_{\rm CKM} = V_{\rm CKM} V_{\rm CKM}^\dagger = \hat{1}, \tag{1.10}$$

where $\hat{1}$ is the 3×3 unit matrix. The matrix equation (1.10) implies 6 orthogonality relations which can be written explicitly as

$$\sum_{i=u,c,t} V_{i\alpha}V_{i\beta}^* = 0, \quad \alpha,\beta = d,s,b, \quad \alpha \neq \beta, \tag{1.11}$$

$$\sum_{\alpha=d,s,b} V_{i\alpha}V_{j\alpha}^* = 0, \quad i,j = u,c,t, \quad i \neq j. \tag{1.12}$$

Each of these six relations can be presented as a triangle in the complex $(\bar{\rho}, \bar{\eta})$ plain. The areas of the triangles are all equal in size and half of the Jarlskog parameter J [17], which is an invariant and a measure of the strength of CP-violation in the SM. In the Standard and Wolfenstein parametrizations it reads as

$$J = s_{12}s_{13}s_{23}c_{12}c_{23}c_{13}^2 \sin\delta_{13} = A^2\lambda^6\eta, \tag{1.13}$$

with the experimental value $J^{\text{exp}} \simeq \mathcal{O}(10^{-5})$. Actually, the smallness of J implies that CP-violating effects are hard to observe. In spite of the equal areas most of the triangles have one suppressed side compared to the other two making their study complicated. Only two triangles have comparable sides. They follow from the relations

$$V_{ud}V_{ub}^* + V_{cd}V_{cb}^* + V_{td}V_{tb}^* = V_{ud}V_{td}^* + V_{us}V_{ts}^* + V_{ub}V_{tb}^* = 0, \tag{1.14}$$

which can be rewritten in terms of Wolfenstein parameters as

$$A\lambda^3(\bar{\rho} + i\bar{\eta}) - A\lambda^3 + A\lambda^3(1 - \bar{\rho} - i\bar{\eta}) + \mathcal{O}\left(\lambda^7\right) = 0. \tag{1.15}$$

Introducing the quantities

$$R_b \equiv \sqrt{\bar{\rho}^2 + \bar{\eta}^2}, \quad R_t \equiv \sqrt{(1-\bar{\rho})^2 + \bar{\eta}^2} \tag{1.16}$$

relation (1.15) leads to the triangle shown in the left-hand plot of Figure 1.1 with unit length base and two sides R_b and R_t. All parameters of the UT, i.e., sides and angles are measurable quantities. Particularly, the angle γ, coinciding with δ_{13}, is $\mathcal{O}(60^\circ)$ according to the experimental data. It means that CP-violation in the SM is nearly maximal.

The various measurements do not serve only to measure particular elements of the CKM matrix but also to verify and overconstrain the complete framework of flavor and CP violations in the SM. The right-hand plot of Figure 1.1 describes such attempts done by the CKMfitter collaboration [18]. Several observables indicated by the bands various bands constrain the position of the UT apex. The global analysis shows that current data are in good agreement with the SM predictions. But still there is a big space for improving the data and hopefully finding some inconsistencies with the SM which helps us to study the physics beyond the SM.

1.2 From Quarks to Hadrons

1.2.1 QCD Lagrangian

After SSB in the SM the unbroken symmetry is $SU(3)_{QCD} \times U(1)_{QED}$, corresponding to *Quantum Chromodynamics*(QCD) and *Quantum Electrodynamics*(QED), respectively. The corresponding degrees of freedom of $SU(3)_{QCD} \times U(1)_{QED}$ are nine

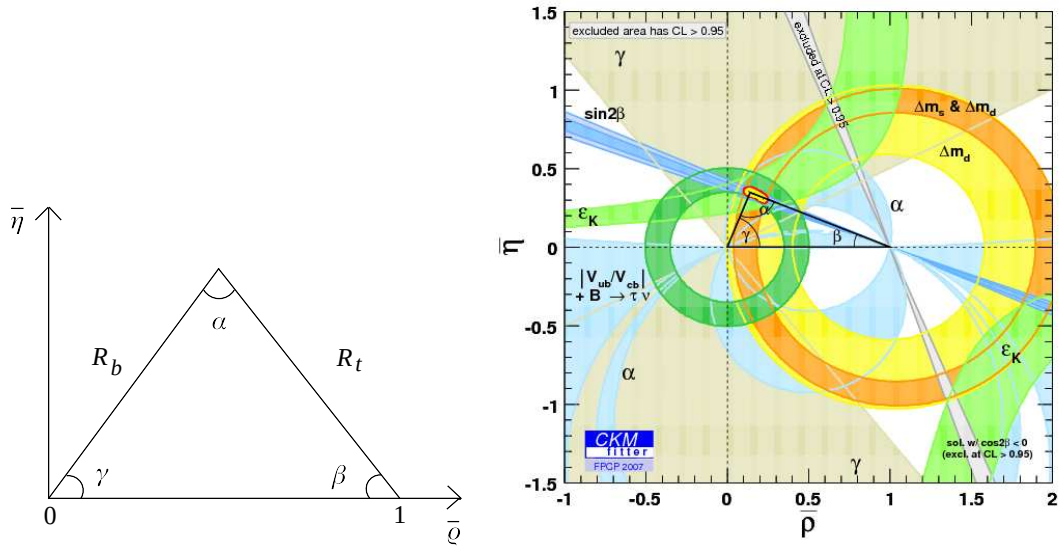

Figure 1.1: Draft of Unitarity triangle (left) and current CKMfitter analyses of UT [18] (right).

massless gauge bosons, i.e., the photon and the eight gluons. Whereas QED is the theory describing interactions of electrically charged quarks and leptons, QCD applies only to quarks. Moreover, the non-abelian nature of the QCD leads to the fact that the only observable form of quarks and gluons at long distances are the hadrons. In this section we discuss the basics of QCD starting from the Lagrangian of the theory, which reads as

$$\mathcal{L}_{\mathrm{QCD}} = -\frac{1}{4} G^a_{\mu\nu} G^{a\mu\nu} + \sum_{q=u,d,s\ldots} \bar{q}(iD_\mu \gamma^\mu - m_q)q, \tag{1.17}$$

where

$$D_\mu = \partial_\mu - i g_s \frac{\lambda^a}{2} A^a_\mu, \tag{1.18}$$

$$G^a_{\mu\nu} = \partial_\mu A^a_\nu - \partial_\nu A^a_\mu + g_s f^{abc} A^b_\mu A^c_\nu. \tag{1.19}$$

Here g_s is the dimensionless coupling of $SU(3)_{QCD}$ and $G^a_{\mu\nu}$ is the field-strength tensor corresponding to the gluon field A^a_μ, where $a = 1...8$. In (1.17) we skip gauge-fixing and ghost terms which are irrelevant for the current discussions. The non-abelian nature of QCD manifests in the fact that the gluon fields carry color charge and the selfinteraction due to the third term in (1.19). In contrast to QED, the quark can change its color-charge after emission or absorption of a gluon field.

If we assume that g_s is small enough for a perturbative treatment, we can calculate different processes in QCD applying (1.17). Going beyond tree level by considering

loop corrections will lead to divergences. This happens because the momentum of virtual particles in the loop is integrated from zero to infinity. Fortunately, similar to QED, QCD is a renormalizable theory. This means that the ultraviolet divergences, appearing in Feynman diagrams with loops, can be isolated by the redefinition of Lagrangian parameters (regularization), i.e., couplings, masses and fields. Thus, the physically observable quantities are finite to all orders in perturbation theory.

Due to the regularization the renormalization technique introduces an additional mass dimension parameter μ, the renormalization scale. All the parameters of the Lagrangian are μ dependent, i.e., $g_s \equiv g_s(\mu)$, $m_q \equiv m_q(\mu)$ etc. The μ-scale dependence is governed by the so-called renormalization group equations (RGE). For example, in QCD the renormalization scale dependence of the gauge coupling and quark masses can be computed by solving the following RGE

$$\begin{aligned}\frac{dg_s(\mu)}{d\ln\mu} &= \beta(g_s(\mu)),\\ \frac{dm_q(\mu)}{d\ln\mu} &= -\gamma_m(g_s(\mu))m_q,\end{aligned} \tag{1.20}$$

where β is the RGE-function of the coupling and γ_m is the anomalous dimension of the mass. They can be calculated in perturbation theory and at two loop order we have

$$\beta(g_s) = -g_s\Big[\frac{g_s^2}{16\pi^2}\beta_0 + \Big(\frac{g_s^2}{16\pi^2}\Big)^2\beta_1\Big], \tag{1.21}$$

$$\gamma_m(g_s) = \frac{g_s^2}{16\pi^2}\gamma_m^{(0)} + \Big(\frac{g_s^2}{16\pi^2}\Big)^2\gamma_m^{(1)}. \tag{1.22}$$

In the so-called $\overline{MS}$ scheme the coefficients read as

$$\beta_0 = 11 - \frac{2n_f}{3}, \tag{1.23}$$

$$\beta_1 = 102 - \frac{38}{3}n_f, \tag{1.24}$$

$$\gamma_m^{(0)} = 8, \tag{1.25}$$

$$\gamma_m^{(1)} = \frac{404}{3} - \frac{40n_f}{9}, \tag{1.26}$$

where n_f is the number of active flavors. In terms of $\alpha_s(\mu) = g_s^2(\mu)/(4\pi)$ the solutions of the differential equations (1.20) are

$$\begin{aligned}\alpha_s(\mu) &= \frac{\beta_0}{\ln(\mu^2/\Lambda^2)}\left[1 - \frac{\beta_1\ln\ln(\mu^2/\Lambda_{QCD}^2)}{\beta_0\ln(\mu^2/\Lambda_{QCD}^2)}\right],\\ m_q(\mu) &= m_q(\mu_0)\Big[\frac{\alpha_s(\mu)}{\alpha_s(\mu_0)}\Big]^{\frac{\gamma_m^{(0)}}{2\beta_0}}\left[1 + \Big(\frac{\gamma_m^{(1)}}{2\beta_0} - \frac{\gamma_m^{(0)}\beta_1}{2\beta_0^2}\Big)\frac{\alpha_s(\mu)-\alpha_s(\mu_0)}{4\pi}\right],\end{aligned} \tag{1.27}$$

where Λ_{QCD} is the momentum scale where α_s diverges. In the case of five active flavors, $\Lambda_{QCD} \sim \mathcal{O}(200\,\mathrm{MeV})$, being the characteristic scale of the breakdown of the perturbative expansion. The growth of α_s, predicted in perturbation theory, indicates the necessity to use non-perturbative methods at long distances of $\mathcal{O}(1/\Lambda_{QCD})$. This regime of QCD is called *confinement*. The interaction between quarks and gluons becomes strong, and they are confined into hadronic bound states. Thus, it is quite natural that the characteristic scale of hadron interactions is of order Λ_{QCD}. The limit $\mu \to \infty$ leads to a vanishing quark-gluon coupling. This regime reveals that at short distances the behavior of quarks and gluons in QCD is *asymptotically* free.

1.2.2 Quark Model of Hadrons

The large amount of hadrons can be nicely systematized and studied with the help of the various approximate symmetries in QCD. First we consider the consequences of the QCD gauge group for the hadron formation. Each quark q carries a color index and transforms as a triplet, whereas an antiquark $\bar{q}$ transforms as an antitriplet under the $SU(3)_{QCD}$ gauge group. Since the hadrons are color-neutral particles, we need such combinations of q and $\bar{q}$ which will be singlets under $SU(3)_{QCD}$. There are two possibilities to form such color neutral combinations. The first one is the so-called meson state, which can be built from quark and antiquark by summing over all color quantum numbers

$$|M\rangle = \sum_{i=1}^{3} |q_1^i\, \bar{q}_{2\,i}\rangle. \tag{1.28}$$

The second possibility is a combination of three quarks (antiquarks) multiplied by the totally antisymmetric tensor ε_{ijk} (ε^{ijk})

$$|B\rangle = \sum_{i,j,k=1}^{3} \varepsilon_{ijk}\, |q_1^i\, q_2^j\, q_3^k\rangle, \tag{1.29}$$

which are called baryons. Therefore the $SU(3)_{QCD}$ group explains naturally the absence of such states as qq (diquark) or $qqqq$ (four-quark) in the hadronic spectrum, since these quark combinations are not color-singlets. It also clarifies the existence of the uuu or sss bound states, i.e., Δ^{++} and Ω^-, respectively, which in the absence of the color quantum number would violate the Pauli principle for fermions.

The quarks in (1.28), (1.29) are called valence quarks since they define the flavor type of the hadron. However, the true structure of hadrons is more complicated. At the distances of $\mathcal{O}(1/\Lambda_{QCD})$ additional quark-antiquark pairs and gluons are created and annihilated inside of hadrons due to quantum fluctuations. The reason

is that the masses of light quarks, i.e., u, d and s, are smaller than Λ_{QCD}. These virtualities are color neutral and flavor conserving. We can qualitatively estimate the importance of these virtual processes for the example of the neutron and the proton. The proton and neutron are the lightest baryons with the quark structure uud and udd, respectively. If we take a look at the quark masses in the $\overline{MS}$ scheme from the Particle Data Group review [15]

$$\begin{aligned} \overline{m}_u(2\,\mathrm{GeV}) &= 3 \pm 1\,\mathrm{MeV}, & \overline{m}_d(2\,\mathrm{GeV}) &= 6.0 \pm 1.5\,\mathrm{MeV}, \\ \overline{m}_s(2\,\mathrm{GeV}) &= 103 \pm 20\,\mathrm{MeV}, & \overline{m}_c(\overline{m}_c) &= 1.24 \pm 0.09\,\mathrm{GeV}, \\ \overline{m}_b(\overline{m}_b) &= 4.2 \pm 0.07\,\mathrm{GeV}, & \overline{m}_t(\overline{m}_t) &= 162.9 \pm 1.3\,\mathrm{GeV}, \end{aligned} \tag{1.30}$$

we can see that u and d quarks are the lightest ones with masses of order several MeV. It should be noted that these masses are due to the interaction with the Higgs-field. If we just sum the masses of u and d correspondingly to the valence quark content of the proton and neutron, we obtain that the nucleon mass should be of $\mathcal{O}\,(10\,\mathrm{MeV})$. This contradicts the well known experimental values of the proton and neutron masses of $\mathcal{O}\,(940\,\mathrm{MeV})$ being three orders of magnitude larger then the naive estimate given above. The transparent example shows the important role of the long-distance quark-gluon dynamics in non-pertubative QCD for the mass generation of hadronic matter, which can not be explained by the SSB-mechanism alone.

1.2.3 Flavor Symmetries: Isospin and $SU(3)$

Since the discovery of Yang-Mills local gauge theories and their role in particle physics, group theory helps to understand high energy physics from the first principles. A physical system having with a symmetry can be studied by group-theoretical methods, since the symmetry transformations form a group. In QCD, besides the space-time (Poincare) and color ($SU(3)_{QCD}$) symmetries the fundamental Lagrangian can be studied using flavor symmetries. One of the well-known examples is the *isospin* symmetry introduced by Heisenberg in the 1930's. If we concentrate on u and d quarks, we can observe the fact that their masses and the mass difference are much smaller with respect to Λ_{QCD}

$$m_u,\, m_d,\, m_u - m_d \ll \Lambda_{QCD}. \tag{1.31}$$

Neglecting the mass difference and introducing a common mass m for up and down quarks the QCD Lagrangian (1.17) can be written in this limit as

$$\mathcal{L}_{\mathrm{QCD}} = \bar{N}(iD_\mu\gamma^\mu - m)N + \sum_{q=s,c,b,t} \bar{q}(iD_\mu\gamma^\mu - m_q)q + \mathcal{L}_{gluon}, \tag{1.32}$$

where we introduce the doublet N as

$$N = \begin{pmatrix} u \\ d \end{pmatrix}. \tag{1.33}$$

The Lagrangian (1.32) has a global symmetry under the following transformations of the new field N

$$N \to N' = e^{i\alpha^a \sigma^a/2} N \tag{1.34}$$

where the summation over $a = 1, 2, 3$ is understood. The σ^a are the well-known 2×2 Pauli matrices, i.e., the generators of the $SU(2)$ group transformations. The isospin symmetry is not exact. The violation is due to the mass difference $m_u - m_d$ and the difference of the electric charges of u and d quarks, being effects of $\mathcal{O}(\alpha)$ and $\mathcal{O}\left(\frac{m_u - m_d}{\Lambda_{QCD}}\right)$, respectively.

The isospin symmetry manifests itself in hadrons. The hadrons which differ in the quark content by the interchange of the u and d quarks, form isodoublets ($I = 1/2$). The components of such doublets differ in their mass by order of few MeV as predicted by the $SU(2)$ symmetry breaking corrections, which is confirmed experimentally. Examples are the proton (uud) and the neutron (udd), K^+ ($u\bar{s}$) and K^- ($d\bar{s}$), B^+ ($u\bar{b}$) and B^0 ($d\bar{b}$), etc. The mesons built only from the N doublets can be written as

$$N^\alpha \bar{N}_\beta = \begin{pmatrix} \frac{u\bar{u} - d\bar{d}}{\sqrt{a}} & u\bar{d} \\ d\bar{u} & -\frac{u\bar{u} - d\bar{d}}{\sqrt{a}} \end{pmatrix}^\alpha_\beta + \delta^\alpha_\beta \frac{u\bar{u} + d\bar{d}}{\sqrt{2}} \tag{1.35}$$

with $\alpha, \beta = 1, 2$. The first term in (1.35) corresponds to the isotriplet ($I = 1$) whereas the second one is the isosinglet ($I = 0$). Examples of such triplets are the pions, π^+, π^0 and π^- and the ρ mesons, ρ^+, ρ^0 and ρ^-. Similarly to the doublet states, the mass difference within the triplet is of order few MeV, which is nicely confirmed by experimental observations.

The smallness of the strange quark mass m_s with respect to Λ_{QCD} allows us to extend the isospin $SU(2)$ symmetry to the $SU(3)$ flavor symmetry group. In analogy with isospin we neglect the mass differences between u, d and s quarks. Introducing the common m_3 mass for u, d and s, the QCD Lagrangian takes the form

$$\mathcal{L}_{\text{QCD}} = \bar{\psi}(iD_\mu \gamma^\mu - m_3)\psi + \sum_{q=c,b,t} \bar{q}(iD_\mu \gamma^\mu - m_q)q + \mathcal{L}_{gluon}, \tag{1.36}$$

where ψ is a triplet

$$\psi = \begin{pmatrix} u \\ d \\ s \end{pmatrix}. \tag{1.37}$$

The Lagrangian (1.36) is invariant under transformations of the new field ψ

$$\psi \to \psi' = e^{i\alpha^a \lambda^a/2}\,\psi, \tag{1.38}$$

where $a = 1...8$ and λ^a are eight Gell-Mann matrices, i.e., the generators of the $SU(3)$ flavor group. This symmetry was introduced by Gell-Mann, Ne'eman and Zweig in early 1960's as an extension of the isotopic spin group $SU(2)$ in order to classify the large amount of baryons and mesons seen in terms of *quarks*. At that time several particles were discovered which besides isospin have an additional quantum number called *strangeness*. It can be shown that the charge of a particle Q is correlated to the strangeness S and the third component of isospin I_3 in the following way

$$Q = I_3 + \frac{Y}{2}, \qquad\qquad Y = B + S, \tag{1.39}$$

where B is the baryon number $B = +1$ for baryons and $B = -1$ for antibaryons. The corresponding quantum numbers for the quarks u, d and s read as

Quarks	Q	I	I_3	Y	S	B
u	2/3	1/2	1/2	1/3	0	1/3
d	-1/3	1/2	-1/2	1/3	0	1/3
s	-1/3	0	0	-2/3	-1	1/3

The meson bound states are formed by the $\psi\bar{\psi}$ combination. As a result of multiplet multiplication

$$3 \otimes 3^* = 1 \oplus 8 \tag{1.40}$$

mesons belong either to the singlet or the octet representations of $SU(3)$. Using (1.40) one can show that the quark content of the scalar meson octet is

$$\begin{aligned} &\pi^+ \sim (\bar{d}u), && \pi^0 \sim (\bar{u}u, \bar{d}d), && \pi^- \sim (\bar{u}d), && \\ &K^+ \sim (\bar{s}u), && K^0 \sim (\bar{s}d), && \bar{K}^0 \sim (\bar{d}s), && K^- \sim (\bar{u}s), \\ &\eta^0 \sim (\bar{u}u, \bar{d}d, \bar{s}s), && && && \end{aligned} \tag{1.41}$$

being the same as for the vector mesons. The baryons are bound states of three quarks $\psi\psi\psi$ and from

$$3 \otimes 3 \otimes 3 = 1 \oplus 8 \oplus 8 \oplus 10 \tag{1.42}$$

follows that they form octets and decuplets. For the spin 1/2 baryon octet we have

$$\begin{aligned} p &\sim (udu), & n &\sim (udd), & & \\ \Sigma^+ &\sim (suu), & \Sigma^0 &\sim (sud, sdu), & \Sigma^- &\sim (sdd), \\ \Xi^0 &\sim (ssu), & \Xi^- &\sim (ssd), & & \\ \Lambda^0 &\sim (suu, sdd, sud) & & & & \end{aligned} \tag{1.43}$$

and the quark content for the spin 3/2 baryon decuplet is

$$\begin{aligned} \Delta^{++} &\sim (uuu), & \Delta^+ &\sim (uud), & \Delta^0 &\sim (udd), & \Delta^- &\sim (ddd), \\ \Sigma^{*+} &\sim (suu), & \Sigma^{*0} &\sim (sud), & \Sigma^{*-} &\sim (sdd), & & \\ \Xi^0 &\sim (ssu), & \Xi^- &\sim (ssd), & & & & \\ \Omega^- &\sim (sss). & & & & & & \end{aligned} \tag{1.44}$$

Of course, the $SU(3)$ is not an exact symmetry. The experimental data shows that the masses of the mesons or baryons differ from component to component in the multiplet. Thus, the violation of $SU(3)$ is characterized by the mass splitting within one multiplet, which varies from $\mathcal{O}(m_u - m_d)$ to $\mathcal{O}(m_s - m)$, where m is the common mass of u and d quarks.

Taking into account the spin of the light quarks, $SU(3)$ can be extended to an $SU(6)$ symmetry group. The fundamental representation of $SU(6)$ is 6, i.e.

$$q = \begin{pmatrix} u\uparrow \\ d\uparrow \\ s\uparrow \\ u\downarrow \\ d\downarrow \\ s\downarrow \end{pmatrix} \tag{1.45}$$

and from the multiplication of representations

$$6 \otimes 6 \otimes 6 = 56 \oplus 70 \oplus 70 \oplus 20 \tag{1.46}$$

it follows that the baryon bound states transform as 56, 70 and 20 representations. The $SU(6)$ multiplets can be decomposed into $SU(3)$ ones as

$$\begin{aligned} 56 &= 10^4 \oplus 8^2, \\ 70 &= 10^2 \oplus 8^4 \oplus 8^2 \oplus 1^2, \\ 20 &= 8^2 \oplus 1^4, \end{aligned} \tag{1.47}$$

where the superscript denotes $(2S+1)$ and S is the spin of a baryon in a particular multiplet. In order to take into account orbitally excited baryons rigorously one extends $SU(6)$ to the $SU(6) \times O(3)$ group ("symmetric" quark model) where $O(3)$ corresponds to the symmetry transformation of the spatial part of baryon wave functions. In this model the 56-plet is a "ground state" and contains such baryons as p, n, $\Delta(1232)$ and $P_{11}(1440)$. The next "excited" multiplet is 70 which includes $D_{13}(1520)$ and $S_{11}(1535)$. Particularly these resonances will be considered in Chapter 2 in the context of neutrino scattering on nucleons.

1.2.4 Heavy Quark Symmetry

Here we focus on the heavy quark sector of the QCD Lagrangian, namely on c and b quarks with m_c, $m_b \gg \Lambda_{QCD}$, see (1.30). We do not consider t quark since it is too heavy to form hadronic bound states before decaying. That leads to the situation when

$$m_c \sim m_b \sim m_Q \to \infty. \tag{1.48}$$

In this limit the Lagrangian (1.17) can be formally rewritten as

$$\mathcal{L}_{\mathrm{QCD}} = \bar{Q}(iD_\mu\gamma^\mu - m_Q)Q + \mathcal{L}_{gluon,\,u,\,d,\,s}, \tag{1.49}$$

where we introduce a new doublet

$$Q = \begin{pmatrix} c \\ b \end{pmatrix}. \tag{1.50}$$

We now rewrite (1.49) such that it does not contain m_Q explicitly. The momentum of the heavy quark Q can be decomposed in the rest frame of the heavy meson as

$$p_Q = m_Q v + k, \tag{1.51}$$

with $v = (1, \vec{0})$ being the 4-velocity of the meson and with the small residual momentum $k \sim \Lambda_{QCD} \ll m_Q$. In this limit the heavy quark field can be decomposed into the large h_v and small χ_v components as

$$Q = e^{-im_Q v\cdot x}(h_v + \chi_v) \tag{1.52}$$

with

$$(\not{v} - 1)h_v = 0, \qquad (\not{v} + 1)\chi_v = 0. \tag{1.53}$$

Since the χ_v part is suppressed by k/m_Q and therefore can be neglected, we rewrite (1.49) in terms of the h_v as

$$\begin{aligned}\bar{Q}(i\not{D} - m_Q)Q \simeq \bar{h}_v i\not{D} h_v &= \bar{h}_v \Big(\frac{\not{v}+1}{2}\Big) i\not{D} h_v \\ &= \bar{h}_v \left[iv\cdot D - i\not{D}\Big(\frac{\not{v}-1}{2}\Big)\right] h_v = \bar{h}_v iv\cdot D h_v. \end{aligned} \tag{1.54}$$

In this form the Lagrangian becomes independent of the m_Q scale. We can generalize this to the case of N heavy quarks as

$$\mathcal{L}_Q = \sum_{i=1}^{N} \bar{h}_v^{(i)} iv\cdot D h_v^{(i)}. \tag{1.55}$$

One can show that the effective Lagrangian possesses a $SU(2N)$ spin-flavor symmetry, which in the case of c and b becomes $SU(4)$. The $SU(2N)$ symmetry becomes broken if one includes $\mathcal{O}\left(1/m_Q\right)$ corrections to the Lagrangian.

The consequence of the heavy quark limit is that the mass of a meson M can be written as

$$m_M = m_Q + \bar{\Lambda} + \mathcal{O}\left(1/m_Q\right), \tag{1.56}$$

where the constant $\bar{\Lambda}$ is of order Λ_{QCD} and characterizes the energy of the light quark and gluon "cloud" in the meson M and is independent of m_Q. In the heavy meson case such a quark-gluon cloud is purely relativistic with a non-perturbative long-distance behavior.

1.3 Effective Theory of Electroweak Processes

1.3.1 Idea

Rare B meson decays, governed by FCNC, consist useful probe to investigate NP. To study FCNC processes one uses a useful technique, called *Effective Weak Hamiltonian*. The effective Hamiltonian notation is nothing but the construction of an effective theory in the presence of several energy scales in the problem. In the effective theories one separates low energy (large distances) dynamics from high energy (small distances) ones by decoupling degrees of freedom which are not actively participating in low energy processes. For FCNC processes, these degrees of freedom correspond to the particles running in loops. Crucially, it is possible to decouple (or integrate out) the virtual degrees of freedom in such a way that they do not appear in the low energy Lagrangian anymore.

One of the examples of such a reduction is the well known Fermi theory of the β-decay. In the SM, on the quark level, the leading contribution to this process comes from the tree level W-boson exchange. Since the typical energy scale of the external momentum (in the center of mass frame) in the β-decay is much smaller than the W-boson mass it is possible to integrate it out from the theory by keeping only the leading term in the expansion of the W-propagator

$$-i\frac{g_{\mu\nu}}{q^2-m_W^2} \simeq ig_{\mu\nu}(\frac{1}{m_W^2}+\frac{q^2}{m_W^2}+...) \tag{1.57}$$

and omitting higher order terms in q^2/m_W^2. Here we denote by q^2 the four momentum transfer and by m_W the W-boson mass, where $q^2 \ll m_W^2$ is understood. (A more elegant formulation can be given with the help of the functional path integral formalism.) Thus, the β-decay can be described with high order of accuracy by the effective theory with the following Hamiltonian

$$H_{\text{eff}} = -\frac{4G_F}{\sqrt{2}}V_{ud}^*(\bar{e}\gamma_\mu P_L\nu_e)\,(\bar{u}\gamma^\mu P_L d) + \mathcal{O}\left(\frac{q^2}{m_W^2}\right), \tag{1.58}$$

$$\frac{G_F}{\sqrt{2}} \equiv \frac{g^2}{8m_W^2} \tag{1.59}$$

and $P_L = (1-\gamma_5)/2$. Here G_F is the well-known Fermi constant and V_{lm} are the CKM matrix elements. Note that the information about small distances is not completely removed from the theory (it is only removed dynamically) but contained in the G_F effective constant.

Generalizing this approach, the amplitude in the effective theory can be written as a projection of the effective Hamiltonian onto external states

$$A(I \to F) = \langle F|H_{\text{eff}}|I\rangle \sim G_F V_{\text{CKM}} C_i(\mu)\langle F|\mathcal{O}_i(\mu)|I\rangle, \tag{1.60}$$

where $\mathcal{O}_i$ are high dimensional operators sandwiched between I and F, i.e., initial and final states respectively. The Wilson coefficients can be computed perturbatively in α_s

$$C_i = C_i^{(0)}(\mu_0) + \frac{\alpha_s}{4\pi}C_i^{(1)}(\mu_0) + \frac{\alpha_s^2}{(4\pi)^2}C_i^{(2)}(\mu_0) + \mathcal{O}\left(\alpha_s^3\right) \tag{1.61}$$

as a function of the high-energy scale (matching scale) $\mu_0 \sim m_W$ of the order of the decoupled heavy degrees of freedom. Technically, one calculates the amplitude in the full theory and in the effective theory, and subsequently determines the Wilson coefficient by requiring the equality of both. In order to add higher order QCD corrections and evaluate the Wilson coefficients at the low scale μ, where particular phenomena are observed (for b-decays $\mu \sim m_b$), one uses the powerful technique of

the RGE. The RGE for the Wilson coefficients has the following general form

$$\frac{dC_i(\mu)}{d\ln\mu} = \gamma_{ij}(\mu)C_j(\mu), \tag{1.62}$$

where γ_{ij} is the so-called anomalous dimension matrix

$$\gamma_{ij}(\mu) = Z^{-1}_{ik}\frac{dZ_{kj}}{d\ln\mu}. \tag{1.63}$$

The Z_{ij} are the renormalization constants appearing during the renormalization of the amplitude $\langle F|H_{\text{eff}}|I\rangle$. The non-diagonal nature of the Z_{ij} leads to the mixing of the different operators under the renormalization procedure. γ_{ij} can be expanded in perturbation theory as

$$\gamma_{ij} = \frac{\alpha_s}{4\pi}\gamma^{(0)}_{ij} + \frac{\alpha_s^2}{(4\pi)^2}\gamma^{(1)}_{ij} + \frac{\alpha_s^3}{(4\pi)^3}\gamma^{(2)}_{ij} + ... \tag{1.64}$$

The RGE (1.62) is a system of ordinary coupled differential equations with the formal solution

$$C_i(\mu) = U_{ij}(\mu,\mu_0)C_j(\mu_0), \tag{1.65}$$

expressing the running of the Wilson coefficients from the scale μ_0 to the scale μ. The evolution matrix $U(\mu,\mu_0)$ allows us to calculate the Wilson coefficients at the low scale.

Let us summarize the important features of the effective Hamiltonian. First, the Wilson coefficients are process independent quantities, i.e., do not depend on the type of the external hadronic states. Therefore, once calculated, they can be used for different processes. This manifests itself by the fact that the Wilson coefficients depend only on the masses of the particles which we integrated out. Second, the hadronic matrix elements are process dependent quantities and have to be calculated using some non-perurbative methods. Third, the physical observables must not depend on the scale μ, which cancels between the short distance (Wilson coefficients) and long distance (hadronic matrix elements) dynamics. Unfortunately, the truncation of the perturbation expansion leaves a remnant μ dependence in the predictions, which introduces an additional uncertainty to the observables and is usually used as an indication of the size of missing higher order corrections. The inclusion of higher order terms is supposed to reduce the μ dependence.

1.3.2 Hadronic Matrix Elements

In order to compute the amplitude (1.60) we should know the Wilson coefficients and matrix elements of the operators $\langle\mathcal{O}_i(\mu)\rangle$ being sandwiched between the initial

and final states. The Wilson coefficients are process independent quantities and can be computed in perturbation theory. The computation of the matrix elements is a sophisticated task. In the so-called *naive factorization* approach the matrix elements of $B \to K, K^* \bar{l}l$ exclusive semileptonic decays are assumed to factorize into the product of a leptonic current and the matrix element of a quark current, which schematically can be written as

$$\langle \bar{l}l K, K^* | \mathcal{O}_i | B \rangle \sim \langle K, K^* | \bar{s}\, \Gamma_1\, b | B \rangle\, (\bar{l}\, \Gamma_2\, l), \tag{1.66}$$

where $\Gamma_{1,2}$ corresponds to different Dirac matrix structures. Applying Lorentz-transformation properties of the matrix element, the hadronic part is parametrized in terms of the form factors $F_i^{B\to K,K^*}$ of the $B \to K, K^*$ transitions and can be formally written as

$$\langle K, K^* | \bar{s}\, \Gamma_1\, b | B \rangle \sim F_i^{B\to K,K^*}, \tag{1.67}$$

where the form factors are functions of Lorentz-scalars. This picture is incomplete due to the presence of so-called *non-factorizable* strong interactions effects which are not contained in the definition of the form factors of the $B \to K, K^*$ transitions [19, 20]. There are two types of such non-factorizable contributions. The first type corresponds to the photon scattering with the spectator quarks of the B-meson or Kaon. The corresponding diagrams are (g), (j) and (k) in Figure B.1 of Appendix B.4 which contribute at LO and NLO in α_s. The second type of the non-factorizable contributions come from the diagrams (d), (e) and (f) in Figure B.1 where the omitted spectator quark is connected to the hard process through soft interactions.

The consistent method which goes beyond the *naive factorization* and is able to include non-factorizable contributions is called QCD factorization (QCDF). It was firstly introduced in [21, 22] for the non-leptonic B-decays and was extended to semileptonic and radiative decays in [19, 20, 23, 24]. The amplitude of the $B \to K, K^* \bar{l}l$ decays computed in QCDF can be schematically written as

$$\langle \bar{l}l K_a^{(*)} | H_{\text{eff}} | B \rangle = C_a \xi_a + \Phi_B \otimes T_a \otimes \Phi_{K^{(*)}} \tag{1.68}$$

where $a = P, \perp, \parallel$ corresponds to a pseudoscalar K-meson, a transversely or longitudinally polarized K^*, respectively. Here ξ_a are universal heavy-to-light form factors [25, 26] and Φ light cone distribution amplitudes of the B and K mesons. The factors C_a and T_a are computed in perturbation theory [19, 20], whose explicit expressions can be found in Appendix B.4.

The resulting calculations are limited to the dilepton invariant mass range $1\,\text{GeV}^2 \lesssim q^2 \lesssim 7\,\text{GeV}^2$. The lower cut is chosen in order to avoid the contributions from light resonances. The proper upper limit is determined by the requirements that the momentum of the Kaon is large $p_K \sim m_b$ and the contributions from charm resonances are evaded [19, 20].

2 Resonance Production by Neutrinos

In this chapter we discuss neutrino scattering on nucleons in the resonance region. Here we will consider first four dominantly contributing resonances. We present the updated fit of the form factors of nucleon-resonance transitions. The form factors are determined from the experimental data on helicity amplitudes and using theory general principles. Employing the new fit we compute cross sections of the neutrinoproduction processes.

2.1 Introduction

The neutrino production of the resonances has been studied for a long time. Together with quasielastic scattering (QE) and deep inelastic scattering (DIS) the resonance production contributes to the total cross section of the neutrino-nucleon interaction. Schematically, this process is shown in Figure 2.1. The first attempts concerned the proton excitation in the delta resonance Δ which gives the main contribution to the cross section [27, 28, 29, 30]. These papers determined the $p \to \Delta$ transition in terms of hadronic form factors using general principles such as conserved vector current (CVC), partially conserved axial-vector currents (PCAC), dispersion relations, etc. In a later article [31], also resonance electroproduction data was used which gives more precise values for the vector form factors and shows that the form factors fall faster with increasing Q^2 than the nucleon form factors in the dipole approximation. The result of the papers [32, 33, 34] are the cross sections depending on several parameters characterizing form factor fits.

In the latest decade the interest to study resonance production has increased because of the discovery of neutrino oscillations. For the precise study of neutrino oscillations the production of resonances by muon- and tau-neutrinos was analyzed [35, 36, 31, 37, 38]. In the paper [38] calculations have been done taking into account the mass of the outgoing muon.

The goal of the present work is to extend the previous investigations for isospin-1/2 resonances $P_{11}(1440)$, $D_{13}(1520)$, $S_{11}(1535)$ whose contribution to the cross section

is sufficient besides $P_{33}(1232)$. Recently, electroproduction of resonance data has become available from the Jefferson Laboratory [39, 40, 41] and Mainz [42] (BATEs and Bonn). The data is mainly given in terms of helicity amplitudes. Here we present the approach of determining the vector form factors of nucleon-resonance transition from the helicity amplitudes of electroproduction data. For the axial form factors we adopt an effective Lagrangian for the $R \to N\pi$ couplings and calculate the decay widths. For each resonance we assume PCAC which gives us one relation between axial form factors. Another coupling is determined from the decay width of each resonance.

Knowing the resonance coupling we will consider different processes of resonance production by neutrinos and predict cross sections.

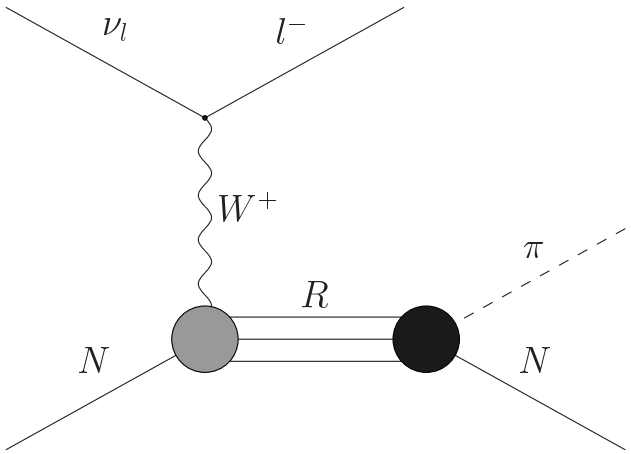

Figure 2.1: Single-pion production through a resonance R in neutrino reaction.

2.2 Formalism of Resonance Production in Neutrino-Nucleon Interactions

2.2.1 Cross Section

In this section we give the parametrization of the cross sections of the neutrino resonance production, involving the following reaction

$$\nu(k)\, n(p) \to \mu^-(k')\, R(p') \to \mu^- \begin{cases} p\,\pi^0 \\ n\,\pi^- \end{cases}, \tag{2.1}$$

where $R = D_{13}(1520)$, $P_{33}(1232)$, $P_{11}(1440)$ and $S_{11}(1535)$. The calculations of cross sections are based on the formalism analogous to the one used in deep inelastic scattering (DIS). The cross section in DIS is given as

$$\frac{d\sigma}{d\Omega dE'} = \frac{G_F^2}{16\pi^2}\cos^2\theta_C \frac{E'}{E} L_{\mu\nu}\mathcal{W}^{\mu\nu}, \tag{2.2}$$

where G_F is Fermi constant, E and E' are the corresponding energies of incoming and outgoing leptons, θ_C is the Cabibbo angle, i.e., $\sin\theta_C = V_{us}$ (see Section 1.1). We prefer to work with variables convenient for the resonance production and write the cross section as

$$\frac{d\sigma}{dQ^2 dW} = \frac{\pi W}{m_N E E'}\frac{d\sigma}{d\Omega dE'}, \tag{2.3}$$

where m_N is the nucleon mass and we use the following standard kinematics

$$\begin{aligned} Q^2 &= -q^2 = (k-k')^2, \\ W^2 &= p'^2 = (q+p)^2 = m_N^2 + 2m_N q_0 - Q^2, \\ q_0 &= E' - E. \end{aligned} \tag{2.4}$$

The leptonic tensor $L_{\mu\nu}$ has the form

$$\begin{aligned} L_{\mu\nu} &= Tr[\gamma_\mu(1-\gamma_5)\not{k}\gamma_\nu \not{k}'] \\ &= 4(k_\mu k'_\nu + k_\nu k'_\mu - g_{\mu\nu} k\cdot k' - i\varepsilon_{\mu\nu\alpha\beta}k^\alpha k'^\beta). \end{aligned} \tag{2.5}$$

The hadronic tensor, which has also to be a Lorentz tensor, can be written in general in terms of the 4-momenta p and q as

$$\begin{aligned} \mathcal{W}^{\mu\nu} &= \frac{1}{2m_N}\sum \langle p|J^\mu(0)|\Delta\rangle\langle\Delta|J^\nu(0)|p\rangle \delta(W^2 - M_R^2) \\ &= -\mathcal{W}_1 g^{\mu\nu} + \frac{\mathcal{W}_2}{m_N^2}p^\mu p^\nu - i\varepsilon^{\mu\nu\sigma\lambda}p_\sigma q_\lambda \frac{\mathcal{W}_3}{2m_N^2} \\ &+ \frac{\mathcal{W}_4}{m_N^2}q^\mu q^\nu + \frac{\mathcal{W}_5}{m_N^2}(p^\mu q^\nu + q^\mu p^\nu) + i\frac{\mathcal{W}_6}{m_N^2}(p^\mu q^\nu - q^\mu p^\nu), \end{aligned} \tag{2.6}$$

where M_R is the mass of the resonance and $\mathcal{W}_i$ are the functions of Q^2 and q_0. In this expression the sum runs over the R resonance polarization states and implies an averaging over the spins of the target. The $\mathcal{W}_i$ are the so-called structure functions which describe the hadron current. The integration over the phase space of the R was carried out and gives the one-dimensional $\delta-$function. Since the resonance has an observable width, the $\delta-$function should be replaced by its resonance representation

$$\delta(W^2 - M_R^2) = \frac{M_R \Gamma_R}{\pi} \frac{1}{(W^2 - M_R^2)^2 + M_R^2 \Gamma_R^2}. \tag{2.7}$$

The presented formalism in this section is general and holds for various resonances. The structure functions $\mathcal{W}_i$ can be expressed through resonance form factors and the corresponding expressions are summarized in the Appendices A.1 and A.2.

2.2.2 Hadronic Matrix Element

First we consider the resonances D_{13} and P_{33} with spin-3/2. According to the Rarita-Schwinger formalism, the spin-3/2 particles are described by the so called Rarita-Schwinger spinor field ψ_μ^a which has two indices, a Lorentz index μ and the spinor index a (later the spinor index will be omitted). The hadronic matrix elements for D_{13} and P_{33} resonances consist of 3 vector C_i^V and 4 axial C_i^A form factors. For example, the parametrization of the matrix element for the D_{13} has the following form

$$\langle D_{13}|J^\nu|N\rangle = \bar{\psi}_\mu^{(D)}(p') d_D^{\mu\nu} u(p) \tag{2.8}$$

with the spinor of the target $u(p)$ and the Rarita-Schwinger field $\psi_\mu^{(D)}$ for the D_{13} resonance. The structure of $d_D^{\mu\nu}$ is given in terms of form factors, which generally are functions of the squared momentum transfer

$$\begin{aligned} d_D^{\mu\nu} &= g^{\mu\nu}\left[\frac{C_3^V}{m_N}\not{q} + \frac{C_4^V}{m_N^2}(p'q) + \frac{C_5^V}{m_N^2}(pq) + C_6^V\right] \\ &- q^\mu\left[\frac{C_3^V}{m_N}\gamma^\nu + \frac{C_4^V}{m_N^2}p'^\nu + \frac{C_5^V}{m_N^2}p^\nu\right] + g^{\mu\nu}\left[\frac{C_3^A}{m_N}\not{q} + \frac{C_4^A}{m_N^2}(p'q)\right]\gamma_5 \\ &- q^\mu\left[\frac{C_3^A}{m_N}\gamma^\nu + \frac{C_4^A}{m_N^2}p'^\nu\right]\gamma_5 + \left[g^{\mu\nu}C_5^A + q^\mu q^\nu \frac{C_6^A}{m_N^2}\right]\gamma_5. \end{aligned} \tag{2.9}$$

In the square of the matrix element also appears the Rarita-Schwinger projection operator

$$\begin{aligned} |\psi_\sigma^{(D)}\rangle\langle\psi_\lambda^{(D)}| &= S^{\sigma\lambda} \\ &= [\not{p}' + M_R]\left(-g_{\sigma\lambda} + \frac{1}{3}\gamma_\sigma\gamma_\lambda + \frac{1}{3M_R}(\gamma_\sigma p'_\lambda - p'_\sigma\gamma_\lambda) + \frac{2}{3M_R^2}p'_\sigma p'_\lambda\right). \end{aligned} \tag{2.10}$$

Another form to write the weak vertex, which will be used later for the determination of the form factors through the helicity amplitudes, is

$$\langle D_{13}|J^{\rho}_{(V)}\varepsilon_{\rho}|N\rangle = \bar{\psi}^{(D)}_{\mu}\left[\Gamma^{(V)}_{\nu}F^{\mu\nu} + \Gamma^{(A)}_{\nu}\gamma^5 F^{\mu\nu} + C^A_5\gamma^5 g^{\mu\nu}\varepsilon_{\nu} + \frac{C^A_6}{m^2_N}\gamma^5 q^{\mu}q^{\nu}\varepsilon_{\nu}\right]u(p), \tag{2.11}$$

where

$$\Gamma^{(V)}_{\nu} = \frac{C^V_3}{m_N}\gamma_{\nu} + \frac{C^V_4}{m^2_N}p'_{\lambda} + \frac{C^V_5}{m^2_N}p_{\lambda}, \quad \Gamma^{(A)}_{\nu} = \frac{C^V_3}{m_N}\gamma_{\nu} + \frac{C^V_4}{m^2_N}p'_{\lambda}, \quad F^{\mu\nu} = q^{\mu}\varepsilon^{\nu} - q^{\nu}\varepsilon^{\mu}. \tag{2.12}$$

In these expressions ε^{μ} denotes the polarization vector of either photon or leptonic vector current. There are right-, left- handed and scalar polarizations of the photon. In the frame of reference, where the photon moves along the $z-$axis the polarization vectors are

$$\begin{gathered}\varepsilon^{\mu(R)} = \tfrac{1}{\sqrt{2}}\big(0,-1,-i,0\big), \qquad \varepsilon^{\mu(L)} = \tfrac{1}{\sqrt{2}}\big(0,1,-i,0\big), \\ \varepsilon^{\mu(S)} = \tfrac{1}{\sqrt{Q^2}}\big(q_3,0,0,q_0\big).\end{gathered} \tag{2.13}$$

The parametrization of the hadronic matrix element for the P_{33} resonance is similar. The only difference with respect to D_{13} is the location of the γ_5 matrix (in the case of the P_{33} resonance it appears in the vector part of the vertex), because these two resonance have opposite parity.

Thus, with this notation the hadronic tensor takes the form

$$\mathcal{W}^{\mu\nu} = \frac{1}{2}\frac{1}{2m_N}Tr\left[(\bar{d})^{\mu\sigma}S_{\sigma\lambda}d^{\lambda\nu}(\not{p}+m_N)\right]\delta(W^2-M^2_R) \tag{2.14}$$

with $(\bar{d})^{\mu\sigma} = \gamma_0(d^{\dagger})^{\mu\sigma}\gamma_0$ and then parametrized according to (2.6). Substituting the $d^{\lambda\nu}$ in (2.14) we find the dependence of the $\mathcal{W}_i$ structure functions on the form factors (see Appendices A.1 and A.2).

For the spin-1/2 resonances the parametrization for the weak vertex of the resonance creation is simpler than for the spin-3/2 resonances and similar to the parametrization for the nucleon. Since the initial nucleon and the outgoing resonance do not enter the same isospin multiplet and have different masses, the term $g^V_1\gamma^{\mu}$ does not vanish due to CVC, but its contribution is proportional to Q^2. There are also two axial form factors g^A_1 and g^A_3, which are related by PCAC.

The matrix element of the P_{11} resonance production can be written as follows:

$$\langle P_{11}|J^{\nu}|N\rangle = \bar{u}(p')\left[\frac{g^V_1}{\mu^2}(Q^2\gamma^{\nu} + \not{q}q^{\nu}) + \frac{g^V_2}{\mu}i\sigma^{\nu\rho}q_{\rho} - g^A_1\gamma^{\nu}\gamma_5 - \frac{g^A_3}{m_N}q^{\nu}\gamma_5\right]u(p), \tag{2.15}$$

where we use the standard notation $\sigma^{\nu\rho} = \frac{i}{2}[\gamma^\nu, \gamma^\rho]$ and the form factors are normalized to $\mu = m_N + M_R$.

For the S_{11} the amplitude of resonance production is similar to that for P_{11}, only now the γ_5 matrix appears in the vector part of the hadronic current

$$\langle S_{11}|J^\nu|N\rangle = \bar{u}(p')\left[\frac{g_1^V}{\mu^2}(Q^2\gamma^\nu + \not{q}q^\nu)\gamma_5 + \frac{g_2^V}{\mu}i\sigma^{\nu\rho}q_\rho\gamma_5 - g_1^A\gamma^\nu - \frac{g_3^A}{m_N}q^\nu\right]u(p). \quad (2.16)$$

2.3 Determination of Helicity Amplitudes in Electroproduction

The data on exclusive electroproduction of π^0, π^+ on protons in the first and second resonance region obtained at the Jefferson Laboratory [39, 40, 41] and Mainz [42] (BATEs and Bonn) accelerators, are mainly expressed through the helicity amplitudes. The extraction of the vector form factors from the helicity amplitudes provides more accurate results than the extraction from cross sections. Thus, these data allow us to obtain more precise information about vector form factors of the four first resonances. In this section we derive the general expressions for the helicity amplitudes and in the next one we present the formulae for the particular resonance case explicitly.

Let us consider unpolarized lepton-nucleon scattering. The cross section of this process has the standard form, which is used widely in the literature:

$$\frac{d\sigma}{dE'd\Omega} = \Gamma_T(\sigma_T + \epsilon\sigma_L), \quad (2.17)$$

where σ_T and σ_L are the transverse and longitudinal cross sections corresponding to the virtual photon polarization, and

$$\Gamma_T = \frac{K\alpha}{2\pi^2Q^2}\frac{E'}{E}\frac{1}{1-\epsilon}, \quad (2.18)$$

$$\epsilon = \left[1 + 2\frac{Q^2+q_0^2}{Q^2}\tan^2\frac{\theta}{2}\right]^{-1}. \quad (2.19)$$

The virtual photoabsorption cross section is given by

$$\sigma_i(W) = \frac{1}{2}K\left|\langle R|\varepsilon^{\nu(i)}J_\nu^{em}|N\rangle\right|^2 R(W, M_R), \quad (2.20)$$

$$K = \frac{4\pi^2\alpha}{2m_N(\nu - Q^2/2m_N)},$$

where $i = R$, L or S is the helicity of the photon and the $R(W, M_R)$ is given by (2.7). $\langle R|\varepsilon^{\nu(i)} J^{em}_{\nu}|N\rangle$ is the matrix element of the resonance electroproduction, which will be specified below for each resonance and expressed through the corresponding form factors. When the invariant mass of the final state equals the mass of a particular resonance, the cross section has a peak and is expressed as

$$\sigma_i(W \;\; = \;\; M_R) = \frac{1}{2} K \left|\langle R, \lambda|\varepsilon^{\nu(i)} J^{em}_{\nu}|N\rangle\right|^2 \frac{1}{\pi M_R \Gamma_R}. \tag{2.21}$$

We write the cross section in this form because analyses of electroproduction data give the cross section as [39, 43, 41, 42]

$$\sigma_T(W = M_R) = \frac{2m_N}{M_R \Gamma_R}(A^2_{1/2} + A^2_{3/2}), \tag{2.22}$$

$$\sigma_L(W = M_R) = \frac{2m_N}{M_R \Gamma_R} \frac{Q^2}{q^2_3} S^2_{1/2}. \tag{2.23}$$

In this way we determine the normalization of the amplitudes

$$\begin{aligned} A_{1/2} &= \mathcal{A}_W \langle R, +\frac{1}{2}|J^{em} \cdot \varepsilon^{(R)}|N, -\frac{1}{2}\rangle, \\ A_{3/2} &= \mathcal{A}_W \langle R, +\frac{3}{2}|J^{em} \cdot \varepsilon^{(R)}|N, +\frac{1}{2}\rangle, \\ S_{1/2} &= \mathcal{A}_W \frac{q_3}{\sqrt{Q^2}} \langle R, +\frac{1}{2}|J^{em} \cdot \varepsilon^{(S)}|N, +\frac{1}{2}\rangle, \end{aligned} \tag{2.24}$$

where $\mathcal{A}_W = \sqrt{\frac{\pi\alpha}{m_N(W^2 - m^2_N)}}$. In the next sections we implement these definitions to extract later the vector couplings C^V_i.

2.4 Calculation of the Amplitudes

Here we present the detailed calculations of the helicity amplitudes for the example of the D_{13} resonance. Following the definition of the helicity amplitudes (2.24) we get the corresponding expressions for spin-3/2 resonances:

$$A^D_{3/2} = \mathcal{A}_W \Big(\overline{\psi}_\mu(p', 3/2) q^\mu \Gamma^{(V)}_\nu \varepsilon^\nu u(p, +) - \overline{\psi}_\mu(p', 3/2) \varepsilon^\mu \Gamma^{(V)}_\nu q^\nu u(p, +)\Big), \tag{2.25}$$

$$A^D_{1/2} = \mathcal{A}_W \Big(\overline{\psi}_\mu(p', 1/2) q^\mu \Gamma^{(V)}_\nu \varepsilon^\nu u(p, -) - \overline{\psi}_\mu(p', 1/2) \varepsilon^\mu \Gamma^{(V)}_\nu q^\nu u(p, -)\Big), \tag{2.26}$$

$$S^D_{1/2} = \frac{q_3}{\sqrt{Q^2}} \mathcal{A}_W \Big(\overline{\psi}_\mu(p', 1/2) q^\mu \Gamma^{(V)}_\nu \varepsilon^\nu u(p, +) - \overline{\psi}_\mu(p', 1/2) \varepsilon^\mu \Gamma^{(V)}_\nu q^\nu u(p, +)\Big). \tag{2.27}$$

The vertex factor $\Gamma_\nu^{(V)}$ is given in (2.12) for the D_{13} resonance. In the following we work in the nucleon rest frame with $p^\mu = (m_N, 0, 0, 0)$ and the virtual photon moving along the z-axis with four-momentum $q^\mu = (q_0, 0, 0, q_3)$. For the resonance we take the Rarita-Scwinger wave function in the representation (see [44])

$$\begin{aligned}
&\psi_\mu(p', 3/2) = e_\mu^{(R)} u(p', +1/2), \\
&\psi_\mu(p', 1/2) = \sqrt{\tfrac{2}{3}} e_\mu^{(S)} u(p', +1/2) + \sqrt{\tfrac{1}{3}} e_\mu^{(R)} u(p', -1/2), \\
&\psi_\mu(p', -1/2) = \sqrt{\tfrac{2}{3}} e_\mu^{(S)} u(p', -1/2) + \sqrt{\tfrac{1}{3}} e_\mu^{(L)} u(p', +1/2), \\
&\psi_\mu(p', -3/2) = e_\mu^{(L)} u(p', -1/2),
\end{aligned} \tag{2.28}$$

where

$$u(p, s_z) = \frac{1}{\sqrt{N}} \begin{bmatrix} 1 \\ \frac{\vec{p}' \cdot \vec{\sigma}}{p'^0 + M_R} \end{bmatrix} u_{s_z} \tag{2.29}$$

and the polarization vectors of the resonance D_{13} are

$$\begin{aligned}
e_\mu^{(R)} = \tfrac{1}{\sqrt{2}}(0, -1, -i, 0), \qquad e_\mu^{(L)} = \tfrac{1}{\sqrt{2}}(0, 1, -i, 0), \\
e_\mu^{(S)} = \tfrac{1}{\sqrt{M_R}}(q_3, 0, 0, q_0 + m_N).
\end{aligned} \tag{2.30}$$

The normalization of the Dirac spinors we choose as

$$\overline{u}(0, s) u(0, s) = 2m_N, \qquad \overline{u}(p', s') u(p', s') = p'^0 + M_R \tag{2.31}$$

where s corresponds to the two spin projections " + " and " − " of the nucleon, and the resonance spin projections $s' = 3/2, 1/2, -1/2, -3/2$.

2.4.1 $A_{3/2}^{D_{13}}$, $A_{1/2}^{D_{13}}$ and $S_{1/2}^{D_{13}}$

Let us first consider the amplitude $A_{3/2}$ for the D_{13}. Here we rewrite the amplitude using the explicit form of the ψ_μ spinor (2.28)

$$A_{3/2}^{D_{13}} = \mathcal{A}_W \Big((e^{(R)*} \cdot q) \overline{u}(p', 3/2) \Gamma_\nu \varepsilon^{(R)\nu} u(0, +) - (e^{(R)*} \cdot \varepsilon^{(R)}) \overline{u}(p', 3/2) \Gamma_\nu q^\nu u(0, +) \Big). \tag{2.32}$$

The first term is equal to zero because of $e^{(R)*} \cdot q = 0$ and only the second term contributes since $e^{(R)*} \cdot \varepsilon^{(R)} = 1$. So, after substituting the explicit form for the spinors and using Dirac matrix properties we obtain:

$$A_{3/2}^{D_{13}} \;=\; \sqrt{\mathcal{N}} \Big(\frac{C_3^V}{m_N} (M_R - m_N) + \frac{C_4^V}{m_N^2} (q_0 m_N - Q^2) + \frac{C_5^V}{m_N} q_0 \Big) \tag{2.33}$$

where

$$\mathcal{N} = \frac{2\pi\alpha(p'^0 + M_R)}{M_R^2 - m_N^2}. \tag{2.34}$$

The matrix element of the $A_{1/2}^{D_{13}}$ is the sum of the four terms:

$$A_{3/2}^{D_{13}} = \mathcal{A}_W\Big(\sqrt{\frac{2}{3}}(e^{S*}\cdot q)\overline{u}(p',+)\Gamma_\nu\varepsilon^{(R)\nu}u(0,-) + \sqrt{\frac{1}{3}}(e^{R*}\cdot q)\overline{u}(p',-)\Gamma_\nu\varepsilon^{(R)\nu}u(0,-)$$
$$- \sqrt{\frac{2}{3}}(e^{S*}\cdot\varepsilon^{(R)})\overline{u}(p',+)\Gamma_\nu q^\nu u(0,-) - \sqrt{\frac{1}{3}}(e^{R*}\cdot\varepsilon^{(R)})\overline{u}(p',-)\Gamma_\nu q^\nu u(0,-)\Big). \tag{2.35}$$

The second and the third terms are equal to zero because of

$$e^{(R)*}\cdot q = 0, \qquad \overline{u}(p',\pm)\Gamma_\nu q^\nu u(0,\mp) = 0, \tag{2.36}$$

and the calculation of the last term is analogous to the one of $A_{3/2}^{D_{13}}$ with the additional factor $\sqrt{\frac{1}{3}}$. For the evaluation of the first term we use:

$$\begin{aligned} e^{(S)*}\cdot q &= -\frac{m_N}{M_R}q_3, \\ \overline{u}(p',+)\Gamma_\nu\varepsilon^{(R)\nu}u(0,-) &= \sqrt{2}\frac{q_3}{p'^0+M_R}\frac{C_3^V}{m_N}. \end{aligned} \tag{2.37}$$

Finally, substituting (2.37) in (2.35), we get the amplitude

$$A_{1/2}^{D_{13}} = \sqrt{\frac{1}{3}}A_{3/2}^{D_{13}} - \frac{2}{\sqrt{3}}\sqrt{\mathcal{N}}\frac{q_3^2}{p'^0+M_R}\frac{C_3^V}{M_R}. \tag{2.38}$$

The same steps should be done for the $S_{1/2}^D$ amplitude

$$\begin{aligned} S_{1/2}^D = \frac{\mathcal{A}_W\, q_3}{\sqrt{Q^2}}\Big(&\sqrt{\frac{2}{3}}(e^{S*}\cdot q)\overline{u}(p',+)\Gamma_\nu\varepsilon^{(S)\nu}u(0,+) \\ &+ \sqrt{\frac{1}{3}}(e^{(R)*}\cdot q)\overline{u}(p',-)\Gamma_\nu\varepsilon^{(S)\nu}u(0,+) \\ &- \sqrt{\frac{2}{3}}(e^{(S)*}\cdot\varepsilon^{(S)})\overline{u}(p',+)\Gamma_\nu q^\nu u(0,+) \\ &- \sqrt{\frac{1}{3}}(e^{(R)*}\cdot\varepsilon^{(S)})\overline{u}(p',-)\Gamma_\nu q^\nu u(0,+)\Big). \end{aligned} \tag{2.39}$$

The second and last terms are zero due to (2.36). Calculating explicitly the expressions

$$\begin{aligned} e^{(S)*}\cdot\varepsilon^{(S)} &= -\frac{\nu m_N - Q^2}{M_R\sqrt{Q^2}}, \\ \overline{u}(p',+)\Gamma_\nu\varepsilon^{(S)\nu}u(0,-) &= \sqrt{2}\frac{q_3}{p'^0+M_R}\frac{C_3^V}{m_N} \end{aligned} \tag{2.40}$$

and substituting them into (2.39) we arrive at

$$\begin{aligned} S_{1/2}^{D_{13}} &= -\sqrt{2/3}\sqrt{\mathcal{N}}\frac{q_3^3}{M_R Q^2}\Big(\frac{m_N+M_R}{p'^0+M_R}C_3^V + C_4^V + C_5^V\Big) \\ &+ \sqrt{2/3}\frac{\nu m_N - Q^2}{M_R Q^2}q_3 A_{3/2}^{D_{13}}. \end{aligned} \tag{2.41}$$

2.4.2 Helicity Amplitudes for the $P_{33}(1232)$ Resonance

Since the P_{33} has positive parity, the $\Gamma_\mu^{(V)}$ vertex has an additional γ_5 matrix

$$\Gamma_\mu^{(V)} = \Big(\frac{C_3^V}{m_N}\gamma_\mu + \frac{C_4^V}{m_N^2}p'_\mu + \frac{C_5^V}{m_N^2}p_\mu\Big)\gamma_5. \tag{2.42}$$

Following the same steps as in the previous section we obtain the expressions for the helicity amplitudes as functions of C_i^V as

$$\begin{aligned} A_{3/2}^{P_{33}} &= \sqrt{\mathcal{N}}\frac{q_3}{p'^0+M_R}\Big(\frac{C_3^V}{m_N}(M_R+m_N) + \frac{C_4^V}{m_N^2}(q_0 m_N - Q^2) + \frac{C_5^V}{m_N}q_0\Big), \\ A_{1/2}^{P_{33}} &= -\sqrt{\frac{1}{3}}A_{3/2}^{D_{13}} - \frac{2}{\sqrt{3}}\sqrt{\mathcal{N}}\frac{q_3 C_3^V}{M_R}, \\ S_{1/2}^{P_{33}} &= -\sqrt{2/3}\sqrt{\mathcal{N}}\frac{m_N q_3^2}{M_R Q^2}\Big(\frac{C_3^V}{m_N}(\frac{q_3^2}{p'^0+M_R} - q_0) - \frac{q_3^2}{(p'^0+M_R)m_N}(C_4^V + C_5^V)\Big) \\ &+ \sqrt{2/3}\frac{\nu m_N - Q^2}{M_R Q^2}q_3 A_{3/2}^{D_{13}}. \end{aligned} \tag{2.43}$$

2.4.3 Helicity Amplitudes for the $P_{11}(1440)$ Resonance

According to (2.15), the hadronic matrix element for electroproduction of resonance can be written as

$$\langle P_{11}|J^\nu|N\rangle = \bar{u}(p')\left[\frac{g_1^V}{(m_N+M_R)^2}(Q^2\gamma^\nu + \not{q}q^\nu) + \frac{g_2^V}{m_N+M_R}i\sigma^{\nu\rho}q_\rho\right]u(p). \tag{2.44}$$

Since the P_{11} resonance is a spin-1/2 particle, only the two helicity amplitudes

$$A_{1/2}^{P_{11}} = \mathcal{A}_W(B_1^R + B_2^R), \quad S_{1/2}^{P_{11}} = \mathcal{A}_W\frac{q_3}{\sqrt{Q^2}}(D_1^S + D_2^S) \tag{2.45}$$

exist. Using Dirac matrices, spinor formalism and (2.13), (2.31) we find

$$\begin{aligned} B_1^R &= \frac{g_1^V}{(m_N+M_R)^2}\bar{u}(p',+)(Q^2\not{\varepsilon}^{(R)}+\not{q}\varepsilon^{(R)}\cdot q)u(0,-) \\ &= \frac{g_1^V}{(m_N+M_R)^2}\sqrt{(p'^0+M_R)2m_N}Q^2\frac{\sqrt{2}q_3}{p'^0+M_R}, \\ B_2^R &= \frac{g_2^V}{(m_N+M_R)}\bar{u}(p',+)i\sigma^{\nu\rho}\varepsilon_\nu^{(R)}q_\rho u(0,-) \\ &= \frac{g_2^V}{(p'^0+M_R)}\sqrt{(p'^0+M_R)2m_N}\sqrt{2}q_3, \end{aligned} \tag{2.46}$$

and

$$\begin{aligned} D_1^S &= \frac{g_1^V}{(m_N+M_R)^2}\bar{u}(p',+)(Q^2\not{\varepsilon}^{(S)}+\not{q}\varepsilon^{(S)}\cdot q)u(0,+) \\ &= \frac{g_1^V}{(m_N+M_R)}\sqrt{(p'^0+M_R)2m_N}Q^2\frac{q_3}{p'^0+M_R}, \\ D_2^S &= \frac{g_2^V}{(m_N+M_R)}\bar{u}(p',+)i\sigma^{\nu\rho}\varepsilon_\nu^{(S)}q_\rho u(0,+) \\ &= -\frac{g_2^V}{(m_N+M_R)}\sqrt{(p'^0+M_R)2m_N}\sqrt{Q^2}\frac{q_3}{p'^0+M_R}. \end{aligned} \tag{2.47}$$

Substituting (2.46) and (2.47) in (2.45) we get the final formulas for the amplitudes as functions of vector form factors g_i^V

$$A_{1/2}^{P_{11}} = \sqrt{\mathcal{N}}\frac{\sqrt{2}q_3}{p'^0+M_R}\left[\frac{g_1^V}{(m_N+M_R)^2}Q^2+g_2^V\right], \tag{2.48}$$

$$S_{1/2}^{P_{11}} = \sqrt{\mathcal{N}}\frac{q_3^2}{p'^0+M_R}\left[\frac{g_1^V}{m_N+M_R}-\frac{g_2^V}{m_N+M_R}\right]. \tag{2.49}$$

2.4.4 Helicity Amplitudes for the $S_{11}(1535)$ Resonance

The parametrization of the matrix element of S_{11} resonance production is similar to P_{11}, except for an additional factor of γ_5 in the matrix element (2.44) due to parity

$$\langle S_{11}|J^\nu|N\rangle = \bar{u}(p')\left[\frac{g_1^V}{(m_N+M_R)^2}(Q^2\gamma^\nu+\not{q}q^\nu)\gamma_5+\frac{g_2^V}{m_N+M_R}i\sigma^{\nu\rho}q_\rho\gamma_5\right]u(p). \tag{2.50}$$

Substituting (2.50) into the definitions (2.24) we get the following expressions for the helicity amplitudes

$$A_{1/2}^{S_{11}} = \sqrt{2\mathcal{N}}\left[\frac{g_1^V}{(m_N+M_R)^2}Q^2+\frac{g_2^V}{(m_N+M_R)}(q_0-\frac{q_3^2}{p'^0+M_R})\right], \tag{2.51}$$

$$S_{1/2}^{S_{11}} = \sqrt{\mathcal{N}} q_3 \left[-\frac{g_1^V}{(m_N + M_R)^2}(q_0 - \frac{q_3^2}{p'^0 + M_R}) + \frac{g_2^V}{m_N + M_R} \right]. \tag{2.52}$$

2.5 Data Analysis and the Extractions of the Form Factors

Having expressed all helicity amplitudes in terms of the vector form factors, we can compare them with the data. In the case of spin-3/2 resonances we have three vector form factors C_i^V and three equations for amplitudes, which allows us unambiguously to extract the form factors. The data in [39, 40, 41], [42] are presented in terms of amplitudes whose numerical value are given as a function of Q^2. We also take into account numerical values of the helicity amplitudes at $Q^2 = 0$ summarized in the Review of Particles Properties [45], where the helicity amplitudes characterize the radiative decay of the resonance $R \to \gamma N$. Fitting form factors at different Q^2 allows us to determine their Q^2-dependence.

To relate electromagnetic to weak form factors we use the isotopic symmetry. The photon has two isospin components $|I, I_3\rangle = |1, 0\rangle$ and $|0, 0\rangle$. The isovector component belongs to the same isomultiplet as the vector part of the weak current. Each of the amplitudes $A_{3/2}$, $A_{1/2}$, $S_{1/2}$ can be further decomposed into three isospin amplitudes. Let us use a general notation and denote by b the contribution from the isoscalar photon; similarly a^1 and a^3 denote contributions of isovector photon to resonances with isospin 1/2 and 3/2, respectively. A general helicity amplitude on a proton (A_p) and neutron (A_n) target has the decomposition

$$\begin{aligned} A_p &= A_p(\gamma p \to R^+) = b - \sqrt{\frac{1}{3}} a^1 + \sqrt{\frac{2}{3}} a^3, \\ A_n &= A_n(\gamma n \to R^0) = b + \sqrt{\frac{1}{3}} a^1 + \sqrt{\frac{2}{3}} a^3. \end{aligned} \tag{2.53}$$

For the weak current we have only an isovector component of the vector current, therefore the b amplitude never occurs in weak interactions. A second peculiarity of the charged currents is that $V_1 \pm iV_2$ does not have the normalization for the Clebsch–Gordon coefficients, it must be normalized as $(V_1 \pm iV_2)/\sqrt{2}$, which brings an additional factor of $\sqrt{2}$ to each of the charged current in comparison with the Clebsch–Gordon coefficients:

$$A(W^+ n \to R^{(1)+}) = \frac{2}{\sqrt{3}} a^1,$$

$$A(W^+p \to R^{(3)++}) = \sqrt{2}a^3,$$
$$A(W^+n \to R^{(3)+}) = \sqrt{\frac{2}{3}}a^3, \tag{2.54}$$

where $R^{(1)}$ and $R^{(3)}$ are the isospin-1/2 and isospin-3/2 resonances, respectively. Comparing (2.53) with (2.54), one easily sees, that, for the isospin-1/2 resonances, the weak amplitude satisfies the equality $A(W^+n \to R^{(1)+}) = A_n - A_p$. Since the amplitudes are linear functions of the form factors, the weak vector form factors are related in the same way to electromagnetic form factors for neutrons C_i^n and protons C_i^p:

$$I = 1/2: \quad C_i^V = C_i^n - C_i^p, \tag{2.55}$$

with the index i distinguishing the Lorenz structure of the form factors.

For the isospin-3/2 resonances one gets $A_n^3(W^+n \to R^{(3)+}) = A_p^3(W^-p \to R^{(3)0}) = \sqrt{2/3}a^3$. The weak form factors, which are conventionally specified for these two processes, are

$$I = 3/2: \quad C_i^V = C_i^p = C_i^n. \tag{2.56}$$

For the process $W^+p \to R^{(3)++}$ the amplitude is $\sqrt{3}$ times bigger: $A(W^+p \to R^{(3)++}) = \sqrt{3}A(W^+n \to R^{(3)+})$.

2.5.1 $D_{13}(1520)$

Matching the equations (2.33), (2.38), (2.41) on the data of helicity amplitudes [39, 40, 41, 42, 45] we extract the form factors and fit the Q^2-dependence for the D_{13} resonance:

$$\begin{aligned}
C_3^{(p)} &= \frac{2.95/D_V}{1+Q^2/8.9M_V^2}, \qquad C_4^{(p)} = \frac{-1.15/D_V}{1+Q^2/8.9M_V^2}, \\
C_5^{(p)} &= \frac{-0.48}{D_V}, \\
C_3^{(n)} &= \frac{-1.13/D_V}{1+Q^2/8.9M_V^2}, \qquad C_4^{(n)} = \frac{0.46/D_V}{1+Q^2/8.9M_V^2}, \\
C_5^{(n)} &= \frac{-0.17}{D_V},
\end{aligned} \tag{2.57}$$

where $D_V = (1+Q^2/M_V^2)$ denotes the dipole function with the vector mass parameter $M_V = 0.84$ GeV. To give an impression, how good this parametrization is, we plot in Figure 2.2 the helicity amplitudes, obtained with these form factors (2.57).

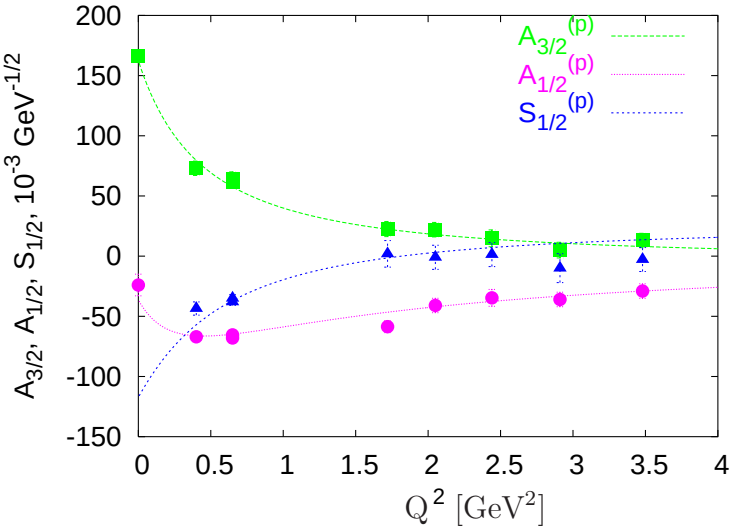

Figure 2.2: The fit of the helicity amplitudes $A^{D_{13}}_{3/2}$, $A^{D_{13}}_{1/2}$ and $S^{D_{13}}_{1/2}$ on the proton data [39, 40, 41, 42, 45], leading to the parametrization (2.57) of the proton form factors.

2.5.2 $P_{33}(1232)$

Using the same method as for the D_{13} we match equations (2.43) on the data [42, 45]. It leads us to the following vector form factors

$$\begin{aligned} C_3^V &= \frac{2.133/D_V}{1+Q^2/4M_V^2}, \\ C_4^V &= \frac{-1.505/D_V}{1+Q^2/4M_V^2}, \\ C_5^V &= \frac{-0.481/D_V}{1+Q^2/0.776M_V^2}, \end{aligned} \tag{2.58}$$

which are the same for proton and neutron since P_{33} is an isospin-3/2 particle. The form factors are in agreement with the generally accepted magnetic dominance approximation within a 5% accuracy and at the same time correctly describe the nonzero scalar helicity amplitude. The fit of the helicity amplitudes for the form factors from (2.58) is shown in Figure 2.3.

2.5.3 $P_{11}(1440)$

In the case of spin-1/2 resonances we have two independent vector form factors and two helicity amplitudes $A_{1/2}$ and $S_{1/2}$. At nonzero Q^2 data on helicity amplitudes

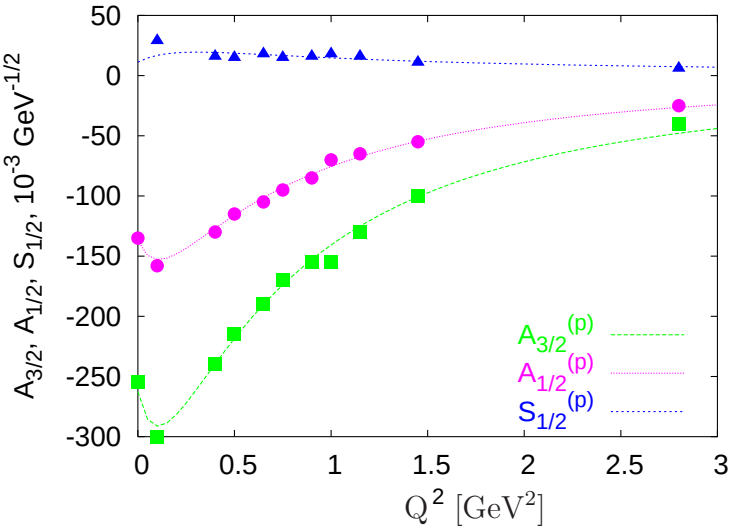

Figure 2.3: The fit of the helicity amplitudes $A^{P_{33}}_{3/2}$, $A^{P_{33}}_{1/2}$ and $S^{P_{33}}_{1/2}$ on the data [42, 45], leading to the parametrization (2.58) of the form factors.

for the P_{11} are available only for the proton. Unlike the case of the other resonances, the accuracy of the data is low and the measurements provided by different groups differ significantly [42, 41, 46], as is illustrated in Figure 2.4. In this case we fit only the recent data from [41, 46]. The uncertainty of the measurements of the helicity amplitudes of the proton turn out to be bigger than the predicted difference between proton and neutron. So we neglect the isoscalar contribution to the electromagnetic current and use $A^{(n)}_{1/2} = -A^{(p)}_{1/2}$, then the isovector form factors become $g_i^V = 2g_i^{(p)}$.

We use for our fit only the recent data [41, 46] and parametrize the proton electromagnetic form factors as follows:

$$P_{11}(1440): \quad \begin{aligned} g_1^{V(p)} &= \frac{2.3/D_V}{1+Q^2/4.3M_V^2}, \\ g_2^{V(p)} &= \frac{-0.76}{D_V}\left[1-2.8\ln\left(1+\frac{Q^2}{1\ \mathrm{GeV}^2}\right)\right]. \end{aligned} \tag{2.59}$$

The fit result of the helicity amplitudes together with the experimental data is plotted in Figure 2.5.

2.5.4 $S_{11}(1535)$

Like the P_{11} resonance, we choose here to fit only proton data [41, 46] and neglect the isoscalar contribution to the electromagnetic current. We get the following form

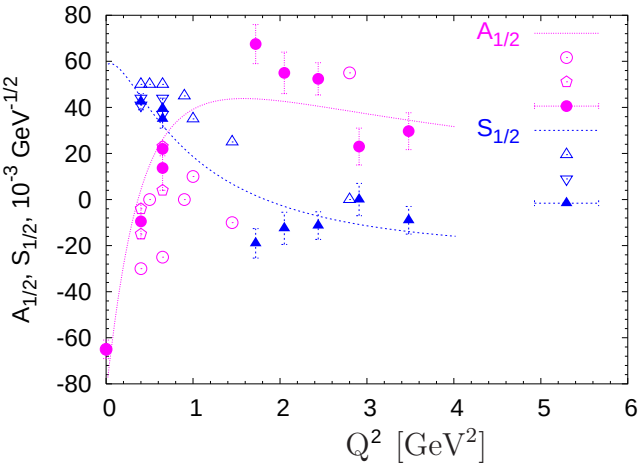

Figure 2.4: Helicity amplitudes for the $P_{11}(1440)$ resonance, calculated with the form factors from (2.59). For $A_{1/2}$ the data are from: [42] (unshaded circles), [41] (unshaded pentagons), [46] (full circles); for $S_{1/2}$: [42] (unshaded up triangles), [41] (unshaded down triangles), [46] (full triangles)

factors:

$$
\begin{aligned}
&S_{11}(1535): \\
&g_1^{V(p)} = \frac{2.0/D_V}{1+Q^2/1.2M_V^2}\left[1+7.2\ln\left(1+\frac{Q^2}{1\ \mathrm{GeV}^2}\right)\right]\ , \\
&g_2^{V(p)} = \frac{0.84}{D_V}\left[1+0.11\ln\left(1+\frac{Q^2}{1\ \mathrm{GeV}^2}\right)\right]\ .
\end{aligned}
\tag{2.60}
$$

The illustration of this parametrization in terms of the helicity amplitudes is plotted in Figure 2.5 together with the data.

2.6 Decays of the Resonances and PCAC

One of the properties of the weak current is the existence of the axial part. The calculation of the divergence of the axial current gives us a nonzero result

$$\langle 0|\partial^\mu A_\mu^a|\pi^b(p)\rangle = f_\pi m_\pi^2 \langle 0|\phi^a(0)|\pi^b(p)\rangle \tag{2.61}$$

where f_π denotes the decay constant. It is measured in the leptonic pion decay $\pi^+ \to l^+\nu_l$. m_π is the pion mass and $\phi^a(0)$ is the pion field. The nonzero divergence of the axial current is explained by $SU(2)_L \times SU(2)_R \to SU(2)_R$ flavor symmetry breaking, according to which the pions get nonzero masses. In the case of an

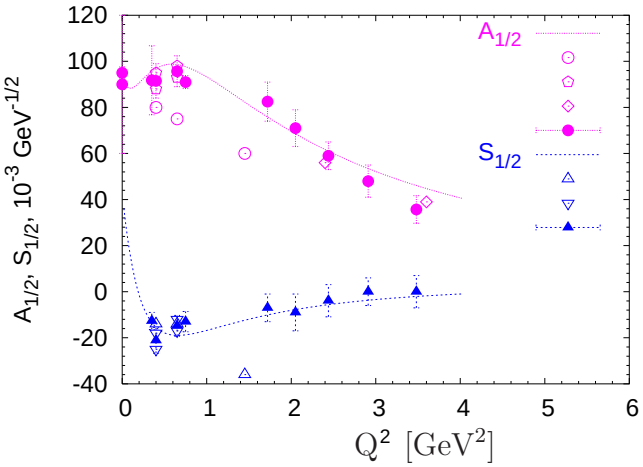

Figure 2.5: Helicity amplitudes for the $S_{11}(1535)$ resonance, calculated with the form factors from (2.60). For $A_{1/2}$ data are from: [42] (unshaded circles), [41] (unshaded pentagons), [46] (full circles), [47] (unshaded diamond); for $S_{1/2}$: [42] (unshaded up triangles), [41] (unshaded down triangles), [46] (full triangles)

unbroken symmetry we have the conserved axial current

$$\langle 0|\partial^\mu A^a_\mu|\pi^b(p)\rangle = 0, \tag{2.62}$$

corresponding to $m_\pi = 0$ as required by the Goldstone theorem.

The generalization of (2.61) leads to an operator relation

$$\partial^\mu A^a_\mu = f_\pi m^2_\pi \phi^a(0), \tag{2.63}$$

which is known as the partial conserved axial-vector current (PCAC) and can be used in hadronic matrix elements. Several applications of PCAC have been established, particularly the so-called Goldberger-Treiman relation analog which we use to determine the axial form factors. This application is based on the assumption that the matrix element of the corresponding pion current is a slowly changing function in the interval from the point where the pion field is off-shell $q^2 = 0$ to point where it goes on-shell $q^2 = m^2_\pi$. Thus, our goal is to calculate the resonance axial form factors C^A_i and g^A_i by using PCAC and by fitting the decay width, the latter taken from [45].

2.6.1 $P_{33}(1232)$

For the $P_{33}(1232)$ the isospin invariance predicts the following phenomenological Lagrangian of the $\Delta N\pi$ interactions:

$$\begin{aligned}\mathcal{L}_{\pi NR}^{P_{33}(1232)} = g_\Delta(&\overline{\Delta_\mu^{++}}p\partial_\mu\pi^+ + \sqrt{\frac{1}{3}}\overline{\Delta_\mu^+}n\partial_\mu\pi^+ \\ &+\sqrt{\frac{1}{3}}\overline{\Delta_\mu^0}p\partial_\mu\pi^- + \sqrt{\frac{2}{3}}\overline{\Delta_\mu^+}p\partial_\mu\pi^0 \\ &+\sqrt{\frac{2}{3}}\overline{\Delta_\mu^0}n\partial_\mu\pi^0 + \overline{\Delta_\mu^-}n\partial_\mu\pi^-),\end{aligned} \tag{2.64}$$

where n, p and π are neutron, proton and pion, respectively. The width is calculated using the standard formula for the decay of the particle in its rest frame

$$d\overline{\Gamma} = \frac{1}{32\pi^2(2J+1)}|\mathcal{M}|^2\frac{|\vec{q}|}{M_R^2}d\Omega \tag{2.65}$$

where J and M_R stand for the spin and mass of the decaying particle, respectively. For the P_{33} resonance we obtain

$$|\mathcal{M}|^2 = \sum_{s,\lambda} g_\Delta^2 q^\nu q^\mu \overline{u}(p)\psi_\mu(\lambda)\overline{\psi}_\nu(\lambda)u(p), \tag{2.66}$$

$$\sum_\lambda q^\nu q^\mu \psi_\mu(\lambda)\overline{\psi}_\nu(\lambda) = \frac{2}{3}(\not{p}' + M_R)(q\cdot e^{(S)})^2. \tag{2.67}$$

Substituting (2.67) in (2.65) and calculating the trace of the matrix element we get the following formula for the width of the Δ resonance decaying into πN

$$\Gamma_\Delta = \frac{g_\Delta^2}{8\pi}\frac{1}{3M_R^2}\left[(M_R+m_N)^2 - m_\pi^2\right]|p_\pi|^3, \tag{2.68}$$

where the pion momentum is

$$p_\pi = \frac{1}{2M_R}\sqrt{(M_R^2 - m_N^2 - m_\pi^2)^2 - 4m_N^2m_\pi^2}. \tag{2.69}$$

For the experimental value $\Gamma_\Delta = 0.114$ GeV, we obtain $g_\Delta = 15.3$ GeV^{-1}.

According to the PCAC relation holds

$$\langle R^+|\partial_\mu A^\mu(0)|n\rangle = -im_\pi^2 f_\pi \frac{1}{q^2 - m_\pi^2}T(\pi^+ n \to R^+), \tag{2.70}$$

where $T(\pi^+ n \to R^+)$ denotes the pion mass shell amplitude for the $\pi^+ n \to R^+$. The weak vertex for all the resonances includes the charged state of the resonance and the neutral state of the initial nucleon, so for the weak vertex we should always take the decay $R^+ \to n\pi^+$.

For the $P_{33}(1232)$ the relation (2.70) turns into

$$i\overline{\Delta^+_\mu}q^\mu\left[C_5^A+\frac{C_6^A}{m_N^2}q^2\right]u_N=-i\sqrt{\frac{1}{3}}\frac{m_\pi^2 f_\pi}{q^2-m_\pi^2}\overline{\Delta^+_\mu}g_\Delta q^\mu u_N, \tag{2.71}$$

and we obtain in the limit $m_\pi \to 0$ a relation between the two form factors

$$C_6^A=-m_N^2\frac{C_5^A}{q^2}. \tag{2.72}$$

The denominator of the above formula is usually phenomenologically extended as $q^2 \to q^2 - m_\pi^2$. Making use of the relation (2.72) for $q^2 \to 0$ one also obtains $C_5^A = g_\Delta f_\pi/\sqrt{3}$. Thus, we find

$$C_5^A(P_{33})=\frac{g_\Delta f_\pi}{\sqrt{3}}=1.2,\quad C_6^A(P_{33})=m_N^2\frac{C_5^A(P_{33})}{m_\pi^2+Q^2}. \tag{2.73}$$

The first relation in (2.73) is an analogy to the Goldberger-Treiman relation of the β-decay, which shows that the vertex constant g_Δ does not vary significantly when the pion goes on-shell $q^2 = m_\pi^2$ with respect to the $q^2 = 0$ value. For the Δ^{++} the πNR vertex is bigger by a factor $\sqrt{3}$, so, strictly speaking, C_5^A is also $\sqrt{3}$ times bigger. However, by historical reasons, this $\sqrt{3}$ is conventionally attributed to the vertex itself and not to the C_5^A.

The same method will be used for the other resonances. We will present the brief calculations of the form factors briefly in the next sections.

2.6.2 $D_{13}(1520)$

For the D_{13} the isospin-invariant Lagrangian of the $D_{13}N\pi$ interactions reads as follows:

$$\begin{aligned}\mathcal{L}_{\pi NR}^{D_{13}}=g_{D_{13}}\Bigg[&\sqrt{\frac{2}{3}}\overline{D^+_\mu}\gamma_5 n\partial_\mu\pi^+-\sqrt{\frac{2}{3}}\overline{D^0_\mu}\gamma_5 p\partial_\mu\pi^-\\&-\sqrt{\frac{1}{3}}\overline{D^+_\mu}\gamma_5 p\partial_\mu\pi^0+\sqrt{\frac{1}{3}}\overline{D^0_\mu}\gamma_5 n\partial_\mu\pi^0\Bigg],\end{aligned} \tag{2.74}$$

where D_μ denotes the D_{13} field. The width of the πN decay is

$$\Gamma_{D_{13}\to\pi N}=\frac{g_{D13}^2}{8\pi}\frac{1}{3M_R^2}\left[(M_R-m_N)^2-m_\pi^2\right]|p_\pi|^3. \tag{2.75}$$

The total width of the D_{13} resonance is about 0.125 GeV and the elasticity (the relation of πN width to the total width) is about 0.5. With $\Gamma_{D_{13}\to\pi N} = 0.0625$ GeV, we obtain $g_{D_{13}} = 15.5\,\mathrm{GeV}^{-1}$ and the running width of the resonance is again

proportional to the third power of the pion momentum. The PCAC relation turn into

$$i\overline{D_\mu}q^\mu\left[C_5^A+\frac{C_6^A}{m_N^2}q^2\right]\gamma_5 u_N=\sqrt{\frac{2}{3}}\overline{D_\mu}g_{D13}q^\mu\gamma_5 u_N, \tag{2.76}$$

which results in

$$C_6^A(D_{13})=m_N^2\frac{C_5^A(D_{13})}{m_\pi^2+Q^2},\quad C_5^A(D_{13})=\sqrt{\frac{2}{3}}g_{D13}f_\pi=2.1. \tag{2.77}$$

2.6.3 $P_{11}(1440)$

For the P_{11} the isospin-invariant Lagrangian is

$$\begin{aligned}\mathcal{L}_{\pi NR}^{P_{11}}=g_{P_{11}}\Bigg[&\sqrt{\frac{2}{3}}\overline{P^+}\gamma_5 n\pi^+-\sqrt{\frac{2}{3}}\overline{P^0}\gamma_5 p\pi^-\\&-\sqrt{\frac{1}{3}}\overline{P^+}\gamma_5 p\pi^0+\sqrt{\frac{1}{3}}\overline{P^0}\gamma_5 n\pi^0\Bigg],\end{aligned}$$

where P is the field corresponding to the P_{11} resonance. The decay width is

$$\Gamma_{P_{11}\to\pi N}=\frac{g_{P_{11}}^2}{8\pi M_R^2}\left[(M_R-m_N)^2-m_\pi^2\right]|p_\pi|. \tag{2.78}$$

With the experimental value $\Gamma_{P_{11}\to\pi N}=0.6\cdot 0.350$ GeV we obtain $g_{P_{11}}=10.9$.

The PCAC relation

$$\begin{aligned}i\bar{u}_R(p')\left[g_1^A\gamma^\mu q_\mu+\tfrac{g_3^A}{m_N}q^2\right]\gamma^5 u_N(p)&=\\=\sqrt{\frac{2}{3}}(-im_\pi^2)\frac{f_\pi}{q^2-m_\pi^2}\bar{u}_R(p')g_{P_{11}}\gamma^5 u_N(p)&\end{aligned} \tag{2.79}$$

at $m_\pi\to 0$ leads to

$$g_3^A(P_{11})=-\frac{m_N(M_R+m_N)}{q^2-m_\pi^2}g_1^A(P_{11}) \tag{2.80}$$

(here the denominator is phenomenologically extended as usual) and at $Q^2\to 0$ the coupling is

$$g_1^A(P_{11})=\sqrt{\frac{2}{3}}\frac{g_{P_{11}}f_\pi}{M_R+m_N}=0.51. \tag{2.81}$$

2.6.4 $S_{11}(1535)$

For the S_{11} the isospin-invariant Lagrangian is

$$\mathcal{L}_{\pi NR}^{S_{11}}=g_{S_{11}}\left[\sqrt{\frac{2}{3}}\overline{S^+}n\pi^+-\sqrt{\frac{2}{3}}\overline{S^0}p\pi^--\sqrt{\frac{1}{3}}\overline{S^+}p\pi^0+\sqrt{\frac{1}{3}}\overline{S^0}n\pi^0\right], \tag{2.82}$$

where S denotes the S_{11} field. The decay width is

$$\Gamma_{S11\to\pi N} = \frac{g_{S_{11}}^2}{8\pi M_R^2}\left[(M_R + m_N)^2 - m_\pi^2\right]|p_\pi|. \tag{2.83}$$

With the experimental value $\Gamma_{S_{11}\to\pi N} = 0.06$ GeV we obtain $g_{S_{11}} = 1.12$.

The PCAC relation

$$\begin{aligned} i\bar{u}_R(p')\left[g_1^A\gamma^\mu q_\mu + \frac{g_3^A}{m_N}q^2\right]u_N(p) \\ = \sqrt{\frac{2}{3}}(-im_\pi^2)\frac{f_\pi}{q^2-m_\pi^2}\bar{u}_R(p')g_{S_{11}}u_N(p) \end{aligned} \tag{2.84}$$

at $m_\pi \to 0$ leads to

$$g_3^A(S_{11}) = -\frac{m_N(M_R - m_N)}{q^2 - m_\pi^2}g_1^A(S_{11}) \tag{2.85}$$

where we used the physical propagator pole. At $Q^2 \to 0$ the coupling is

$$g_1^A(S_{11}) = \sqrt{\frac{2}{3}}\frac{g_{S_{11}}f_\pi}{M_R - m_N} = 0.21. \tag{2.86}$$

2.7 Cross Sections in the Second Resonance Region

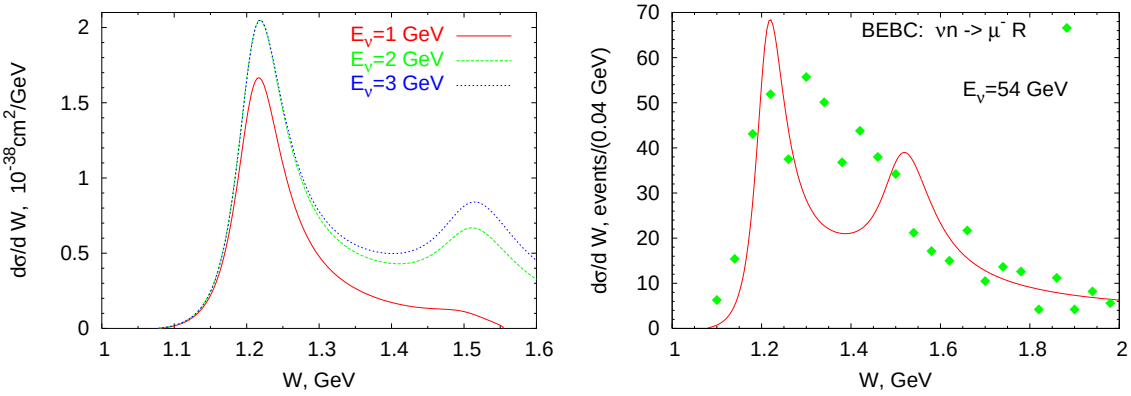

Figure 2.6: The left-hand plot shows the differential cross section $d\sigma/dW$ for the one-pion neutrinoproduction on neutron for the neutrino energy $E_\nu = 1, 2, 3$ GeV. The right-hand plot shows the differential cross section $d\sigma/dW$ for the one-pion neutrinoproduction for the BEBC experiment [48] with the neutrino energy $E_\nu = 54$ GeV.

In this section we present the cross sections of neutrinoproduction of the resonances for the second resonance region using the isovector form factors. We specialize to the final states $\nu n \to R \to \mu^- p\pi^0$ and $\nu n \to R \to \mu^- n\pi^+$, where both

$I = 3/2$ and $I = 1/2$ resonances contribute. We use the form factors obtained in Section 2.5 and plot the differential cross section $d\sigma/dW$ in Figure 2.6 for incoming neutrino energies $E_\nu = 1, 2$ and 3 GeV. We note, that the second resonance peak grows faster than the first one with the neutrino energy and becomes more pronounced for the higher neutrino energies. For this purpose we show in Figure 2.6 also the theoretical curve together with the experimental data from the BEBC experiment [48] for $E_\nu = 54$ GeV. The theoretical curve clearly shows two peaks with comparable areas under the peaks. The experimental points are of the same order of magnitude and follow general trends of our curves, but are not accurate enough to resolve two resonant peaks.

We also present the integrated cross sections for the final states $\mu^- p\pi^0$ and $\mu^- n\pi^+$ as functions of the neutrino energy. Together with the theoretical curves we show the experimental data taken from the ANL [49, 50], SKAT [51] and BNL [52] experiments. The experiments use different neutrino energy spectra, however, with an overlap region for $E_\nu < 2.0$ GeV where different results can be compared. The solid curves in Fig. 2.7 show the theoretically calculated cross sections with the cut $W < 2.0$ GeV and the dashed ones with the cut $W < 1.6$ GeV. For $p\pi^0$ the solid curve goes through most of the experimental points except for those of the BNL experiment, which are consistently higher than the ones of the other experiments.

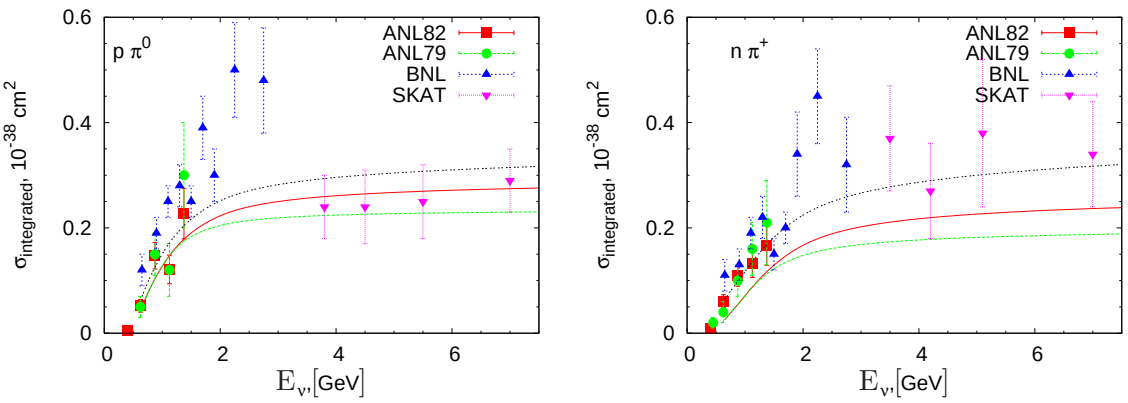

Figure 2.7: Integrated cross section for the $\mu^- p\pi^0$ (left-hand plot) and $\mu^- n\pi^+$ (right-hand plot) final states. The solid curves show the theoretically calculated cross sections with the cut $W < 2.0$ GeV and the dashed ones with the cut $W < 1.6$ GeV. The double dashed curve in the case $\mu^- n\pi^+$ state includes a smooth background (see text). The data are taken from ANL [49] (red full squares) and [50] (green full circles), SKAT [51] (magenta triangles) and BNL [52] (blue triangles) experiments.

For the $n\pi^+$ channel our prediction is a little lower than the data. This means that there are contributions from higher resonances or axial form factors that cannot be

fixed using available data. Another possibility is to add a smooth background which grows with energy. By isospin conservation, the background for the $p\pi^0$ channel is determined to be half as big as the one for $n\pi^+$. Including this background, which may originate from various sources, produces the double-dashed curves in Fig. 2.7.

2.8 Conclusions

The production of resonances in neutrino-nucleon collisions can be uniquely described by the form factors of the nucleon-resonance transitions. Thank to the recent electroproduction data from JLAB and the Mainz accelerators we were able to determine the vector form factors by fitting the measured helicity amplitudes. We found, that several of the form factors fall slower than the dipole form factor, at least for $Q^2 < (2-3)$ GeV^2. The fit of the form factors is illustrated in Figures 2.2, 2.3, 2.4, 2.5. We obtain values for two axial form factors by applying PCAC whenever the decay width and elasticity are known. For the spin-3/2 resonances there is still freedom for two additional axial form factors whose contribution may be important. This should be tested in the experiments. The impact of the second resonance region to the cross section is sizable. For the differential cross section it has a noticeable peak in $d\sigma/dW$ (Fig.2.6), which grows as E_ν increases from 1 to 3 GeV. The integrated cross section for the $I = 1/2$ channel also grows with the energy of the beam and requires a stronger contribution from the resonances and a non-resonant background (Fig.2.7).

3 Angular Analysis of $B \to K, K^* \bar{l} l$ Decays

In this chapter we present the detailed study of the exclusive $B \to K, K^* \bar{l} l$ decays. We give the precise SM values of observables constructed by angular distributions of decay rates. The sensitivity of these observables to NP is analyzed.

3.1 Introduction

In the SM due to the absence of tree level FCNC, $B \to K, K^* \bar{l} l$ with $l = e, \mu$ occur at loop level, what makes these processes very rare. The experimental measurements of the branching ratios confirm the SM predictions within uncertainties, estimating it in the region of $\mathcal{O}\left(10^{-7}\right)$ [53, 54, 55, 56, 57, 58]. The early theoretical studies [57, 58] were devoted to phenomenological analyses of different observables in the SM and beyond, such as integrated rates, dilepton mass spectra, lepton angle distributions and dimuon to dielectron ratios. Taking into account the subsequent decay $K^* \to K\pi$ enlarges the number of obsevables of $B \to K^* \bar{l} l$ offering the angular analysis of the $\bar{K}\pi\bar{l}l$ final state [59, 60, 61, 62, 63, 64].

In spite of recent improvements of the theoretical methods, the resulting theory uncertainties in the rates are still large, making them not so useful to test the SM. Therefore additional more convenient observables need to be discussed. Particularly, the source of such observables is the angular distributions of the decay rates with respect to angles defined by outgoing particles. Normalizing the angular distribution to the decay rate makes the corresponding observables less sensitive to the various input uncertainties.

Particularly, in the SM the normalized angular distribution of $B \to K \bar{l} l$ with respect to the the lepton charge asymmetry angle θ has a simple structure [57, 58]:

$$\frac{d\Gamma_l{}^{\mathrm{SM}}}{d\cos\theta} \propto \sin^2\theta + \mathcal{O}(m_l^2), \tag{3.1}$$

which is very attractive to test the SM, since any modifications of it can reveal underling NP. A closer analysis shows that the $\cos\theta$-dependence of the (normalized)

angular distribution can be parametrized as [55, 57, 58]

$$\frac{1}{\Gamma_l}\frac{d\Gamma_l}{d\cos\theta} = \frac{3}{4}(1 - F_H^l)(1 - \cos^2\theta) + \frac{1}{2}F_H^l + A_{\rm FB}^l \cos\theta, \tag{3.2}$$

with a flat term $F_H^l/2$ and a linear term in $\cos\theta$, the forward-backward asymmetry $A_{\rm FB}^l$. Both are small within the SM, and therefore can signal the presence of NP.

The richer structure of the $B \to K^*(\to K\pi)\bar{l}l$ decay product gives a possibility to study eight CP asymmetries, the one in the decay rate plus seven more requiring angular information. Three of them are T-odd CP-odd and five are T-even CP-odd, where T-transformation reverses the sign of all particle momenta and spins. The advantage of T-odd CP asymmetries is a maximal sensitivity to CP violation in the case of vanishing small strong phases. Denoting by δ_S and δ_W strong and weak phases, respectively, it can be shown that T-odd CP asymmetries $\propto \cos\delta_S \sin\delta_W$, whereas T-even CP asymmetries $\propto \sin\delta_S \sin\delta_W$.

Here, we compute the observables in the SM using the formalism of QCD factorization (QCDF), which has been applied to $B \to K, K^*\bar{l}l$ decays [19, 20] and is valid in the low q^2 region. Presenting a model-independent analysis of NP, we give the predictions of the the F_H^l, $A_{\rm FB}^l$ and CP asymmetries while implementing constrains on NP from other rare B-decay observables. The various NP models are also discussed which can be tested by the observables in (3.2).

3.2 Effective Hamiltonian for $b \to s\bar{l}l$

In this section we focus on the $b \to s\bar{l}l$ transition which is the dominant quark level process contributing to $B \to K\bar{l}l$ and $B \to K^*\bar{l}l$ semileptonic exclusive decays. The effective Hamiltonian for the $\Delta B = 1$ flavor changing processes [65, 20] reads as

$$H_{\rm eff} = -\frac{4G_F}{\sqrt{2}}\left(\lambda_t H_{\rm eff}^{(t)} + \lambda_u H_{\rm eff}^{(u)}\right) + h.c., \tag{3.3}$$

where $\lambda_q = V_{qs}^* V_{qb}$ and

$$\begin{aligned} H_{\rm eff}^{(t)} &= C_1\mathcal{O}_1^c + C_2\mathcal{O}_2^c + \sum_{i=3}^{10} C_i\mathcal{O}_i, \\ H_{\rm eff}^{(u)} &= C_1(\mathcal{O}_1^c - \mathcal{O}_1^u) + C_2(\mathcal{O}_2^c - \mathcal{O}_2^u). \end{aligned} \tag{3.4}$$

The second term in (3.3) is CKM-suppressed and can often be neglected, but we keep it when we discuss CP asymmetries for $B \to K^*\bar{l}l$ decays since it contains the CP violating phase of the SM. The $\mathcal{O}_i$ are dimension six operators and the C_i are Wilson coefficients being both dependent on the renormalization scale μ. Since the

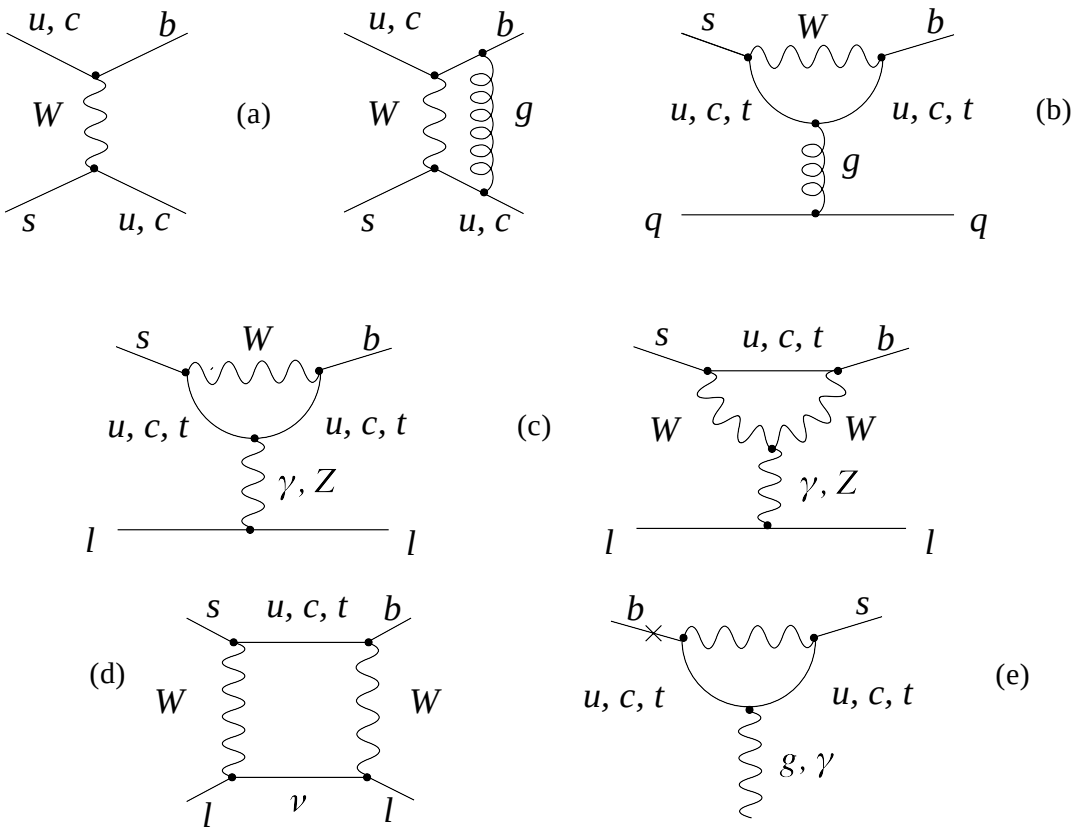

Figure 3.1: The SM diagrams giving rise to the operators in the effective Hamiltonian of $\Delta B = 1$ decays.

characteristic scale of $b \to s\bar{l}l$ decays is $\mathcal{O}(m_b)$ we assume μ to be of the same order. The $\mathcal{O}_i$ $i = 1, 2$ correspond to the current-current operators

$$\mathcal{O}_1^q = [\bar{s}\gamma_\mu T^a P_L q][\bar{q}\gamma^\mu T^a P_L b], \tag{3.5}$$

$$\mathcal{O}_2^q = [\bar{s}\gamma_\mu P_L q][\bar{q}\gamma^\mu P_L b] \tag{3.6}$$

with $q = u, c$. They originate from the diagrams (a) in Figure 3.1. One should emphasize that $\mathcal{O}_1^q$ does not contribute at leading order (LO) in α_s. The QCD-penguin operators $\mathcal{O}_i$, $i = 3, 4, 5, 6$ are shown in diagram (b) in Figure 3.1 and read as

$$\mathcal{O}_3 = [\bar{s}\gamma_\mu P_L b]\sum_q [\bar{q}\gamma^\mu q], \qquad \mathcal{O}_4 = [\bar{s}\gamma_\mu T^a P_L b]\sum_q [\bar{q}\gamma^\mu T^a q], \tag{3.7}$$

$$\mathcal{O}_5 = [\bar{s}\gamma_\mu\gamma_\nu\gamma_\rho P_L b]\sum_q [\bar{q}\gamma^\mu\gamma^\nu\gamma^\rho q], \qquad \mathcal{O}_6 = [\bar{s}\gamma_\mu\gamma_\nu\gamma_\rho T^a P_L b]\sum_q [\bar{q}\gamma^\mu\gamma^\nu\gamma^\rho T^a q],$$

where the sum is over $q = u, d, s, c, b$. The photon and gluon dipole operators $\mathcal{O}_i$, $i = 7, 8$, stem from diagrams (e), and the semileptonic operators $i = 9, 10$, from diagrams (c) in Figure 3.1, and read as

$$\mathcal{O}_7 = \frac{e}{(4\pi)^2}\overline{m}_b[\bar{s}\sigma^{\mu\nu}P_R b]F_{\mu\nu}, \qquad \mathcal{O}_9 = \frac{e^2}{(4\pi)^2}[\bar{s}\gamma_\mu P_L b][\bar{l}\gamma^\mu l],$$

$$\mathcal{O}_8 = \frac{g_s}{(4\pi)^2}\overline{m}_b[\bar{s}\sigma^{\mu\nu}P_R T^a b]G^a_{\mu\nu}, \qquad \mathcal{O}_{10} = \frac{e^2}{(4\pi)^2}[\bar{s}\gamma_\mu P_L b][\bar{l}\gamma^\mu\gamma_5 l], \tag{3.8}$$

where $P_{R/L} = (1 \pm \gamma_5)/2$ denote chiral projectors, T^a are $SU(3)_{QCD}$ generators and $\overline{m}_b(\mu)$ the $\overline{\text{MS}}$ b-quark mass at the scale μ. For completeness we also introduce the chirality-flipped operators

$$\mathcal{O}'_7 = \frac{e}{(4\pi)^2}\overline{m}_b[\bar{s}\sigma^{\mu\nu}P_L b]F_{\mu\nu},$$

$$\mathcal{O}'_9 = \frac{e^2}{(4\pi)^2}[\bar{s}\gamma_\mu P_R b][\bar{l}\gamma^\mu l],$$

$$\mathcal{O}'_{10} = \frac{e^2}{(4\pi)^2}[\bar{s}\gamma_\mu P_R b][\bar{l}\gamma^\mu\gamma_5 l], \tag{3.9}$$

though in the SM the corresponding Wilson coefficients are suppressed, namely $C'_i \sim m_s/m_b C_i$. They can only compete with $\mathcal{O}_{7,9,10}$ in models beyond the SM. This set of operators suffices to describe $b \to s\bar{l}l$ induced processes in the SM, which are dominated by C_7, C_9 and C_{10}, whereas C_8 enters at higher order in the strong coupling.

Using NNLO results from [65, 66, 67] we calculate Wilson coefficients in the SM and show their numerical values in Table 3.1 for the different values of the lower scale.

	$m_b/2$			m_b			$2m_b$		
	LO	NLO	NNLO	LO	NLO	NNLO	LO	NLO	NNLO
C_1	−0.754	−0.507	−0.458	−0.504	−0.297	−0.265	−0.340	−0.156	−0.132
C_2	1.053	1.022	1.022	1.025	1.008	1.009	1.012	1.002	1.003
C_3	−0.0107	−0.0112	−0.0124	−0.0049	−0.0045	−0.0054	−0.0023	−0.0017	−0.0024
C_4	−0.111	−0.137	−0.136	−0.068	−0.082	−0.080	−0.043	−0.052	−0.051
C_5	0.0010	0.0008	0.0009	0.0005	0.0003	0.0004	0.0002	0.0001	0.0002
C_6	0.0023	0.0025	0.0027	0.0010	0.0009	0.0010	0.0005	0.0003	0.0003
C_7	0	−0.395	−0.370	0	−0.342	−0.330	0	−0.302	−0.298
C_8	0	−0.193	−0.207	0	−0.167	−0.178	0	−0.148	−0.160
C_9	2.234	4.381	4.532	2.015	4.130	4.218	1.671	3.750	3.801
C_{10}	0	−4.194	−4.092	0	−4.194	−4.092	0	−4.194	−4.092

Table 3.1: Wilson coefficients at the low scale for $\mu = m_b/2$, m_b and $2m_b$ with $m_b = 4.6\,\text{GeV}$.

Beyond the SM, NP might contribute in various ways. Assuming that NP manifests itself at and above the electroweak scale, it can be model-independently analyzed in the effective theory framework by allowing for NP contributions to the Wilson coefficients of the SM operators and by additional operators not present in the SM. To account also for the latter we include the most general $b \to s$ (pseudo-) scalar and tensor operators with dileptons into our analysis:

$$\begin{aligned}
\mathcal{O}_S^l &= \frac{e^2}{(4\pi)^2}[\bar{s}P_R b][\bar{l}l], & \mathcal{O}_S^{l\prime} &= \frac{e^2}{(4\pi)^2}[\bar{s}P_L b][\bar{l}l], \\
\mathcal{O}_P^l &= \frac{e^2}{(4\pi)^2}[\bar{s}P_R b][\bar{l}\gamma_5 l], & \mathcal{O}_P^{l\prime} &= \frac{e^2}{(4\pi)^2}[\bar{s}P_L b][\bar{l}\gamma_5 l], \\
\mathcal{O}_T^l &= \frac{e^2}{(4\pi)^2}[\bar{s}\sigma_{\mu\nu} b][\bar{l}\sigma^{\mu\nu} l], & \mathcal{O}_{T5}^l &= \frac{e^2}{(4\pi)^2}[\bar{s}\sigma_{\mu\nu} b][\bar{l}\sigma^{\mu\nu}\gamma_5 l],
\end{aligned} \tag{3.10}$$

where we made the dependence on the lepton flavor explicit by the superscript l. Note that there are only two independent tensor operators in four dimensions. At higher order also 4-quark operators with scalar, pseudoscalar and tensor structure contribute to rare radiative and semileptonic decays [68, 69]. As these studies show 4-quark operators with scalar and pseudoscalar structure mix under QCD into $\mathcal{O}_{7,8,9}$. Here we assume that scalar and pseudoscalar 4-quark operators are not affected by NP.

The additional NP operators (3.10) mix under QCD only with themselves. Their 1-loop anomalous dimensions $\gamma_i = \frac{\alpha_s}{4\pi}\gamma_i^{(0)}$ are

$$\gamma_i^{(0)} = -6C_F = -8, \qquad i = S, S', P, P',$$

$$\gamma_i^{(0)} = 2C_F = \frac{8}{3}, \qquad i = T, T5. \tag{3.11}$$

In our NP analyses all Wilson coefficients are taken at the low scale μ_b.

3.3 Some New Physics Models

In this section we give a short description of several possible extensions of the SM. We concentrate on the models originating large (pseudo-) scalar and tensor interactions contributing to $b \to s\bar{l}l$ transitions. Particularly, the most promising and interesting are the models with lepton flavor violation.

3.3.1 MSSM with Large $\tan\beta$

One of the NP theories contributing to (pseudo-) scalar operators is a minimal extension of the SM with $N = 1$ broken global supersymmetry called *Minimal Supersymmetric Standard Model* (MSSM) [70]. In the MSSM one introduces superpartners to the SM matter fields. They are taken to be spin zero scalars and called *squarks* and *sleptons*. For the first generations we have

$$\tilde{q}_L = \begin{pmatrix} \tilde{u} \\ \tilde{d} \end{pmatrix}_L, \quad \tilde{u}_R, \tilde{d}_R, \quad \tilde{l}_L = \begin{pmatrix} \tilde{\nu_e} \\ \tilde{e} \end{pmatrix}_L, \quad \tilde{e}_R, \tag{3.12}$$

where $\tilde{q}_L$ and $\tilde{l}_L$ are the $SU(2)_L$ squark and slepton doublets, whereas $\tilde{u}_R$, $\tilde{d}_R$ and $\tilde{e}_R$ singlets. In the gauge sector of the SM we have three type of twelve spin one bosons B_μ, W_μ^i, A_μ^a, $i = 1, 2, 3; a = 1, ..., 8$, corresponding to symmetry groups $U(1)_Y$, $SU(2)_L$, $SU(3)_C$ respectively. Their superpartners are spin 1/2 Majorana gauginos $\tilde{\lambda}_0$ (bino), $\tilde{\lambda}^i$ (wino), $\tilde{g}^a$ (gluino).

The Higgs sector of the MSSM is more complicated. In the SM we have only one Higgs field h which after electroweak symmetry breaking gives masses to "up" quarks. The lepton and "down" quark masses are generated by conjugated Higgs field h^C. In the MSSM such Yukawa interactions are derived from the superpotential which is a function of chiral superfields (a field which contains particles and their superpartners). This superpotential has to be an analytic function of superfield, which forbids the simultaneous appearance of both h and h^C fields. This restriction requires the introduction of a second Higgs field in order to give leptons and "down" quarks their masses. Thus, in the supersymmetric theory we need to have two Higgs doublets denoting them as h_d ("down" type) and h_u ("up" type). The vacuum expectation values (VEVs) of the neutral components of the Higgs fields are related

to the mass of the Z^0 boson and the electowek gauge couplings

$$\langle h_u^0 \rangle = v_u, \quad \langle h_d^0 \rangle = v_d, \tag{3.13}$$

$$v_u^2 + v_d^2 = v^2 = 2m_Z^2/(g^2 + g^{'2}) \simeq (174\text{GeV})^2, \tag{3.14}$$

where the couplings g' and g couplings correspond to $U(1)_Y$ and $SU(2)_L$ respectively. In the MSSM the ratio of VEV's is commonly written as

$$\frac{v_u}{v_d} = \tan\beta, \tag{3.15}$$

which is a free parameter of the theory appearing also in processes involving the fermion mass spectrum. The theoretical estimates, based on the pertubative running of the top and bottom Yukawa couplings, require that the values of $\tan\beta$ lie in the range $1 \lesssim \tan\beta \lesssim 65$, whereas the experimental data require lower bound $\tan\beta > 2$ [15].

The superpartners of the MSSM Higgs particles are two higgsino doublets. After electroweak symmetry breaking, the charged higgsinos mix with the charged winos giving two massive Dirac charginos $\tilde{\chi}_i^{\pm}$(i=1,2). The two neutral higgsinos $\tilde{h}_d^0$ and $\tilde{h}_v^0$ mix with the neutral bino $\tilde{\lambda}_0$ and wino $\tilde{\lambda}_3$ giving rise to four Majorana particles called neutralinos $\tilde{\chi}_i^0$(i=1,...,4).

Omitting the $SU(2)_L$ and generation indices, the superpotential of the MSSM is given by

$$W_{\text{MSSM}} = \mu H_d H_u - y_e H_d L_L \bar{e}_R - y_d H_d L_Q \bar{d}_R - y_u Q_L H_u \bar{u}_R, \tag{3.16}$$

where $L_L(Q_L)$ and $e_R(d_R, u_R)$ denote the superfields containing the lepton (quark) doublet and the charged lepton (down-type quark, up-type quark) singlet, respectively. The H_u and H_d are Higgs superfields. The y_e, y_d and y_u are Yukawa couplings presented in terms of 3×3 matrices in family space. Thus, (3.16) is just the supersymmetric generalization of Yukawa couplings and leads to the standard Yukawa Lagrangian from (3.16) by applying the following rule

$$\mathcal{L}_{\text{Yukawa}} = -\frac{1}{2}\psi_i\psi_j \frac{\partial^2 W(\phi)}{\partial\phi_i \partial\phi_j} + \text{h.c.}, \tag{3.17}$$

where ψ_i are fermions and ϕ_i are their scalar superpartners. The first term in the superpotential (3.16), called "μ-term", is the supersymmetric version of the Higgs boson mass term in the SM. The consistent incorporation of spontaneous EW symmetry breaking requires the μ parameter to be of the order of the weak scale.

After brief introduction to the MSSM let us consider the case with large value of $\tan\beta$. Similarly to the SM, the MSSM has Higgs-like interactions and one can expect the appearance of operators with (pseudo-)scalar structure in the Weak Hamiltonian.

Figure 3.2 shows MSSM diagrams contributing to $b \to s\bar{l}l$. These diagrams have been calculated in [58] considering the box, penguin and wave-function counterterm diagrams. As a result they obtained that for a regime when $\tan\beta$ is large the contributions to $C^l_{S,P}$ from the box and penguin diagrams are

$$C^{l,\text{box}}_{S,P} \sim \mathcal{O}\left(\frac{m_l m_b \tan^2\beta}{m^2_{\tilde{\chi}}}\right), \tag{3.18}$$

$$C^{l,\text{penguin}}_{S,P} \sim \mathcal{O}\left(\frac{m_l m_b \tan^2\beta}{m^2_{A^0}}\right), \tag{3.19}$$

where m_{A^0} is the mass of the CP odd neutral Higgs (pseudoscalar Higgs) A^0 being a linear combination of the imaginary components of the neutral h^0_d, h^0_u Higgs fields. The counterterms contribute with third power of $\tan\beta$ (for the exact formulas, see [58])

$$C^{l,\text{count}}_{S,P} \sim \mathcal{O}\left(\frac{m_l m_b \tan^3\beta}{m^2_{A^0}}\right). \tag{3.20}$$

Note that at this order the following relation holds

$$C^{l,\text{count}}_{S} = -C^{l,\text{count}}_{P}. \tag{3.21}$$

The chirality-flipped Wilson coefficients $C^{l'}_{S,P}$ are also enhanced by $\tan\beta$ but suppressed by a factor m_s/m_b compared to $C^l_{S,P}$, thus, can be neglected. Evidently, the impact on the electron channel from such interactions is negligible since $C^e \sim m_e$.

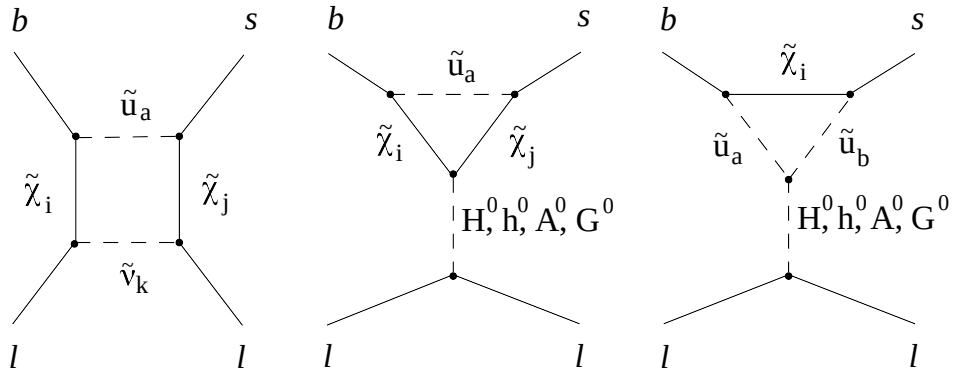

Figure 3.2: The box and penguin contributions to $b \to s\bar{l}l$ in the MSSM.

3.3.2 Models with Broken R-parity

In the previous section we introduced the superpotential (3.16), which is a supersymmetric version of the Yukawa couplings and the Higgs mass term. The construction

of this superpotential is dictated by Lorentz invariance and of course invariance under the SM gauge group $SU(3)_C \otimes SU(2)_L \otimes U(1)_Y$. We did not mention though that (3.16) has an additional symmetry, called R-parity (R_p). This symmetry follows in the MSSM from the assumption that baryon number B and lepton number L are conserved as in the SM. Denoting by S the spin of the MSSM particle, R_p can be written in the form

$$\begin{aligned} R_p &= (-1)^{3(B-L)+2S}, \quad \text{or} \\ R_p &= (-1)^{3B-L+2S} = (-1)^{3B+L+2S}. \end{aligned} \tag{3.22}$$

From (3.22) it follows that particles always have positive R-parity whereas their superpartners (sparticles) have negative R_p. This symmetry forbids proton decay at the renormalizable level and predicts the existence of a stable lightest supersymmetric particle (LSP).

Once lifting the requirement of R-parity conservation the following additional terms to (3.16) are allowed by gauge and supersymmetry

$$W_{\not R_p} = -\epsilon_i L_L^i H_u + \lambda_{ijk} L_L^i L_L^j e_R^k + \lambda'_{ijk} L_L^i Q_L^j d_R^k + \lambda''_{ijk} u_R^i d_R^j d_R^k, \tag{3.23}$$

where i, j, k are flavor indices and ϵ, λ, λ', λ'' are R-parity violating couplings (ϵ has the dimension of mass and the λ's are dimensionless). The invariance under $SU(2)_L$ and $SU(3)_C$ requires λ_{ijk} to be antisymmetric in i, j and λ''_{ijk} to be antisymmetric in j, k, respectively. If $L = \sum_i L_i$ is the sum of lepton type numbers then ϵ, λ and λ' violate both L and L_i, whereas the couplings λ'' violate baryon number B. If both λ' and λ'' are present and unsuppressed, it would lead to extremely rapid proton decay. Thus, already from the lower bound on the proton lifetime one can strongly constrain these couplings. We do not discuss this problem in detail and theoretical solutions (see review [71] and references therein). Here, we just assume for further consideration that $W_{\not R_p}$ contains only λ and λ' couplings. Such models without R-parity can enhance (pseudo-) scalar interactions. Figure 3.3 shows a diagram which can contribute to $b \to s\bar{l}l$ transitions in rare decays. The corresponding effective couplings are [72]

$$C_S^l = -C_P^l = \frac{\lambda'^*_{k23}\lambda_{kll}}{\sqrt{2}G_F\alpha_e\, V_{tb}V_{ts}^*\, m^2_{\tilde{\nu}_k}}, \tag{3.24}$$

$$C_S^{l'} = C_P^{l'} = \frac{\lambda'_{k32}\lambda^*_{kll}}{\sqrt{2}G_F\alpha_e\, V_{tb}V_{ts}^*\, m^2_{\tilde{\nu}_k}}, \tag{3.25}$$

where $m_{\tilde{\nu}_k}$ is the sneutrino mass of the k-th generation. The R_p violating models do not generate effective tensor interactions. The difference with respect to the MSSM is that now the primed Wilson coefficients $C'_{S,P}$ are not suppressed by lepton mass and can be sizeable.

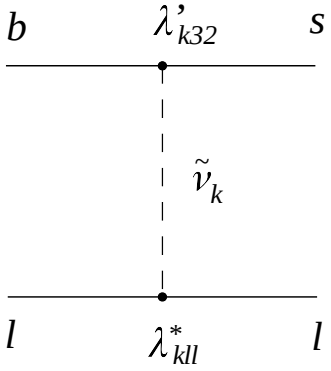

Figure 3.3: Sneutrino exchange diagram contributing to $b \to s\bar{l}l$ in the R-parity violating MSSM.

3.3.3 Leptoquarks

Here we consider models generating tensor interactions based on the concept of Leptoquark (LQ). LQs, particles carrying both lepton and baryon numbers, emerge naturally in some high-energy scale theories, such as GUT, technicolor and composite models (see [73], [74] and references therein). The low-energy theory of LQs can be introduced by constructing the most general Lagrangian assuming two generic principles taken from the SM [74]: *i*) renormalizability of the theory and *ii*) invariance under the SM gauge group. Thus, the LQ interactions with leptons and quarks have the following form [74]

$$\begin{aligned}\mathcal{L}_{S-l-q} = {} & \lambda^{(R)}_{S_0} \cdot \overline{u^c} P_R e \cdot S^{R\dagger}_0 + \lambda^{(R)}_{\tilde{S}_0} \cdot \overline{d^c} P_R e \cdot \tilde{S}^{\dagger}_0 + \lambda^{(R)}_{S_{1/2}} \cdot \overline{u} P_L l \cdot S^{R\dagger}_{1/2} \\ & + \underline{\lambda^{(R)}_{\tilde{S}_{1/2}} \cdot \overline{d} P_L l \cdot \tilde{S}^{\dagger}_{1/2}} + \lambda^{(L)}_{S_0} \cdot \overline{q^c} P_L i\tau_2 l \cdot S^{L\dagger}_0 + \underline{\lambda^{(L)}_{S_{1/2}} \cdot \overline{q} P_R i\tau_2 e \cdot S^{L\dagger}_{1/2}} \\ & + \lambda^{(L)}_{S_1} \cdot \overline{q^c} P_L i\tau_2 \hat{S}^{\dagger}_1 l + h.c. \end{aligned} \tag{3.26}$$

and

$$\begin{aligned}\mathcal{L}_{V-l-q} = {} & \lambda^{(R)}_{V_0} \cdot \overline{d} \gamma^\mu P_R e \cdot V^{R\dagger}_{0\mu} + \lambda^{(R)}_{\tilde{V}_0} \cdot \overline{u} \gamma^\mu P_R e \cdot \tilde{V}^{\dagger}_{0\mu} + \lambda^{(R)}_{V_{1/2}} \cdot \overline{d^c} \gamma^\mu P_L l \cdot V^{R\dagger}_{1/2\mu} \\ & + \lambda^{(R)}_{\tilde{V}_{1/2}} \cdot \overline{u^c} \gamma^\mu P_L l \cdot \tilde{V}^{\dagger}_{1/2\mu} + \lambda^{(L)}_{V_0} \cdot \overline{q} \gamma^\mu P_L l \cdot V^{L\dagger}_{0\mu} + \lambda^{(L)}_{V_{1/2}} \cdot \overline{q^c} \gamma^\mu P_R e \cdot V^{L\dagger}_{1/2\mu} \\ & + \lambda^{(L)}_{V_1} \cdot \overline{q} \gamma^\mu P_L \hat{V}^{\dagger}_{1\mu} l + h.c. \end{aligned} \tag{3.27}$$

The LQ field Φ^j_i can be scalar (S) or vector like (V) under the Lorentz group. The index i corresponds to the transformation properties under the $SU(2)_L$ gauge group and index j shows the chirality of the quarks coupled to LQ (j=L,R). The LQ

LQ	$SU(3)_C$	$SU(2)_L$	Y	Q_{em}
S_0	**3**	**1**	-2/3	-1/3
$\tilde{S}_0$	**3**	**1**	-8/3	-4/3
$S_{1/2}$	$\mathbf{3}^*$	**2**	-7/3	(-2/3, -5/3)
$\tilde{S}_{1/2}$	$\mathbf{3}^*$	**2**	-1/3	(1/3, -2/3)
S_1	**3**	**3**	-2/3	(2/3, -1/3,-4/3)
V_0	$\mathbf{3}^*$	**1**	-4/3	-2/3
$\tilde{V}_0$	$\mathbf{3}^*$	**1**	-10/3	-5/3
$V_{1/2}$	**3**	**2**	-5/3	(-1/3, -4/3)
$\tilde{V}_{1/2}$	**3**	**2**	1/3	(2/3, -1/3)
V_1	$\mathbf{3}^*$	**3**	-4/3	(1/3, -2/3,-5/3)

Table 3.2: SM gauge group assignments of leptoquarks ($Y = 2(Q_{em} - T_3)$).

interaction with the SM $H = \begin{pmatrix} H^+ \\ H^0 \end{pmatrix}$ Higgs doublet is

$$\begin{aligned}
\mathcal{L}_{LQ-H} &= h^{(i)}_{S_0} H i\tau_2 \tilde{S}_{1/2} \cdot S^i_0 + h^{(i)}_{V_0} H i\tau_2 \tilde{V}^\mu_{1/2} \cdot V^i_{0\mu} \\
&+ h_{S_1} H i\tau_2 \hat{S}_1 \cdot \tilde{S}_{1/2} + h_{V_1} H i\tau_2 \hat{V}^\mu_1 \cdot \tilde{V}_{1/2\mu} \\
&+ \underline{Y^{(i)}_{S_{1/2}} \left(H i\tau_2 S^i_{1/2}\right) \cdot \left(\tilde{S}^\dagger_{1/2} H\right)} + Y^{(i)}_{V_{1/2}} \left(H i\tau_2 V^{\mu(i)}_{1/2}\right) \cdot \left(\tilde{V}^\dagger_{1/2\mu} H\right) \\
&+ Y_{S_1} \left(H i\tau_2 \hat{S}^\dagger_1 H\right) \cdot \tilde{S}_0 + Y_{V_1} \left(H i\tau_2 \hat{V}^\dagger_{1\mu} H\right) \cdot \tilde{V}^\mu_0 \\
&+ \kappa^{(i)}_S \left(H^\dagger \hat{S}_1 H\right) \cdot S^{i\dagger}_0 + \kappa^{(i)}_V \left(H^\dagger \hat{V}^\mu_1 H\right) \cdot V^{i\dagger}_{0\mu} + h.c. \\
&- \left(\eta_\Phi M^2_\Phi - g^{(i_1 i_2)}_\Phi H^\dagger H\right) \Phi^{i_1 \dagger} \Phi^{i_2}.
\end{aligned} \tag{3.28}$$

The general study of the Lagrangian above shows that vector-like LQs alone can not generate an effective tensor interaction. It is easy to see that when integrating out the vector-like V field and fierzing the effective interactions does not yield tensor operators, but gives rise to scalar operators:

$$[\bar{s}\gamma_\mu P_L l][\bar{l}\gamma^\mu P_R b] = 2[\bar{s}P_R b][\bar{l}P_L l], \tag{3.29}$$

$$[\bar{s}\gamma_\mu P_R l][\bar{l}\gamma^\mu P_L b] = 2[\bar{s}P_L b][\bar{l}P_R l]. \tag{3.30}$$

Considering only scalar LQ interactions with leptons and quarks is also not sufficient to generate tensor operators because the Lagrangian (3.26) does not provide the necessary operator structure. Integrating out LQs one has

$$[\bar{q}P_L l][\bar{l}P_R q], \quad [\bar{q}P_R l][\bar{l}P_L q], \tag{3.31}$$

which after "fierzing" lead to the vanishing tensor operators

$$[\bar{q}P_R\sigma_{ab}P_Lq][\bar{l}P_L\sigma^{ab}P_Rl] = 0, \qquad [\bar{q}P_L\sigma_{ab}P_Rq][\bar{l}P_L\sigma^{ab}P_Rl] = 0. \tag{3.32}$$

In order to produce non-vanishing tensor operators one needs initially (before Fierz transformation) the following form for the effective interaction

$$[\bar{q}P_Ll][\bar{l}P_Lq], \quad [\bar{q}P_Rl][\bar{l}P_Rq] \tag{3.33}$$

and this structure is provided by the LQ interaction with the SM Higgs. The spontaneous symmetry breaking of $SU(2)_L \times U(1)_Y$ leads to the non-trivial mixing between different types of LQ's according to (3.28). As one possibility we consider the mixing between the $\tilde{S}_{1/2}$ and $S^L_{1/2}$ (where the relevant terms in Lagrangian (3.26) and (3.28) have been underlined) which, as we see later, could generate tensor like effective operators in the $(\bar{s}b)(\bar{l}l)$ transition. The relevant mass matrix for the LQs with charge $Q = -2/3$ has the form [74]

$$\mathcal{M}^2_S = \begin{pmatrix} \bar{M}^2_{\tilde{S}_{1/2}} & \sqrt{2}Y_{S_{1/2}}v^2 \\ \sqrt{2}Y_{S_{1/2}}v^2 & \bar{M}^2_{S^L_{1/2}} \end{pmatrix}, \tag{3.34}$$

where $\bar{M}^2_S = M^2_S + g_S|v|^2$ is the "shifted" diagonal mass and v is the vacuum expectation value (VEV) of the SM Higgs field. This mass matrix can be diagonalized by an orthogonal transformation and as a result we have in the mass eigenstate basis two new LQ fields as a mixture of the $\tilde{S}_{1/2}$ and $S^L_{1/2}$. The masses of the new LQ fields S_a and S_b are

$$M^2_{a,b} = \frac{1}{2}(\bar{M}^2_{\tilde{S}_{1/2}}) + \bar{M}^2_{S^L_{1/2}} \pm \sqrt{(\bar{M}^2_{\tilde{S}_{1/2}} - \bar{M}^2_{S^L_{1/2}})^2 + 8Y^2_{S_{1/2}}v^4} \tag{3.35}$$

and the mixing

$$\begin{aligned} S_a &= \cos\theta\tilde{S}_{1/2} + \sin\theta S^L_{1/2}, & \tilde{S}_{1/2} &= \cos\theta S_a - \sin\theta S_b, \\ S_b &= \cos\theta S^L_{1/2} - \sin\theta\tilde{S}_{1/2}, & S^L_{1/2} &= \cos\theta S_b + \sin\theta S_a. \end{aligned} \tag{3.36}$$

The mixing angle can be written in terms of couplings and masses

$$\tan 2\theta = \frac{4Y_{S_{1/2}}v^2}{(\bar{M}^2_{\tilde{S}_{1/2}} - \bar{M}^2_{S^L_{1/2}})}. \tag{3.37}$$

Substituting (3.36) in the Lagrangian (3.26) we derive the interaction in terms of the LQ mass eigenstates and keep only relevant terms one has

$$\mathcal{L} = \lambda^{(R)}_{\tilde{S}_{1/2}}\bar{d}P_Ll[\cos\theta S_a - \sin\theta S_b] - \lambda^{(L)}_{S_{1/2}}\bar{l}P_Ld[\cos\theta S^\dagger_b + \sin\theta S^\dagger_a] + h.c. \tag{3.38}$$

where we omitted generation indices. Now, it is easy to see that after integrating out LQs one gets the necessary structures (3.33)

$$[\bar{d}P_L l][\bar{l}P_L q],\ \ [\bar{q}P_R l][\bar{l}P_R d]. \tag{3.39}$$

Finally one can deduce the tensor Wilson coefficients for the $(\bar{s}b)(\bar{l}l)$ transition in terms of the LQ Lagrangian parameters

$$C_{T,T5} = \frac{\cos\theta \sin\theta (M_b^2 - M_a^2)}{\sqrt{2} G_F \alpha_e V_{tb} V_{ts}^*\, M_a^2 M_b^2} \Big([\lambda^{(L)*}_{S_{1/2}}]_{l3} [\lambda^{(R)}_{\tilde{S}_{1/2}}]_{2l} \pm [\lambda^{(L)}_{S_{1/2}}]_{l2} [\lambda^{(R)*}_{\tilde{S}_{1/2}}]_{3l}. \Big) \tag{3.40}$$

From this expressions one can see that we get an additional suppression from the mixing of order $\sin\theta \sim \mathcal{O}\left(v^2/M_S^2\right)$ where M_S is a general scalar LQ mass.

3.4 Form Factors and Large Recoil Limit

As we see from Section 1.3.2 $B \to K, K^* \bar{l}l$ transitions can be partly factorized. This factorizable parts are described by $B \to K, K^*$ transition form factors. In this section we show that in particular regime, i.e., large recoil, the number of the form factors can be substantially reduced.

In QCD the $B \to K$ transition can be defined in terms of three form factors $f_+(q^2)$, $f_0(q^2)$, $f_T(q^2)$

$$\begin{aligned} \langle K(p_B - q)|\bar{s}\gamma_\mu b|B(p_B)\rangle &= f_+(q^2)\Big[(2p_B - q)_\mu - \frac{M_B^2 - M_K^2}{q^2} q_\mu\Big] \\ &\quad + \frac{M_B^2 - M_K^2}{q^2} f_0(q^2) q_\mu, \\ \langle K(p_B - q)|\bar{s}\sigma_{\mu\nu} q^\nu b|B(p_B)\rangle &= i\Big[(2p_B - q)_\mu q^2 - q_\mu (M_B^2 - M_K^2)\Big] \frac{f_T(q^2)}{M_B + M_K}, \end{aligned} \tag{3.41}$$

where the momentum transfer q is in the range $4m_l^2 \le q^2 \le (M_B - M_K)^2$, but as we show later in QCDF this range is quite restricted. As a consequence of this parametrization the relation $f_+(0) = f_0(0)$ holds.

Since K^* is a vector meson, the parametrization of the $B \to K^*$ transition is more complicated and needs seven q^2-dependent QCD form factors $V, A_{0,1,2}$ and $T_{1,2,3}$. It reads as

$$\begin{aligned} &\langle K^*(p_B - q)|\bar{s}\gamma_\mu(1 - \gamma_5) b|B(p_B)\rangle = \\ &- 2\epsilon_{\mu\nu\alpha\beta}\varepsilon^{*\nu} p_B^\alpha q^\beta \frac{V}{M_B + M_{K^*}} - i\varepsilon_\mu^* (M_B + M_{K^*}) A_1 \\ &+ i(2p_B - q)_\mu (\varepsilon^* \cdot q) \frac{A_2}{M_B + M_{K^*}} + i q_\mu (\varepsilon^* \cdot q) \frac{2M_{K^*}}{q^2} [A_3 - A_0], \end{aligned} \tag{3.42}$$

$$\langle K^*(p_B - q)|\bar{s}\sigma_{\mu\nu}q^\nu(1+\gamma_5)b|B(p_B)\rangle =$$
$$-2i\,\epsilon_{\mu\nu\alpha\beta}\varepsilon^{*\nu}p_B^\alpha q^\beta\, T_1 + [\varepsilon_\mu^*(M_B^2 - M_{K^*}^2) - (\varepsilon^*\cdot q)(2p_B - q)_\mu]\, T_2$$
$$+ (\varepsilon^*\cdot q)\left[q_\mu - \frac{q^2}{M_B^2 - M_{K^*}^2}(2p_B - q)_\mu\right] T_3 \tag{3.43}$$

and

$$A_3 = \frac{M_B + M_{K^*}}{2M_{K^*}}A_1 - \frac{M_B - M_{K^*}}{2M_{K^*}}A_2, \tag{3.44}$$

where $\epsilon^{*\mu}$ denotes the polarization vector of the K^* and p_B^μ the four momentum of the B meson.

Let us assume the case when the outgoing Kaon (K or K^*) is energetic (small q^2). We also require that the s quark in the Kaon is created by the $b \to s$ transition. The b quark interacts with the spectator quark only via soft gluon exchange (hard interactions imply large momenta of the spectator quarks in the B meson which is highly improbable). The effective theory applied to this case is called heavy quark effective theory (HQET) [75, 76, 77, 78]. In this theory the heavy quark momentum p_b expanded as (1.51). A similar expression can be written for the energetic s quark. Introducing a light-like vector n_-^μ ($n_-^2 = 0$) parallel to the Kaon momentum we can write

$$p_s^\mu = En_-^\mu + k'^\mu, \quad k' \ll E, \tag{3.45}$$

where k' is a small residual momentum and E is the Kaon energy $E = (M_B^2 + M_K^2 - q^2)/(2M_B) \sim M_B/2$ for $q^2 \ll M_B^2$. The QCD form factors obey symmetry relations in this limit (Large Recoil) limit and can be expressed at leading order in the $1/E$ expansion in terms of universal form factors ξ_P, $\xi_\perp$ and $\xi_\parallel$ [25, 26] as

$$f_+(q^2) = \frac{M_B}{E}f_0(q^2) = \frac{M_B}{M_B + M_K}f_T(q^2) = \xi_P(q^2), \tag{3.46}$$

$$\frac{M_{K^*}}{E}A_0(q^2) = \frac{M_B + M_{K^*}}{2E}A_1(q^2) - \frac{M_B - M_{K^*}}{M_B}A_2(q^2) = \frac{M_B}{2E}T_2(q^2) - T_3(q^2) = \xi_\parallel(q^2),$$

$$\frac{M_B}{M_B + M_{K^*}}V(q^2) = \frac{M_B + M_{K^*}}{2E}A_1(q^2) = T_1(q^2) = \frac{M_B}{2E}T_2(q^2) = \xi_\perp(q^2). \tag{3.47}$$

Symmetry breaking corrections at order α_s have been calculated using QCDF in Ref. [26]. For the case of the $B \to K$ transition they can be written in a schematically simple form

$$\frac{f_0}{f_+} = \frac{2E}{M_B}\left[1 + \mathcal{O}(\alpha_s) + \mathcal{O}\left(\frac{q^2}{M_B^2}\sqrt{\frac{\Lambda_{\rm QCD}}{E}}\right)\right],$$
$$\frac{f_T}{f_+} = \frac{M_B + M_K}{M_B}\left[1 + \mathcal{O}(\alpha_s) + \mathcal{O}\left(\sqrt{\frac{\Lambda_{\rm QCD}}{E}}\right)\right], \tag{3.48}$$

up to higher order QCD, power and mixed corrections. The α_s-corrections from the soft-overlap and hard scattering contributions indicated in (3.48) have been calculated in QCDF and are given in [26]. The symmetry relation breaking corrections due to sub-leading orders in the $\Lambda_{\rm QCD}/E$ expansion have been considered for the soft-overlap part using SCET [79]. The corresponding corrections are indicated in (3.46). Note that the expansion parameter is rather $\sqrt{\Lambda_{\rm QCD}/E}$ than $\Lambda_{\rm QCD}/E$, and that for f_0/f_+ an additional suppression of q^2/M_B^2 appears.

The q^2 dependence of the only form factor $f_+(q^2) = \xi_P(q^2)$ is adopted from LCSR calculations [80]. This parametrization is given in terms of the Gegenbauer moments of the K-meson LCDA, a_1^K, a_2^K and a_4^K as

$$f_+(q^2) = f_+^{as}(q^2) + a_1^K(\mu_{IR}) f_+^{a_1}(q^2) + a_2^K(\mu_{IR}) f_+^{a_2}(q^2) + a_4^K(\mu_{IR}) f_+^{a_4}(q^2). \qquad (3.49)$$

where

$$f_+^{as}(q^2) = \frac{0.0244}{1 - q^2/(5.41\,\text{GeV})^2} + \frac{0.2590}{(1 - q^2/(5.41\,\text{GeV})^2)^2} \qquad (3.50)$$

and f^{a_i} are fitted by polynomials of 3rd degree

$$f^{a_i} = a + bq^2 + c(q^2)^2 + d(q^2)^3. \qquad (3.51)$$

where the numerical values of $\{a, b, c, d\}$ are $\{0.310, 0.930{\times}10^{-2}, 0.139{\times}10^{-2}, -0.083{\times}10^{-3}\}$ respectively. Here we use "set 2" of the fit with $m_b^{pole} = 4.8$ GeV corresponding to the infrared factorization scale $\mu_{IR} = \sqrt{M_B^2 - m_b^{pole\,2}} = 2.2$ GeV. The running of the Gegenbauer moments given in Table 3.4 from 1 GeV to 2.2 GeV is accounted for by the scaling factors $\{0.793, 0.696, 0.590\}$ for $\{a_1^K, a_2^K, a_4^K\}$. The relative uncertainty of f_+ due to the asymptotic form factor f_+^{as} (which is independent of the a_i^K) at $q^2 = 0$ is approximately $\Delta_{as}/f_+(0) = 10\%$, see Table 2 of [80]. In order to estimate the form factor uncertainty in the low-q^2 region we scan over the Gegenbauer moments according to the ranges in Table 3.4 translated to $\mu_{IR} = 2.2$ GeV and add the uncertainty from Δ_{as} in quadrature. The form factor $f_+(q^2) = \xi_P(q^2)$ with its uncertainties with and without Δ_{as} is shown in Figure 3.4. The total uncertainty is 16% at maximal recoil and reduces to 12% at $q^2 = 7\,\text{GeV}^2$. The reduction of the relative form factor uncertainty towards larger values of q^2 stems from the increase of the form factor in this region while keeping Δ_{as} from $q^2 = 0$.

For the q^2 dependence of the form factors $\xi_\perp$ and $\xi_\parallel$ we adopt also the results from light cone sum rule (LCSR) calculations [81] for the $V(q^2)$, $A_1(q^2)$ and $A_2(q^2)$ form

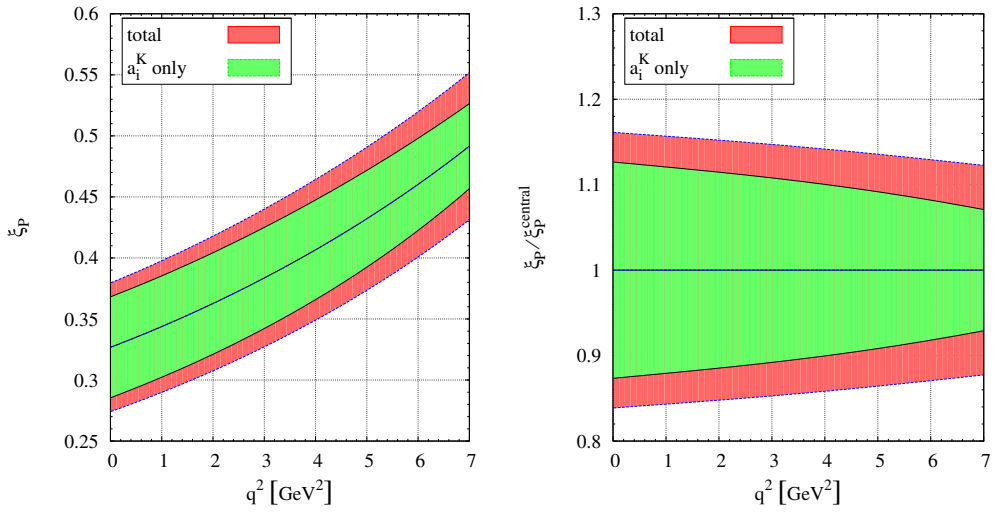

Figure 3.4: The form factor $\xi_P(q^2) = f_+(q^2)$ in the low-q^2 region including uncertainties from the Gegenbauer moments a_i^K (lighter shaded area) and from a_i^K and Δ_{as} with their uncertainties added in quadrature (darker shaded area), for details see text. In the left-hand plot is shown $\xi_P(q^2)$, and in the right-hand plot the form factor normalized to its central value, $\xi_P(q^2)/\xi_P^{\text{central}}(q^2)$.

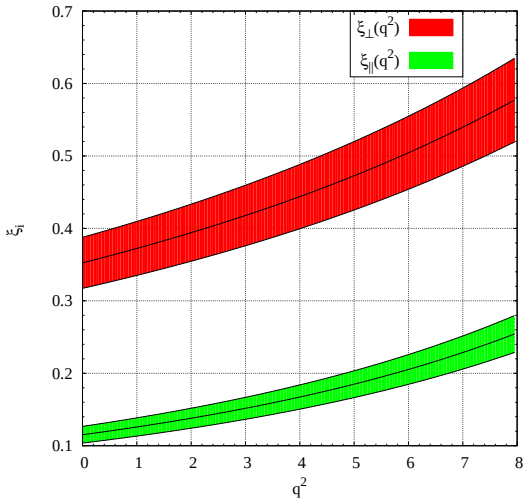

Figure 3.5: The universal form factors $\xi_\perp$ and $\xi_\parallel$ in the low-q^2 region and their uncertainty indicated by the bands.

factors. Here the q^2 dependence is parametrized as

$$V(q^2) = \frac{r_1}{1 - q^2/m_R^2} + \frac{r_2}{1 - q^2/m_{fit}^2}, \tag{3.52}$$

$$A_1(q^2) = \frac{r_2}{1 - q^2/m_{fit}^2}, \tag{3.53}$$

$$A_2(q^2) = \frac{r_1}{1 - q^2/m_{fit}^2} + \frac{r_2}{(1 - q^2/m_{fit}^2)^2}, \tag{3.54}$$

where the fit parameters $r_{1,2}, m_R^2$ and m_{fit}^2 are shown in Table 3.3. Also given in this table are the values of the form factors at $q^2 = 0$ and the corresponding parametric uncertainties within the LCSR approach. We give the uncertainties independent of the Gegenbauer moments $a_{1,K^*}^{\perp,\parallel}$ and the ones due to $a_{1,K^*}^{\perp,\parallel}$ separately. We use $a_{1,K^*}^{\perp,\parallel}(1\text{ GeV}) = 0.1 \pm 0.07$ [81]. The relative uncertainty of the form factors $V(0), A_1(0)$ and $A_2(0)$ amounts to 8%, 10% and 10% without, and 11%, 12% and 14% after adding the a_{1,K^*} induced uncertainty in quadrature, respectively. We use the total relative uncertainty from maximal recoil as an estimate for the form factor uncertainties for $q^2 > 0$. The form factors $\xi_{\perp,\parallel}$ defined via (3.47) are shown as a function of q^2 in Figure 3.5. Here the bands indicate the uncertainty in $\xi_\perp$ and $\xi_\parallel$ of 11% and 14%, respectively.

	r_1	r_2	$m_R^2\,[\,\text{GeV}^2]$	$m_{fit}^2\,[\,\text{GeV}^2]$	$F(0)$	$\Delta_0 F(0)$	$\Delta_{a_1} F(0)$
V	0.923	−0.511	5.32^2	49.40	0.411	0.033	$0.44\delta_{a_1}$
A_1		0.290		40.38	0.292	0.028	$0.33\delta_{a_1}$
A_2	−0.084	0.342		52.00	0.259	0.027	$0.31\delta_{a_1}$

Table 3.3: The parameters $r_{1,2}, m_R^2$ and m_{fit}^2 describing the q^2 dependence of the form factors V and $A_{1,2}$ in the LCSR approach [81]. Also shown are the corresponding values of the form factors at $q^2 = 0$, $F(0)$, their uncertainties independent of the Gegenbauer moment a_{1,K^*}, $\Delta_0 F(0)$ and the uncertainties induced by a_{1,K^*} in terms of $\delta_{a_1} = (a_{1,K^*}(1\text{ GeV}) - 0.1)$, $\Delta_{a_1} F(0)$.

3.5 Standard Model Analysis

In this section we concentrate on the SM contributions in $B \to K, K^* \bar{l} l$. We introduce several observables constructed by angular distributions. We give their SM predictions and dominant uncertainties computed in QCDF.

$\alpha_s(m_Z) = 0.1176 \pm 0.0020$	[15]	$f_K = (159.8 \pm 1.4 \pm 0.44)$ MeV	[15]
$\alpha_e(m_b) = 1/133$		$f_{B_{u,d}} = (200 \pm 30)$ MeV	
$m_W = 80.403$ GeV	[15]	$f_{B_s} = (240 \pm 30)$ MeV	[82]
$m_t^{pole} = (170.9 \pm 1.8)$ GeV	[83]	$\lambda_{B,+}(1.5\text{ GeV}) = (0.458 \pm 0.115)$ GeV	[20, 84]
$m_b = (4.6 \pm 0.1)$ GeV	[19]	$\tau_{B^\pm} = (1.638 \pm 0.011)$ ps	[15]
$m_c^{pole} = (1.4 \pm 0.2)$ GeV		$\tau_{B^0} = (1.530 \pm 0.009)$ ps	[15]
$\mathcal{B}(\bar{B} \to X_c l \bar{\nu}_l) = (10.57 \pm 0.15)\%$	[15]	$\tau_{B_s} = (1.425 \pm 0.041)$ ps	[15]
$f_K = (159.8 \pm 1.4 \pm 0.44)$ MeV	[15]†	$f_\perp^{K^*}(1\text{ GeV}) = (185 \pm 10)$ MeV	[85]††
$a_1^K(1\text{ GeV}) = 0.06 \pm 0.03$	[86]†	$f_\parallel^{K^*} = (217 \pm 5)$ MeV	[15]††
$a_2^K(1\text{ GeV}) = 0.25 \pm 0.15$	[86]†	$a_{1,K^*}^{\perp,\parallel}(1\text{ GeV}) = 0.1 \pm 0.07$	[81]††
$a_4^K(1\text{ GeV}) = -0.015 \pm 0.1$	[80]†	$a_{2,K^*}^{\perp,\parallel}(1\text{ GeV}) = 0.1 \pm 0.1$	[81]††
$\xi_P(0) = 0.327 \pm 0.053$	[86, 80]†	$\lambda = 0.2258^{+0.0016}_{-0.0017}$ (95% C.L.)	[18]††
$\lvert V_{ts}\rvert = 0.0409 \pm 0.0021$	[87]†	$\lvert V_{cb}\rvert = 0.0417 \pm 0.0013$ (95% C.L.)	[18]††
$\lvert V_{cb}\rvert = 0.0416 \pm 0.0007$	[87]†	$\bar{\rho} = [0.108, 0.243]$ (95% C.L.)	[18]††
		$\bar{\eta} = [0.288, 0.375]$ (95% C.L.)	[18]††

Table 3.4: The numerical input used in $B \to K, K^* \bar{l} l$ analysis. We neglect the strange quark mass throughout this work. We denote by m_b the PS mass at the factorization scale $\mu_f = 2$ GeV. We neglect the strange quark mass throughout this work unless otherwise stated. The numerical input for the form factors $\xi_{\perp,\parallel}$ is given in Section 3.4. † The numerical input relevant only for $B \to K \bar{l} l$. †† The numerical input relevant only for $B \to K^* \bar{l} l$.

3.5.1 Angular Distribution in $B \to K \bar{l} l$

A systematic treatment of the matrix element $\mathcal{M}[B \to K \bar{l} l]$ is available in the large recoil region. According to the symmetry relations (3.46) only one soft form factor $\xi_P(q^2)$ appears in the $B \to K$ heavy-to-light decay amplitude in the large energy limit of QCD [25, 26]. Denoting by p_B, p, p_- and p_+ the 4-momenta of the B-meson, Kaon, lepton l and antilepton $\bar{l}$, respectively, the SM $B \to K \bar{l} l$ matrix element can be written as

$$\begin{aligned} \mathcal{M}[B \to K \bar{l} l] &= \langle l(p_-) \bar{l}(p_+) K(p) | \mathcal{H}_{\text{eff}} | \bar{B}(p_B) \rangle \\ &= i \frac{G_F \alpha_e}{\sqrt{2}\pi} V_{tb}^* V_{ts}\, \xi_P(q^2) \left(F_V\, p_B^\mu\, [\bar{l} \gamma_\mu l] + F_A\, p_B^\mu\, [\bar{l} \gamma_\mu \gamma_5 l] + F_P\, [\bar{l} \gamma_5 l] \right). \end{aligned} \tag{3.55}$$

The functions $F_i \equiv F_i(q^2)$, $i = P, A, V$ are given as

$$F_P = m_l C_{10} \left[\frac{M_B^2 - M_K^2}{q^2} \left(\frac{f_0(q^2)}{f_+(q^2)} - 1 \right) - 1 \right], \tag{3.56}$$

$$F_A = C_{10}, \qquad F_V = C_9 + \frac{2 m_b}{M_B} \frac{\mathcal{T}_P(q^2)}{\xi_P(q^2)} + \frac{8 m_l}{M_B + M_K} \frac{f_T(q^2)}{f_+(q^2)} C_T^l, \tag{3.57}$$

where

$$\lambda = M_B^4 + M_K^4 + q^4 - 2(M_B^2 M_K^2 + M_B^2 q^2 + M_K^2 q^2), \qquad \beta_l = \sqrt{1 - 4\frac{m_l^2}{q^2}}. \tag{3.58}$$

The quantity $\mathcal{T}_P(q^2)$ appearing in the vector coupling to leptons, F_V, takes into account virtual one-photon exchange between the hadrons and the lepton pair and hard scattering contributions. $\mathcal{T}_P(q^2)$ can be extracted from [19] and is given in Appendix B.4. At lowest order (denoted by the superscript $^{(0)}$) up to numerically small annihilation contributions, it has the simple form

$$\mathcal{T}_P^{(0)}(q^2) = \xi_P(q^2) \left[C_7^{\text{eff}(0)} + \frac{M_B}{2m_b} Y^{(0)}(q^2) \right]. \tag{3.59}$$

Here C_7^{eff} is an effective Wilson coefficient and Y denotes 1-loop matrix elements of 4-quark operators contributing to $b \to s\bar{l}l$ which can be found in Appendix B.4.

Based on the matrix element (3.55) the double differential decay rate with respect to q^2 and $\cos\theta$ with lepton flavor l reads as

$$\frac{d^2\Gamma_l}{dq^2\, d\cos\theta} = a_l(q^2) + b_l(q^2)\cos\theta + c_l(q^2)\cos^2\theta, \tag{3.60}$$

where

$$\begin{aligned} \frac{a_l(q^2)}{\Gamma_0 \sqrt{\lambda}\, \beta_l\, \xi_P^2} &= q^2 |F_P|^2 + \frac{\lambda}{4}(|F_A|^2 + |F_V|^2) \\ &\quad + 2m_l(M_B^2 - M_K^2 + q^2) Re(F_P F_A^*) + 4 m_l^2 M_B^2 |F_A|^2, \end{aligned} \tag{3.61}$$

$$\frac{b_l(q^2)}{\Gamma_0 \sqrt{\lambda}\, \beta_l\, \xi_P^2} = 0, \tag{3.62}$$

$$\frac{c_l(q^2)}{\Gamma_0 \sqrt{\lambda}\, \beta_l\, \xi_P^2} = -\frac{\lambda}{4} \beta_l^2 (|F_A|^2 + |F_V|^2) \tag{3.63}$$

and

$$\Gamma_0 = \frac{G_F^2 \alpha_e^2 |V_{tb}^* V_{ts}|^2}{512 \pi^5 M_B^3}. \tag{3.64}$$

Here, θ denotes the angle between the direction of motion of the B and the negatively charged lepton l in the dilepton center of mass frame. In the limit $m_l \to 0$ further relation $a_l(q^2) = -c_l(q^2)$ holds.

With (3.60) at hand the angular distribution

$$\frac{d\Gamma_l}{d\cos\theta} = A_l + B_l \cos\theta + C_l \cos^2\theta \tag{3.65}$$

is given in terms of the q^2-integrated coefficients

$$A_l = \int_{q^2_{\rm min}}^{q^2_{\rm max}} dq^2\, a_l(q^2), \qquad B_l = \int_{q^2_{\rm min}}^{q^2_{\rm max}} dq^2\, b_l(q^2), \qquad C_l = \int_{q^2_{\rm min}}^{q^2_{\rm max}} dq^2\, c_l(q^2). \tag{3.66}$$

Their values depend on the cuts in q^2. We recall that while the boundaries of the phase space allow for dilepton masses in the range $4m_l^2 < q^2 \leq (M_B - M_K)^2$, the QCDF approach is valid only in the low-q^2 region. Note that for very low dilepton masses there is sensitivity to light resonances. We therefore restrict our analysis to $1\ \text{GeV}^2 \lesssim q^2 < 7\ \text{GeV}^2$.

The decay rate Γ_l and the integrated and normalized forward-backward asymmetry $A^l_{\rm FB}$ of the lepton pair can be expressed in terms of A_l, B_l and C_l

$$\Gamma_l = 2\left(A_l + \frac{1}{3}C_l\right), \qquad\qquad A^l_{\rm FB} = \frac{B_l}{\Gamma_l}. \tag{3.67}$$

We further introduce the observable

$$F^l_H \equiv \frac{2}{\Gamma_l}(A_l + C_l) = \int_{q^2_{\rm min}}^{q^2_{\rm max}} dq^2 \left[a_l(q^2) + c_l(q^2)\right] \Bigg/ \int_{q^2_{\rm min}}^{q^2_{\rm max}} dq^2 \left[a_l(q^2) + \frac{1}{3}c_l(q^2)\right]. \tag{3.68}$$

Since F^l_H is normalized to Γ_l, we expect reduced uncertainties in the former compared to the latter due to cancellations between numerator and denominator. As already anticipated after (3.64) within the SM a cancellation takes place in (3.68) between a_l and c_l such that $F^{l\,\rm SM}_H$ vanishes in the limit $m_l \to 0$. From here follows the approximate $\propto \sin^2\theta$ angular dependence of $B \to K\bar{l}l$ decays in the SM.

We would like to comment on the possibility of corrections to (3.65) from higher powers of $\cos\theta$, that is, a polynomial dependence in the angular distribution on $\cos^n\theta$ with $n > 2$. Higher angular momenta arise from higher (> 6) dimensional operators in the weak Hamiltonian (3.3) or from QED corrections. Hence, they are suppressed by powers of external low energy momenta or masses over the electroweak scale, and $\alpha_e/4\pi$, respectively.

A further useful observable in $B \to K\bar{l}l$ decays is R_K, the ratio of $B \to K\bar{\mu}\mu$ to $B \to K\bar{e}e$ decay rates with the same q^2 cuts [68]

$$R_K \equiv \frac{\Gamma_\mu}{\Gamma_e} = \int_{q^2_{\rm min}}^{q^2_{\rm max}} dq^2\, \frac{d\Gamma_\mu}{dq^2} \Bigg/ \int_{q^2_{\rm min}}^{q^2_{\rm max}} dq^2\, \frac{d\Gamma_e}{dq^2} = \frac{\Gamma_\mu F^\mu_H - 4/3\, C_\mu}{\Gamma_e}, \tag{3.69}$$

which probes lepton flavor dependent effects in and beyond the SM. We find that F^l_H and R_K are model-independently related

$$R_K \cdot (1 - F^\mu_H - \Delta) = 1, \qquad \text{where} \qquad \Delta = \frac{4}{3}\frac{C_e - C_\mu}{\Gamma_\mu} - \frac{F^e_H}{R_K}. \tag{3.70}$$

The expression for Δ simplifies in models where chiral couplings to electrons can be neglected as, for example, in the SM with $m_e = 0$. Then $F_H^e = 0$ and $\Gamma_e = -4/3 C_e$ and in the SM $\Delta^{\rm SM} \propto m_\mu^2$.

Let us examine the observables F_H^l, R_K and Γ_l and the corresponding branching ratios $\mathcal{B}_l \equiv \mathcal{B}(B \to K\bar{l}l)$ for low dilepton mass. We start with Γ_l and analyze the lepton flavor dependence. In the SM this effect is purely of kinematical origin, i.e., proportional to the lepton mass, and often negligible in the analysis of branching ratios. Here we try to keep these contributions and quantify them analytically. For that we use the form factor symmetry relations (3.48) and as a consequence of it the useful relation holds

$$\frac{q^2}{M_B^2}|\tilde{F}_P|^2 + 4|F_A|^2 + \frac{M_B^2 - M_K^2 + q^2}{M_B^2} 2Re(\tilde{F}_P F_A^*) = \mathcal{O}\left(\alpha_s, \frac{q^2}{M_B^2}\sqrt{\frac{\Lambda_{\rm QCD}}{E}}\right), \quad (3.71)$$

which enters both $a_l^{\rm SM} + c_l^{\rm SM}$ and $a_l^{\rm SM} + c_l^{\rm SM}/3$ combinations. Here, the explicit SM expressions for $F_{V,A,P}$ (3.56) have been used and $F_P = m_l \tilde{F}_P$ has been rescaled. The relation (3.71) involves only the ratio f_0/f_+ and results in a beneficial q^2/M_B^2 suppression of the power corrections. Thus, Γ_l in the low q^2 region reads as

$$\Gamma_l{}^{\rm SM} = \frac{\Gamma_0}{3}\int_{q^2_{\rm min}}^{q^2_{\rm max}} dq^2\, \xi_P^2(q^2)\sqrt{\lambda}^3(|F_A|^2 + |F_V|^2) \quad (3.72)$$
$$\times \left\{1 + \mathcal{O}\left(\frac{m_l^4}{q^4}\right) + \frac{m_l^2}{M_B^2} \times \mathcal{O}\left(\alpha_s, \frac{q^2}{M_B^2}\sqrt{\frac{\Lambda_{\rm QCD}}{E}}\right)\right\},$$

where we get the higher order lepton flavor depending terms $\mathcal{O}(m_l^4)$ and $\mathcal{O}(m_l^2)$. Here, we neglect terms of order M_K^2/M_B^2 and in $\lambda \approx M_B^4$ drop q^2/M_B^2 terms which is consistent with the $\Lambda_{\rm QCD}/E$ expansion. These corrections are obtained expanding the coefficients a_l and c_l in m_l. It is necessary to note that the $\mathcal{O}(m_l^2)$ term is additionally suppressed by a factor of order $\mathcal{O}\left(\alpha_s, \frac{q^2}{M_B^2}\sqrt{\frac{\Lambda_{\rm QCD}}{E}}\right)$ and numerically negligible with respect to $\mathcal{O}(m_l^4)$ one. Thus, there is no term of $\mathcal{O}(m_l^2)$ up to symmetry breaking corrections. The leading order term is proportional to $\xi_P^2(q^2)(|F_A|^2+|F_V|^2)$. The functions F_A ($|F_A| = |C_{10}^{\rm SM}| \sim 4$) and F_V are quantities of the same order, since F_V is a sum of $|C_9^{\rm SM}| \sim 4$ and a term containing $\mathcal{T}_P$, where $|\mathcal{T}_P(q^2)| \sim 0.1$.

Thus, as a conclusion one should note that the SM $B \to K\bar{l}l$ decay rate is highly insensitive to lepton mass (or lepton flavor) dependent effects. For the muon channel these effects are of order $m_\mu^4/q^4 \sim 10^{-4}$ in the low q^2 $(1 - 7{\rm GeV}^2)$. These effects are even more suppressed for electrons by the factor $m_e^2/m_\mu^2 \simeq 2 \cdot 10^{-5}$.

In view of the large form factor uncertainties and the insensitivity to lepton mass effects of $\Gamma_l{}^{\rm SM}$ it is proposed to investigate the ratio Γ_μ/Γ_e, i.e., R_K [68]. First, one expects cancellations of the hadronic uncertainties in R_K for low dilepton mass.

	$B^- \to K^- \bar{l}l$			$\bar{B} \to \bar{K} \bar{l}l$		
	SM value	$\xi_P[\%]$	$\mu_b[\%]$	SM value	$\xi_P[\%]$	$\mu_b[\%]$
$\mathcal{B}_\mu$	$1.60^{+0.51}_{-0.46}$	$^{+29.9}_{-27.0}$	$^{+2.0}_{-1.8}$	$1.46^{+0.47}_{-0.43}$	$^{+30.4}_{-27.4}$	$^{+2.1}_{-2.0}$
	$1.27^{+0.40}_{-0.36}$	$^{+29.4}_{-26.6}$	$^{+2.2}_{-2.1}$	$1.16^{+0.37}_{-0.33}$	$^{+29.8}_{-27.0}$	$^{+2.3}_{-2.2}$
$[10^{-7}]$	$1.91^{+0.59}_{-0.54}$	$^{+29.2}_{-26.6}$	$^{+2.2}_{-2.2}$	$1.74^{+0.55}_{-0.50}$	$^{+29.6}_{-26.8}$	$^{+2.3}_{-2.3}$
	$1.59^{+0.48}_{-0.44}$	$^{+28.7}_{-26.0}$	$^{+2.4}_{-2.4}$	$1.45^{+0.45}_{-0.41}$	$^{+29.0}_{-26.3}$	$^{+2.5}_{-2.6}$
F_H^μ	$0.0244^{+0.0003}_{-0.0003}$	$^{+0.8}_{-1.0}$	$^{+0.7}_{-0.5}$	$0.0243^{+0.0003}_{-0.0003}$	$^{+0.9}_{-1.1}$	$^{+0.7}_{-0.4}$
	$0.0188^{+0.0002}_{-0.0001}$	$^{+0.4}_{-0.5}$	$^{+0.7}_{-0.4}$	$0.0187^{+0.0002}_{-0.0001}$	$^{+0.5}_{-0.5}$	$^{+0.7}_{-0.4}$
	$0.0221^{+0.0003}_{-0.0003}$	$^{+1.2}_{-1.4}$	$^{+0.9}_{-0.6}$	$0.0221^{+0.0003}_{-0.0004}$	$^{+1.2}_{-1.5}$	$^{+0.9}_{-0.6}$
	$0.0172^{+0.0002}_{-0.0002}$	$^{+0.7}_{-0.8}$	$^{+0.9}_{-0.6}$	$0.0172^{+0.0002}_{-0.0002}$	$^{+0.7}_{-0.8}$	$^{+0.9}_{-0.6}$
R_K	$1.00030^{+0.00010}_{-0.00007}$	$^{+0.004}_{-0.003}$	$^{+0.010}_{-0.006}$	$1.00031^{+0.00010}_{-0.00007}$	$^{+0.004}_{-0.003}$	$^{+0.010}_{-0.006}$
	$1.00037^{+0.00010}_{-0.00007}$	$^{+0.004}_{-0.003}$	$^{+0.010}_{-0.006}$	$1.00038^{+0.00011}_{-0.00007}$	$^{+0.004}_{-0.003}$	$^{+0.010}_{-0.006}$
	$1.00032^{+0.00010}_{-0.00007}$	$^{+0.004}_{-0.003}$	$^{+0.010}_{-0.006}$	$1.00033^{+0.00011}_{-0.00007}$	$^{+0.004}_{-0.003}$	$^{+0.010}_{-0.006}$
	$1.00039^{+0.00011}_{-0.00007}$	$^{+0.004}_{-0.003}$	$^{+0.010}_{-0.006}$	$1.00040^{+0.00011}_{-0.00007}$	$^{+0.004}_{-0.003}$	$^{+0.010}_{-0.007}$

Table 3.5: SM predictions for $\mathcal{B}_\mu$ (in units of 10^{-7}), F_H^μ and R_K for charged and neutral B-meson decays and different q^2 cuts $(q^2_{\rm min}, q^2_{\rm max}) = (1,6), (2,6), (1,7), (2,7)\,{\rm GeV}^2$ (from top to bottom). The uncertainties from the form factor $\xi_P(q^2)$ and the renormalization scale μ_b varied between $m_b/2$ and $2m_b$ are also given separately in percent of the central value. The corresponding branching ratios with electrons, $\mathcal{B}_e$, agree within uncertainties with the ones with muons, $\mathcal{B}_\mu$.

Second, the deviation of $R_K^{\rm SM}$ from 1 is mainly due to the inclusion of effects of $\mathcal{O}\left(m_\mu^4/q^4\right) \sim 10^{-4}$ given in (3.72).

The numerical analysis, carried out within the numerical input from Table 3.4, confirms the qualitative properties of Γ_l and R_K described above. In Table 3.5 we summarize our numerics giving the predictions for the two channels, $B^- \to K^- \bar{l}l$ and $\bar{B}^0 \to \bar{K}^0 \bar{l}l$. The splitting between the B^- and $\bar{B}^0$ modes branching ratios is of $\mathcal{O}\,(10\%)$ due to the difference in lifetime and small isospin breaking terms in $\mathcal{T}_P$. For the Γ_l the dominant errors come from uncertainties in the form factor ξ_P, the CKM matrix element V_{ts} and the renormalization scale μ_b. Adding errors in quadrature gives the combined uncertainty from $\xi_P(q^2)$, μ_b and V_{ts} which can be as large as 32% (see Table 3.5). At low dilepton mass, the form factor has an uncertainty between $(12-16)\%$, with smaller uncertainty for larger q^2 due to the findings from Light Cone Sum Rules (LCSR) [80]. We find that the μ_b-dependence of the decay rate is rather small, about a few percent, as can be seen from Figure 3.6 (left-hand plot). The small uncertainty due to μ_b is not unexpected because of the inclusion of NNLL

corrections to the matrix elements of the current-current operators [88, 89, 90] in $\mathcal{T}_P$, which cancels the μ_b-dependence of $C_9^{\rm SM}$. Further subleading sources are the lifetime with 0.7% uncertainty and $\alpha_e(\mu)$, which enters quadratically and brings in about 6% uncertainty to the $B \to K\bar{l}l$ decay rates. The uncertainties in Γ_l from the charm, bottom and top mass are $2\%, 0.4\%$ and 2%, respectively.

In the right-hand plot of Figure 3.6 we plot Γ_μ for three lower cuts $q^2_{\rm min} = \{0.5, 1, 2\}$ GeV^2 as a function of the upper boundary $q^2_{\rm max}$. The bands show dependence on the uncertainties from $\xi_P(q^2)$, μ_b and V_{ts}. The Figure 3.7 presents a dependence on $q^2_{\rm max}$ done for different cuts $q^2_{\rm min} = \{0.5, 1, 2\}$ GeV^2. As already expected above, the cancellation of the hadronic uncertainties is observed in R_K, see also Table 3.5. The combined error from form factor and the renormalization scale is tiny. One can conclude that in the SM R_K is 1 with high precision (deviation from 1 is of $\mathcal{O}\left(m_\mu^4/q^4\right)$, see (3.72)), what makes this observable so attractive to study possible NP effects characterized by non-universal lepton couplings. It should be noticed that the additional lepton flavor dependence can appear in R_K due to the QED bremsstrahlung corrections. In the case of the inclusive $B \to X_s\bar{l}l$ decay these corrections are computed in [67] and enhanced by the logarithms $\ln(m_b^2/m_l^2)$. However, in the exclusive decay case such corrections are unknown.

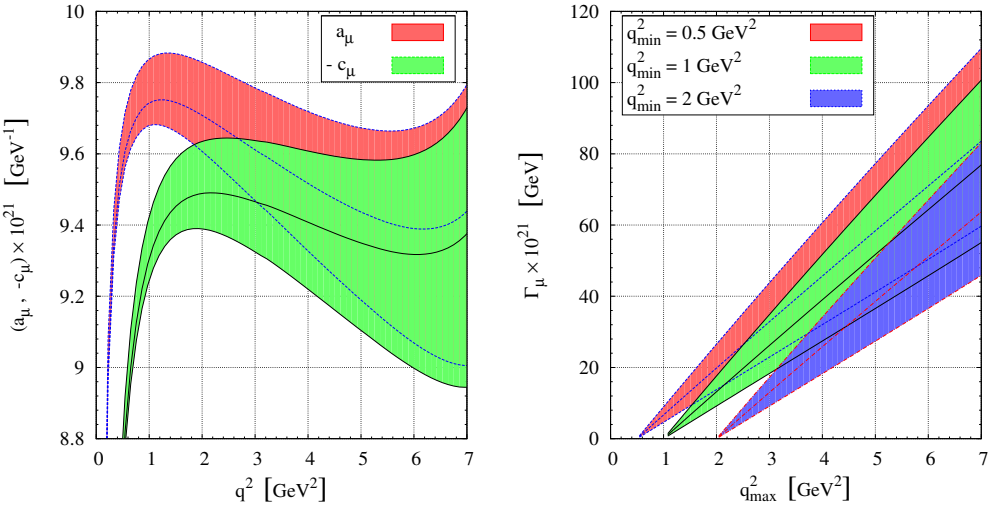

Figure 3.6: In the left-hand plot $a_l(q^2)$ and $-c_l(q^2)$ defined in (3.60) are shown for $l = \mu$ in the SM as a function of q^2 for the renormalization scale μ_b between $m_b/2$ and $2m_b$. In the right-hand plot the SM $B \to K\bar{\mu}\mu$ decay rate is given for three different cuts $q^2_{\rm min} = \{0.5, 1, 2\}$ GeV^2 as a function of $q^2_{\rm max}$. Here the bands take into account uncertainties from the form factor ξ_P, μ_b and V_{ts}.

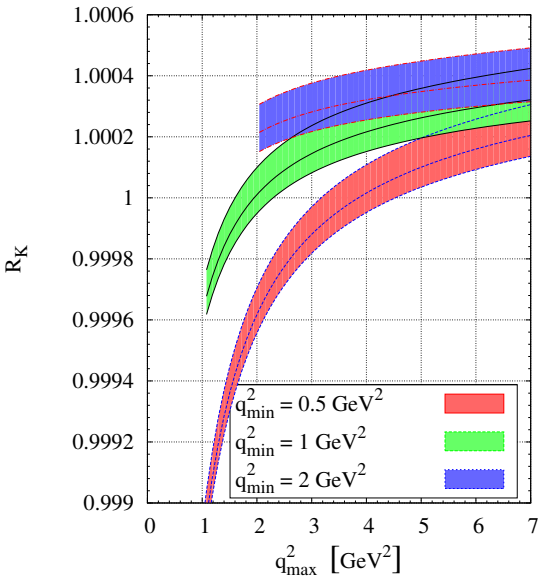

Figure 3.7: The ratio R_K in the SM for different cuts $q^2_{\text{min}} = \{0.5, 1, 2\}$ GeV^2 as a function of q^2_{max}. The uncertainties from the scale μ_b and the form factor are added in quadrature.

The other interesting observable is F_H^l (3.68), being similarly to R_K a ratio which leads to cancellation of hadronic and other uncertainties. This concerns the ones from the form factor, the renormalization scale, V_{ts} and unknown subleading $1/E$ corrections in $\mathcal{T}_P$. In the same way as for Γ_l we apply symmetry relations for the form factors (3.48) and (3.71) in order to obtain an expression for F_H^l in the SM at low q^2:

$$F_H^{l\,\text{SM}} = 2m_l^2 \frac{\Gamma_0}{\Gamma_l{}^{\text{SM}}} \int_{q^2_{\text{min}}}^{q^2_{\text{max}}} \frac{dq^2}{q^2}\, \xi_P^2(q^2) \sqrt{\lambda}^3 \beta_l (|F_A|^2 + |F_V|^2) \times \left\{ 1 + \frac{q^2}{M_B^2} \times \mathcal{O}\left(\alpha_s, \frac{q^2}{M_B^2} \sqrt{\frac{\Lambda_{\text{QCD}}}{E}} \right) \right\}, \tag{3.73}$$

where the denominator $\Gamma_l{}^{\text{SM}}$ is given in (3.72). The leading terms cancel in the sum $a_l + c_l$ and as a result $F_H^{l\,\text{SM}} \propto m_l^2$ and $F_H^{e\,\text{SM}}/F_H^{\mu\,\text{SM}} \propto m_e^2/m_\mu^2$ such that $F_H^{e\,\text{SM}}$ is negligible. This fact can be also seen from the Figure 3.6 (left-hand plot). In Figure 3.8 (also Table 3.5) one can see the cancellation of uncertainties transparently, where F_H^μ is plotted for $q^2_{\text{min}} = 0.5, 1, 2$ GeV^2 versus the upper integration boundary q^2_{max}. The value of F_H^μ becomes larger for smaller dilepton mass intervals. It also increases for lower values of the lower cut q^2_{min}. The tiny bands indicate small errors due to ξ_P and μ_b, combining which gives the uncertainty of $F_H^\mu \lesssim 2\%$. Here, in the numerical analysis we skip an additional uncertainty from the subleading power

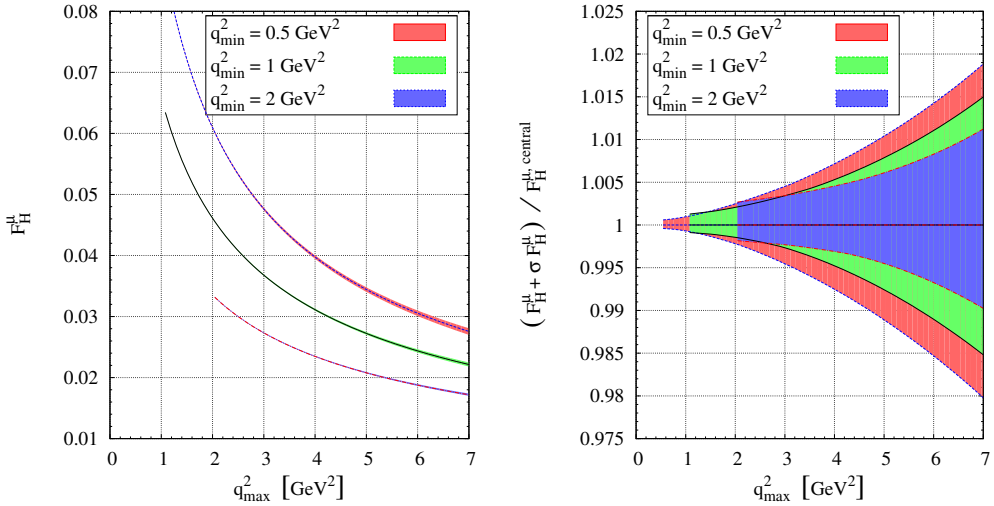

Figure 3.8: The observable F_H^μ in the SM depending on q^2_{max} for three cuts $q^2_{\text{min}} = \{0.5, 1, 2\}\,\text{GeV}^2$ (left-hand plot) and normalized to the central value (right-hand plot). The bands include combined uncertainties from μ_b and the form factor $\xi_P(q^2)$.

corrections. These subleading corrections contributing to form factor symmetry breaking relations are known [79] and give additional uncertainties to F_H^μ of order $q^4/M_B^4\sqrt{\Lambda_{\text{QCD}}/E} \sim 3\%$. We expect, that the subleading corrections for the hard scattering part which have not been calculated yet, contribute to F_H^μ at the order $q^2/M_B^2\alpha_s\sqrt{\Lambda_{\text{QCD}}/E} \sim 3\%$ assuming the same power counting as for the soft overlap part. Thus, combining the errors one can predict F_H^μ with maximal precision of $\sim \mathcal{O}(6\%)$ in the SM. For the electron channel F_H^e becomes a null test of the SM due to the huge suppression coming from m_e^2.

3.5.2 Angular Distribution in $B \to K^*(\to K\pi)\bar{l}l$

In the most general case the decay $\bar{B}^0 \to \bar{K}^{*0}(\to K^-\pi^+)\bar{l}l$ can be characterized by five kinematic variables considering an off-shell K^* meson in narrow width approximation [59]. Here we follow [63] where the limit of an on-shell K^* has been considered. In this approximation the differential decay rate of $\bar{B}^0 \to \bar{K}^{*0}(\to K^-\pi^+)\bar{l}l$, when summing over the spin of the final state particles, reads

$$\frac{d^4\Gamma}{dq^2\, d\cos\theta_l\, d\cos\theta_{K^*}\, d\phi} = \frac{3}{8\pi} J(q^2, \theta_l, \theta_{K^*}, \phi). \tag{3.74}$$

Note that we use $\bar{B} \equiv (b\bar{d})$ and $\bar{K}^{0*} \equiv (s\bar{d})$. The angular dependence can be explicitly written as

$$\begin{aligned} J(q^2, \theta_l, \theta_{K^*}, \phi) = {} & J_1^s \sin^2\theta_{K^*} + J_1^c \cos^2\theta_{K^*} + (J_2^s \sin^2\theta_{K^*} + J_2^c \cos^2\theta_{K^*}) \cos 2\theta_l \\ & + J_3 \sin^2\theta_{K^*} \sin^2\theta_l \cos 2\phi + J_4 \sin 2\theta_{K^*} \sin 2\theta_l \cos\phi \\ & + J_5 \sin 2\theta_{K^*} \sin\theta_l \cos\phi + J_6 \sin^2\theta_{K^*} \cos\theta_l + J_7 \sin 2\theta_{K^*} \sin\theta_l \sin\phi \\ & + J_8 \sin 2\theta_{K^*} \sin 2\theta_l \sin\phi + J_9 \sin^2\theta_{K^*} \sin^2\theta_l \sin 2\phi, \end{aligned} \tag{3.75}$$

where the coefficients $J_i^{(a)} = J_i^{(a)}(q^2)$ for $i = 1, \ldots, 9$ and $a = s, c$ are functions of the dilepton mass q^2. Here θ_l is the angle between the negatively charged lepton and the $\bar{B}$ in the dilepton center of mass system (CMS) and θ_{K^*} denotes the angle between the K^- and the $\bar{B}$ in the $(K^-\pi^+)$ CMS. The angle ϕ is given by the normals of the two planes defined by the $(K^-\pi^+)$ and (l^+l^-) pairs, respectively, in the rest frame of the $\bar{B}$. The kinematically accessible phase space is

$$4m_l^2 \leqslant q^2 \leqslant (M_B - M_{K^*})^2, \quad -1 \leqslant \cos\theta_l \leqslant 1, \quad -1 \leqslant \cos\theta_{K^*} \leqslant 1, \quad 0 \leqslant \phi \leqslant 2\pi. \tag{3.76}$$

The corresponding distribution of the CP conjugated decay $B^0 \to K^{*0}(\to K^+\pi^-)\bar{l}l$ can be written as

$$\frac{d^4\bar{\Gamma}}{dq^2\, d\cos\theta_l\, d\cos\theta_{K^*}\, d\phi} = \frac{3}{8\pi} \bar{J}(q^2, \theta_l, \theta_{K^*}, \phi). \tag{3.77}$$

Here, θ_{K^*} denotes the angle between the Kaon and the B meson in the $(K^+\pi^-)$ CMS. The definition of θ_l is identical for both B and $\bar{B}$ decays. Again, the angle ϕ is given by the normals of the two planes defined by the $(K^+\pi^-)$ and (l^+l^-) pairs. The functions $\bar{J}_i$ are obtained from J_i in (3.75) by the replacements (see Appendix B.1)

$$J_{1,2,3,4,7}^{(a)} \to \bar{J}_{1,2,3,4,7}^{(a)}(\delta_W \to -\delta_W), \qquad J_{5,6,7} \to -\bar{J}_{5,6,8,9}(\delta_W \to -\delta_W), \tag{3.78}$$

the conjugation of weak phases denoted collectively by δ_W is understood [59].

Let us discuss the CP properties of the angles in the angular distributions (3.75) and (3.78). We have three angles θ_l, θ_{K^*} and ϕ which correspond to the decay $\bar{B} \to \bar{K}^{0*}(\to K^-\pi^+)l^+l^-$, and the angles $\bar{\theta}_l, \bar{\theta}_{K^*}$ and $\bar{\phi}$ of the CP conjugate decay $B \to K^{0*}(\to K^+\pi^-)l^+l^-$ (in (3.77) we have skipped the bars in the notation of the angles, but reintroduce them here for clearness). We denote by $\mathbf{p}_i(\bar{\mathbf{p}}_i), \mathbf{q}_i(\bar{\mathbf{q}}_i)$ and $\mathbf{k}_i(\bar{\mathbf{k}}_i)$ the three momentum vectors of particle i in the $\bar{B}(B)$, lepton pair and $\bar{K}^*(K^*)$ rest frame, respectively. Let us further take the direction of motion of the $\bar{K}^*$ meson along the z-axis in the $\bar{B}$ rest frame. One can then define three unit

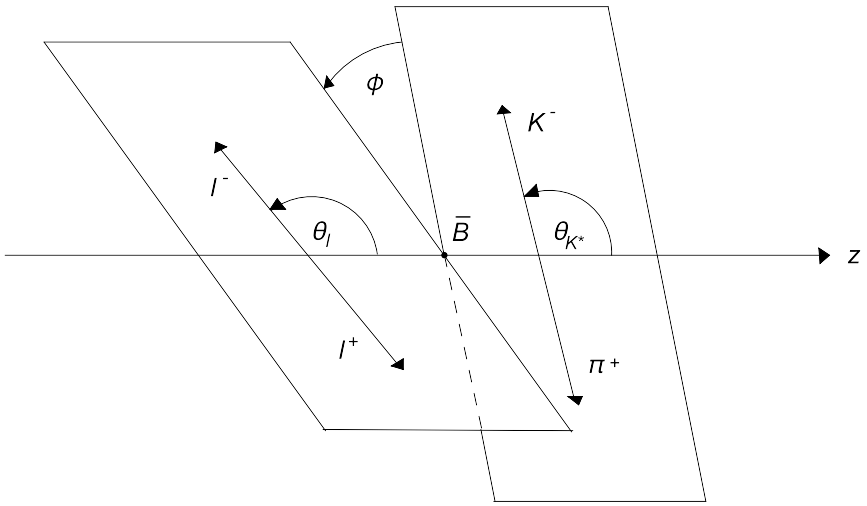

Figure 3.9: The kinematical angles in $\bar{B} \to \bar{K}^{0*}(\to K^-\pi^+)l^+l^-$ decays.

vectors

$$\mathbf{e}_z = \frac{\mathbf{p}_{K^-} + \mathbf{p}_{\pi^+}}{|\mathbf{p}_{K^-} + \mathbf{p}_{\pi^+}|}, \qquad \mathbf{e}_l = \frac{\mathbf{p}_{l^-} \times \mathbf{p}_{l^+}}{|\mathbf{p}_{l^-} \times \mathbf{p}_{l^+}|}, \qquad \mathbf{e}_K = \frac{\mathbf{p}_{K^-} \times \mathbf{p}_{\pi^+}}{|\mathbf{p}_{K^-} \times \mathbf{p}_{\pi^+}|} \tag{3.79}$$

for the $\bar{B}$ decay and correspondingly

$$\bar{\mathbf{e}}_z = \frac{\bar{\mathbf{p}}_{K^+} + \bar{\mathbf{p}}_{\pi^-}}{|\bar{\mathbf{p}}_{K^+} + \bar{\mathbf{p}}_{\pi^-}|}, \qquad \bar{\mathbf{e}}_l = \frac{\bar{\mathbf{p}}_{l^+} \times \bar{\mathbf{p}}_{l^-}}{|\bar{\mathbf{p}}_{l^+} \times \bar{\mathbf{p}}_{l^-}|}, \qquad \bar{\mathbf{e}}_K = \frac{\bar{\mathbf{p}}_{K^+} \times \bar{\mathbf{p}}_{\pi^-}}{|\bar{\mathbf{p}}_{K^+} \times \bar{\mathbf{p}}_{\pi^-}|} \tag{3.80}$$

for the decay of the B meson. One can now define the angles $\theta_l, \theta_{K^*}, \phi$ for $\bar{B} \to \bar{K}^{0*}(\to K^-\pi^+)l^+l^-$ decays as

$$\sin\theta_l = \frac{(\mathbf{k}_{l^-} \times \mathbf{e}_z) \cdot \mathbf{e}_l}{|\mathbf{k}_{l^-}|}, \qquad \cos\theta_l = \frac{\mathbf{k}_{l^-} \cdot \mathbf{e}_z}{|\mathbf{k}_{l^-}|}, \tag{3.81}$$

$$\sin\theta_{K^*} = \frac{(\mathbf{q}_{K^-} \times \mathbf{e}_z) \cdot \mathbf{e}_l}{|\mathbf{q}_{K^-}|}, \qquad \cos\theta_{K^*} = \frac{\mathbf{q}_{K^-} \cdot \mathbf{e}_z}{|\mathbf{q}_{K^-}|}, \tag{3.82}$$

$$\sin\phi = (\mathbf{e}_l \times \mathbf{e}_K) \cdot \mathbf{e}_z, \qquad \cos\phi = \mathbf{e}_K \cdot \mathbf{e}_l. \tag{3.83}$$

Likewise, we have for $B \to K^{0*}(\to K^+\pi^-)l^+l^-$ decays

$$\sin\bar{\theta}_l = \frac{(\bar{\mathbf{k}}_{l^-} \times \bar{\mathbf{e}}_z) \cdot \bar{\mathbf{e}}_l}{|\bar{\mathbf{k}}_{l^-}|}, \qquad \cos\bar{\theta}_l = \frac{\bar{\mathbf{k}}_{l^-} \cdot \bar{\mathbf{e}}_z}{|\bar{\mathbf{k}}_{l^-}|}, \tag{3.84}$$

$$\sin\bar{\theta}_{K^*} = \frac{(\bar{\mathbf{q}}_{K^+} \times \bar{\mathbf{e}}_z) \cdot \bar{\mathbf{e}}_l}{|\bar{\mathbf{q}}_{K^+}|}, \qquad \cos\bar{\theta}_{K^*} = \frac{\bar{\mathbf{q}}_{K^+} \cdot \bar{\mathbf{e}}_z}{|\bar{\mathbf{q}}_{K^+}|}, \tag{3.85}$$

$$\sin\bar{\phi} = (\bar{\mathbf{e}}_l \times \bar{\mathbf{e}}_K) \cdot \bar{\mathbf{e}}_z, \qquad \cos\bar{\phi} = \bar{\mathbf{e}}_K \cdot \bar{\mathbf{e}}_l. \tag{3.86}$$

Since under CP $\mathbf{p}_{i^\pm} \to -\bar{\mathbf{p}}_{i^\mp}$, the unit vectors transform as

$$\mathbf{e}_z \to \bar{\mathbf{e}}_z = -\mathbf{e}_z, \qquad \mathbf{e}_{K,l} \to \bar{\mathbf{e}}_{K,l} = \mathbf{e}_{K,l}. \tag{3.87}$$

It is easy to see from the formulae above that only $\sin\phi$ is odd under the CP transformation and the other are CP even where we apply (3.87). We summarize the CP properties of the following quantities:

$$\sin\phi \xrightarrow{CP} \sin\bar{\phi} = -\sin\phi, \tag{3.88}$$

$$\cos\phi \xrightarrow{CP} \cos\bar{\phi} = \cos\phi, \tag{3.89}$$

$$\sin\theta_{l,K^*} \xrightarrow{CP} \sin\bar{\theta}_{l,K^*} = -\sin\theta_{l,K^*}, \tag{3.90}$$

$$\cos\theta_{l,K^*} \xrightarrow{CP} \cos\bar{\theta}_{l,K^*} = -\cos\theta_{l,K^*}. \tag{3.91}$$

Transversity Amplitudes

The functions J_i^a are expressed in terms of transversity amplitudes (see Appendix B.1) $A_\perp$, $A_\parallel$ and A_0 being the functions of Wilson coefficients and form factors. Here we are giving the expressions for the transversity amplitudes in the presence of NP Wilson coefficients within QCDF and neglecting kinematical terms[1] $M_{K^*}^2/M_B^2$. They read as

$$\begin{aligned}
A_\perp^{L,R} &= +\sqrt{2} N M_B (1-\hat{s}) \left\{ \Big[(C_9 + C_9') \mp (C_{10} + C_{10}') \Big] \xi_\perp + \frac{2\hat{m}_b}{\hat{s}} \mathcal{T}_\perp^+ \right\}, \\
A_\parallel^{L,R} &= -\sqrt{2} N M_B (1-\hat{s}) \left\{ \Big[(C_9 - C_9') \mp (C_{10} - C_{10}') \Big] \xi_\perp + \frac{2\hat{m}_b}{\hat{s}} \mathcal{T}_\perp^- \right\}, \\
A_0^{L,R} &= -\frac{N M_B^2 (1-\hat{s})^2}{2 M_{K^*} \sqrt{\hat{s}}} \left\{ \Big[(C_9 - C_9') \mp (C_{10} - C_{10}') \Big] \xi_\parallel - 2\hat{m}_b \mathcal{T}_\parallel^- \right\}, \\
A_t &= \frac{N M_B^2 (1-\hat{s})^2}{M_{K^*} \sqrt{\hat{s}}} (C_{10} - C_{10}') \frac{\xi_\parallel}{\Delta_\parallel},
\end{aligned} \tag{3.92}$$

where

$$\hat{s} = \frac{q^2}{M_B^2}, \qquad \hat{m}_b = \frac{m_b}{M_B}, \qquad N = \left[\frac{G_F^2 \alpha_e^2}{3 \cdot 2^{10} \pi^5 M_B} |V_{tb} V_{ts}^*|^2 \, \hat{s} \, \sqrt{\lambda} \, \beta_l \right]^{1/2} \tag{3.93}$$

and

$$\lambda = M_B^4 + M_{K^*}^4 + q^4 - 2(M_B^2 M_{K^*}^2 + M_B^2 q^2 + M_{K^*}^2 q^2), \quad \beta_l = \sqrt{1 - \frac{4m_l^2}{q^2}}. \tag{3.94}$$

[1] These formally subleading terms in the $1/E$ expansion are included in the numerical evaluation.

Note that A_t contributes only for $m_l \neq 0$ and contains $\Delta_\parallel$, see [19], which represents form factor symmetry breaking QCD corrections. Note that helicity conservation dictates $A_\perp^{L,R} = -A_\parallel^{L,R}$ for $C_i' = 0$ up to $1/E$ corrections [91].

In the framework of QCDF, the functions $\mathcal{T}_{\perp,\parallel}^{\pm}$ are calculated at $1/m_b$ order in heavy quark mass expansion and at NLO in α_s for the SM operators and the corresponding chirality flipped operators, see (3.9). The $\mathcal{T}_{\perp,\parallel}^{\pm}$ have the following CKM and QCD structure

$$\begin{aligned}
\mathcal{T}_a^{\pm} &= \mathcal{T}_a^{\pm(t)} + \hat{\lambda}_u \mathcal{T}_a^{(u)}, \\
\mathcal{T}_a^{\pm(t)} &= \mathcal{T}_a^{\pm(t),\mathrm{LO}} + \frac{\alpha_s}{4\pi}\mathcal{T}_a^{\pm(t),\mathrm{NLO}}, \qquad \mathcal{T}_a^{(u)} = \mathcal{T}_a^{(u),\mathrm{LO}} + \frac{\alpha_s}{4\pi}\mathcal{T}_a^{(u),\mathrm{NLO}},
\end{aligned} \tag{3.95}$$

where $a = \perp, \parallel$. At LO in α_s (denoted by the superscript (0)) and neglecting numerically small weak annihilation terms in $\mathcal{T}_\parallel^{\pm(t),}$ we have

$$\begin{aligned}
\mathcal{T}_\perp^{\pm(t),\mathrm{LO}} &= \xi_\perp \left[C_7^{\mathrm{eff}(0)} \pm C_7^{\prime(0)} + \frac{q^2}{2m_b M_B} Y^{(0)} \right], \qquad \mathcal{T}_\perp^{(u),\mathrm{LO}} = \xi_\perp \frac{q^2}{2m_b M_B} Y^{(u)(0)}, \\
\mathcal{T}_\parallel^{\pm(t),\mathrm{LO}} &= -\xi_\parallel \left[C_7^{\mathrm{eff}(0)} \pm C_7^{\prime(0)} + \frac{M_B}{2m_b} Y^{(0)} \right] + HS, \quad \mathcal{T}_\parallel^{(u),\mathrm{LO}} = -\xi_\parallel \frac{M_B}{2m_b} Y^{(u)(0)} + HS
\end{aligned} \tag{3.96}$$

where spectator effects are denoted by HS (complete expressions can be found in Appendix B.4). Two kind of phases are contained in the $\mathcal{T}_{\perp,\parallel}^{\pm}$ functions. The weak phase comes from the CKM matrix, i.e. $\hat{\lambda}_u$ pre-factor. The strong phases come at LO in α_s from $Y(q^2)$ and $Y^{(u)}(q^2)$, [19, 20], containing 1-loop contributions of four-quark operators $\sim \bar{s}b\bar{q}q$ with an imaginary part if $q^2 > 4m_q^2$. These phases are small in the low q^2-region, where the $1/E$ expansion of QCDF is valid, which is below the charm threshold (the origin of large phases coming from the $c\bar{c}$ resonances). In this low q^2-region the lighter quarks induce either CKM suppressed or penguin contributions leading to small strong phases. At higher order in α_s, strong phases are further generated in $\mathcal{T}_a^{(i),\mathrm{NLO}}$ and from spectator interactions [19, 20], which have been included in our numerical analysis. The form factors $\xi_\perp$ and $\xi_\parallel$ are discussed in Section 3.4.

Branching Ratio and A_{FB}

The differential decay rate for $\bar{B}^0 \to \bar{K}^{*0}(\to K^-\pi^+)\bar{l}l$ decays can be obtained after integration of (3.75) over all angles. It is simply a linear combination of J_1 and J_2

$$\frac{d\Gamma}{dq^2} = J_1 - \frac{J_2}{3}, \quad \text{where} \quad J_{1,2} \equiv 2J_{1,2}^s + J_{1,2}^c. \tag{3.97}$$

It can be also rewritten more explicitly, i.e., in terms of the transversity amplitudes (3.92) as

$$\frac{d\Gamma}{dq^2} = |A_\perp^L|^2 + |A_\parallel^L|^2 + |A_0^L|^2 + (L \to R) + \mathcal{O}\left(m_l^2/q^2\right) \tag{3.98}$$

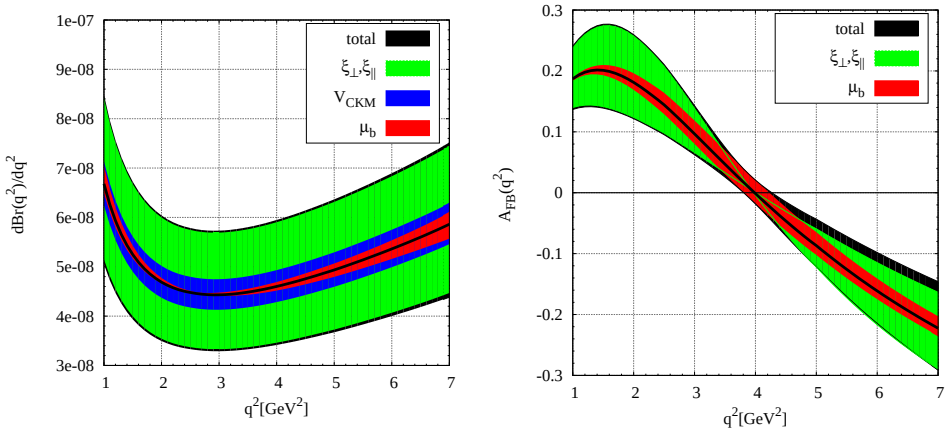

Figure 3.10: The differential branching ratio (right-hand plot) and $A_{\rm FB}(q^2)$ (left-hand plot) in the SM as functions of the dilepton invariant mass calculated in the QCDF. The bands show the uncertainties of the form factors, the CKM parameters, μ_b and the total uncertainties (by adding errors in quadrature) separately.

up to contributions suppressed by the lepton mass.

The (normalized) forward-backward asymmetry $A_{\rm FB}$ is given after full ϕ and θ_{K^*} integration as [2]

$$A_{\rm FB}(q^2) \equiv \left[\int_0^1 - \int_{-1}^0\right] d\cos\theta_l \frac{d^2\Gamma}{dq^2\, d\cos\theta_l} \Bigg/ \frac{d\Gamma}{dq^2} = J_6 \Bigg/ \frac{d\Gamma}{dq^2}. \tag{3.99}$$

By $d\bar{\Gamma}/dq^2$ and $\bar{A}_{\rm FB}(q^2)$ we refer to the corresponding spectra of the CP conjugated decays.

We worked out both $d\Gamma/dq^2$ and $A_{\rm FB}(q^2)$ in the SM using QCDF. In Figure 3.10 we plot the differential branching ratio, which is just $d\Gamma/dq^2$ multiplied by life time τ_{B^0}, and $A_{\rm FB}(q^2)$ as functions of q^2. The various bands represent the three dominant uncertainties coming from the form factors, renormalization scale μ_b and the CKM parameters. We vary the scale between $m_b/2$ and $2m_b$ and allow for an uncertainty of 11% and 14% for $\xi_\perp$ and $\xi_\parallel$, respectively. The CKM input is given in Table 3.4. For the total uncertainty estimate, all three sources of uncertainty are added in quadrature.

[2] Since we define the lepton angle θ_l with respect to the l^-, our definiton of the forward-backward asymmetry (3.99) differs from the one in other works using the l^+, e.g., [19, 20, 92], by a global sign.

In the left-hand plot of Figure 3.10 one can see that the dominant uncertainties to the decay rate come from the form factors $\xi_\perp$ and $\xi_\parallel$. From the formulae (3.92) and (3.98) follows that the longitudinal amplitudes $A_0^{L,R}$ are enhanced by M_B/M_{K^*} with respect to $A_\perp^{L,R}$, $A_\parallel^{L,R}$, what implies a stronger dependence of $d\Gamma/dq^2$ on $\xi_\parallel$ than on $\xi_\perp$.

In the framework of QCDF we calculate numerically in the SM the quantities $\mathcal{F}_{L,T}$ defined as

$$\mathcal{F}_L = \frac{\langle |A_0^L|^2 + |A_0^R|^2 \rangle}{\langle d\Gamma/dq^2 \rangle}, \tag{3.100}$$

and

$$\mathcal{F}_T = \frac{\langle |A_\perp^L|^2 + |A_\perp^R|^2 + |A_\parallel^L|^2 + |A_\parallel^R|^2 \rangle}{\langle d\Gamma/dq^2 \rangle}, \tag{3.101}$$

being the longitudinal and transversal K^* contribution to the total decay rate, respectively. Here we introduce a short notation for q^2-integrated quantities

$$\langle X \rangle = \int_{q^2_{\rm min}}^{q^2_{\rm max}} dq^2\, X(q^2). \tag{3.102}$$

For the cuts $(q^2_{\rm min}, q^2_{\rm max}) = (1,6)\,\text{and}\,(1,7)$ GeV^2 $\mathcal{F}_L$ is $0.73^{+0.08}_{-0.10}$ and $0.72^{+0.08}_{-0.11}$, respectively. Whereas $\mathcal{F}_T$ for the same cuts is $0.27^{+0.11}_{-0.08}$ and $0.28^{+0.11}_{-0.09}$.

The dominant error to $A_{\rm FB}$ comes also from form factors. The numerator of $A_{\rm FB}$ presented by function J_6 is proportional to $\xi_\perp^2$ at LO in QCDF, whereas the denominator being the decay rate is dominated by $\xi_\parallel$. The independent variation of $\xi_\perp$ and $\xi_\parallel$ gives about 30% error of $A_{\rm FB}$ for the upper part of the region $1-7$ GeV^2.

CP Asymmetries

To reveal CP violation effects of a theory there should exist a non-trivial phase, which can not be removed by any field transformations and there should exist an observable which depends on this phase. Particularly, in the SM this phase resides in the CKM matrix, as a result of the fact that the SM has three generations.

To construct CP-odd observables having the structure of $|M|^2 - |\bar{M}|^2$, where M and $\bar{M}$ are the matrix elements of to each other CP conjugated processes, one needs several contributing amplitudes. The relative phases appearing in the matrix element can be of two kinds, conventionally called "weak" and "strong" phases. A weak phase has an opposite sign in the CP-conjugated process and a strong one has the same one. As an example, we consider the matrix element of the $i \to f$ transition in terms of two contributing amplitudes A_1 and A_2

$$M(i \to f) = A_1 e^{i\delta_W} + A_2 e^{i\delta_S} \tag{3.103}$$

where the phase δ_W changes the sign in the CP-conjugated matrix element $\bar{M}$ and δ_S not. Computing $|M|^2 - |\bar{M}|^2$ one finds that CP-odd observables are proportional to $\sin\delta_W \sin\delta_S$ and vanishes when one of the phases goes to zero.

There are basically two types of origins of the strong phases. In perturbative calculations they appear as absorptive parts in the loop integrals. The second origin is the so-called final-state-interaction scattering. In this case the transition $i \to f' \to f$ has two parts, $i \to f'$ is due to the weak interaction and $f' \to f$ is due to the strong interaction. If the f' intermediate state is on mass shell then this generates an absorptive part (strong phase) in the amplitude.

Using the discrete symmetry T (is not same as the time reversal invariance), which changes the signs of all particle momenta and spins, one can classify CP-odd observables. The observable discussed above is CP-odd and T-even and generally proportional to quantities like $\sin\delta_W \sin\delta_S$. T-even observables depend on a strong phase and can be additionally suppressed in the case if the latter is small. On the other hand CP-odd T-odd observables are proportional to quantities like $\sin\delta_W \cos\delta_S + \cos\delta_W \sin\delta_S$ and survive in the case $\delta_S \to 0$. Typically, CP-odd T-odd observables are proportional to the triple product of three momenta or spin vectors $\vec{p}_1 \cdot \vec{p}_2 \times \vec{p}_3$ originating from the Lorenz invariant expression $\epsilon_{\mu\nu\alpha\beta} p_1^\mu p_2^\nu p_3^\alpha p_4^\beta$ (in the rest of frame of p_4). Particularly, considering $B \to K^*$ transitions one can find the Levi-Civita tensor in the definition of QCD form factors (3.42)-(3.43). Such terms with a triple product generate terms in the decay rate, as for the CP-conjugated process, being

$$\mathrm{Im}[A_1 A_2^*]\, \vec{p}_1 \cdot \vec{p}_2 \times \vec{p}_3 \tag{3.104}$$

which will contribute to CP-odd observables if the relative weak phase is contained either in A_1 or A_2. The nice property of CP-odd T-odd observables is that they are non zero even in the case when the strong phases vanish.

In the case of $\bar{B}^0 \to \bar{K}^{*0}(\to K^- \pi^+) \bar{l} l$ decays CP violating effects in the angular distribution are signaled by non-vanishing differences between the (q^2-dependent) angular coefficients

$$\Delta J_i^{(a)} = \Delta J_i^{(a)}(q^2) \equiv J_i^{(a)} - \bar{J}_i^{(a)}. \tag{3.105}$$

Using these differences one can construct CP-odd T-even and T-odd observables. Under T-transformation the coefficients $J_{7,8,9}$ are odd ($\phi \to -\phi$ under T) and hence induce T-odd asymmetries $\Delta J_{7,8,9}$ which are not suppressed by small strong phases predicted from QCDF. The remaining coefficients J_i will induce T-even asymmetries which will be suppressed by small strong phases.

The CP asymmetry in the dilepton mass distribution, being T-even quantity, is

commonly defined as (see (3.97))

$$A_{\rm CP}(q^2) \equiv \frac{d(\Gamma-\bar{\Gamma})}{dq^2}\Bigg/\frac{d(\Gamma+\bar{\Gamma})}{dq^2} = \frac{1}{N_\Gamma}\left[\Delta J_1 - \frac{\Delta J_2}{3}\right], \quad N_\Gamma = N_\Gamma(q^2) = \frac{d(\Gamma+\bar{\Gamma})}{dq^2}. \tag{3.106}$$

Following [59], we define in addition to $A_{\rm CP}$ seven normalized CP asymmetries as

$$A_i(q^2) \equiv \frac{2\Delta J_i}{N_\Gamma} \text{ for } i=3,6,9, \qquad A_i^D(q^2) \equiv -\frac{2\Delta J_i}{N_\Gamma} \text{ for } i=4,5,7,8, \tag{3.107}$$

where again $A_{3,6}$ and $A_{4,5}^D$ are T-even, and A_9 and $A_{7,8}^D$ are T-odd observables. We then define the normalized q^2-integrated CP asymmetries as

$$\langle A_i\rangle \equiv 2\frac{\langle\Delta J_i\rangle}{\langle N_\Gamma\rangle} \text{ for } i=3,6,9, \qquad \left\langle A_i^D\right\rangle \equiv -2\frac{\langle\Delta J_i\rangle}{\langle N_\Gamma\rangle} \text{ for } i=4,5,7,8, \tag{3.108}$$

where the numerator and the denominator are integrated with the same q^2 cuts which should be in the low dilepton mass region in order to be consistent with the QCDF formalism (see Section 3.5.2).

These CP asymmetries can be extracted from the differential decay rate (3.74) by partial integration over the angles. Particularly, integrating (3.74) over θ_{K^*} gives the double-differential distribution in θ_l and ϕ,

$$\begin{aligned}\frac{d^2\langle\Gamma\rangle}{d\cos\theta_l\, d\phi} = \frac{1}{4\pi}\big\{ &\langle J_1\rangle + \langle J_2\rangle\cos 2\theta_l + 2\langle J_3\rangle\sin^2\theta_l\cos 2\phi \\ &+ 2\langle J_6\rangle\cos\theta_l + 2\langle J_9\rangle\sin^2\theta_l\sin 2\phi\big\},\end{aligned} \tag{3.109}$$

which can be used to extract the CP asymmetry $\langle A_6\rangle$. Further integration over θ_l gives

$$\frac{d\langle\Gamma\rangle}{d\phi} = \frac{1}{2\pi}\left\{\langle J_1\rangle - \frac{\langle J_2\rangle}{3} + \frac{4}{3}\langle J_3\rangle\cos 2\phi + \frac{4}{3}\langle J_9\rangle\sin 2\phi\right\}, \tag{3.110}$$

which shows the possibility of finding $\langle\Delta J_9\rangle$ from $d\left\langle\Gamma+\bar{\Gamma}\right\rangle/d\phi$, whereas $\langle\Delta J_3\rangle$ can be obtained from $d\left\langle\Gamma-\bar{\Gamma}\right\rangle/d\phi$, with $\langle\Delta J_1\rangle - \langle\Delta J_2\rangle/3$ from $A_{\rm CP}$ without angular study, see (3.106).

The construction of the CP asymmetries $\langle A_i^D\rangle$ $(i=4,5,7,8)$ requires binning into $\cos\theta_{K^*}$ as

$$\begin{aligned}\frac{d^2\langle A_{\theta_{K^*}}\rangle}{d\cos\theta_l\, d\phi} &\equiv \left[\int_0^1 - \int_{-1}^0\right] d\cos\theta_{K^*}\,\frac{d^3\langle\Gamma\rangle}{d\cos\theta_{K^*}\, d\cos\theta_l\, d\phi} \\ &= \frac{1}{2\pi}\big\{\langle J_4\rangle\sin 2\theta_l\cos\phi + \langle J_5\rangle\sin\theta_l\cos\phi \\ &\quad + \langle J_7\rangle\sin\theta_l\sin\phi + \langle J_8\rangle\sin 2\theta_l\sin\phi\big\}.\end{aligned} \tag{3.111}$$

Performing the θ_l-integration leads to the distribution

$$\frac{d\left\langle A_{\theta_{K^*}}\right\rangle}{d\phi} = \frac{1}{4}\left\{\langle J_5\rangle \cos\phi + \langle J_7\rangle \sin\phi\right\} \tag{3.112}$$

giving the possibility of extracting $\langle \Delta J_5 \rangle$ from $d\left\langle A_{\theta_{K^*}} + \bar{A}_{\theta_{K^*}}\right\rangle/d\phi$ whereas $\langle \Delta J_7 \rangle$ can be obtained from $d\left\langle A_{\theta_{K^*}} - \bar{A}_{\theta_{K^*}}\right\rangle/d\phi$.

The double asymmetry in θ_{K^*} and θ_l,

$$\frac{d\left\langle A_{\theta_{K^*},\theta_l}\right\rangle}{d\phi} \equiv \left[\int_0^1 - \int_{-1}^0\right] d\cos\theta_l \, \frac{d^2\left\langle A_{\theta_{K^*}}\right\rangle}{d\cos\theta_l \, d\phi} = \frac{2}{3\pi}\left\{\langle J_4\rangle \cos\phi + \langle J_8\rangle \sin\phi\right\}, \tag{3.113}$$

then allows to obtain $\langle \Delta J_4 \rangle$ from $d\left\langle A_{\theta_{K^*},\theta_l} - \bar{A}_{\theta_{K^*},\theta_l}\right\rangle/d\phi$, whereas $\langle \Delta J_8 \rangle$ can be extracted from $d\left\langle A_{\theta_{K^*},\theta_l} + \bar{A}_{\theta_{K^*},\theta_l}\right\rangle/d\phi$.

Note that only A_3, A_6 and A_9 can be obtained from a genuinely single differential distribution. A_9 is the only T-odd asymmetry with this property.

Another way of the extraction is based on the construction of corresponding weight functions W_i which project out J_i from the decay distribution (3.74), see Appendix B.2.

Let us discuss the SM predictions of the CP asymmetries applying the framework of QCDF. The complete NLO in α_s and LO in $1/E$ analytical expressions for CP asymmetries in the low-q^2 region are given in Appendix B.3. Those expressions can be reduced to the SM ones by setting NP Wilson coefficients $C_{7,9,10}^{(\prime),\mathrm{NP}} = 0$. In the large recoil limit the symmetry relations reduce the seven QCD form factors to the two form factors $\xi_\perp$ and $\xi_\parallel$. To calculate $\xi_{\perp,\parallel}$ we use q^2-dependent fits of $B \to K^*$ form factors from light cone QCD sum rules (LCSR) [81], see Section 3.4.

In the SM CP asymmetries $A_i^{(D)}$ are uniquely induced by the phase of the CKM matrix. Therefore an overall factor

$$\mathrm{Im}[\hat{\lambda}_u] = \mathrm{Im}\Big[\frac{V_{ub}V_{us}^*}{V_{tb}V_{ts}^*}\Big] \simeq \bar{\eta}\lambda^2, \tag{3.114}$$

where λ and $\bar{\eta}$ are Wolfenstein parameters, gives a suppression of $\mathcal{O}(10^{-2})$. Due to this fact all CP asymmetries obtain a universal 15% uncertainty coming from the variation of the CKM matrix parameters in the ranges given in Table 3.4.

Together with the CKM parameters, the form factors and the renormalization scale μ_b are dominant sources of uncertainties in CP asymmetries. Similarly as in Section 3.5.2, we vary the scale between $m_b/2$ and $2m_b$ and for $\xi_\perp$ and $\xi_\parallel$ we assume a flat (not depending on q^2) uncertainty of 11% and 14%, respectively. For the total uncertainty estimate, all three sources of uncertainty are added in quadrature.

In the Figure 3.11 we plot T-even CP asymmetries, i.e., $A_{\mathrm{CP},6}(q^2)$ and $A_{4,5}^D(q^2)$ as functions of q^2. From the plots one can see that LO and NLO results are comparable to each other, therefore impact of higher order terms to these particular T-even

	SM $\cdot 10^{-3}$	$\xi_{\perp,\parallel}[\%]$	$\mu_b[\%]$	SM LO $\cdot 10^{-3}$	SM($B^{\mp}$) $\cdot 10^{-3}$
$\langle A_{CP}\rangle$	$4.2^{+1.7}_{-2.5}$	$^{+19}_{-24}$	$^{+33}_{-51}$	$3.0^{+1.2}_{-1.5}$	$10.0^{+2.3}_{-2.9}$
	$4.8^{+1.7}_{-2.4}$	$^{+13}_{-17}$	$^{+29}_{-44}$	$3.1^{+1.2}_{-1.6}$	$9.9^{+2.2}_{-2.8}$
$\langle A_4^D\rangle$	$-1.8^{+0.3}_{-0.3}$	$^{+11}_{-8}$	$^{+2}_{-6}$	$-0.7^{+0.4}_{-0.4}$	$-0.7^{+0.4}_{-0.3}$
	$-2.0^{+0.4}_{-0.4}$	$^{+11}_{-8}$	$^{+7}_{-8}$	$-0.8^{+0.5}_{-0.4}$	$-1.1^{+0.4}_{-0.4}$
$\langle A_5^D\rangle$	$7.6^{+1.5}_{-1.6}$	$^{+10}_{-13}$	$^{+7}_{-8}$	$2.7^{+0.8}_{-1.2}$	$10.0^{+2.2}_{-2.3}$
	$7.6^{+1.5}_{-1.6}$	$^{+9}_{-12}$	$^{+7}_{-9}$	$2.7^{+0.8}_{-1.2}$	$9.8^{+2.1}_{-2.1}$
$\langle A_6\rangle$	$-6.4^{+2.2}_{-2.7}$	$^{+31}_{-39}$	$^{+0}_{-2}$	$-1.9^{+1.0}_{-0.9}$	$-6.3^{+2.1}_{-2.6}$
	$-6.7^{+2.2}_{-2.7}$	$^{+30}_{-37}$	$^{+1}_{-3}$	$-2.0^{+1.1}_{-1.0}$	$-6.6^{+2.2}_{-2.7}$
$\langle A_7^D\rangle$	$-5.1^{+2.4}_{-1.6}$	$^{+11}_{-8}$	$^{+42}_{-26}$	$< 10^{-2}$	$-7.1^{+2.6}_{-1.9}$
	$-4.6^{+2.1}_{-1.4}$	$^{+10}_{-6}$	$^{+42}_{-25}$		$-6.5^{+2.3}_{-1.7}$
$\langle A_8^D\rangle$	$3.5^{+1.4}_{-2.0}$	$^{+7.4}_{-10}$	$^{+37}_{-53}$	$0.2^{+0.04}_{-0.08}$	$3.4^{+1.4}_{-2.0}$
	$3.1^{+1.3}_{-1.7}$	$^{+6}_{-10}$	$^{+37}_{-53}$	$0.14^{+0.03}_{-0.06}$	$3.1^{+1.3}_{-1.8}$
$\langle A_{3,9}\rangle^{\dagger}$	$\mathcal{O}(1)$			$\mathcal{O}(1)$	$\mathcal{O}(1)$

Table 3.6: SM predictions for the integrated CP asymmetries in units of 10^{-3} with the integration boundaries $(q^2_{\rm min}, q^2_{\rm max}) = (1,6), (1,7)$ GeV^2 (from top to bottom). We take into account uncertainties from the form factors, the scale dependence μ_b and the CKM parameters, all of them added in quadrature. The form factor uncertainty employed is 11% and 14% for $\xi_\perp$ and $\xi_\parallel$, respectively, and μ_b is varied within $[m_b/2, 2m_b]$. The relative uncertainties due to $\xi_\perp, \xi_\parallel$ and μ_b are also shown separately. The asymmetries at LO in α_s and the NLO ones for charged B-decays are given as well, see text for details. †The leading contributions $\langle A_{3,9}\rangle$ in the SM are power counting estimates only.

asymmetries is numerically sizeable, but qualitatively less pronounced. For the NLO result we also show separately the uncertainty dependence from the form factors, CKM parameters and μ_b by plotting various bands.

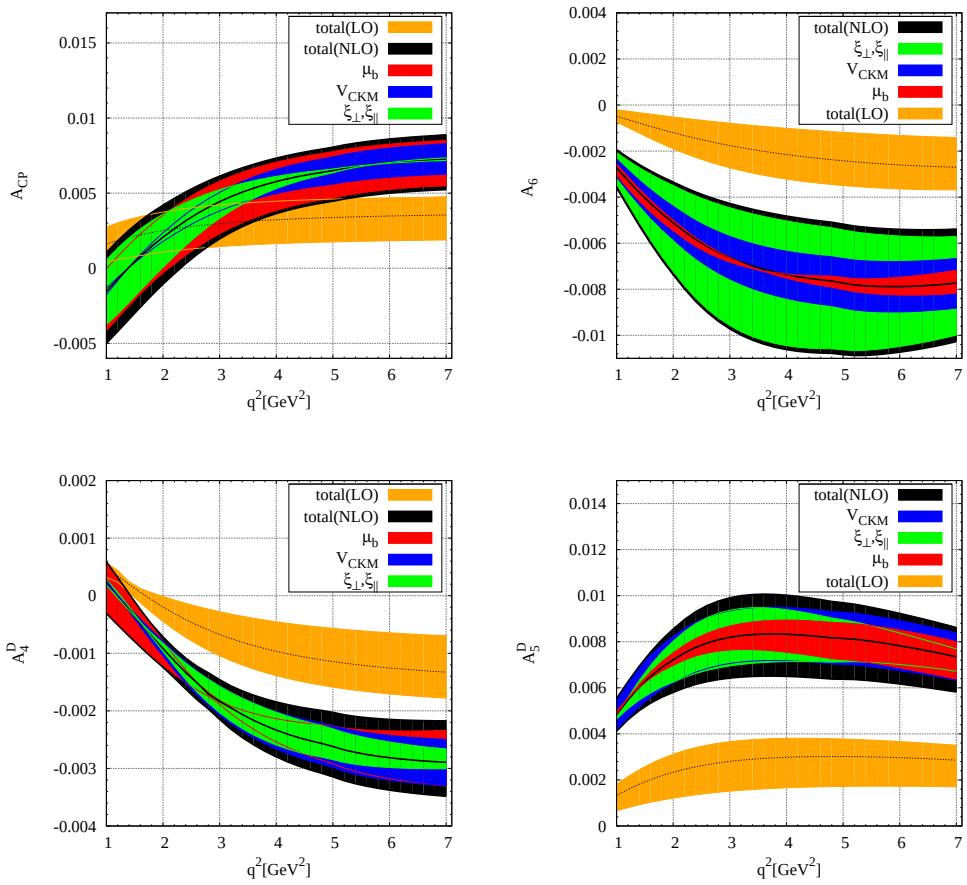

Figure 3.11: The T-even CP asymmetries $A_{\mathrm{CP},6}(q^2)$ and $A^D_{4,5}(q^2)$ in the SM in the low-q^2 region at LO and NLO in QCDF. The various bands show the uncertainty due to the form factors, the CKM parameters and μ_b separately, whereas the overall band indicates the total uncertainty.

In contrast to T-even asymmetries the higher order terms in the T-odd $A^D_{7,8}(q^2)$ asymmetries are even more dominant, see Figure 3.12. Particularly, at LO in α_s A^D_7 asymmetry, i.e.,

$$A_7^D \sim \mathrm{Im}[\hat{\lambda}_u]\mathrm{Re}\left[\frac{\mathcal{T}_\perp^{(u)}}{\xi_\perp} + \frac{q^2}{M_B^2}\frac{\mathcal{T}_\parallel^{(u)}}{\xi_\parallel}\right], \tag{3.115}$$

vanishes due to cancellations of the terms in the square brackets [93]. (Our value of A^D_7 at LO is tiny but finite since in the numerical analysis we do not neglect kinematical factors $M^2_{K^*}/M^2_B$.) Therefore adding higher order α_s corrections increase

the value of A_7^D drastically. That is what we observe on the left-hand plot of Figure 3.12.

The similar cancellations at LO happens in the A_8^D asymmetry, i.e.,

$$A_8^D \sim \mathrm{Im}[\hat{\lambda}_u]\mathrm{Re}\left[\frac{2m_b}{M_B}\frac{\left(\mathcal{T}_\perp^{(u)}\mathcal{T}_\parallel^{(t)*} - \mathcal{T}_\perp^{(t)}\mathcal{T}_\parallel^{(u)*}\right)}{\xi_\perp\xi_\parallel} - \left(\frac{\mathcal{T}_\perp^{(u)}}{\xi_\perp} + \frac{q^2}{M_B^2}\frac{\mathcal{T}_\parallel^{(u)}}{\xi_\parallel}\right)C_9^{\mathrm{SM}}\right], \tag{3.116}$$

although here an additional numerically subleading LO term exists (the first term in square brackets), giving a small contribution, see Figure 3.12.

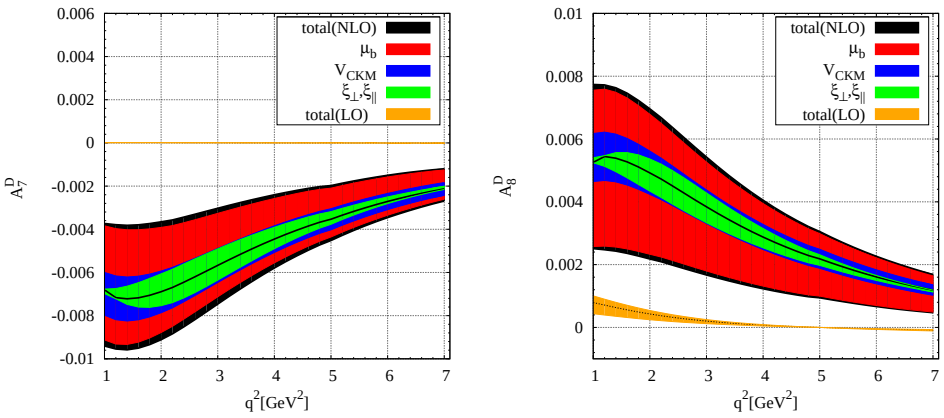

Figure 3.12: The T-odd CP asymmetries $A_{7,8}^D(q^2)$ in the SM in the low-q^2 region at LO and NLO in QCDF. The various bands show the uncertainty due to the form factors, the CKM parameters and μ_b separately, whereas the overall band indicates the total uncertainty.

The T-even A_3 and T-odd A_9 CP asymmetries are considered separately since they vanish in the SM at lowest order in $1/E$. Being the result of higher order in $1/E$

$$A_{3,9} \sim \mathrm{Im}[\hat{\lambda}_u]\,\mathcal{O}(\Lambda_{\mathrm{QCD}}/E) \sim \mathcal{O}(10^{-3}), \tag{3.117}$$

the numerical values of $A_{3,9}$ are expected to be smaller then the other CP asymmetries.

We present in Table 3.6 the integrated CP asymmetries for the two cuts $(q^2_{\mathrm{min}}, q^2_{\mathrm{max}}) = (1,6)$ GeV^2 (upper entries) and $(1,7)$ GeV^2 (lower entries), respectively. The predictions are given for both neutral and charged B-decays. In the case of neutral modes we consider the results in detail, by showing LO values of CP asymmetries and giving separate information about form factor and renormalization scale uncertainties.

The form factor induced uncertainty in the asymmetries depends on the amount of cancellations between the numerator and the decay rate in the denominator. We recall that we vary the two form factors within their uncertainties independently. The denominators of CP asymmetries, i.e., decay rates, are dominated by $\xi_\parallel$ (see Section 3.5.2), whereas the numerators are proportional to $\xi_\perp^2$ for A_6 and $\xi_\perp \xi_\parallel$ for the $A^D_{4,5,7,8}$. Therefore the cancellations in $A^D_{4,5,7,8}$ are expected to be more pronounced than in A_6. The numerator of $A_{\rm CP}$ has a more complicated structure leading to an intermediate size of cancellations. From the second column of the Table 3.6 one can see that the biggest, about 40%, form factor uncertainties appear in A_6, whereas for $A^D_{4,5,7,8}$ the errors do not exceed 13%.

As can be seen from Table 3.6, $\langle A_{\rm CP} \rangle$, $\langle A_7^D \rangle$ and $\langle A_8^D \rangle$ exhibit a massive μ_b dependence of order 50 %. The CP asymmetries $A_i^{(D)}$ with $i = 4, 5, 6$ are not subject of the cancellations mentioned after (3.115) and have a smaller residual μ_b uncertainty below ten percent. The μ_b dependence of $\langle A_6 \rangle$ of a few percent is accidentally small due to significant cancellations between different q^2-regions, see the crossing of the μ_b bands in A_6 near $q^2 \simeq (3-4)\,{\rm GeV}^2$ in Figure 3.11.

The last column in Table 3.6 shows the NLO SM predictions for charged B-decays. The splitting between the CP asymmetries in neutral versus charged B-decays is dominated by weak annihilation contributions from current-current operators and varies a lot in size: $\langle A^D_{5,7} \rangle$ ($\langle A_{\rm CP} \rangle$) increase by $\mathcal{O}(30\%)$ (a factor of two) from neutral to charged B-decays, whereas $\langle A_4^D \rangle$ decreases by $\sim 1/2$. The splitting for $\langle A^{(D)}_{6,8} \rangle$ is at the few percent level.

In conclusion it should be said that in spite of large theoretical uncertainties for the SM predictions, CP asymmetries are very attractive for the search of NP CP violating phases. This advantage comes from the smallness of the CP asymmetries in the SM due to the CKM suppression. In the next section we will show that current experimental bounds on NP allow for huge enhancement of CP asymmetries, particularly T-odd ones, up to $\mathcal{O}\,(1)$.

3.6 New Physics Analysis

The NP section is split into two parts. In the first one we discuss the experimental constraints on NP from various FCNC B-decay observables. The second part is devoted to NP model-independent analysis of the obsevables defined in Section 3.5. It is shown that the large enhancements with respect to the SM contributions are allowed by the present data.

observable	sensitive to	SM value	data
F_H^μ	$C_{S,P}^\mu + C_{S,P}^{\mu\prime}$, $C_{T(5)}^\mu$	$\mathcal{O}(m_\mu^2/q^2)$	$0.81^{+0.58}_{-0.61} \pm 0.46^\dagger$ [55]
$A_{\rm FB}^\mu$	$C_{S,P}^\mu + C_{S,P}^{\mu\prime}$, $C_{T(5)}^\mu$	$\mathcal{O}(\alpha_e/(4\pi))$	$0.15^{+0.21}_{-0.23} \pm 0.08^\dagger$ [55] $0.10 \pm 0.14 \pm 0.01^\dagger$ [54]
$R_K - 1$	$C_{S,P}^l + C_{S,P}^{l\prime}$, $C_{T(5)}^l$, e vs. μ	$\mathcal{O}(10^{-4})$	$0.24 \pm 0.31^\dagger$ [53, 55]
$\mathcal{B}(\bar{B}_s \to \bar{\mu}\mu)$	$C_{S,P}^\mu - C_{S,P}^{\mu\prime}$	$(3.23 \pm 0.44) \cdot 10^{-9}$	$< 8.0 \cdot 10^{-8}$ [56]
$\mathcal{B}(\bar{B}_s \to \bar{e}e)$	$C_{S,P}^e - C_{S,P}^{e\prime}$	$(7.56 \pm 0.32) \cdot 10^{-14}$	$< 5.4 \cdot 10^{-5}$ [94]
$\mathcal{B}_\mu^{\rm incl}\vert_{[>0.04]}$	$C_S^{\mu(\prime)} \pm C_P^{\mu(\prime)}$, $C_{T(5)}^\mu$	$(4.15 \pm 0.70) \cdot 10^{-6}$ [57, 92]	$(4.3 \pm 1.2) \cdot 10^{-6}$ [15]
$\mathcal{B}_e^{\rm incl}\vert_{[>0.04]}$	$C_S^{e(\prime)} \pm C_P^{e(\prime)}$, $C_{T(5)}^e$	$(4.15 \pm 0.70) \cdot 10^{-6}$ [57, 92]	$(4.7 \pm 1.3) \cdot 10^{-6}$ [15]

Table 3.7: Observables in $b \to s\bar{l}l$ induced transitions and used in the NP analysis of $B \to K^*\bar{l}l$ decays. Upper bounds are given at 90% C.L. For details see text. †Data include q^2-regions where QCDF does not apply and both $l = e$ and μ are included.

observable	sensitive to	SM	data
$\mathcal{B}(\bar{B} \to X_s\gamma)^a$	C_7, C_7'	$(3.15 \pm 0.23) \cdot 10^{-4}$ [95]	$(3.52 \pm 0.25) \cdot 10^{-4}$ [96]
$S^b_{K^*\gamma}$	C_7, C_7'	$(-2.8^{+0.4}_{-0.5}) \cdot 10^{-2}$	-0.19 ± 0.23 [96, 97, 98]
$\mathcal{B}(\bar{B} \to X_s\bar{l}l)\vert_{[1,6]}$	$C_7^{(\prime)}$, $C_9^{(\prime)}$, $C_{10}^{(\prime)}$	$(1.59 \pm 0.11) \cdot 10^{-6}$ [67]	$(1.60 \pm 0.51) \cdot 10^{-6}$ [99]
$\mathcal{B}(\bar{B} \to X_s\bar{l}l)\vert_{[>0.04]}$	$C_7^{(\prime)}$, $C_9^{(\prime)}$, $C_{10}^{(\prime)}$	$(4.15 \pm 0.70) \cdot 10^{-6}$ [92]	$(4.5 \pm 1.0) \cdot 10^{-6}$ [15]
$\langle A_{\rm FB}\rangle^c_{[high\,q^2]}$	$C_7^{(\prime)}$, $C_9^{(\prime)}$, $C_{10}^{(\prime)}$	< 0	$-(0.76^{+0.52}_{-0.32} \pm 0.07)$ [55], also [53, 54]
$\mathcal{B}(\bar{B}_s \to \bar{\mu}\mu)$	$C_{10} - C_{10}^{'}$	$\simeq 3 \cdot 10^{-9}$	$< 4.7 \cdot 10^{-8}$ at 90% C.L. [100]

Table 3.8: Relevant $b \to s\gamma$ and $b \to s\bar{l}l$ observables used in the NP analysis of $B \to K^*\bar{l}l$ decays. ^{a}With photon energy cut $E_\gamma > 1.6$ GeV. ^{b}SM value obtained with $m_s = 0.12$ GeV. ^{c}Note the different lepton angle convention between [54, 55] and this work.

3.6.1 Experimental Constraints

In this section we discuss the experimental constraints on NP from different FCNC B-decay observables. For the case of the angular distribution in $B \to K\bar{l}l$ decays we discuss the observables sensitive to (pseudo-) scalar and tensor interactions. Relevant to $B \to K^*\bar{l}l$ decay analysis, we consider the observables being able to constrain the NP Wilson coefficients $C_i^{\rm NP}$ and $C_i^{\prime\rm NP} = C_i'$ for $i = 7, 9, 10$ corresponding to $\mathcal{O}_{7,9,10}$ and chirality-flipped $\mathcal{O}'_{7,9,10}$ operators in model-independent way. We allow the respective NP coefficients to be varied in a magnitude and a phase, denoted by ϕ_i.

$\bar{B}_s \to \bar{l}l$ Decay

A detailed study of the $b \to s\bar{l}l$ operators shows that not all contribute to the $\bar{B}_s \to \bar{l}l$. For instance, the matrix element $\langle 0|\bar{s}\sigma^{\mu\nu}b|\bar{B}_s\rangle$ vanishes since it depends

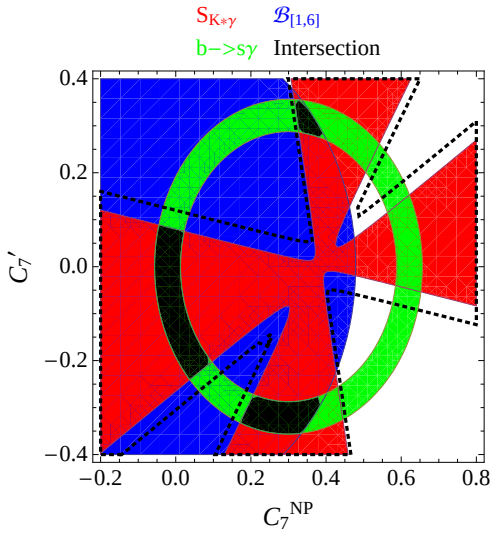

Figure 3.13: Allowed region for real $C_7^{\rm NP}$ and C_7'. The regions allowed by $\mathcal{B}(\bar{B} \to X_s\gamma)$, $S_{K^*\gamma}$ and $\mathcal{B}(\bar{B} \to X_s\bar{l}l)|_{[1,6]}$ are shown as the green ring, the red cross and the blue half circle, respectively.

only on the momentum p_{B_s} of the B_s meson, making it impossible to construct an antisymmetric tensor with respect to μ and ν indices. The contribution from the axial-vector matrix element $\langle 0|\bar{s}\gamma^\mu\gamma_5 b|B\rangle$ contracted with the leptonic vector current $\bar{l}\gamma^\mu l$ also vanishes since it is proportional $p^\mu_{B_s} = p^\mu_{l^+} + p^\mu_{l^-}$. Since $\bar{B}_s$ is a pseudoscalar particle the matrix elements of the $\bar{s}b$ and $\bar{s}\gamma^\mu b$ operators vanish too.

Thus, the remaining relevant operators relevant for $\bar{B}_s \to \bar{l}l$ are

$$(\bar{s}\gamma_\mu\gamma_5 b)(\bar{l}\gamma^\mu\gamma_5 l), \quad (\bar{s}\gamma_5 b)(\bar{l}\gamma_5 l), \quad (\bar{s}\gamma_5 b)(\bar{l}l). \tag{3.118}$$

Applying for these PCAC relations

$$\langle 0|\bar{s}\gamma^\mu\gamma_5 b|B\rangle = ip^\mu_{B_s} f_{B_s}, \qquad \langle 0|\bar{s}\gamma_5 b|B\rangle = -if_{B_s}\frac{M_{B_s}}{m_b + m_s}, \tag{3.119}$$

which express the matrix elements in terms of the decay constant f_{B_s}, momentum $p^\mu_{B_s}$ and mass M_{B_s} of the $\bar{B}_s$ meson, we can write the matrix element for the $\bar{B}_s \to \bar{l}l$ as [101, 72, 58]

$$\mathcal{M} = \frac{G_F\alpha_e}{\sqrt{2}\pi}V_{tb}V_{ts}^*\big[F_s\bar{l}l + (F_P + 2m_l F_A)\bar{l}\gamma_5 l\big], \tag{3.120}$$

where

$$F_A = -\frac{i}{2}f_{B_s}C_{10}, \qquad F_i = -\frac{i}{2}M^2_{B_s}f_{B_s}\Big[\frac{C_i - C_i'}{m_b + m_s}\Big], \quad i = S, P, \tag{3.121}$$

where $C^{(\prime)}_{S,P}$ are (pseudo-) scalar Wilson coefficients needed to be constrained for the $B \to K\bar{l}l$ analysis.

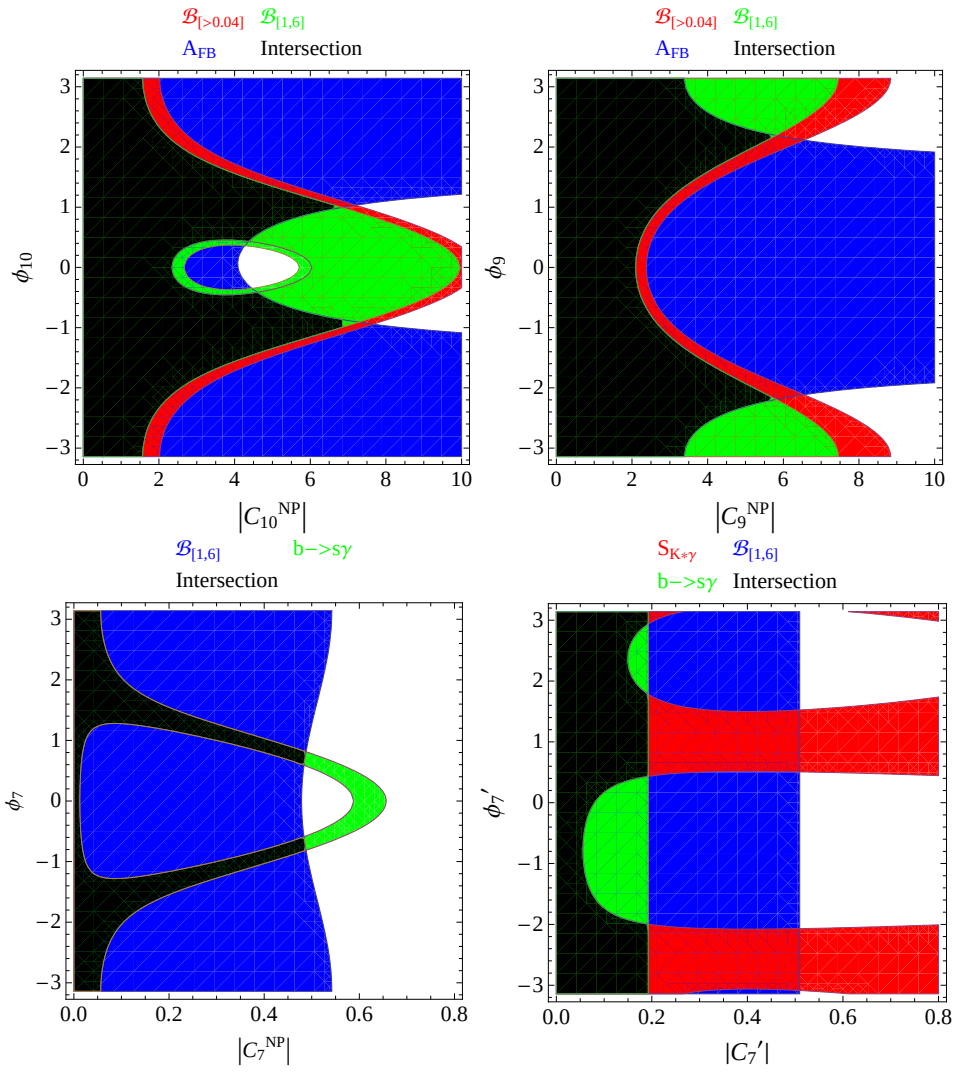

Figure 3.14: Allowed areas for the NP Wilson coefficients in particular scenarios: "C_9^{NP} only", "C_{10}^{NP} only", "C_7^{NP} only" and "C_7' only". The regions are constrained by $\mathcal{B}(\bar{B} \to X_s\gamma)$, $S_{K^*\gamma}$, $\mathcal{B}(\bar{B} \to X_s\bar{l}l)|_{[1,6]}$, $\mathcal{B}(\bar{B} \to X_s\bar{l}l)|_{[>0.04]}$ and integrated A_{FB}.

Finally, we ca write the branching ratio $\mathcal{B}(\bar{B}_s \to \bar{l}l)$ explicitly in terms of NP Wilson coefficients

$$\mathcal{B}(\bar{B}_s \to \bar{l}l) = \frac{G_F^2 \alpha_e^2 M_{B_s}^5 f_{B_s}^2 \tau_{B_s}}{64\pi^3} |V_{tb} V_{ts}^*|^2 \sqrt{1 - \frac{4m_l^2}{M_{B_s}^2}} \times \left\{ \left(1 - \frac{4m_l^2}{M_{B_s}^2}\right) \left| \frac{C_S^l - C_S^{l\prime}}{m_b + m_s} \right|^2 + \left| \frac{C_P^l - C_P^{l\prime}}{m_b + m_s} + \frac{2m_l}{M_{B_s}^2} C_{10} \right|^2 \right\}. \quad (3.122)$$

Tensor operators do not contribute to $\bar{B}_s \to \bar{l}l$ decays and hence $C_{T,T5}^l$ are not constrained by these decays. The $\bar{B}_s \to \bar{l}l$ branching ratios depend on the difference of Wilson coefficients $(C_{S,P}^l - C_{S,P}^{l\prime})$. It means that constraints from (3.122) can be evaded in the presence of both unprimed and primed (pseudo-)scalar Wilson coefficients. In the exclusive $B \to K, K^* \bar{l}l$ decays this can be avoided by the presence of a sum $(C_{S,P}^l + C_{S,P}^{l\prime})$ [68].

In the Table 3.7 we give current experimental upper bound on $\mathcal{B}(\bar{B}_s \to \bar{l}l)$ together with their SM values obtained with the input from Table 3.4. One should note that in the SM the branching ratio of $\bar{B}_s \to \bar{l}l$ is proportional to m_l^2 and for the electron mode is of order $\mathcal{O}(10^{-14})$, i.e., nine orders of magnitude smaller than the current upper bound from L3 [94]. As we show later, the current $\mathcal{B}(\bar{B}_s \to \bar{e}e)$ constraint is nevertheless on the verge of being useful, since NP in $C_{S,P}^{l(\prime)}$ does not enter the $\bar{B}_s \to \bar{l}l$ modes with m_l-suppression as the SM contribution, see (3.122). The current upper bound on $\mathcal{B}(\bar{B}_s \to \bar{\mu}\mu)$ comes from CDF and DØ [56]([102]) presented at 90% C.L. (95% C.L. $\mathcal{B}(\bar{B}_s \to \bar{\mu}\mu) < 5.8 \cdot 10^{-8}$) which is quite close to the SM prediction.

Inclusive $\bar{B} \to X_s \bar{l}l$ and $\bar{B} \to X_s \gamma$ Decays

In our analysis we take into account the further constraint which comes from the branching ration of the inclusive $\bar{B} \to X_s \bar{l}l$ decay. Currently, the inclusive decays can be predicted with better accuracy, especially in the low-q^2 region it has reached the level of $\lesssim 10\%$ [66, 90, 67, 103], but also the high-q^2 region is theoretically accessible [90, 104, 103] with larger uncertainties. In our analysis we use two regimes, i.e., the integrated branching ratio in the low-q^2 region with $q^2 \in [1, 6]$ GeV^2 $\mathcal{B}(\bar{B} \to X_s \bar{l}l)|_{[1,6]}$ as well as the whole q^2 region with $q^2 > 0.04$ GeV^2 $\mathcal{B}(\bar{B} \to X_s \bar{l}l)|_{[>0.04]}$. One should note that the latter case has some model-dependence due to the cuts of the first and second charm resonances in the experimental analysis.

The computational method of the $\bar{B} \to X_s \bar{l}l$ inclusive branching ratio differs from the exclusive ones. The matrix element of the $\bar{B} \to X_s$ transition (X_s is a sum of the states with strangeness S=1) can be computed in perturbation theory based on the method of the heavy quark expansion (HQE). Considering a non-relativistic theory of the b quark, the expansion takes place in terms of the inverse powers of the heavy

quark mass m_b. Employing the optical theorem, one can relate the decay rate to the absorptive part of the forward scattering amplitude $\mathrm{Im}(\langle\bar{B}|A|\bar{B}\rangle)$, with

$$A = i\int d^4x\, \mathrm{T}[H_{\mathrm{eff}}(x)H_{\mathrm{eff}}(0)], \tag{3.123}$$

where T is a time-ordering operation and H_{eff} is defined in (3.3). Inserting a complete set of the states inside of the time-ordered product we get an expression for the decay rate of the $\bar{B}\to X_s$

$$\Gamma(\bar{B}\to X_s) = \frac{1}{2M_B}\sum_{X_s}(2\pi)^4\delta^4(p_B - p_{X_s})|\langle X_s|H_{\mathrm{eff}}|\bar{B}\rangle|^2. \tag{3.124}$$

The leading term of the OPE in A corresponds to the lowest dimension operator $\bar{b}b$. It means that in the limit of $m_b\to\infty$ the decay rate of B meson is given by the decay rate of the b quark. The corrections to the leading order result are of $\mathcal{O}\,(1/m_b^2)$ with corresponding operators $\bar{b}(D)^2b$ and $\bar{b}\sigma^{\mu\nu}G_{\mu\nu}b$. There is no correction of $\mathcal{O}\,(1/m_b)$ because the corresponding operator $\bar{b}\not{D}b$ can be reduced to $\bar{b}b$.

Since for the $B\to K\bar{l}l$ decays we are interested in lepton flavor dependent physics, we apply the effective Hamiltonian H_{eff} extended by the NP operators (3.10) and write the q^2-cut dependent $\bar{B}\to X_s\bar{l}l$ branching ratios in terms of (pseudo-) scalar and tensor Wilson coefficients as (see, e.g., [105])

$$\begin{aligned}\mathcal{B}_l^{\mathrm{incl}}|_{[q^2_{\mathrm{min}},\,q^2_{\mathrm{max}}]} \equiv \mathcal{B}(\bar{B}\to X_s\bar{l}l) = {}& \mathcal{B}_l^{\mathrm{incl}}|_{[q^2_{\mathrm{min}},\,q^2_{\mathrm{max}}],\mathrm{SM}} + (|C_T^l|^2 + |C_{T5}^l|^2)\mathcal{M}_T \\ &+ (|C_S^l + C_P^l|^2 + |C_S^{l\prime} + C_P^{l\prime}|^2 + |C_S^l - C_P^l|^2 + |C_S^{l\prime} - C_P^{l\prime}|^2)\mathcal{M}_S,\end{aligned} \tag{3.125}$$

where

$$\mathcal{M}_{S,T} = \frac{\mathcal{B}_0}{2m_b^8}\int_{q^2_{\mathrm{min}}}^{q^2_{\mathrm{max}}} dq^2\; M_{S,T}(q^2), \qquad \mathcal{B}_0 = \frac{3\alpha_e^2}{(4\pi)^2}\frac{|V_{tb}V_{ts}^*|^2}{|V_{cb}|^2}\frac{\mathcal{B}(\bar{B}\to X_c l\bar{\nu}_l)}{f(m_c/m_b)\kappa(m_c/m_b)} \tag{3.126}$$

and

$$M_S(q^2) = 2q^2(m_b^2 - q^2)^2, \qquad M_T(q^2) = \frac{64}{3}(m_b^2 - q^2)^2(2m_b^2 + q^2). \tag{3.127}$$

The factor $\mathcal{B}_0$, is fixed due the normalization of $\mathcal{B}(\bar{B}\to X_s\bar{l}l)$ to the well measured experimental value of $\mathcal{B}(\bar{B}\to X_c l\bar{\nu}_l)$

$$\mathcal{B}(\bar{B}\to X_s\bar{l}l) = \mathcal{B}(\bar{B}\to X_c l\bar{\nu}_l)\int d\,q^2\frac{1}{\Gamma(\bar{B}\to X_c l\bar{\nu}_l)}\frac{d\,\Gamma(\bar{B}\to X_s\bar{l}l)}{d\,q^2} \tag{3.128}$$

in order to avoid a strong dependence on m_b^5.

In the expressions (3.127) we neglect kinematical factors of m_s and m_l in the NP part and evaluate (3.126) and (3.127) with a b-quark mass of 4.8 GeV, corresponding

to the pole mass in accordance with [57, 92]. The functions $f(m_c/m_b)$ and $\kappa(m_c/m_b)$ represent the phase space function and QCD corrections of the decay $\bar{B} \to X_c l \bar{\nu}_l$, respectively, and can be seen in [105].

Since $M_{S,T} > 0$ are positive for the whole kinematic region, (pseudo-) scalar and tensor like NP enhances the $\bar{B} \to X_s \bar{l}l$ branching ratios, and only the upper boundary of the experimental value of $\mathcal{B}(\bar{B} \to X_s \bar{l}l)$ becomes a constraint on the corresponding Wilson coefficients. Also, since $M_T \gg M_S$, the inclusive branching ratios are more sensitive to tensor than scalar and pseudoscalar operators.

There are two interesting kinematical ranges. First, the range $0.04\ \text{GeV}^2 < q^2 \leq m_b^2$ where the lepton flavor specified data exist, and we use these data as a constraint. For this range numerical values of $\mathcal{M}_{S,T}$ are

$$\mathcal{M}_S = 1.92 \cdot 10^{-8}, \quad \mathcal{M}_T = 1.84 \cdot 10^{-6}. \tag{3.129}$$

The $\mathcal{M}_{S,T}$-coefficients for the low dilepton mass region $1\ \text{GeV}^2 < q^2 \leq 6\ \text{GeV}^2$ are

$$\mathcal{M}_S = 0.52 \cdot 10^{-8}, \quad \mathcal{M}_T = 0.83 \cdot 10^{-6}. \tag{3.130}$$

Note that we used here the b-quark pole mass in the NP part of $\mathcal{B}(\bar{B} \to X_s \bar{l}l)$ as well. To be consistent with the SM results of [67] the $1S$ mass should be used once the next-to-leading order corrections to the NP part are known.

For the $B \to K \bar{l}l$ decay studies we neglect with (pseudo-) scalar and tensor interactions and rewrite the branching ratio of $\bar{B} \to X_s \bar{l}l$ decays as The branching ratio of $\bar{B} \to X_s \bar{l}l$ is

$$\begin{aligned}
&\mathcal{B}(\bar{B} \to X_s \bar{l}l)|_{[q^2_{\text{min}}, q^2_{\text{max}}]} = \mathcal{B}(\bar{B} \to X_s \bar{l}l)|_{[q^2_{\text{min}}, q^2_{\text{max}}],\text{SM}} \\
&+ \Bigg\{ \Big[|C_7^{\text{NP}}|^2 + |C_7'|^2 + 2\text{Re}(C_7^{\text{eff,SM}} C_7^{\text{NP}*}) \Big] \mathcal{M}_1 \\
&\quad + \text{Re}\Big(C_9 C_7^{\text{NP}*} + C_9^{\text{NP}} C_7^{\text{eff,SM}*} + C_9' C_7'^* \Big) \mathcal{M}_2 \\
&\quad + \Big(|C_9^{\text{NP}}|^2 + |C_9'|^2 + |C_{10}^{\text{NP}}|^2 + |C_{10}'|^2 + 2\text{Re}(C_9^{\text{SM}} C_9^{\text{NP}*} + C_{10}^{\text{SM}} C_{10}^{\text{NP}*}) \Big) \mathcal{M}_3 \Bigg\},
\end{aligned} \tag{3.131}$$

where the SM contribution has been splitted off. The q^2-cut-dependent functions

$\mathcal{M}_i$ read as

$$\mathcal{M}_1 = \frac{\mathcal{B}_0^{b\to s\bar{l}l}}{m_b^8}\int_{q^2_{\rm min}}^{q^2_{\rm max}} dq^2\,\frac{16}{3}\frac{m_b^2}{q^2}(m_b^2-q^2)(2m_b^4-m_b^2q^2-q^4),$$

$$\mathcal{M}_2 = \frac{\mathcal{B}_0^{b\to s\bar{l}l}}{m_b^8}\int_{q^2_{\rm min}}^{q^2_{\rm max}} dq^2\,16\,m_b^2(m_b^2-q^2)^2,$$

$$\mathcal{M}_3 = \frac{\mathcal{B}_0^{b\to s\bar{l}l}}{m_b^8}\int_{q^2_{\rm min}}^{q^2_{\rm max}} dq^2\,\frac{4}{3}(m_b^2-q^2)(m_b^4+m_b^2q^2-2q^4). \tag{3.132}$$

The experimental data as well as theory predictions are shown in Table 3.8. For those two integrations regions the quantities $\mathcal{M}_i$ have following values

- for $q^2 \in [1,6]$ GeV^2: $\mathcal{M}_1 = 3.61\cdot 10^{-6}$, $\mathcal{M}_2 = 0.58\cdot 10^{-6}$, $\mathcal{M}_3 = 0.06\cdot 10^{-6}$,
- for $q^2 \in [> 0.04]$ GeV^2: $\mathcal{M}_1 = 1.05\cdot 10^{-5}$, $\mathcal{M}_2 = 0.12\cdot 10^{-5}$, $\mathcal{M}_3 = 0.02\cdot 10^{-5}$,

where we used the b-quark pole mass $m_b^{pole} = 4.8$ GeV.

Since the NP parts of branching ratios are at LO, we take for the theoretical uncertainties of the NP part twice the SM uncertainty in order to account for the missing higher order terms.

For the NP analysis of the $C_{S,P}^{l(\prime)}$ and $C_{T,T5}^{l}$ Wilson coefficients we use branching ratios of the $\bar{B}\to X_s\bar{e}e$ and $\bar{B}\to X_s\bar{\mu}\mu$ decays for $q^2 > 0.04\,\text{GeV}^2$ denoted by $\mathcal{B}_l^{\rm incl}|_{[>0.04]}$ in Table 3.7. Since only for this kinematical region the numbers are accessible for the muon and electron channels separately. The experimental values can be compared with SM predictions taken from [57, 92]. The second region, $1\,\text{GeV}^2 < q^2 \leq 6\,\text{GeV}^2$, will be consider to predict $\mathcal{B}_l^{\rm incl}|_{[1,6]}$ for $l = e,\mu$ using $\mathcal{B}_e^{\rm incl}|_{[1,6],\rm SM} = (1.64\pm 0.11)\cdot 10^{-6}$ and $\mathcal{B}_\mu^{\rm incl}|_{[1,6],\rm SM} = (1.59\pm 0.11)\cdot 10^{-6}$ [67]. These values are close to the experimental world average $\mathcal{B}_l^{\rm incl}|_{[1,6],\rm exp} = (1.60\pm 0.51)\cdot 10^{-6}$ [99, 106, 107] which is lepton flavor averaged and we therefore can not use it as a constraint.

On the other hand for the analysis of the $C_i^{(\prime)\rm NP}$ Wilson coefficients we employ the branching ratios in the both q^2 regions, see Table 3.8, using the experimental data averaged over lepton flavor.

The most important and currently best measured are $\bar{B}\to X_s\gamma$ being sensitive to C_7' and $\bar{B}\to X_s\bar{l}l$ testing all 6 Wilson coefficients. For these processes branching ratios can be splitted into the SM and NP contributions. In the case of $\bar{B}\to X_s\gamma$ it reads as

$$\mathcal{B}(\bar{B}\to X_s\gamma) = \mathcal{B}(\bar{B}\to X_s\gamma)|_{\rm SM} + \mathcal{B}_0^{b\to s\gamma}\left(|C_7^{\rm NP}|^2 + 2{\rm Re}(C_7^{\rm eff,SM}C_7^{\rm NP\,*}) + |C_7'|^2\right) \tag{3.133}$$

with $C_7^{\text{eff,SM}}$ being real and

$$\mathcal{B}_0^{b\to s\gamma} = 6\frac{\alpha_e}{\pi}\left|\frac{V_{tb}V_{ts}^*}{V_{cb}}\right|^2 \frac{\mathcal{B}(\bar{B}\to X_c l\bar{\nu}_l)}{f(m_c/m_b)\kappa(m_c/m_b)}. \tag{3.134}$$

Here $f(m_c/m_b)$ and $\kappa(m_c/m_b)$ represent the phase space function and the QCD corrections of the semileptonic decay [108]. Both the SM branching ratio at NNLO and experimental one are given in Table 3.8 for the photon energy $E_\gamma > 1.6$ GeV cut.

A_{FB} Forward-Backward Asymmetry of $B \to K^* \bar{l} l$ Decays

We should notice that we do not consider in our analysis $B \to K\bar{l}l$ and $B \to K^*\bar{l}l$ decays as a constraint. The main reason is that currently available data are presented with q^2-cuts where QCDF does not apply. In addition the experimental and theoretical uncertainties are much larger.

Instead we consider the less stringent but important measurement of the forward-backward asymmetry A_{FB} of $B \to K^*\bar{l}l$ decays. We employ early data from Belle and BaBar [53, 54, 55], which strongly indicate that the sign of A_{FB} in the high-q^2 region above the second charmonium peak is SM-like. A rigorous theory calculation of the exclusive $B \to K^*\bar{l}l$ decays in this kinematical region can be facilitated with an operator product expansion in Λ_{QCD}/Q and m_c^2/Q^2 where $Q = \{\sqrt{q^2}, m_b\}$ put forward in [109]. The leading contribution and also the order m_c^2/Q^2 terms do not introduce new non-perturbative matrix elements beyond naive factorization. Corrections start to enter at $\mathcal{O}(\alpha_s \Lambda_{\text{QCD}}/Q)$. The framework holds at low recoil, $(M_B - M_{K^*})^2 - 2M_B\Lambda_{\text{QCD}} \lesssim q^2 < (M_B - M_{K^*})^2$, which covers the large dilepton mass region above the Ψ' resonance, $q^2 \gtrsim 14\ \text{GeV}^2$.

To leading order in the $1/Q$-expansion we obtain the A_{FB} at low recoil as

$$A_{\text{FB}}(q^2) \propto \text{Re}\Big[(C_9^{\text{eff}}(q^2) + \frac{2m_b^2}{q^2}C_7^{\text{eff}})\, C_{10}^* - (C_9' + \frac{2m_b^2}{q^2}C_7')\, C_{10}'^*\Big]. \tag{3.135}$$

The effective coefficients read as

$$C_7^{\text{eff}} = C_7 - \frac{C_3}{3} - \frac{4}{9}C_4 - \frac{20}{3}C_5 - \frac{80}{9}C_6 + \frac{\alpha_s}{4\pi}\Big[(C_1 - 6C_2)A(q^2) - C_8 F_8^{(7)}(q^2)\Big],$$

$$C_9^{\text{eff}} = C_9 + Y(q^2)|_{m_c=0}$$

$$+ \frac{\alpha_s}{4\pi}\Big[\frac{9}{2}C_1\, C(q^2) + (C_1 - 6C_2)(B(q^2) - \frac{1}{2}C(q^2)) - C_8 F_8^{(9)}(q^2)\Big], \tag{3.136}$$

where $Y(q^2)$ is given in Appendix B.4. The functions $F_8^{(7,9)}$ can be found in [19], whereas functions $A(q^2)$, $B(q^2)$ and $C(q^2)$ are given in [110].

Interestingly, the dependence on form factors can be factored out in $A_{\rm FB}$ (3.135) at this order. We require that the sign of the integrated $A_{\rm FB}$ over $q^2 > 14\,{\rm GeV}^2$ to be negative according to experimental observations, see Table 3.8 .

Time-Dependent CP Asymmetry in $\bar{B}_d, B_d \to K^{*0}(\to K^0\pi^0)\gamma$ Decays

Since the branching ratio of $\bar{B} \to X_s\gamma$ is not sensitive to interference of the $\mathcal{O}_7$ and $\mathcal{O}_7'$ operators (the interference of photons with different polarizations), we discuss the additional important constraint from the time-dependent CP asymmetry in $\bar{B}_d, B_d \to K^{*0}(\to K^0\pi^0)\gamma$ decays [111]. The asymmetry is given by

$$A_{\rm CP}(t) = \frac{\Gamma(\bar{B}(t) \to \bar{K}^*\gamma) - \Gamma(B(t) \to K^*\gamma)}{\Gamma(\bar{B}(t) \to \bar{K}^*\gamma) + \Gamma(B(t) \to K^*\gamma)} = S_{K^*\gamma}\sin(\Delta M_B t) - C_{K^*\gamma}\cos(\Delta M_B t), \tag{3.137}$$

where the term proportional to $S_{K^*\gamma}$ is responsible for the interference of photons with different polarizations. To illustrate this we give an expression of $S_{K^*\gamma}$ at the lowest order (indicated by the superscript (0) for the contributions already presented in the SM):

$$S_{K^*\gamma} = -\frac{2|r|}{1+|r|^2}\sin\left(2\beta - \arg(C_7^{(0)}C_7')\right), \qquad r = C_7'/C_7^{(0)}\,. \tag{3.138}$$

Here we assume that there is no physics beyond the SM in $B_d - \bar{B}_d$-mixing, and its phase is given by the CKM matrix elements. The dimensional analysis suggests that the SM value of $S_{K^*\gamma}$ can be larger than naive SM estimate $\mathcal{O}(m_s/m_b)$. Power corrections can give additional contributions to r of the order $C_2\Lambda_{\rm QCD}/(3m_bC_7) \sim 0.1$ [112]. We calculate $S_{K^*\gamma}$ using QCDF following [20] including α_s-corrections adding a rough estimate of power corrections according to [112].

Assuming $C_7^{\rm NP}$ and C_7' to be real and applying the data from Table 3.8 we plot the constrained parameter space in Figure 3.13. One can see that together with semileptonic decays $S_{K^*\gamma}$ plays significant role as a NP constraint. The regions allowed by $\mathcal{B}(\bar{B} \to X_s\gamma)$, $S_{K^*\gamma}$ and $\mathcal{B}(\bar{B} \to X_s\bar{l}l)|_{[1,6]}$ are shown as the green ring, the red cross and the blue half circle, respectively. Including the power corrections enlarges red cross to the dashed area. Therefore the present experimental situation is not sensitive to the inclusion of the power corrections, which enlarge a little bit the red cross to the dashed area, see Figure 3.13.

3.6.2 $B \to K\bar{l}l$: Beyond the Standard Model

New Physics in F_H^l, R_K and $A_{\rm FB}^l$

In this section we present expressions for F_H^l, R_K and $A_{\rm FB}^l$ depending on NP Wilson coefficients corresponding to the operators (3.10). The matrix element is modified

due to additional contributions from scalars and tensors and is written as

$$\mathcal{M}[B \to K\bar{l}l] = i\frac{G_F \alpha_e}{\sqrt{2}\pi} V_{tb} V_{ts}^* \, \xi_P(q^2) \Bigg(F_V \, p_B^\mu \, [\bar{l}\gamma_\mu l] + F_A \, p_B^\mu \, [\bar{l}\gamma_\mu\gamma_5 l] \tag{3.139}$$
$$+ (F_S + \cos\theta F_T) \, [\bar{l}l] + (F_P + \cos\theta F_{T5}) \, [\bar{l}\gamma_5 l] \Bigg).$$

where the functions $F_{V,P}$ get additional terms and the $F_{S,T,T5}$ are completely new:

$$F_A = C_{10}, \qquad F_T = \frac{2\sqrt{\lambda}\,\beta_l}{M_B + M_K} \frac{f_T(q^2)}{f_+(q^2)} \, C_T^l \,, \qquad F_{T5} = \frac{2\sqrt{\lambda}\,\beta_l}{M_B + M_K} \frac{f_T(q^2)}{f_+(q^2)} \, C_{T5}^l,$$

$$F_P = \frac{1}{2} \frac{M_B^2 - M_K^2}{m_b - m_s} \frac{f_0(q^2)}{f_+(q^2)} (C_P^l + C_P^{l\prime}) + m_l C_{10} \left[\frac{M_B^2 - M_K^2}{q^2} \left(\frac{f_0(q^2)}{f_+(q^2)} - 1 \right) - 1 \right], \tag{3.140}$$

$$F_S = \frac{1}{2} \frac{M_B^2 - M_K^2}{m_b - m_s} \frac{f_0(q^2)}{f_+(q^2)} (C_S^l + C_S^{l\prime}), \quad F_V = C_9 + \frac{2m_b}{M_B} \frac{\mathcal{T}_P(q^2)}{\xi_P(q^2)} + \frac{8m_l}{M_B + M_K} \frac{f_T(q^2)}{f_+(q^2)} \, C_T^l.$$

The coefficients of the double differential expansion (3.60) read in the presence of NP wilson coefficients as follows

$$\frac{a_l(q^2)}{\Gamma_0 \sqrt{\lambda}\,\beta_l\,\xi_P^2} = q^2 \left(\beta_l^2 |F_S|^2 + |F_P|^2 \right) + \frac{\lambda}{4} (|F_A|^2 + |F_V|^2)$$
$$+ 2m_l (M_B^2 - M_K^2 + q^2) Re(F_P F_A^*) + 4 m_l^2 M_B^2 |F_A|^2, \tag{3.141}$$

$$\frac{b_l(q^2)}{\Gamma_0 \sqrt{\lambda}\,\beta_l\,\xi_P^2} = 2 \Big\{ q^2 \left[\beta_l^2 Re(F_S F_T^*) + Re(F_P F_{T5}^*) \right]$$
$$+ m_l \left[\sqrt{\lambda} \beta_l Re(F_S F_V^*) + (M_B^2 - M_K^2 + q^2) Re(F_{T5} F_A^*) \right] \Big\}, \tag{3.142}$$

$$\frac{c_l(q^2)}{\Gamma_0 \sqrt{\lambda}\,\beta_l\,\xi_P^2} = q^2 \left(\beta_l^2 |F_T|^2 + |F_{T5}|^2 \right) - \frac{\lambda}{4} \beta_l^2 (|F_A|^2 + |F_V|^2) + 2 m_l \sqrt{\lambda} \beta_l Re(F_T F_V^*) \tag{3.143}$$

We assume in the following all NP Wilson coefficients to be real and at the low scale μ_b, i.e., here $C_i^l = C_i^l(\mu_b)$. The LO RGE evolution from the electroweak scale can be done with the anomalous dimensions given in (3.11).

If we keep the lepton mass non-zero and integrate our observables over the dilepton mass region $1\ \mathrm{GeV}^2 < q^2 \leq 7\ \mathrm{GeV}^2$, then using the central values of the input

parameters given in Table 3.4 we find the following expressions for the branching ratio

$$\mathcal{B}_l = \left[\frac{\tau_{B^\pm}}{1.64\text{ps}}\right]\Bigg[1.91 + 0.02\,(C_S^{l2}+C_P^{l2}) + 0.06\,(C_T^{l2}+C_{T5}^{l2}) + \frac{m_l}{\text{GeV}}\Big(\frac{C_T^l}{0.99}-\frac{C_P^l}{2.92}\Big) + \frac{m_l^2}{\text{GeV}^2}\Big(\frac{C_T^{l2}}{3.28^2}-\frac{C_{T5}^{l2}}{3.28^2}-\frac{C_P^{l2}}{10.36^2}-\frac{C_S^{l2}}{5.98^2}\Big)+\mathcal{O}\left(m_l^3\right)\Bigg]\cdot 10^{-7}, \tag{3.144}$$

the numerator of F_H^l (3.68) multiplied to $\tau_{B^\pm}$

$$2\,\tau_{B^\pm}\,(A_l+C_l) = \left[\frac{\tau_{B^\pm}}{1.64\text{ps}}\right]\Bigg[\frac{m_l^2}{(0.51\text{ GeV})^2} + 0.02\,(C_S^{l2}+C_P^{l2}) + 0.19\,(C_T^{l2}+C_{T5}^{l2}) \tag{3.145}$$
$$+\frac{m_l}{\text{GeV}}\Big(\frac{C_T^l}{0.99}-\frac{C_P^l}{2.92}\Big) + \frac{m_l^2}{\text{GeV}^2}\Big(\frac{C_T^{l2}}{3.28^2}-\frac{C_{T5}^{l2}}{1.89^2}-\frac{C_P^{l2}}{10.36^2}-\frac{C_S^{l2}}{5.98^2}\Big)+\mathcal{O}\left(m_l^3\right)\Bigg]\cdot 10^{-7},$$

and the numerator of the normalized forward-backward asymmetry multiplied by $\tau_{B^\pm}$ (3.67)

$$\tau_{B^\pm}\,B_l = \left[\frac{\tau_{B^\pm}}{1.64\text{ps}}\right]\Bigg[0.06(C_S^l C_T^l + C_P^l C_{T5}^l) + \frac{m_l}{\text{GeV}}\Big(\frac{C_S^l}{6.25}-\frac{C_{T5}^l}{1.85}\Big) - \frac{m_l^2}{\text{GeV}^2}\Big(\frac{C_S^l C_T^l}{4.12^2}+\frac{C_P^l C_{T5}^l}{4.12^2}\Big)+\mathcal{O}\left(m_l^3\right)\Bigg]\cdot 10^{-7}. \tag{3.146}$$

Thus, F_H^l is given by the ratio of (3.145) and (3.144), R_K by the ratio of (3.144) for $l=\mu$ and $l=e$ and A_{FB}^l by the ratio of (3.146) and (3.144), respectively. Replacing $C_{S,P}^l \to C_{S,P}^l + C_{S,P}^{l\prime}$ we can include the contributions from the chirality-flipped operators $\mathcal{O}_{S,P}^{l\prime}$. The higher order terms in the expressions (3.144)-(3.146) are suppressed kinematically by higher power of the lepton mass. The equation (3.144) illustrates the fact that the $B\to K\bar{l}l$ branching ratio is not very sensitive to NP effects from scalar and tensor operators due to the small coefficients in front of the NP couplings with respect to the SM contribution. In the Section 3.5.1 we found that $\mathcal{B}_l$ possesses large uncertainties in the SM which in addition will hide NP effects unless the NP Wilson coefficients become large $C_i^{l\,\text{NP}} \gtrsim 1$. This can be avoided in R_K being the ratio of two decay rates and having tiny SM uncertainties. Thus, R_K is a much more powerful probe of NP than the $B\to K\bar{l}l$ branching ratios. Particularly, a combination R_K-1 can be significantly modified with respect to the SM value by the terms both zeroth and first order in the lepton mass.

Similarly to the combination R_K-1, F_H^l (3.145) and A_{FB}^l have the clean SM predicted values (see Section 3.5.1). Both observable are also more sensitive to the tensor Wilson coefficients than to (pseudo-) scalar ones. Note that the dependence

of $\mathcal{B}_l$ and F_H^l on the (pseudo-) scalar Wilson coefficients is the same. In the leading order in the lepton mass, the deviation of $A_{\rm FB}^l$ from its zero SM value requires the presence of both (pseudo-) scalar and tensor like NP.

In the Table 3.7 we present current experimental information on F_H^l, $R_K - 1$ and $A_{\rm FB}^l$ observables. In the second column we give estimates of the SM predictions. Unfortunately, these data can not be used in the analysis being aimed to constrain NP Wilson coefficients. The reason is that the data on R_K include large dilepton masses where QCDF is not applicable and the values of F_H^l and $A_{\rm FB}^l$ are in addition lepton flavor averaged. We do not take these constraints into account since a straightforward application of these data is impossible.

Model-Independent NP Analysis

Summarizing previous sections, we have four experimental bounds at our disposition, i.e., $\bar{B}_s \to \bar{l}l$ and $\mathcal{B}_l^{\rm incl}|_{[>0.04]}$ with $l = e, \mu$, and twelve NP Wilson coefficients. Since the existing experimental constraints do not allow us to perform at present a full model-independent fit of all Wilson coefficients, we split our study into four steps. We consider the following four benchmark scenarios with (pseudo-) scalar operators (Scenario I-III) and the tensor operators (Scenario IV) defined as:

- Scenario I: NP in C_S^l and C_P^l, all other NP contributions vanish.
- Scenario II: Same as Scenario I, but with the additional assumptions $C_S^l = -C_P^l$ and $C^l \propto m_l$.
- Scenario III: NP in C_S^l, C_P^l and $C_S^{l\prime}$, $C_P^{l\prime}$, the tensor coefficients $C_{T,T5}^l$ vanish.
- Scenario IV: NP in the tensor coefficients C_T^l, C_{T5}^l, all other NP contributions vanish.

Scenario II is inspired by the MSSM for large values of $\tan\beta$ (see also Section 3.3.1).

One should comment that we employ all experimental bounds in the analysis at 90% C.L. The resulting allowed ranges of the NP Wilson coefficients in each of the scenarios are summarized in Table 3.9. These values of the parameters (Wilson coefficients) predict numerical values of $B \to K\bar{l}l$ observables obtained for $1\ {\rm GeV}^2 < q^2 \leq 7\ {\rm GeV}^2$ and given in the Table 3.10. Since the current experimental errors dominate the theoretical uncertainties, in the analysis we do not take into account SM uncertainties. Their inclusion would allow for slightly bigger NP effects.

Scenario I: Scalars C_S^l and C_P^l

In the Scenario I we consider only scalar and pseudoscalar Wilson coefficients C_S^l and C_P^l per lepton species. We start with a discussion of the Wilson coefficients for

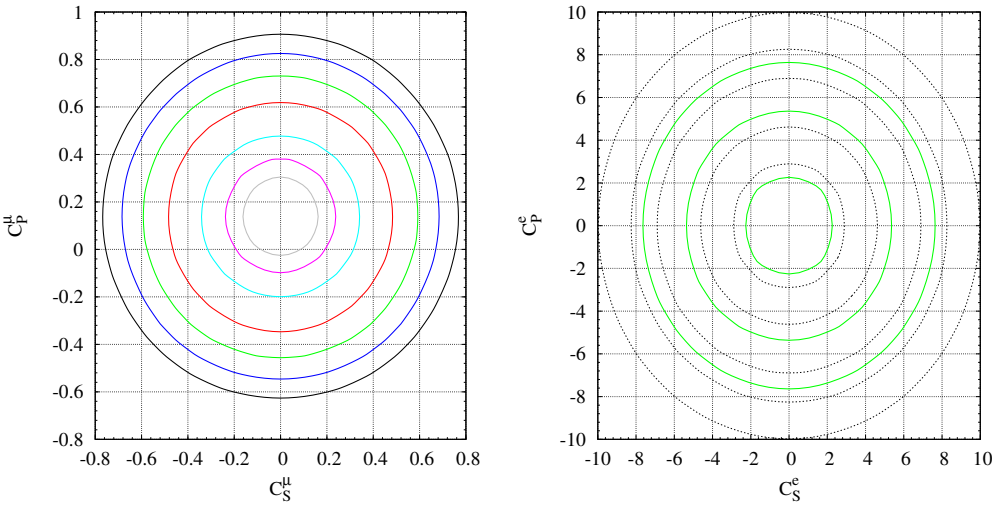

Figure 3.15: In the left-hand plot contours of $\mathcal{B}(\bar{B}_s \to \bar{\mu}\mu)$ are shown in the $C_S^\mu - C_P^\mu$ plane in Scenario I. The contours enclose values of $\mathcal{B}(\bar{B}_s \to \bar{\mu}\mu) < \{0.05, 0.1, 0.2, 0.4, 0.6, 0.8, 1.0\} \cdot 10^{-7}$ starting with the innermost. In the right-hand plot contours of $\mathcal{B}_e^{\text{incl}}|_{[>0.04]} < \{4.5, 5.0, 6.0, 6.8, 8.0\} \cdot 10^{-6}$ (dashed black) and $\mathcal{B}(\bar{B}_s \to \bar{e}e) < \{0.1, 0.5, 1.0\} \cdot 10^{-5}$ (solid green) are shown in the $C_S^e - C_P^e$ plane in Scenario I starting with the innermost.

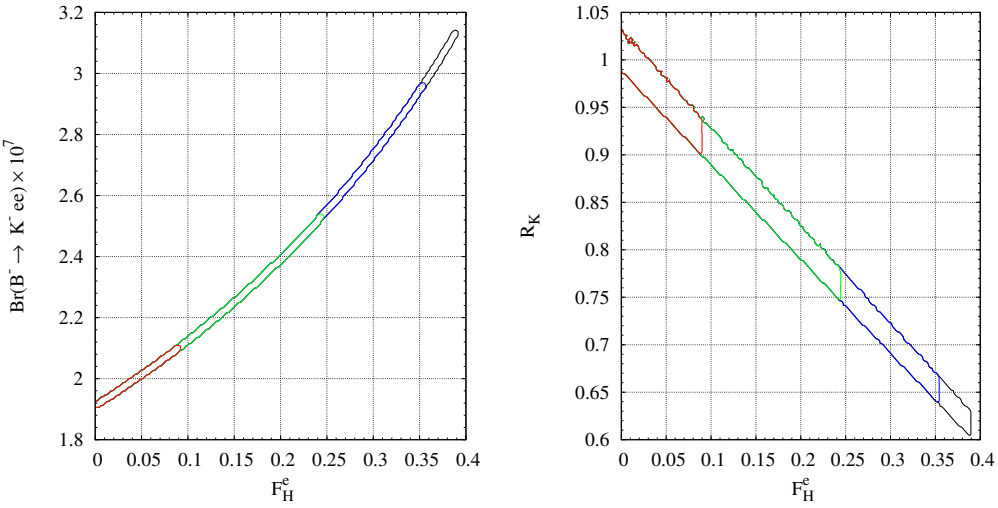

Figure 3.16: Contours of $\mathcal{B}_e^{\text{incl}}|_{[1,6]} < \{1.75, 2.0, 2.25, 2.35\} \cdot 10^{-6}$ in the $F_H^e - \mathcal{B}_e$ plane (left-hand plot) and the $F_H^e - R_K$ plane (right-hand plot) in Scenario I.

muons, $C^{\mu}_{S,P}$ where the bound from $\mathcal{B}(\bar{B}_s \to \bar{\mu}\mu)$ is stronger than that from the inclusive decay $\mathcal{B}^{\rm incl}_{\mu}|_{[>0.04]}$. In Figure 3.15 various bounds on $C^{\mu}_{S,P}$ as contours corresponding to different upper bounds on $\mathcal{B}(\bar{B}_s \to \bar{\mu}\mu) < \{0.05, 0.1, 0.2, 0.4, 0.6, 0.8, 1.0\} \cdot 10^{-7}$ are displayed, reminding that the current experimental bound is $\mathcal{B}(\bar{B}_s \to \bar{\mu}\mu) < 0.8 \cdot 10^{-7}$ 90% C.L.. Employing the ranges for the C^{μ}_S and C^{μ}_P we calculate the ranges for $B \to K\bar{l}l$ and $\bar{B} \to X_s\bar{l}l$ observables which can be seen in Table 3.10. The F^{μ}_H can deviate from the SM by about 40% whereas the forward-backward asymmetry is less then 1% in agreement with and updating earlier findings [58]. The forward-backward asymmetry $A^{\mu}_{\rm FB}$ is small, of order one percent. The impact on the branching ratio $\mathcal{B}_{\mu}$ is about 2% and can be completely neglected as soon as one takes into account SM uncertainties. Also the NP contributions to $\mathcal{B}^{\rm incl}_{\mu}|_{[1,6]}$ and $\mathcal{B}^{\rm incl}_{\mu}|_{[>0.04]}$ are small compared to the theoretical uncertainties.

Concerning the Wilson coefficients for electrons the case is different. The current experimental bound from $\mathcal{B}(\bar{B}_s \to \bar{e}e)$ is much weaker than the one from $\mathcal{B}^{\rm incl}_{e}|_{[>0.04]}$. Similarly to the muon case, in Figure 3.15 we plot the contours in the $C^{e}_S - C^{e}_P$ plane corresponding to the different bounds from $\mathcal{B}^{\rm incl}_{e}|_{[>0.04]} < \{4.5, 5.0, 6.0, 6.8, 8.0\} \cdot 10^{-6}$. Additionally we plot in the same figure hypothetical future bounds from $\mathcal{B}(\bar{B}_s \to \bar{e}e) < \{0.1, 0.5, 1.0\} \cdot 10^{-5}$. As can be seen, the improved measurements on $\mathcal{B}(\bar{B}_s \to \bar{e}e)$ would be important when restricting $C^{e}_{S,P}$. The allowed ranges for $C^{e}_{S,P}$ determined by $\mathcal{B}^{\rm incl}_{e}|_{[>0.04]} < 6.8 \cdot 10^{-6}$ at 90% C.L. are given in the Table 3.7. The corresponding ranges for the decay observables for $l = e$ are presented in Table 3.10. The flat term in the angular distribution, F^{e}_H is strongly enhanced and can be of order 40%. The branching ratio $\mathcal{B}_e$ can be enhanced by about 60% with respect to its SM value. Since, R_K has inverse dependence on $\mathcal{B}_e$, its allowed region is extended to lower values and currently can be 40% smaller than the SM value. In the Figure 3.16 we plot correlations $\mathcal{B}_e - F^{e}_H$ and $R_K - F^{e}_H$. Particularly, one can see a significant decrease of R_K and huge increase of F^{e}_H with respect to their SM values. The forward-backward asymmetry $A^{e}_{\rm FB}$ is one order smaller than the one for muons. The $\mathcal{B}^{\rm incl}_{e}|_{[1,6]}$ is enhanced by 60% with respect to the SM value.

Scenario II: MSSM-like $C^{\mu}_S = -C^{\mu}_P$

The discussion of such scenario can be interesting due to similarity with the MSSM at large $\tan\beta$. For instance, similar to the SM the Wilson coefficients in the MSSM $C^{l}_{S,P} \sim m_l$ and in turn $C^{e}_{S,P}$ can be safely neglected with the result that all observables corresponding to $b \to s\bar{e}e$ are SM-like. A further restriction appears due to the relation $C^{\mu}_S = -C^{\mu}_P$ which holds in the large $\tan\beta$ MSSM only for the dominant leading order term $\sim \tan^3\beta$. We also neglect chirality-flipped Wilson coefficients $C^{\mu\prime}_{S,P}$ because of the additional suppression m_s/m_b. These additional assumptions

Wilson coefficient	Sc I	Sc II	Sc III	Sc IV
$C^e_{S,P}$	$[-8.3, 8.3]$	–	$[-8.3, 8.3]$	–
C^μ_S	$[-0.69, 0.69]$	$[-0.55, 0.41]$	$[-5.6, 5.6]$	–
C^μ_P	$[-0.55, 0.82]$	$= -C^\mu_S$	$[-5.6, 5.6]$	–
$C^{e\prime}_{S,P}$	–	–	$[-8.3, 8.3]$	–
$C^{\mu\prime}_{S,P}$	–	–	$[-5.6, 5.6]$	–
$C^e_{T,T5}$	–	–	–	$[-1.2, 1.2]$
$C^\mu_{T,T5}$	–	–	–	$[-1.1, 1.1]$

Table 3.9: The allowed ranges for the NP Wilson coefficients C^l_i in Scenarios I-IV after using the constraints $\mathcal{B}(\bar{B}_s \to \bar{e}e) < 5.4 \cdot 10^{-5}$, $\mathcal{B}(\bar{B}_s \to \bar{\mu}\mu) < 0.8 \cdot 10^{-7}$, $\mathcal{B}^{\rm incl}_e|_{>0.04} < 6.8 \cdot 10^{-6}$ and $\mathcal{B}^{\rm incl}_\mu|_{>0.04} < 6.3 \cdot 10^{-6}$, see Table 3.7. A "–" means that the corresponding coefficient is zero in this NP scenario.

Observable	Sc I	Sc II	Sc III	Sc IV
F^e_H	< 0.39	–	< 0.56	< 0.13
F^μ_H	$[0.013, 0.035]$	$[0.018, 0.032]$	$[0.013, 0.56]$	$[0.014, 0.18]$
R_K	$[0.61, 1.01]$	$[0.996, 1.01]$	$[0.44, 2.21]$	$[0.93, 1.10]$
$\mathcal{B}_e\,[10^{-7}]$	$[1.91, 3.14]$	–	$[1.91, 4.36]$	$[1.91, 2.00]$
$\mathcal{B}_\mu\,[10^{-7}]$	$[1.90, 1.94]$	$[1.90, 1.93]$	$[1.90, 4.26]$	$[1.87, 2.10]$
$A^e_{\rm FB}\,[\%]$	$[-0.02, 0.02]$	–	$[-0.02, 0.02]$	$[-0.02, 0.02]$
$A^\mu_{\rm FB}\,[\%]$	$[-0.6, 0.6]$	$[-0.5, 0.3]$	$[-4.46, 4.46]$	$[-3.1, 3.1]$
$\mathcal{B}(\bar{B}_s \to \bar{e}e)\,[10^{-5}]$	< 1.17	–	< 2.33	–
$\mathcal{B}(\bar{B}_s \to \bar{\mu}\mu)\,[10^{-7}]$	< 0.8	< 0.8	< 0.8	–
$\mathcal{B}^{\rm incl}_e\|_{[1,6]}\,[10^{-6}]$	$[1.64, 2.35]$	–	$[1.64, 2.35]$	$[1.64, 2.83]$
$\mathcal{B}^{\rm incl}_\mu\|_{[1,6]}\,[10^{-6}]$	$[1.59, 1.60]$	$[1.59, 1.60]$	$[1.59, 2.17]$	$[1.59, 2.56]$
$\mathcal{B}^{\rm incl}_e\|_{[>0.04]}\,[10^{-6}]$	$[4.15, 6.8]$	–	$[4.15, 6.8]$	$[4.15, 6.8]$
$\mathcal{B}^{\rm incl}_\mu\|_{[>0.04]}\,[10^{-6}]$	$[4.15, 4.18]$	$[4.15, 4.17]$	$[4.15, 6.3]$	$[4.15, 6.3]$

Table 3.10: Allowed ranges for $b \to s\bar{l}l$ observables in Scenarios I-IV after taking into account the constraints from $\mathcal{B}(\bar{B}_s \to \bar{l}l)$ and $\mathcal{B}^{\rm incl}_l|_{[>0.04]}$ for $l = e$ and $l = \mu$, see Table 3.7 and the text for details. A "–" means that the corresponding observable is SM-like.

give rise to the expectation of smaller deviations from the SM than in Scenario I.

The allowed range of C_S^μ and the effects of NP on the rare decay observables are given in Table 3.9 and Table 3.10, respectively. In the Figure 3.17 we show the dependence of $B \to K\bar{l}l$ observables on the only Wilson coefficient C_S. The NP contributions enhance F_H^μ by 30% with respect to the SM value. The deviations of $\mathcal{B}_\mu$ from the SM are of the order of 2%, much smaller than the theoretical uncertainties. The same holds for $\mathcal{B}_\mu^{\text{incl}}|_{[1,6]}$, which confirms earlier studies within the MSSM [113]. Since $\mathcal{B}_e$ is SM-like in Scenario II, the deviation of R_K from the SM is much reduced with respect to the one in Scenario I. We find NP effects of 1%, which are larger than the uncertainties of the SM prediction. The forward-backward asymmetry is smaller then 1% in agreement with previous works in the framework of the MSSM [114].

Scenario III: Scalars C_S^l, C_P^l and $C_S^{l\prime}$, $C_P^{l\prime}$

In the third scenario we consider the full set of (pseudo-) scalar Wilson coefficients including the chirality flipped ones $C_{S,P}^{l\prime}$ for $l = e$ and $l = \mu$. Thus, as we have already mentioned in the Section 3.6.1 the only bounds from $\bar{B}_s \to \bar{l}l$ can be evaded since $C_{S,P}^l$ and corresponding $C_{S,P}^{l\prime}$ Wilson coefficients contribute as a difference in the expression for the branching ratio. Therefore, one needs to use the whole set of our experimental data, i.e., both $\mathcal{B}(\bar{B}_s \to \bar{l}l)$ and $\mathcal{B}_l^{\text{incl}}|_{[>0.04]}$. The allowed ranges are given in the Table 3.9. The chirality-flipped Wilson coefficients have identical ranges as the unprimed one and all C_i's are comparable in magnitude.

The large Wilson coefficients lead to big NP effects in the rare decay observables, see Table 3.10. In Scenario III R_K can both increase and decrease significantly with respect to the SM as opposed to Scenario I where $\mathcal{B}(\bar{B}_s \to \bar{\mu}\mu)$ permits only a large decrease of R_K. This happens due to the fact that the muon Wilson coefficients become less constrained. The correlation between F_H^l and R_K can be seen in the Figure 3.18, where in addition we show contours corresponding to the predictions of $\mathcal{B}_\mu^{\text{incl}}|_{[1,6]} < \{1.75, 2.0, 2.17\} \cdot 10^{-6}$ for muons and $\mathcal{B}_e^{\text{incl}}|_{[1,6]} < \{1.75, 2.0, 2.25, 2.35\} \cdot 10^{-6}$ for electrons. The NP contributions enhance both $\mathcal{B}_e$ and $\mathcal{B}_\mu$ by order 200% above the SM such that measurements of these observables in the low-q^2 region could provide constraints regardless of the large form factor uncertainties. In this scenario the forward-backward asymmetry of the muon channel reaches bigger values in comparison with other scenarios, which is of order $(4-5)\%$. For the electron channel the forward-backward asymmetry is negligible.

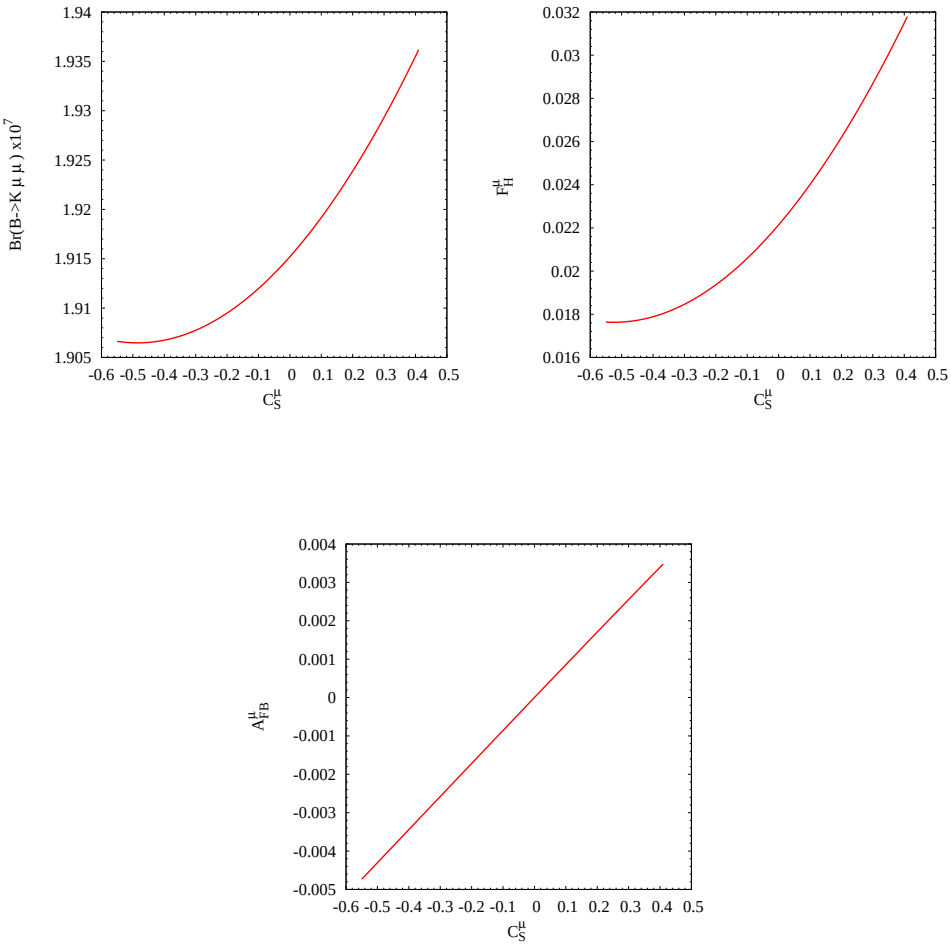

Figure 3.17: Dependence of $B \to K\bar{l}l$ observables, integrated over the interval $1\ \text{GeV}^2 < q^2 \leq 7\ \text{GeV}^2$, on NP Wilson coefficient C_S in the Scenario II.

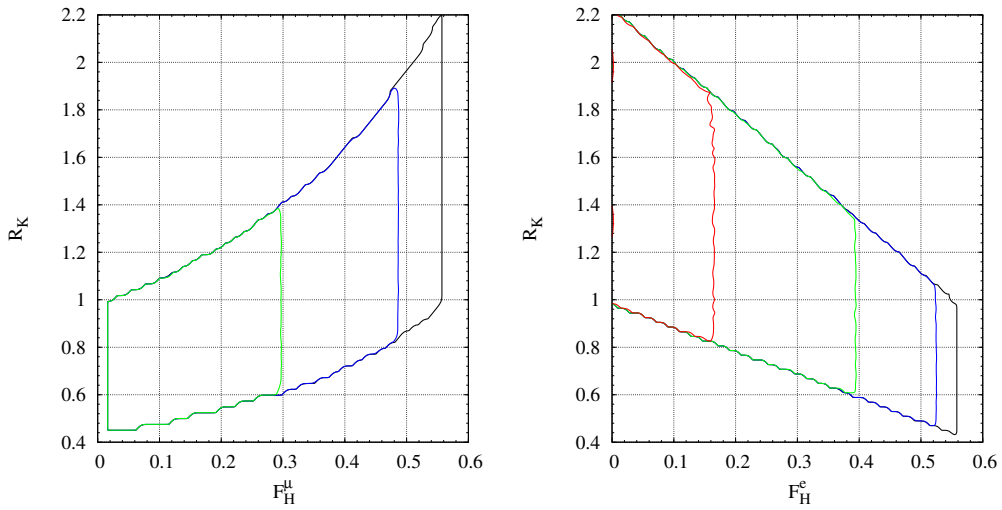

Figure 3.18: Contours of $\mathcal{B}_\mu^{\text{incl}}|_{[1,6]} < \{1.75, 2.0, 2.17\} \cdot 10^{-6}$ in the $F_H^\mu - R_K$ plane in Scenario III (left-hand plot). In the right-hand plot contours of $\mathcal{B}_e^{\text{incl}}|_{[1,6]} < \{1.75, 2.0, 2.25, 2.35\} \cdot 10^{-6}$ are shown in the $F_H^e - R_K$ plane in Scenario III. For details see text.

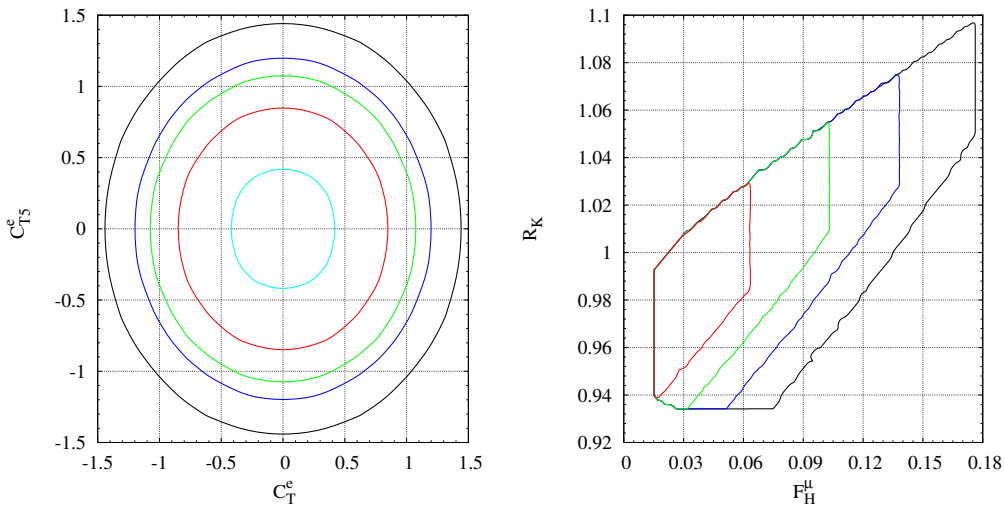

Figure 3.19: In the left-hand plot contours of $\mathcal{B}_e^{\text{incl}}|_{[>0.04]}$ are shown in the $C_T^e - C_{T5}^e$ plane in Scenario IV. Each contour encloses values of $\mathcal{B}_e^{\text{incl}}|_{[>0.04]} < \{4.5, 5.5, 6.3, 6.8, 8.0\} \cdot 10^{-6}$ starting with the innermost. Corresponding constraints for $C_T^\mu - C_{T5}^\mu$ can be read off from the left-hand plot as well. In the right-hand plot contours of $\mathcal{B}_\mu^{\text{incl}}|_{[1,6]} < \{1.75, 2.0, 2.25, 2.56\} \cdot 10^{-6}$ are shown for F_H^μ versus R_K in Scenario IV starting with the innermost.

Scenario IV: Tensors C_T^l, C_{T5}^l

In Scenario IV we consider only NP in $C_{T,T5}^l$ and only inclusive $\bar{B} \to X_s \bar{l} l$ decays (3.125) are sensitive to tensor interactions. The allowed ranges for tensor Wilson coefficients can be seen in the Table 3.9. We plot the bounds on $C_{T,T5}^l$ in the left-hand plot of Figure 3.19, where contours of $\mathcal{B}_e^{\text{incl}}|_{[>0.04]} < \{4.5, 5.5, 6.3, 6.8, 8.0\} \cdot 10^{-6}$ are shown in the $C_T^e - C_{T5}^e$ plane starting with the innermost. The constraints on $C_{T,T5}^\mu$ from upper bounds on $\mathcal{B}_\mu^{\text{incl}}|_{[>0.04]}$ can be read off from the same plot.

The NP effects in F_H^e and F_H^μ are comparable with Scenario III and huge with respect to the SM. R_K receives order 10% corrections from NP which are well above the theoretical uncertainties. The branching ratios $\mathcal{B}_l$ are subject to NP contributions $\lesssim +10\%$, which cannot be separated from the larger form factor induced uncertainties. Whereas $\mathcal{B}_l^{\text{incl}}|_{[1,6]}$ gets large enhancement, about 70%, which makes the inclusive decays a sensitive probe of tensor operators. The correlation between the three observables F_H^μ, R_K and $\mathcal{B}_\mu^{\text{incl}}|_{[1,6]}$ is shown in the right-hand plot of Figure 3.19 for contours of $\mathcal{B}_\mu^{\text{incl}}|_{[1,6]} < \{1.75, 2.0, 2.25, 2.56\} \cdot 10^{-6}$. Similarly to other scenarios $|A_{\text{FB}}^\mu|$ is small and does not exceed 3%.

3.6.3 CP Asymmetries in the Presence of New Physics

In this sections we discuss NP effects on CP asymmetries defined in Appendix B.3 in terms of 6 NP Wilson coefficients. We consider two main possibilities:

- We vary all twelve parameters, i.e., six absolute values and six phases. We call this scenario "Generic NP".

- We vary one particular Wilson coefficient assuming for the remaining Wilson coefficients their SM values. We call each scenario "C_i only".

We make several plots corresponding for the particular "$C_i^{(\prime)}$ only" scenarios applying the constraints from Table 3.8. In Figure 3.14 we see the constrained regions for Wilson coefficients in "C_9^{NP} only", "C_{10}^{NP} only", "C_7^{NP} only" and "$C_7^\prime$ only" scenarios. From the plots we can see that the rare decays give the strongest bounds. The A_{FB} plays an important role in the "C_9^{NP} only" and "C_{10}^{NP} only" cutting out the regions with large absolute values of Wilson coefficients. The time-dependent asymmetry $S_{K^*\gamma}$ is only relevant for "$C_7^\prime$ only". In the case of "Generic NP" both A_{FB} and $S_{K^*\gamma}$ become less important.

The dependence of the CP asymmetries $A_i^{(D)}$ on the Wilson coefficients can be seen from the analytical (NLO) formulae in Appendix B.3. Explicit LO expressions

	generic NP	$C_{10}^{\rm NP}$ only	$C_{10}^{\prime\rm NP}$ only	$C_9^{\rm NP}$ only
$\langle A_{\rm CP}\rangle$	$[-0.1, 0.1]$	$[3, 8]\cdot 10^{-3}$	SM-like	$[-0.02, 0.02]$
$\langle A_3\rangle$	$[-0.08, 0.08]$	SM-like	SM-like	SM-like
$\langle A_4^D\rangle$	$[-0.04, 0.04]$	$[-4, -1]\cdot 10^{-3}$	$[-3, -1]\cdot 10^{-3}$	$[-0.01, 0.01]$
$\langle A_5^D\rangle$	$[-0.07, 0.07]$	$[-0.04, 0.04]$	$[-0.02, 0.04]$	$[5, 9]\cdot 10^{-3}$
$\langle A_6\rangle$	$[-0.1, 0.1]$	$[-0.05, 0.05]$	$[-9, -3]\cdot 10^{-3}$	SM-like
$\langle A_7^D\rangle$	$[-0.76, 0.76]$	$[-0.48, 0.48]$	$[-0.38, 0.38]$	SM-like
$\langle A_8^D\rangle$	$[-0.48, 0.48]$	$[2.2, 6.8]\cdot 10^{-3}$	$[-0.28, 0.28]$	$[-0.17, 0.17]$
$\langle A_9\rangle$	$[-0.62, 0.60]$	SM-like	$[-0.20, 0.20]$	SM-like
$\mathcal{B}(\bar{B}_s \to \bar{\mu}\mu)$	$< 1.4\cdot 10^{-8}$	$< 6.3\cdot 10^{-9}$	$< 1.3\cdot 10^{-8}$	SM-like

	$C_9^{\prime}$ only	$C_7^{\rm NP}$ only	$C_7^{\prime}$ only
$\langle A_{CP}\rangle$	$[-3, 6]\cdot 10^{-3}$	$[-0.03, 0.04]$	$[3.5, 4.5]\cdot 10^{-3}$
$\langle A_3\rangle^\dagger$	$[-0.02, 0.02]$	SM-like	$[-0.02, 0.01]$
$\langle A_4^D\rangle$	$[-0.01, 0.01]$	$[-3, -1]\cdot 10^{-3}$	$[-3, -1]\cdot 10^{-3}$
$\langle A_5^D\rangle$	$[0.003, 0.01]$	$[5, 8]\cdot 10^{-3}$	$[7, 8]\cdot 10^{-3}$
$\langle A_6\rangle$	$[-8, -3]\cdot 10^{-3}$	$[-6, -4]\cdot 10^{-3}$	$[-7, -5]\cdot 10^{-3}$
$\langle A_7^D\rangle$	$[-6.2, -2.2]\cdot 10^{-3}$	$[-0.3, 0.32]$	$[-0.22, 0.18]$
$\langle A_8^D\rangle$	$[-0.07, 0.07]$	$[-0.17, 0.16]$	$[-0.09, 0.10]$
$\langle A_9\rangle^\dagger$	$[-0.036, 0.032]$	$[-3.1, 3.2]\cdot 10^{-3}$	$[-0.070, -0.080]$

Table 3.11: The ranges of the integrated CP asymmetries $\langle A_i^{(D)}\rangle$ for $(q^2_{\rm min}, q^2_{\rm max}) = (1, 6)$ GeV^2 are given after applying the experimental constraints at 90% C.L. for the general scenario and the scenarios with particular Wilson coefficient only. Note that in the scenarios "$C_{7,9}^{NP}$ only" and "$C_{7,9}^{\prime}$ only " $\mathcal{B}(\bar{B}_s \to \bar{\mu}\mu)$ is SM-like.

for the T-odd asymmetries, which present the most interest, read as

$$A_7^D = 2\mathcal{A}^D \frac{\hat{m}_b}{\hat{s}}(1-\hat{s})\mathrm{Im}\left[(C_{10}^{(0)} - C_{10}')(C_7^{\mathrm{eff}(0)} - C_7')^*\right], \tag{3.147}$$

$$\begin{aligned} A_8^D = \mathcal{A}^D \beta_l \Bigg\{ \mathrm{Im}\Bigg[& C_9^{(0)} C_9'^* + C_{10}^{(0)} C_{10}'^* + \frac{4\hat{m}_b^2}{\hat{s}} C_7^{\mathrm{eff}(0)} C_7'^* \\ & + \frac{\hat{m}_b}{\hat{s}}\big((1-\hat{s})(C_7' C_9'^* - C_7^{\mathrm{eff}(0)} C_9^{(0)*}) + (1+\hat{s})(C_7^{\mathrm{eff}(0)} C_9'^* - C_7' C_9^{(0)*})\big)\Bigg] \\ & - \mathrm{Re}(Y^{(0)})\mathrm{Im}\left[C_9' + \frac{\hat{m}_b}{\hat{s}}\big((1-\hat{s})C_7^{\mathrm{eff}(0)} + (1+\hat{s})C_7'\big)\right]\Bigg\} + \mathcal{O}(\hat{\lambda}_u), \end{aligned} \tag{3.148}$$

$$\begin{aligned} A_9 = 4\mathcal{A}^D \beta_l \Bigg\{ & \mathrm{Im}\left[C_9^{(0)} C_9'^* + C_{10}^{(0)} C_{10}'^* + \frac{4\hat{m}_b^2}{\hat{s}^2} C_7^{\mathrm{eff}(0)} C_7'^* + \frac{2\hat{m}_b}{\hat{s}}(C_7^{\mathrm{eff}(0)} C_9'^* - C_7' C_9^{(0)*})\right] \\ & - \frac{\hat{m}_b}{\hat{s}}\mathrm{Re}(Y^{(0)})\mathrm{Im}\left[2C_7' + \frac{\hat{m}_b}{\hat{s}} C_9'\right]\Bigg\} + \mathcal{O}(\hat{\lambda}_u), \end{aligned} \tag{3.149}$$

where for A_8^D, A_9 we neglected the SM CP violation suppressed by $\hat{\lambda}_u$. From numerical model-independent formulae for the $B \to K^*(\to K\pi)\bar{l}l$ branching ratio and CP asymmetries in Appendix B.5 one can read out the dependence CP asymmetries on a particular NP Wilson coefficient. The numerators of $A_{\mathrm{CP},3,4}^{(D)}$ are sensitive to $C_{7,9}$ and $C_{7,9}'$ whereas the numerators of $A_{5,7}^D$ and A_6 probe $C_{7,10}$ and $C_{7,10}'$. The numerators of $A_{8,9}^{(D)}$ can be affected by all Wilson coefficients considered here. The $A_{3,9}$ are very sensitive to the flipped Wilson coefficients and vanish in the limit $C_i' \to 0$ at lowest order in the $1/E$-expansion. In Appendix B.5 we provide numerical model-independent formulae for branching ratios and CP asymmetries as functions of all NP Wilson coefficients.

In Table 3.11 we show the allowed ranges of the CP asymmetries in various NP scenarios. The asymmetries are integrated over low dilepton masses, $q^2 \in [1,6]$ GeV^2. Numerically we find that the CP asymmetries can deviate significantly from their SM values, which are doubly Cabibbo-suppressed and below the percent level. Especially, this concerns T-odd asymmetries $A_{7,8,9}^{(D)}$ which can receive large NP enhancements, up to order one. T-even CP asymmetries can be enhanced by one order of magnitude up to $\lesssim 10\%$. By "SM-like" we denote a residual tiny contribution coming from the normalization to the CP averaged decay rate, which can not be distinguished from the SM value at 1σ. In Table 3.11 we also predict an upper bound for the purely leptonic decay $\bar{B}_s \to \bar{\mu}\mu$ which has strong sensitivity to the combination $|C_{10} - C_{10}'|$ of NP Wilson coefficients (see [115]). We find a possible enhancement of $\mathcal{B}(\bar{B}_s \to \bar{\mu}\mu)$ up to almost an order of magnitude in NP scenarios with these coefficients modified, see Table 3.11. The largest branching ratio, obtained with generic NP, is still a factor of two below the current experimental upper bound

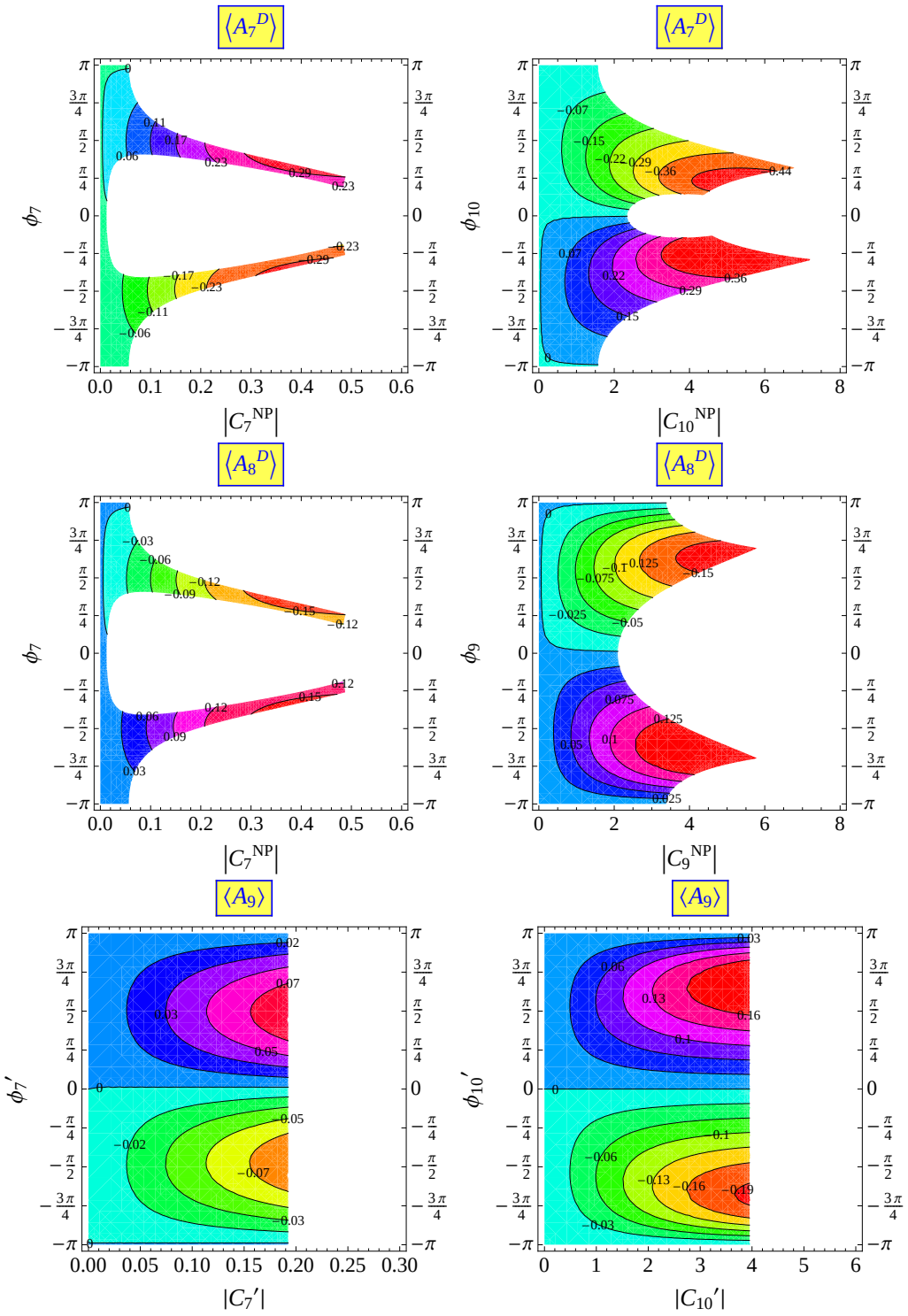

Figure 3.20: The dependence of the integrated T-odd CP asymmetries $\langle A_{7,8,9}^{(D)} \rangle$ for $(q^2_{\rm min}, q^2_{\rm max}) = (1, 6)$ GeV^2 on NP Wilson coefficients after applying the experimental constraints. In each plot all other NP Wilson coefficients have been set to zero.

given in Table 3.8. We conclude that improved data on or a discovery of $\bar{B}_s \to \bar{\mu}\mu$ decays will have a strong impact on this type of analysis.

In Figure 3.20 we show the dependence of the T-odd asymmetries integrated over $(q^2_{\rm min}, q^2_{\rm max}) = (1, 6)$ GeV^2 on the absolute value and the phase of the NP Wilson coefficients in particular scenario. The plots indicate the strong dependence on phases. In Figure 3.21 we also present correlations between T-even and T-odd asymmetries in several scenarios. Falsifying such correlations can establish the nature of the NP.

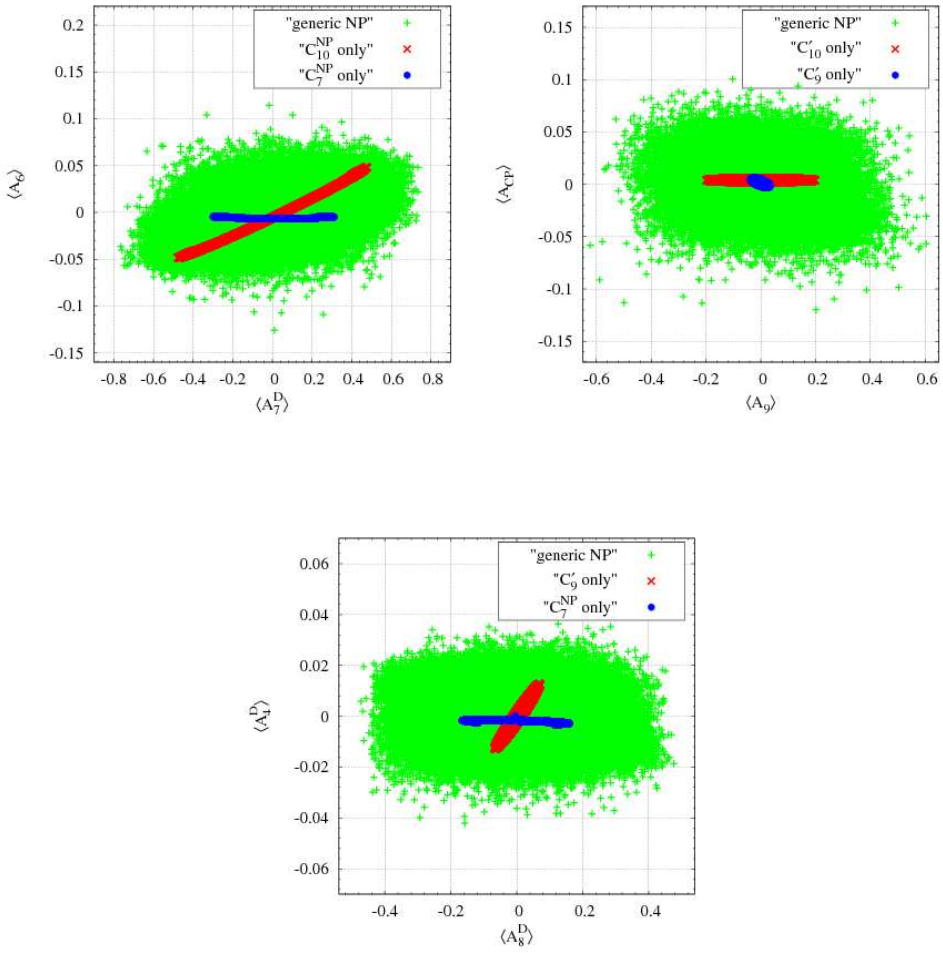

Figure 3.21: Correlations between T-odd ($\langle A_7^D\rangle$,$\langle A_7^D\rangle$ and $\langle A_9\rangle$) and T-even ($\langle A_4^D\rangle$,$\langle A_6\rangle$ and $\langle A_{CP}\rangle$) asymmetries integrated over $(q^2_{\rm min}, q^2_{\rm max}) = (1, 6)$ GeV^2 in different scenarios.

3.7 Conclusion

We have shown, that the observables appearing in normalized $1/\Gamma_l \, d\Gamma_l/d\cos\theta$ of $B \to K\bar{l}l$ decay angular distribution offer great opportunities to test the SM and search for NP. Namely, they are the flat term in the distribution, $F_H^l/2$ and the forward-backward asymmetry $A_{\rm FB}^l$. The angular distribution can be presented as the power series in $\cos\theta$ truncated after power two. The powers greater than two appear only if we include either higher dimensional operators in $\mathcal{H}_{\rm eff}$ or QED corrections. Both are strongly suppressed by powers of the low energy masses and momenta over the scale of electroweak NP and by $\alpha_e/(4\pi)$, respectively.

Whereas the SM predictions of $B \to K\bar{l}l$ branching ratios suffer from $\mathcal{O}(30\%)$ uncertainties, the SM value of F_H^μ is order few percent, and can be cleanly predicted using QCDF for low dilepton masses with $\sim 6\%$ accuracy, see Table 3.5. Being $F_H^l \propto m_l^2$ in the SM, F_H^e is negligible. At the same time the forward-backward asymmetry vanishes exactly in the SM up to the aforementioned higher order OPE and QED corrections. We also analyzed the ratio of $B \to K\bar{\mu}\mu$ to $B \to K\bar{e}e$ decay rates, denoted as $R_K^{\rm SM}$, being one at the level of $m_\mu^4/q^4 \sim 10^{-4}$ in the SM. Such strong suppression comes due to the cancellations of $\mathcal{O}(m_l^2)$-corrections at LO in $1/E$ and α_s in the decay rate. However, lepton flavor dependence in R_K can be increased by taking into account collinear QED logarithms, which have not be computed for $B \to K\bar{l}l$ decays yet.

The clean and definite predictions of F_H^l, $A_{\rm FB}^l$ and R_K in the SM makes these observables very attractive for NP studies. All observables, i.e., F_H^l, $A_{\rm FB}^l$ and R_K are sensitive to Higgs and tensor interactions. We have worked out NP signatures and correlations by taking into account existing data on $\mathcal{B}(\bar{B}_s \to \bar{l}l)$ and $\mathcal{B}(\bar{B} \to X_s\bar{l}l)$ for $l = e$ and $l = \mu$ separately. We found that the NP modifications to the angular observables F_H^e, F_H^μ, $A_{\rm FB}^\mu$ and $R_K - 1$ can be sizeable, see Table 3.10.

The current experimental situation for the observables F_H^l, $A_{\rm FB}^l$ and R_K is at a very early stage, see Table 3.7. In particular, all measurements average $l = e$ and $l = \mu$ final states except the ones of R_K [53, 55]. In addition the data include q^2-regions where QCDF does not apply. Therefore, for the future improvements and abilities to compare with the theory all data in rare semileptonic decays $B \to K\bar{l}l, B \to K^*\bar{l}l$ and $\bar{B} \to X_s\bar{l}l$ should be available for each lepton flavor separately since deviations from the SM could be l-dependent. Appropriate cuts in q^2 should be taken into account to maximally exploit the theoretical predictions.

We also studied eight CP asymmetries, which can be constructed from the angular distribution of the $B \to K^*(\to K\pi)\bar{l}l$, in the SM and the presence of NP phases. The SM predictions suffer from large uncertainties, i.e., $\sim 20\%$ for $A_{4,5}^D$, $\sim 50\%$ for $A_{\rm CP}, A_6, A_{7,8}^D$ and order one for $A_{3,9}$, coming from uncertainties in μ_b scale, CKM

matrix elements and form factor uncertainties. In spite of large SM errors, the magnitude of the CP asymmetries $\lesssim 10^{-2}$ makes them all ideal to search for a variety of different NP effects. We summarize here specific features of the asymmetries:

- A_7^D, A_8^D, A_9 are T-odd and can be order one with NP.
- A_5^D, A_6, A_8^D, A_9 are CP-odd and can be obtained without tagging from $d\Gamma + d\bar{\Gamma}$.
- A_3, A_9 are very sensitive to right-handed currents.
- $A_3, A_9, (A_6)$ can be extracted from a single-differential distribution in $\phi(\theta_l)$.
- A_7^D is very sensitive to the phase of the Z-penguins $\sim C_{10}^{(\prime)}$.

Therefore CP asymmetries are sensitive to the whole set of NP Wilson coefficients. Large NP effects are possible, which survive also the current experimental FCNC constraints, see Table 3.11. The future measurements of the CP asymmetries will make possible to test the SM mechanism of CP violation through the CKM matrix. Further, the correlations between various CP asymmetries will be able to reveal the peculiar nature of NP, see Figure 3.21.

4 Summary

Today particle physics appears to be at the border of new discoveries which will shed light on fundamental questions of physics. Thank to experiments at LHC we might find the most important missing particle of the SM, Higgs boson. The existence of it will confirm the mechanism of the mass generation of the SM particles. Besides, it might be discovered a lot of other particles predicted by models beyond the SM.

On the other side B-factories and the Tevatron have studied and continue to investigate a large number of observables to test the SM and directly or/and indirectly to demystify the nature of NP. In spite of the fact that the B-factory data agree globally with CKM mechanism of flavor and CP violations in the quark sector, the uncertainties of measurements are still too large to make some definite and final conclusions. Collecting statistics at the B-factories and the future Super$B$-factory with high luminosity will continue improve the precision of CKM pattern by accessing to branching fractions, kinematic distributions, asymmetries of rare processes in the SM. In the forthcoming perspective with a help of LHCb, i.e., experiment devoted to B physics at LHC, we have additional tool to learn more about flavor physics with a higher precision.

Such rich experimental potential needs elaboration of appropriate observables. Such important observables are those from processes proceeding through FCNC. Being loop suppressed in the SM they could be very sensitive to NP contributions which can be easily detected. Practically all extensions of the SM, e.g, Higgs doublet models, fourth gereration, generic SUSY models, left-right models, extra dimensions etc., lead to new sources of CP-odd phases. Therefore additional tools to probe NP are CP violating observables. In this thesis we presented the example of the observables in semileptonic $b \to s$ penguins with the above discussed properties. Those are branching rates, angular distributions in rates, forward-backward asymmetries, CP-odd asymmetries where some of them present null tests of the SM. In the presence of NP we showed that the current experimental bounds from various rare decays give large enhancements for these observables.

In the leptonic sector the neutrino oscillation experiments of the last decade confirmed the existence of physics beyond the SM. In comparison with quark sector neutrino mixing is large, whereas the neutrino mass scale is $\mathcal{O}(0.1\,\mathrm{eV})$ being much smaller than quark and lepton masses. The topic of CP violation in the leptonic

sector is still untested. Depending on the neutrino mass nature, i.e., Dirac or Majorana mass, the number of CP violating phases can be three. The neutrino oscillation experiments can not distinguish neutrino mass type. Whereas, in the future the possible discovery of the neutrinoless double β-decay in some nuclei will claim that neutrino mass has Majorana origin.

The important role in the analysis of the neutrino oscillation experiments play the pion production from the nucleons with resonances as intermediate states. Therefore, it is crucial to understand the production of leptons and pions by neutrinos. The cross section of these processes depend on the nucleon-resonance form factors, which can be mainly extracted form the experimental data. The currently available neutrinoproduction data [49, 50, 51, 52] is not useful fot it due to low statistic and inconsistency with each other. The future experiments like Minerνa, MiniBooNE, OPERA, MINOS will improve this situation. Since the electroproduction data from JLAB and the Mainz accelerators is more consistent and precise we used it to define the vector form factors of nucleon-resonance transitions for first four resonances, $P_{33}(1232)$, $D_{13}(1520)$, $P_{11}(1440)$ and $S_{11}(1535)$. The calculated cross sections with the updated form factors claim the importance of the second resonance region, i.e., $D_{13}(1520)$, $P_{11}(1440)$ and $S_{11}(1535)$, with the energy increase of scattered neutrinos. The future improvements of lepton-nucleon scattering will also be useful to understand the phenomenon of quark-hadron duality (see more [116, 117]). For this the resonance production region is particularly interesting having possibility to link it with DIS region. These all dictate the need for further investigation in this field both from experimental (next generation of accelerators) and theoretical (precise calculations, background extraction, medium impact etc.) sides.

Thus, we expect that the near future of particle physics phenomenology will be extremely exciting and fruitful for new discoveries which are just around the corner.

A Resonance Production by Neutrinos

In this appendix we collect the relevant formulae for Chapter 2. Particularly, we give the explicit expressions for the structure functions of all four resonances, i.e., $P_{33}(1232)$, $D_{13}(1520)$, $P_{11}(1440)$ and $S_{11}(1535)$.

A.1 Structure of Hadronic Tensor for P_{33} and D_{13}

Following the notations of [38], we write the cross section of the resonance production in a form close to DIS, that is, express it via the hadronic structure functions $\mathcal{W}_{1...5}$ as

$$\begin{aligned}\frac{d\sigma}{dQ^2dW} &= \frac{G_F^2}{4\pi}\cos^2\theta_C\frac{W}{m_N E^2}\Bigg\{\mathcal{W}_1(Q^2+m_\mu^2)\\ &+ \frac{\mathcal{W}_2}{m_N^2}\left[2(k\cdot p)(k'\cdot p)-\frac{1}{2}m_N^2(Q^2+m_\mu^2)\right]\\ &+ \frac{\mathcal{W}_3}{m_N^2}\left[Q^2 k\cdot p-\frac{1}{2}q\cdot p(Q^2+m_\mu^2)\right]\\ &+ \frac{\mathcal{W}_4}{m_N^2}m_\mu^2\frac{(Q^2+m_\mu^2)}{2}-2\frac{\mathcal{W}_5}{m_N^2}m_\mu^2(k\cdot p)\Bigg\}. \end{aligned} \tag{A.1}$$

where m_μ is the mass of the muon. The hadronic structure functions for the resonance D_{13} are similar to those for the P_{33}, presented in paper [38] (see Appendix) and can be obtained from them by replacing $m_N M_R$ by $-m_N M_R$. In the formulae below the upper sign corresponds to the P_{33} resonance, whereas the lower sign corresponds to the D_{13}.

$$\mathcal{W}_i(Q^2,\nu)=\frac{2}{3m_N}V_i(Q^2,\nu)R(W,M_R), \tag{A.2}$$

$$
\begin{aligned}
V_1 = {} & \frac{(C_3^V)^2}{m_N^2 M_R^2}\left[(q\cdot p - Q^2)^2(q\cdot p + m_N^2) + M_R^2(m_N^2\nu^2 + Q^2 m_N^2 \pm Q^2 m_N M_R)\right] \\
& + \frac{(C_4^V)^2(q\cdot p - Q^2)^2 + (C_5^V)^2(q\cdot p)^2}{m_N^4}(q\cdot p + m_N^2 \mp m_N M_R) \\
& + \frac{C_3^V C_4^V(q\cdot p - Q^2) + C_3^V C_5^V q\cdot p}{m_N^3 M_R}\left[(q\cdot p - Q^2)(q\cdot p + m_N^2 \mp 2m_N M_R) + M_R^2 q\cdot p\right] \\
& + 2\frac{C_4^V C_5^V}{m_N^4} q\cdot p(q\cdot p - Q^2)(q\cdot p + m_N^2 \mp m_N M_R) \\
& + \left[\frac{(C_4^A)^2}{m_N^4}(q\cdot p - Q^2)^2 + (C_5^A)^2 + 2\frac{C_4^A C_5^A}{m_N^2}(q\cdot p - Q^2)\right]\left[q\cdot p + m_N^2 \pm m_N M_R\right],
\end{aligned}
\tag{A.3}
$$

$$
\begin{aligned}
V_2 = {} & \frac{(C_3^V)^2}{M_R^2}Q^2\left[q\cdot p + m_N^2 + M_R^2\right] + \frac{C_3^V C_4^V}{m_N M_R}Q^2\left[q\cdot p + (M_R \mp m_N)^2\right] \\
& + \frac{C_3^V C_5^V}{m_N M_R}\left[q\cdot p + (M_R \mp m_N)^2 + Q^2\right] \\
& + \left(\frac{(C_4^V)^2}{m_N^2} + \frac{(C_5^V)^2(Q^2 + M_R^2)}{m_N^2 M_R^2} + \frac{2C_4^V C_5^V}{m_N^2}\right)Q^2\left[q\cdot p + m_N^2 \mp m_N M_R\right] \\
& + \left[(C_5^A)^2\frac{m_N^2}{M_R^2} + \frac{(C_4^A)^2}{m_N^2}Q^2\right]\left[q\cdot p + m_N^2 \pm m_N M_R\right],
\end{aligned}
\tag{A.4}
$$

$$
\begin{aligned}
V_3 = {} & 2\left[C_3^V C_5^A\frac{m_N}{M_R} - \frac{C_3^V C_4^A}{M_R m_N}(Q^2 - q\cdot p)\right]\left(2M_R^2 \pm 2m_N M_R + Q^2 - q\cdot p\right) \\
& + 2\left[\frac{C_4^V C_4^A}{m_N^2}(Q^2 - q\cdot p) - C_4^V C_5^A\right](Q^2 - q\cdot p) \\
& + 2\left[C_5^V C_5^A - \frac{C_5^V C_4^A}{m_N^2}(Q^2 - q\cdot p)\right] q\cdot p.
\end{aligned}
\tag{A.5}
$$

These are the dominant structure functions for most of the kinematical region. There are two additional structure functions, whose contribution to the cross section is proportional to the square of the muon mass.

$$
\begin{aligned}
V_4 = {} & \frac{(C_3^V)^2}{M_R^2}\left[(2q\cdot p - Q^2)(q\cdot p + m_N^2) - M_R^2(m_N^2 \pm m_N M_R)\right] \\
& + \left(\frac{(C_4^V)^2(2q\cdot p - Q^2)}{m_N^2} + \frac{(C_5^V)^2(q\cdot p)^2}{m_N^2 M_R^2} + 2\frac{C_4^V C_5^V}{m_N^2}pq\right)\left[q\cdot p + m_N^2 \mp m_N M_R\right] \\
& + \frac{C_3^V C_4^V}{m_N M_R}\left[(2q\cdot p - Q^2)(q\cdot p + m_N^2 \mp 2m_N M_R) + q\cdot p M_R^2\right]
\end{aligned}
$$

$$
\begin{aligned}
&+ \frac{C_3^V C_5^V}{m_N M_R} q\cdot p \left[2q\cdot p + m_N^2 \mp 2m_N M_R + M_R^2 + Q^2\right] \\
&+ \Big[(C_5^A)^2 \frac{m_N^2}{M_R^2} + \frac{(C_4^A)^2}{m_N^2}(2q\cdot p - Q^2) + \frac{(C_6^A)^2}{m_N^2 M_R^2}\left((Q^2 - q\cdot p)^2 + Q^2 M_R^2\right) \\
&+ 2C_4^A C_5^A - 2\frac{C_4^A C_6^A}{m_N^2} q\cdot p \\
&- 2\frac{C_5^A C_6^A}{M_R^2}(M_R^2 + Q^2 - q\cdot p)\Big] \left[q\cdot p + m_N^2 + m_N M_R\right], \qquad \text{(A.6)}
\end{aligned}
$$

$$
\begin{aligned}
V_5 = &\frac{(C_3^V)^2}{M_R^2} q\cdot p \left[q\cdot p + m_N^2 + M_R^2\right] + \frac{C_3^V C_4^V}{m_N M_R} q\cdot p \left[q\cdot p + (M_R \mp m_N)^2\right] \\
&+ \frac{C_3^V C_5^V}{m_N M_R} q\cdot p \left[q\cdot p + (M_R \mp m_N)^2 + Q^2\right] \\
&+ 2\left(\frac{(C_4^V)^2}{m_N^2} + \frac{(C_5^V)^2(Q^2 + M_R^2)}{m_N^2 M_R^2} + \frac{C_4^V C_5^V}{m_N^2}\right) q\cdot p \left[q\cdot p + m_N^2 \mp m_N M_R\right] \\
&+ \Big[\frac{(C_4^A)^2}{m_N^2} q\cdot p + (C_5^A)^2 \frac{m_N^2}{M_R^2} + C_4^A C_5^A - \frac{C_4^A C_6^A}{m_N^2} Q^2 \\
&+ \frac{C_5^A C_6^A}{M_R^2}(q\cdot p - Q^2)\Big] \left[q\cdot p + m_N^2 \pm m_N M_R\right]. \qquad \text{(A.7)}
\end{aligned}
$$

A.2 Structure of the Hadronic Tensor for P_{11} and S_{11}

The hadronic structure functions for P_{11} and S_{11} resonances are:

$$
\begin{aligned}
V_1 = &\frac{(g_1^V)^2}{\mu^4}\left[(q\cdot p + m_N^2 \mp m_N M_R)\right] Q^4 \\
&+ \frac{(g_2^V)^2}{\mu^2}\left[2(q\cdot p)^2 + Q^2(m_N^2 \pm m_N M_R - q\cdot p)\right] \\
&+ \frac{g_1^V g_2^V}{\mu^3} 2Q^2\left[(q\cdot p)(M_R \mp m_N) \pm m_N Q^2\right] + (g_1^A)^2(m_N^2 \pm m_N M_R + q\cdot p), \qquad \text{(A.8)}
\end{aligned}
$$

$$
V_2 = 2m_N^2\left[\frac{(g_1^V)^2}{\mu^4} Q^4 + \frac{(g_2^V)^2}{\mu^2} Q^2 + (g_1^A)^2\right], \qquad \text{(A.9)}
$$

$$
V_3 = 4m_N^2\left[\frac{g_1^V g_1^A}{\mu^2} Q^2 + \frac{g_2^V g_1^A}{\mu}(M_R \pm m_N)\right], \qquad \text{(A.10)}
$$

$$
\begin{aligned}
V_4 = m_N^2 \Bigg[& \frac{(g_2^V)^2}{\mu^2} \left[q \cdot p - m_N^2 \mp m_N M_R \right] \\
& + \frac{(g_1^V)^2}{\mu^4} \left[2(q \cdot p)^2 - Q^2 (q \cdot p + m_N^2 \mp m_N M_R) \right] \\
& - \frac{g_1^V g_2^V}{\mu^3} \left[q \cdot p (M_R \mp m_N) \pm m_N Q^2 \right] \mp 2 g_1^A g_3^A + \frac{(g_3^A)^2}{m_N^2} \left[(q \cdot p) + m_N^2 \mp m_N M_R \right] \Bigg],
\end{aligned}
\tag{A.11}
$$

$$
V_5 = m_N^2 \left[2 \frac{(g_1^V)^2}{\mu^4} Q^2 q \cdot p + 2 \frac{(g_2^V)^2}{\mu^2} q \cdot p + (g_1^A)^2 + \frac{g_1^A g_3^A}{m_N} (M_R \mp m_N) \right], \tag{A.12}
$$

where the upper sign correspond to the P_{11} and the lower sign to the S_{11} resonances.

B Angular Analysis of $B \to K, K^* \bar{l} l$ Decays

Here we present auxiliary expressions and formulae which are important for the discussions in Chapter 3.

B.1 Angular Coefficients $J_i^{(a)}$

Here the functions $J_i^{(a)}$ in the angular distribution (3.74) are given in terms of the transversity amplitudes $A_{\perp,\parallel,0,t}$ [63]:

$$J_1^s = \frac{3}{4}\left\{ \frac{(2+\beta_l^2)}{4}\left[|A_\perp^L|^2 + |A_\parallel^L|^2 + (L \to R)\right] + \frac{4m_l^2}{q^2}\mathrm{Re}\left(A_\perp^L A_\perp^{R*} + A_\parallel^L A_\parallel^{R*}\right) \right\}, \tag{B.1}$$

$$J_1^c = \frac{3}{4}\left\{ |A_0^L|^2 + |A_0^R|^2 + \frac{4m_l^2}{q^2}\left[|A_t|^2 + 2\mathrm{Re}(A_0^L A_0^{R*})\right] \right\}, \tag{B.2}$$

$$J_2^s = \frac{3\beta_l^2}{16}\left[|A_\perp^L|^2 + |A_\parallel^L|^2 + (L \to R)\right], \tag{B.3}$$

$$J_2^c = -\frac{3\beta_l^2}{4}\left[|A_0^L|^2 + (L \to R)\right], \tag{B.4}$$

$$J_3 = \frac{3}{8}\beta_l^2\left[|A_\perp^L|^2 - |A_\parallel^L|^2 + (L \to R)\right], \tag{B.5}$$

$$J_4 = \frac{3}{4\sqrt{2}}\beta_l^2\left[\mathrm{Re}(A_0^L A_\parallel^{L*}) + (L \to R)\right], \tag{B.6}$$

$$J_5 = \frac{3\sqrt{2}}{4}\beta_l\left[\mathrm{Re}(A_0^L A_\perp^{L*}) - (L \to R)\right], \tag{B.7}$$

$$J_6 = \frac{3}{2}\beta_l\left[\mathrm{Re}(A_\parallel^L A_\perp^{L*}) - (L \to R)\right], \tag{B.8}$$

$$J_7 = \frac{3\sqrt{2}}{4}\beta_l\left[\mathrm{Im}(A_0^L A_\parallel^{L*}) - (L \to R)\right], \tag{B.9}$$

$$J_8 = \frac{3}{4\sqrt{2}}\beta_l^2\left[\mathrm{Im}(A_0^L A_\perp^{L*}) + (L \to R)\right], \tag{B.10}$$

$$J_9 = \frac{3}{4}\beta_l^2\left[\mathrm{Im}(A_\parallel^{L*} A_\perp^L) + (L \to R)\right]. \tag{B.11}$$

The transversity amplitudes in QCDF can be seen in (3.92) and have the following CP transformation properties [59]

$$A_0^{L,R} \xrightarrow{CP} \bar{A}_0^{L,R} = A_0^{L,R}(\delta_W \to -\delta_W), \tag{B.12}$$
$$A_\parallel^{L,R} \xrightarrow{CP} \bar{A}_\parallel^{L,R} = A_\parallel^{L,R}(\delta_W \to -\delta_W), \tag{B.13}$$
$$A_\perp^{L,R} \xrightarrow{CP} \bar{A}_\perp^{L,R} = -A_\perp^{L,R}(\delta_W \to -\delta_W). \tag{B.14}$$

B.2 Optimal Observables from Optimal Weights

It is possible to construct weight functions W_i which project out the J_i from the differential decay distribution (3.74). For this purpose it is convenient to rewrite the distribution J in terms of associated Legendre polynomials $P_l^m(x)$ in $\cos\theta_{K^*}$ and $\cos\theta_l$. The requisite polynomials read as

$$P_0^0(\cos\theta) = 1, \qquad P_1^0(\cos\theta) = \cos\theta, \tag{B.15}$$
$$P_1^1(\cos\theta) = -\sin\theta, \qquad P_2^0(\cos\theta) = \frac{1}{2}(3\cos^2\theta - 1), \tag{B.16}$$
$$P_2^1(\cos\theta) = -3\sin\theta\cos\theta, \qquad P_2^2(\cos\theta) = 3\sin^2\theta. \tag{B.17}$$

Introducing $x_1 = \cos\theta_{K*}$ and $x_2 = \cos\theta_l$, and using the orthonormality property of the Legendre polynomials one can compute weight functions defined as

$$J_i = \int dq^2\, dx_1\, dx_2\, d\phi\, W_i \frac{d^4\Gamma_{data}}{dq^2\, dx_1\, dx_2\, d\phi}, \tag{B.18}$$

where

$$W_{3,9} = \frac{25}{96} P_2^2(x_1) P_2^2(x_2) \cdot \begin{Bmatrix} \cos 2\phi \\ \sin 2\phi \end{Bmatrix}, \tag{B.19}$$
$$W_{4,8} = \frac{25}{24} P_2^1(x_1) P_2^1(x_2) \cdot \begin{Bmatrix} \cos\phi \\ \sin\phi \end{Bmatrix}, \tag{B.20}$$
$$W_{5,7} = \frac{5}{4} P_2^1(x_1) P_1^1(x_2) \cdot \begin{Bmatrix} \cos\phi \\ \sin\phi \end{Bmatrix}, \tag{B.21}$$
$$W_6 = \frac{5}{8} P_2^2(x_1) P_1^0(x_2). \tag{B.22}$$

B.3 CP Asymmetries and A_{FB} beyond the SM

Here we give analytical expressions of the CP asymmetries defined in (3.106) and (3.107) including contributions from NP operators (3.9). The asymmetries have

been obtained from the transversity amplitudes in QCDF, see (3.92), valid in the low dilepton mass region. The coefficients $C_7^{\rm eff} = C_7^{\rm eff,SM} + C_7^{\rm NP}$ and C_7' are taken into account by $\mathcal{T}_{\perp,\parallel}^{\pm}$. Except for $A_{\rm CP}$, the CP asymmetries are given with their full lepton mass dependence which is confined to powers of β_l. Neglecting kinematical factors $M_{K^*}^2/M_B^2$, the CP asymmetries as a function of the dilepton mass read as

$$A_{\rm CP} = \mathcal{A}\frac{8\hat{m}_b}{3\hat{s}}{\rm Re}\Bigg\{\frac{\xi_\parallel^2}{\xi_\perp^2}\frac{M_B^2}{M_{K^*}^2}\frac{(1-\hat{s})^2}{8}\left[\hat{m}_b\frac{|\mathcal{T}_\parallel^-|^2}{\xi_\parallel^2} - \frac{\mathcal{T}_\parallel^-}{\xi_\parallel}(C_9 - C_9')^*\right] + \frac{\hat{m}_b}{\hat{s}}\frac{|\mathcal{T}_\perp^+|^2 + |\mathcal{T}_\perp^-|^2}{\xi_\perp^2} + \frac{\mathcal{T}_\perp^+ - \mathcal{T}_\perp^-}{\xi_\perp}C_9^* + \frac{\mathcal{T}_\perp^+ + \mathcal{T}_\perp^-}{\xi_\perp}C_9'^* - (\delta_W \to -\delta_W)\Bigg\} + \mathcal{O}\left(m_l^2/q^2\right), \tag{B.23}$$

$$A_3 = \mathcal{A}\frac{2\hat{m}_b\beta_l}{\hat{s}}{\rm Re}\Bigg\{\frac{\hat{m}_b}{\hat{s}}\frac{|\mathcal{T}_\perp^+|^2 - |\mathcal{T}_\perp^-|^2}{\xi_\perp^2} + \frac{\mathcal{T}_\perp^+ - \mathcal{T}_\perp^-}{\xi_\perp}C_9^* + \frac{\mathcal{T}_\perp^+ + \mathcal{T}_\perp^-}{\xi_\perp}C_9'^* - (\delta_W \to -\delta_W)\Bigg\}, \tag{B.24}$$

$$A_4^D = -\mathcal{A}^D\frac{\hat{m}_b\beta_l}{2\hat{s}}{\rm Re}\Bigg\{\left(\frac{\mathcal{T}_\perp^-}{\xi_\perp} - \hat{s}\frac{\mathcal{T}_\parallel^-}{\xi_\parallel}\right)(C_9 - C_9')^* - 2\hat{m}_b\frac{\mathcal{T}_\perp^-(\mathcal{T}_\parallel^-)^*}{\xi_\perp\xi_\parallel} - (\delta_W \to -\delta_W)\Bigg\}, \tag{B.25}$$

$$A_5^D = -\mathcal{A}^D\frac{\hat{m}_b}{\hat{s}}{\rm Re}\Bigg\{\left(\frac{\mathcal{T}_\perp^-}{\xi_\perp} - \hat{s}\frac{\mathcal{T}_\parallel^-}{\xi_\parallel}\right)C_{10} - \left(\frac{\mathcal{T}_\perp^-}{\xi_\perp} + \hat{s}\frac{\mathcal{T}_\parallel^-}{\xi_\parallel}\right)C_{10}'^* - (\delta_W \to -\delta_W)\Bigg\}, \tag{B.26}$$

$$A_6 = \mathcal{A}\frac{4\hat{m}_b}{\hat{s}}{\rm Re}\Bigg\{\frac{\mathcal{T}_\perp^+ + \mathcal{T}_\perp^-}{\xi_\perp}C_{10}^* - \frac{\mathcal{T}_\perp^+ - \mathcal{T}_\perp^-}{\xi_\perp}C_{10}'^* - (\delta_W \to -\delta_W)\Bigg\}, \tag{B.27}$$

$$A_7^D = \mathcal{A}^D\frac{\hat{m}_b}{\hat{s}}{\rm Im}\Bigg\{(C_{10} - C_{10}')\left(\frac{\mathcal{T}_\perp^-}{\xi_\perp} + \hat{s}\frac{\mathcal{T}_\parallel^-}{\xi_\parallel}\right)^* - (\delta_W \to -\delta_W)\Bigg\}, \tag{B.28}$$

$$A_8^D = \mathcal{A}^D\frac{\beta_l}{2}\,{\rm Im}\Bigg\{\frac{2\hat{m}_b^2}{\hat{s}}\frac{\mathcal{T}_\perp^+(\mathcal{T}_\parallel^-)^*}{\xi_\perp\xi_\parallel} - \frac{\hat{m}_b}{\hat{s}}\left[\left(\frac{\mathcal{T}_\perp^+}{\xi_\perp} + \hat{s}\frac{\mathcal{T}_\parallel^-}{\xi_\parallel}\right)C_9^* - \left(\frac{\mathcal{T}_\perp^+}{\xi_\perp} - \hat{s}\frac{\mathcal{T}_\parallel^-}{\xi_\parallel}\right)C_9'^*\right] + C_9C_9'^* + C_{10}C_{10}'^* - (\delta_W \to -\delta_W)\Bigg\}, \tag{B.29}$$

$$A_9 = -\mathcal{A}\,2\beta_l{\rm Im}\Bigg\{\frac{2\hat{m}_b^2}{\hat{s}^2}\frac{\mathcal{T}_\perp^+(\mathcal{T}_\perp^-)^*}{\xi_\perp^2} + \frac{\hat{m}_b}{\hat{s}}\left[\frac{\mathcal{T}_\perp^+ - \mathcal{T}_\perp^-}{\xi_\perp}C_9^* - \frac{\mathcal{T}_\perp^+ + \mathcal{T}_\perp^-}{\xi_\perp}C_9'^*\right] - C_9C_9'^* - C_{10}C_{10}'^* - (\delta_W \to -\delta_W)\Bigg\}, \tag{B.30}$$

where $(\delta_W \to -\delta_W)$ is short hand notation for conjugating all weak phases. Furthermore,

$$\mathcal{A} = \frac{G_F^2\,\alpha_e^2}{3^2 \cdot 2^6\,\pi^5}|V_{tb}V_{ts}^*|^2 \frac{M_B^3 \beta_l^2 \hat{s}(1-\hat{s})^3 \xi_\perp^2}{N_\Gamma},$$
$$\mathcal{A}^D = \frac{G_F^2\,\alpha_e^2}{3^2 \cdot 2^6\,\pi^5}|V_{tb}V_{ts}^*|^2 \frac{M_B^4 \beta_l^2 \sqrt{\hat{s}}(1-\hat{s})^4 \xi_\parallel \xi_\perp}{M_{K^*} N_\Gamma}, \tag{B.31}$$

where N_Γ is defined in (3.106).

At lowest order in α_s, the expressions for the above CP asymmetries simplify by

$$\frac{\mathcal{T}_\perp^{+,\mathrm{LO}} \pm \mathcal{T}_\perp^{-,\mathrm{LO}}}{\xi_\perp} = \begin{cases} 2C_7^{\mathrm{eff}(0)} + \frac{\hat{s}}{\hat{m}_b}(Y^{(0)} + \hat{\lambda}_u Y^{(u)(0)}) \\ 2C_7^{\prime(0)} \end{cases}, \tag{B.32}$$

$$\frac{\mathcal{T}_\perp^{\pm,\mathrm{LO}}}{\xi_\perp} + \hat{s}\frac{\mathcal{T}_\parallel^{-,\mathrm{LO}}}{\xi_\parallel} = \begin{cases} (1-\hat{s})C_7^{\mathrm{eff}(0)} + (1+\hat{s})C_7^{\prime(0)} \\ (1-\hat{s})(C_7^{\mathrm{eff}(0)} - C_7^{\prime(0)}) \end{cases}, \tag{B.33}$$

$$\frac{\mathcal{T}_\perp^{\pm,\mathrm{LO}}}{\xi_\perp} - \hat{s}\frac{\mathcal{T}_\parallel^{-,\mathrm{LO}}}{\xi_\parallel} = \begin{cases} (1+\hat{s})C_7^{\mathrm{eff}(0)} + (1-\hat{s})C_7^{\prime(0)} + \frac{\hat{s}}{\hat{m}_b}(Y^{(0)} + \hat{\lambda}_u Y^{(u)(0)}) \\ (1+\hat{s})(C_7^{\mathrm{eff}(0)} - C_7^{\prime(0)}) + \frac{\hat{s}}{\hat{m}_b}(Y^{(0)} + \hat{\lambda}_u Y^{(u)(0)}) \end{cases}. \tag{B.34}$$

Note that in the SM, or more general, in any model without right-handed contributions to the electromagnetic dipole operator, $\mathcal{T}_\perp^+ = \mathcal{T}_\perp^-$, see Section 3.5.2.

The lepton forward-backward asymmetry is written as

$$A_{\mathrm{FB}} = \frac{12\beta_l N^2 M_B^2 (1-\hat{s})^2 \xi_\perp^2}{d\Gamma/dq^2} \times \mathrm{Re}\Bigg\{ \left[C_9 + \frac{\hat{m}_b}{\hat{s}}\frac{(\mathcal{T}_\perp^+ + \mathcal{T}_\perp^-)}{\xi_\perp}\right] C_{10}^* - \left[C_9' + \frac{\hat{m}_b}{\hat{s}}\frac{(\mathcal{T}_\perp^+ - \mathcal{T}_\perp^-)}{\xi_\perp}\right] C_{10}^{\prime *} \Bigg\}. \tag{B.35}$$

B.4 $\mathcal{T}_a$ Amplitudes

Here we present the expressions of the $\mathcal{T}_a$ $(a = P, \perp, \parallel)$ amplitudes calculated in QCDF [19, 20]. The matrix elements of the $\mathcal{O}_{9,10}$ operators of (3.3) can be directly expressed through the $B \to K, K^*$ form factors, whereas the remaining operators contribute via the exchange of a virtual photon which decays subsequently into the lepton pair. For the later part in QCDF one defines the matrix element as

$$\begin{aligned} \langle \gamma^* K^*(p,\varepsilon)|H_{\mathrm{eff}}^{(i)}|B(p_B)\rangle &= \frac{iem_b}{4\pi^2}\Big(2\,\mathcal{T}_\perp^{(i)}(q^2)\epsilon^{\mu\nu\rho\sigma}\varepsilon_\nu^* p_{B\rho} p_\sigma \\ &- 2i\,\mathcal{T}_\perp^{(i)}(q^2)[E_{K^*} M_B \varepsilon_\mu^* - (\varepsilon^* \cdot q)p^\mu] \\ &- i\,\mathcal{T}_\parallel^{(i)}(q^2)(\varepsilon^* \cdot q)\big[q^\mu - \frac{q^2}{M_B^2}(p_B^\mu + p^\mu)\big]\Big), \end{aligned} \tag{B.36}$$

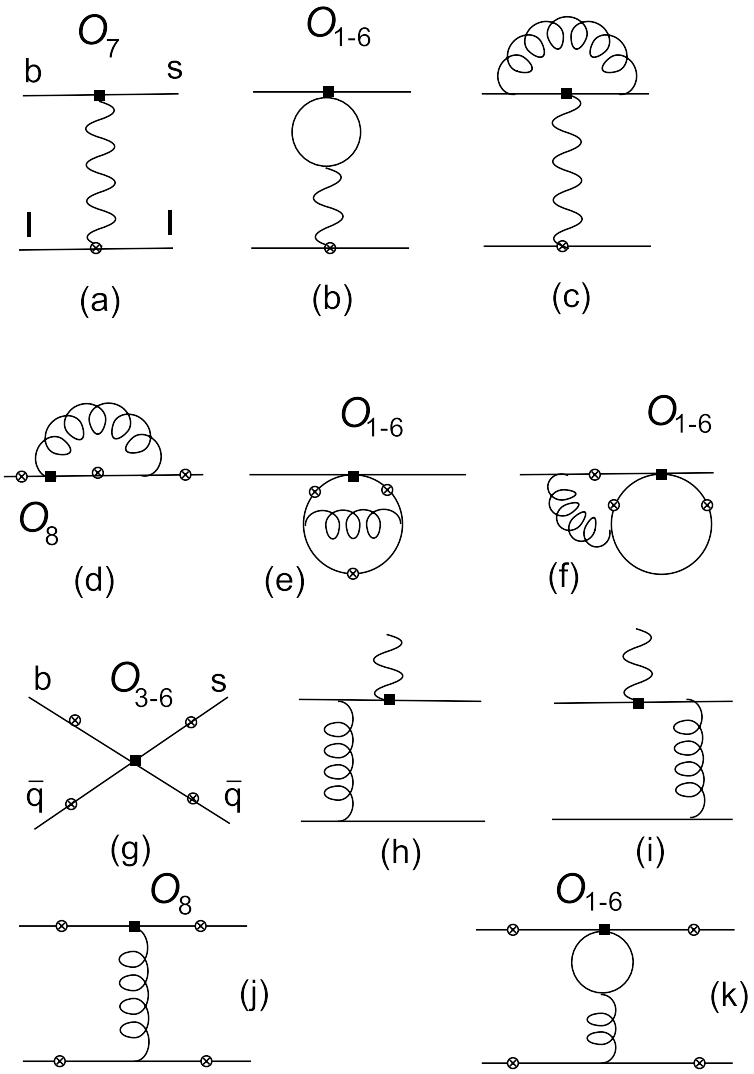

Figure B.1: The diagrams contributing to the matrix elements $\langle \gamma^* K, K^* | H_{\text{eff}}^{(i)} | B \rangle$. The crossed circles mark the interaction vertices of the photon (see Appendix B.4 for details).

for $B \to K^* \bar{l} l$ decays and

$$\langle \gamma^* K(p,\varepsilon)|H_{\rm eff}^{(t)}|B(p_B)\rangle = \frac{e m_b}{4\pi^2\, M_B}\, \mathcal{T}_P(q^2)\big[q^2(p_B^\mu + p^\mu) - (M_B^2 - M_K^2)q^\mu\big], \quad \text{(B.37)}$$

for $B \to K \bar{l} l$ decays. $\mathcal{T}_a$ $(a = \perp, \parallel, P)$ contain factorizable (f) and non-factorizable (nf) contributions [19, 20]:

$$\mathcal{T}_a^{(i)} = C_a^{(i)} \xi_a(q^2) + \frac{\pi^2}{N_c}\frac{f_B\, f_a^{(K^*)}}{M_B}\Xi_a \sum_{\pm} \int \frac{d\omega}{\omega}\Phi_{B,\pm}(\omega) \int_0^1 du\, \Phi_a^{(K^*)}(u) T_{a,\pm}^{(i)}(u,w), \quad \text{(B.38)}$$

where $\Xi_{\perp,P} = 1$ and $\Xi_\parallel = m_{K^*}/E_{K^*}$. The first term depends on "soft" form factors $\xi_\perp$, $\xi_\parallel$ and ξ_P. f_B,f_K and f_a^K denote the B-, K- and K^*-meson decay constants, respectively, whereas $\Phi_{B,\pm}(\omega)$, $\Phi_K(u)$ and $\Phi_a^{(K^*)}(u)$ are corresponding the light cone distribution amplitudes (explicit expressions for the Φ_a, $\Phi_{B,\pm}$ one can find in [19]). The remaining quantities C's and T's are calculable perturbatively

$$\begin{aligned} C_a^{(i)} &= C_a^{(0,i)} + \tfrac{\alpha_s C_F}{4\pi} C_a^{(1,i)} + ..., \\ T_{a,\pm}^{(i)}(u,w) &= T_{a,\pm}^{(0,i)} + \tfrac{\alpha_s C_F}{4\pi} T_{a,\pm}^{(1,i)} + ... \end{aligned} \quad \text{(B.39)}$$

The strong coupling α_s is evaluated differently for C and T coefficients, at the scale $\mu_b \sim m_b$ and the scale $\mu_f \sim (m_b \Lambda_{\rm QCD})^{1/2}$. At leading order the diagrams in Figure B.1 (a), (b) and (g) contribute where the crossed circles mark the interaction vertices of the photon. Leading order coefficients C equal

$$\begin{aligned} C_\perp^{(0,t)} &= C_7^{\rm eff} + \frac{q^2}{2m_b M_B} Y(q^2), & C_\parallel^{(0,t)} &= -C_7^{\rm eff} - \frac{M_B}{2m_b} Y(q^2), \\ C_\perp^{(0,u)} &= \frac{q^2}{2m_b M_B} Y^{(u)}(q^2), & C_\parallel^{(0,u)} &= -\frac{M_B}{2m_b} Y^{(u)}(q^2), \\ C_P^{(0)} &= -C_\parallel^{(0,t)}, \end{aligned} \quad \text{(B.40)}$$

where $C_7^{\rm eff} = C_7 - C_3/3 - 4C_4/9 - 20C_5/3 - 80C_6/9$. Explicitly $Y(q^2)$ and $Y^{(u)}(q^2)$ read as

$$\begin{aligned} Y(q^2) = {} & h(q^2,0)\Big[-\frac{1}{2}C_3 - \frac{2}{3}C_4 - 8C_5 - \frac{32}{3}C_6\Big] \\ & + h(q^2,m_c)\Big[\frac{4}{3}C_1 + C_2 + 6C_3 + 60C_5\Big] \\ & + h(q^2,m_b)\Big[-\frac{7}{2}C_3 - \frac{2}{3}C_4 - 38C_5 - \frac{32}{3}C_6\Big] + \frac{4}{3}C_3 + \frac{64}{9}C_5 + \frac{64}{27}C_6, \\ Y^{(u)}(q^2) = {} & \Big[\frac{4}{3}C_1 + C_2\Big](h(q^2,m_c) - h(q^2,0)), \end{aligned} \quad \text{(B.41)}$$

where

$$h(q^2,m_q)=-\frac{4}{9}\left(\ln\frac{m_q^2}{\mu^2}-\frac{2}{3}-z\right)-\frac{4}{9}(2+z)\sqrt{|z-1|}\begin{cases}\arctan\dfrac{1}{\sqrt{z-1}} & z>1\\ \ln\dfrac{1+\sqrt{1-z}}{\sqrt{z}}-\dfrac{i\pi}{2} & z\le 1\end{cases}, \tag{B.42}$$

defining $z=4m_q^2/q^2$. The diagram Figure B.1 (c) contributes to $C_P^{(\mathrm{f})}$ and the diagrams Figure B.1 (d), (e) and (f) to the quantity $C_P^{(\mathrm{nf})}$.

The first-order corrections to C's are separated into "factorizable" (diagram (c) of the Figure B.1) and "non-factorizable" (diagrams (d), (e) and (f) of the Figure B.1) parts $C_a^{(1,i)}=C_a^{(f,i)}+C_a^{(nf,i)}$ and they read as

$$\begin{aligned} C_\perp^{(f,t)}&=C_7^{\mathrm{eff}}\left(\ln\frac{m_b^2}{\mu^2}-L+\Delta M\right), & C_\parallel^{(f,t)}&=-C_7^{\mathrm{eff}}\left(\ln\frac{m_b^2}{\mu^2}+2L+\Delta M\right),\\ C_\perp^{(f,u)}&=C_\parallel^{(f,u)}=0, & C_P^{(\mathrm{f})}&=-C_\parallel^{(f,t)}. \end{aligned} \tag{B.43}$$

The ΔM depends on the renormalization scheme of m_b which is the overall factor in the (B.36) and (B.37). In the scheme (PS scheme) used here ΔM and L are defined as

$$L=-\frac{m_b^2-q^2}{q^2}\ln\left(1-\frac{q^2}{m_b^2}\right), \qquad \Delta M=3\ln\frac{m_b^2}{\mu^2}-4\left(1-\frac{\mu_f}{m_b}\right). \tag{B.44}$$

The factorization scale in the PS scheme is chosen $\mu_f=2\,\mathrm{GeV}$, see also Table 3.4. The "non-factorizable" parts of the $C_a^{(1,i)}$ have the following form

$$\begin{aligned} C_\perp^{(nf,t)}&=\frac{3}{4}\Bigg(-(C_2-\frac{1}{6}C_1)F_2^{(7)}-C_8^{\mathrm{eff}}F_8^{(7)}\\ &\quad-\frac{q^2}{m_bM_B}\big[(C_2-\frac{1}{6}C_1)F_2^{(9)}+2C_1\big(F_1^{(9)}+\frac{1}{6}F_2^{(9)}\big)+C_8^{\mathrm{eff}}F_8^{(9)}\big]\Bigg), \end{aligned} \tag{B.45}$$

$$\begin{aligned} C_\parallel^{(nf,t)}&=\frac{3}{4}\Bigg((C_2-\frac{1}{6}C_1)F_2^{(7)}+C_8^{\mathrm{eff}}F_8^{(7)}\\ &\quad+\frac{M_B}{2m_b}\big[(C_2-\frac{1}{6}C_1)F_2^{(9)}+2C_1\big(F_1^{(9)}+\frac{1}{6}F_2^{(9)}\big)+C_8^{\mathrm{eff}}F_8^{(9)}\big]\Bigg), \end{aligned} \tag{B.46}$$

$$C_P^{(nf)}=-C_\parallel^{(nf,t)}, \tag{B.47}$$

where $C_8^{\mathrm{eff}}=C_8+C_3-C_4/6+20C_5-10C_6/3$. The functions $F_8^{(7),(9)}$ correspond to 1-loop matrix element of the operator $\mathcal{O}_8$ and can be found in [19], whereas $F_{1,2}^{(7),(9)}$ being 2-loop matrix element of the $\mathcal{O}_{1,2}$ operators, can be extracted from [110]. The corresponding expressions for $C_a^{(nf,u)}$ one can be obtained by replacing the $F_8^{(7,9)}\to 0$ and $F_{1,2}^{(7,9)}\to F_{1,2}^{(7,9)}-F_{1,2,u}^{(7,9)}$ with $F_{1,2,u}^{(7,9)}$ given in [110].

Only the longitudinal amplitude receives contribution from spectator scattering at leading order. This contribution comes from the so-called weak annihilation diagram

where the photon is emitted from the spectator quark in the B meson which later decays into lepton-antilepton pair (diagram (g) of Figure B.1):

$$T_{\perp,+}^{(0,i)}(u,\omega) = T_{\perp,-}^{(0,i)}(u,\omega) = T_{\parallel,+}^{(0,i)}(u,\omega) = 0, \tag{B.48}$$

$$T_{\parallel,-}^{(0,t)}(u,\omega) = -e_q \frac{M_B\omega}{M_B\omega - q^2 - i\epsilon} \frac{4M_B}{m_b} (C_3 + \frac{4}{3}C_4 + 16C_5 + \frac{64}{3}C_6), \tag{B.49}$$

$$T_{\parallel,-}^{(0,u)}(u,\omega) = e_q \frac{M_B\omega}{M_B\omega - q^2 - i\epsilon} \frac{4M_B}{m_b} \delta_{qu} 3C_2, \tag{B.50}$$

$$T_{P,-}^{(0)} = -T_{\parallel,-}^{(0,t)}, \qquad T_{P,+}^{(0)} = 0, \tag{B.51}$$

where $T_{\parallel,-}^{(0,u)}$ is relevant only for charged B-meson modes.

The $T_{a,\pm}^{1,i}$ are also divided into "factorizable" (diagrams (h), (i) of Figure B.1) and "non-factorizable" (diagrams (j), (k) of Figure B.1) parts $T_{a,\pm}^{(1,i)} = T_{a,\pm}^{(f,i)} + T_{a,\pm}^{(nf,i)}$. The factorizable contributions read as

$$T_{\perp,+}^{(f,t)}(u,\omega) = C_7^{eff} \frac{2M_B}{\bar{u}E_{K^*}}, \qquad T_{\parallel,+}^{(f,t)}(u,\omega) = C_7^{eff} \frac{4M_B}{\bar{u}E_{K^*}}, \tag{B.52}$$

$$T_{\perp,-}^{(f,t)}(u,\omega) = T_{\parallel,-}^{(f,t)}(u,\omega) = T_{\perp,\pm}^{(f,u)}(u,\omega) = T_{\parallel,\pm}^{(f,u)}(u,\omega) = 0, \tag{B.53}$$

$$T_{P,+}^{(\mathrm{f})} = -T_{\parallel,+}^{(f,t)}, \qquad T_{P,-}^{(\mathrm{f})} = 0. \tag{B.54}$$

The non-factorizable contributions of the top-sector read as

$$\begin{aligned} T_{\perp,+}^{(\mathrm{nf,t})}(u,\omega) = &-\frac{4e_d\, C_8^{\mathrm{eff}}}{u + \bar{u}q^2/M_B^2} + \frac{M_B}{2m_b} \Big[e_u t_\perp(u,m_c) (C_2 - \frac{1}{2}C_1 + 6C_6) \\ &+ e_d\, t_\perp(u,m_b) (C_3 - \frac{1}{6}C_4 + 16C_5 + \frac{10}{3}C_6 - \frac{4m_b}{M_B}(C_3 - \frac{1}{6}C_4 + 4C_5 - \frac{2}{3}C_6)) \\ &+ e_d\, t_\perp(u,0) (C_3 - \frac{1}{6}C_4 + 16C_5 - \frac{8}{3}C_6) \Big], \end{aligned}$$

$$T_{\perp,-}^{(\mathrm{nf,t})}(u,\omega) = 0,$$

$$\begin{aligned} T_{\parallel,+}^{(\mathrm{nf,t})}(u,\omega) = &\frac{M_B}{m_b} \Big[e_u t_\parallel(u,m_c) (C_2 - \frac{1}{2}C_1 + 6C_6) \\ &+ e_d\, t_\parallel(u,m_b) (C_3 - \frac{1}{6}C_4 + 16C_5 + \frac{10}{3}C_6) \\ &+ e_d\, t_\parallel(u,0) (C_3 - \frac{1}{6}C_4 + 16C_5 - \frac{8}{3}C_6) \Big], \end{aligned}$$

$$\begin{aligned} T_{\parallel,-}^{(\mathrm{nf,t})}(u,\omega) = &e_q \frac{M_B\omega}{M_B\omega - q^2 - i\epsilon} \Big[\frac{8\, C_8^{\mathrm{eff}}}{\bar{u} + uq^2/M_B^2} \\ &+ \frac{6M_B}{m_b} \Big(h(\bar{u}M_B^2 + uq^2, m_c) (C_2 - \frac{1}{2}C_1 + C_4 + 10C_6) \end{aligned}$$

$$+ h(\bar{u}M_B^2 + uq^2, m_b)\,(C_3 + \frac{5}{6}C_4 + 16C_5 + \frac{22}{3}C_6)$$
$$+ \; h(\bar{u}M_B^2 + uq^2, 0)\,(C_3 + \frac{17}{6}C_4 + 16C_5 + \frac{82}{3}C_6)$$
$$- \frac{8}{27}\,(-\frac{15}{2}C_4 + 12C_5 - 32C_6)\Big)\Big],$$

$$T_{P,\pm}^{(\mathrm{nf})}(u,\omega) = -T_{\parallel,\pm}^{(\mathrm{nf,t})}. \tag{B.55}$$

Here $\bar{u} = 1-u$, $e_u = 2/3$, $e_d = -1/3$ and e_q is the electric charge of the spectator quark in the B meson. The explicit expressions for the $t_a(u, m_q)$ can be found in [19].

B.5 Model-independent CP Asymmetries beyond the SM

We give numerical formulae for the q^2-integrated quantities $\mathcal{B} = \tau_{B^0}\langle d\Gamma/dq^2\rangle$, $\overline{\mathcal{B}} = \tau_{B^0}\left\langle d\bar{\Gamma}/dq^2\right\rangle$ and $\mathrm{Num}\left\langle A_i^{(D)}\right\rangle$ for $q^2 \in [1,6]\ \mathrm{GeV}^2$ in terms of the NP Wilson coefficients C_i^{NP}. Here, $\mathrm{Num}\left\langle A_i^{(D)}\right\rangle$ denotes the numerators of the CP asymmetries multiplied by the B-meson lifetime such that the normalized CP asymmetries (see (3.108)) are obtained from

$$\left\langle A_i^{(D)}\right\rangle = \frac{\mathrm{Num}\left\langle A_i^{(D)}\right\rangle}{\mathcal{B} + \overline{\mathcal{B}}}. \tag{B.56}$$

The dependence of the branching ratios on the NP Wilson coefficients can be written as

$$X = X_{\mathrm{SM}}\Big[1 + \sum_i \left(a_i|C_i^{\mathrm{NP}}|^2 + b_i\mathrm{Re}C_i^{\mathrm{NP}} + c_i\mathrm{Im}C_i^{\mathrm{NP}}\right) + \sum_{j>i} d_{ij}\mathrm{Re}(C_i^{\mathrm{NP}}C_j^{\mathrm{NP}*})\Big] \tag{B.57}$$

for $\mathcal{B}$, $\overline{\mathcal{B}}$, whereas the numerators of the T-odd CP asymmetries are parametrized as

$$X = X_{\mathrm{SM}}\Big[1 + \sum_i \left(b_i\mathrm{Re}C_i^{\mathrm{NP}} + c_i\mathrm{Im}C_i^{\mathrm{NP}}\right) + \sum_{j>i} e_{ij}\mathrm{Im}(C_i^{\mathrm{NP}}C_j^{\mathrm{NP}*})\Big] \text{ for } \mathrm{Num}\left\langle A_{7,8}^D\right\rangle. \tag{B.58}$$

The numerators of the T-even CP asymmetries read as

$$X = X_{\mathrm{SM}}\Big[1 + \sum_i \left(b_i\mathrm{Re}C_i^{\mathrm{NP}} + c_i\mathrm{Im}C_i^{\mathrm{NP}}\right)\Big] \quad \text{for } \mathrm{Num}\left\langle A_{\mathrm{CP},6}\right\rangle, \mathrm{Num}\left\langle A_{4,5}^D\right\rangle. \tag{B.59}$$

$X_{\rm SM}$		$i=7$	$i=7'$	$i=9$	$i=9'$	$i=10$	$i=10'$
$\mathcal{B}_{\rm SM}$	a_i	2.634	2.634	0.035	0.035	0.035	0.035
	b_i	−0.271	−0.373	0.162	−0.179	−0.288	0.205
$= 2.444 \cdot 10^{-7}$	c_i	−0.156	0.001	−0.009	−0.0002	0	0
$\overline{\mathcal{B}}_{\rm SM}$	a_i	2.656	2.656	0.036	0.036	0.035	0.035
	b_i	−0.312	−0.370	0.158	−0.178	−0.290	0.206
$= 2.423 \cdot 10^{-7}$	c_i	0.106	0.003	0.004	0.002	0	0
$\mathrm{Num}\,\langle A_{\rm CP}\rangle_{\rm SM}$	b_i	4.469	−0.726	0.587	−0.345	0	0
$= 2.068 \cdot 10^{-9}$	c_i	−30.770	−0.275	−1.500	−0.259	0	0
$\mathrm{Num}\,\langle A_3\rangle_{\rm SM}$	b_i	−0.077	5.720	−0.012	0.378	0	0
$= 0^\dagger$	c_i	0.542	−47.174	0.081	−2.743	0	0
$\mathrm{Num}\,\langle A_4^D\rangle_{\rm SM}$	b_i	3.604	−3.604	0.536	−0.536	0	0
$= -8.642 \cdot 10^{-10}$	c_i	−1.435	1.435	−2.487	2.487	0	0
$\mathrm{Num}\,\langle A_5^D\rangle_{\rm SM}$	b_i	0	0	0	0	−0.244	0.068
$= 3.718 \cdot 10^{-9}$	c_i	0	0	0	0	1.152	−1.258
$\mathrm{Num}\,\langle A_6\rangle_{\rm SM}$	b_i	0	0	0	0	−0.244	0.004
$= -3.117 \cdot 10^{-9}$	c_i	0	0	0	0	1.774	−0.026
$\mathrm{Num}\,\langle A_7^D\rangle_{\rm SM}$	b_i	0	0	0	0	−0.244	0.244
$= -2.496 \cdot 10^{-9}$	c_i	−247.248	247.248	0	0	23.019	−23.019
$\mathrm{Num}\,\langle A_8^D\rangle_{\rm SM}$	b_i	−0.491	−1.423	0.176	−0.288	0	0
$= 1.706 \cdot 10^{-9}$	c_i	−189.333	−170.364	−16.524	−7.160	0	26.834
$\mathrm{Num}\,\langle A_9\rangle_{\rm SM}$	b_i	0	−8.390	0.007	−0.491	0	0
$= 0^\dagger$	c_i	−6.514	225.487	−0.568	6.064	0	31.913

Table B.1: The SM predictions $X_{\rm SM}$ and the corresponding coefficients a_i, b_i and c_i for $i = 7, 7', 9, 9', 10, 10'$. †For $\mathrm{Num}\,\langle A_{3,9}\rangle$ $X_{\rm SM}$ has been set to zero and the corresponding coefficients are given in units of 10^{-9}.

d_{ij}	$\mathcal{B}$	$\overline{\mathcal{B}}$	e_{ij}	Num $\langle A_7^D \rangle$	Num $\langle A_8^D \rangle$	Num $\langle A_9 \rangle^\dagger$
$7, 7'$	-0.255	-0.257	$7, 7'$	0	200.542	1801.269
$7, 9$	0.394	0.397	$7, 9$	0	-43.413	-1.547
$7, 9'$	-0.107	-0.108	$7, 9'$	0	56.532	105.869
$7, 10$	0	0	$7, 10$	60.420	0	0
$7, 10'$	0	0	$7, 10'$	-60.420	0	0
$7', 9$	-0.107	-0.108	$7', 9$	0	-56.532	-105.869
$7', 9'$	0.394	0.397	$7', 9'$	0	43.413	1.547
$7', 10$	0	0	$7', 10$	-60.420	0	0
$7', 10'$	0	0	$7', 10'$	60.420	0	0
$9, 9'$	-0.050	-0.050	$9, 9'$	0	6.558	7.799
$10, 10'$	-0.050	-0.050	$10, 10'$	0	6.558	7.799

Table B.2: The coefficients d_{ij} and e_{ij} for $i, j = 7, 7', 9, 9', 10, 10'$ and $j > i$. †For Num $\langle A_9 \rangle$ $X_{\rm SM}$ has been set to zero and the corresponding coefficients are given in units of 10^{-9}.

Here, the summations are over $i, j = 7, 7', 9, 9', 10, 10'$ and $X_{\rm SM}$ denotes the SM prediction of the corresponding quantity. Note that for Num $\langle A_{3,9} \rangle$ we have set $X_{\rm SM}$ to zero, see Section 3.5.2, and, hence, the corresponding formulae read as

$$X = \sum_i \left(b_i \mathrm{Re} C_i^{\rm NP} + c_i \mathrm{Im} C_i^{\rm NP} \right) \quad \text{for Num} \langle A_3 \rangle \,, \tag{B.60}$$

$$X = \sum_i \left(b_i \mathrm{Re} C_i^{\rm NP} + c_i \mathrm{Im} C_i^{\rm NP} \right) + \sum_{j>i} e_{ij} \mathrm{Im} (C_i^{\rm NP} C_j^{\rm NP *}) \quad \text{for Num} \langle A_9 \rangle \,. \tag{B.61}$$

The SM predictions $X_{\rm SM}$ and the coefficients a_i, b_i, c_i and d_{ij}, e_{ij} are given in Table B.1 and Table B.2, respectively. We assumed central values for all parameters.

Bibliography

[1] S. L. Glashow, "Partial Symmetries of Weak Interactions," *Nucl. Phys.*, vol. 22, pp. 579–588, 1961.

[2] S. Weinberg, "A Model of Leptons," *Phys. Rev. Lett.*, vol. 19, pp. 1264–1266, 1967.

[3] A. Salam, "Weak and Electromagnetic Interactions," Originally printed in *Svartholm: Elementary Particle Theory, Proceedings Of The Nobel Symposium Held 1968 At Lerum, Sweden*, Stockholm 1968, 367-377.

[4] P. H. Frampton, P. Q. Hung, and M. Sher, "Quarks and leptons beyond the third generation," *Phys. Rept.*, vol. 330, p. 263, 2000, hep-ph/9903387.

[5] P. Q. Hung and M. Sher, "Experimental constraints on fourth generation quark masses," *Phys. Rev.*, vol. D77, p. 037302, 2008, 0711.4353.

[6] A. D. Sakharov, "Violation of CP Invariance, c Asymmetry, and Baryon Asymmetry of the Universe," *Pisma Zh. Eksp. Teor. Fiz.*, vol. 5, pp. 32–35, 1967.

[7] R. N. Mohapatra and A. Y. Smirnov, "Neutrino mass and new physics," *Ann. Rev. Nucl. Part. Sci.*, vol. 56, pp. 569–628, 2006, hep-ph/0603118.

[8] P. W. Higgs, "Broken Symmetries and the Masses of Gauge Bosons," *Phys. Rev. Lett.*, vol. 13, pp. 508–509, 1964.

[9] G. S. Guralnik, C. R. Hagen, and T. W. B. Kibble, "Global Conservation Laws and Massless Particles," *Phys. Rev. Lett.*, vol. 13, pp. 585–587, 1964.

[10] J. F. Gunion, H. E. Haber, G. L. Kane, and S. Dawson, "The Higgs Hunter's Guide," SCIPP-89/13.

[11] A. Strumia and F. Vissani, "Neutrino masses and mixings and.," 2006, hep-ph/0606054.

[12] T. Schwetz, "Neutrino oscillations: present status and outlook," *AIP Conf. Proc.*, vol. 981, pp. 8–12, 2008, 0710.5027.

[13] N. Cabibbo, "Unitary Symmetry and Leptonic Decays," *Phys. Rev. Lett.*, vol. 10, pp. 531–532, 1963.

[14] M. Kobayashi and T. Maskawa, "CP Violation in the Renormalizable Theory of Weak Interaction," *Prog. Theor. Phys.*, vol. 49, pp. 652–657, 1973.

[15] W. M. Yao *et al.*, "Review of particle physics," *J. Phys.*, vol. G33, pp. 1–1232, 2006.

[16] L. Wolfenstein, "Parametrization of the Kobayashi-Maskawa Matrix," *Phys. Rev. Lett.*, vol. 51, p. 1945, 1983.

[17] C. Jarlskog, "Commutator of the Quark Mass Matrices in the Standard Electroweak Model and a Measure of Maximal CP Violation," *Phys. Rev. Lett.*, vol. 55, p. 1039, 1985.

[18] "CKMfitter webpage: http://ckmfitter.in2p3.fr,"

[19] M. Beneke, T. Feldmann, and D. Seidel, "Systematic approach to exclusive $B \to V l^+ l^-, V\gamma$ decays," *Nucl. Phys.*, vol. B612, pp. 25–58, 2001, hep-ph/0106067.

[20] M. Beneke, T. Feldmann, and D. Seidel, "Exclusive radiative and electroweak $b \to d$ and $b \to s$ penguin decays at NLO," *Eur. Phys. J.*, vol. C41, pp. 173–188, 2005, hep-ph/0412400.

[21] M. Beneke, G. Buchalla, M. Neubert, and C. T. Sachrajda, "QCD factorization for $B \to \pi\pi$ decays: Strong phases and CP violation in the heavy quark limit," *Phys. Rev. Lett.*, vol. 83, pp. 1914–1917, 1999, hep-ph/9905312.

[22] M. Beneke, G. Buchalla, M. Neubert, and C. T. Sachrajda, "QCD factorization for exclusive, non-leptonic B meson decays: General arguments and the case of heavy-light final states," *Nucl. Phys.*, vol. B591, pp. 313–418, 2000, hep-ph/0006124.

[23] S. W. Bosch and G. Buchalla, "The radiative decays $B \to V\gamma$ at next-to-leading order in QCD," *Nucl. Phys.*, vol. B621, pp. 459–478, 2002, hep-ph/0106081.

[24] A. Ali and A. Y. Parkhomenko, "Branching ratios for $B \to \rho\gamma$ decays in next-to- leading order in $alpha_s$ including hard spectator corrections," *Eur. Phys. J.*, vol. C23, pp. 89–112, 2002, hep-ph/0105302.

[25] J. Charles, A. Le Yaouanc, L. Oliver, O. Pene, and J. C. Raynal, "Heavy-to-light form factors in the heavy mass to large energy limit of QCD," *Phys. Rev.*, vol. D60, p. 014001, 1999, hep-ph/9812358.

[26] M. Beneke and T. Feldmann, "Symmetry-breaking corrections to heavy-to-light B meson form factors at large recoil," *Nucl. Phys.*, vol. B592, pp. 3–34, 2001, hep-ph/0008255.

[27] S. L. Adler, "Photoproduction, electroproduction and weak single pion production in the (3,3) resonance region," *Ann. Phys.*, vol. 50, pp. 189–311, 1968.

[28] P. A. Zucker, "Weak production of nucleon resonances," *Phys. Rev.*, vol. D4, p. 3350, 1971.

[29] C. H. Llewellyn Smith, "Neutrino reactions at accelerator energies," *Phys. Rept.*, vol. 3, p. 261, 1972.

[30] P. A. Schreiner and F. Von Hippel, "Neutrino production of the $\delta(1236)$," *Nucl. Phys.*, vol. B58, pp. 333–362, 1973.

[31] E. A. Paschos, J.-Y. Yu, and M. Sakuda, "Neutrino production of resonances," *Phys. Rev.*, vol. D69, p. 014013, 2004, hep-ph/0308130.

[32] G. L. Fogli and G. Nardulli, "A new approach to the charged current induced weak one pion production," *Nucl. Phys.*, vol. B160, p. 116, 1979.

[33] G. L. Fogli and G. Nardulli, "Neutral current induced one pion production: A new model and its comparison with the experiment," *Nucl. Phys.*, vol. B165, p. 162, 1980.

[34] D. Rein and L. M. Sehgal, "Neutrino excitation of baryon resonances and single pion production," *Ann. Phys.*, vol. 133, p. 79, 1981.

[35] E. A. Paschos, L. Pasquali, and J. Y. Yu, "Single pion production in neutrino reactions and estimates for charge-exchange effects," *Nucl. Phys.*, vol. B588, pp. 263–280, 2000, hep-ph/0005255.

[36] E. A. Paschos and J. Y. Yu, "Neutrino interactions in oscillation experiments," *Phys. Rev.*, vol. D65, p. 033002, 2002, hep-ph/0107261.

[37] L. Alvarez-Ruso, S. K. Singh, and M. J. Vicente Vacas, "$\nu d \to \mu^- \delta^{++} n$ reaction and axial vector $n\delta$ coupling," *Phys. Rev.*, vol. C59, pp. 3386–3392, 1999, nucl-th/9804007.

[38] O. Lalakulich and E. A. Paschos, "Resonance production by neutrinos. i: J = 3/2 resonances," *Phys. Rev.*, vol. D71, p. 074003, 2005, hep-ph/0501109.

[39] V. D. Burkert, R. De Vita, M. Battaglieri, M. Ripani, and V. Mokeev, "Single quark transition model analysis of electromagnetic nucleon resonance excitations in the (70,1-) supermultiplet," *Phys. Rev.*, vol. C67, p. 035204, 2003, hep-ph/0212108.

[40] V. D. Burkert and T. S. H. Lee, "Electromagnetic meson production in the nucleon resonance region," *Int. J. Mod. Phys.*, vol. E13, pp. 1035–1112, 2004, nucl-ex/0407020.

[41] I. G. Aznauryan *et al.*, "Electroexcitation of the $P_{33}(1232)$, $P_{11}(1440)$, $D_{13}(1520)$, $S_{11}(1535)$ at $Q^2 = 0.4 - (\mathrm{GeV/c})^2$ and $0.65 - (\mathrm{GeV/c})^2$," *Phys. Rev.*, vol. C71, p. 015201, 2005, nucl-th/0407021.

[42] L. Tiator *et al.*, "Electroproduction of nucleon resonances," *Eur. Phys. J.*, vol. A19, pp. 55–60, 2004, nucl-th/0310041.

[43] M. Gorchtein, D. Drechsel, M. M. Giannini, E. Santopinto, and L. Tiator, "Generalized sum rules of the nucleon in the constituent quark model," *Phys. Rev.*, vol. C70, p. 055202, 2004, hep-ph/0404053.

[44] A. J. Dufner and Y.-S. Tsai, "Phenomenological analysis of the γnn^* formfactors," *Phys. Rev.*, vol. 168, pp. 1801–1809, 1968.

[45] S. Eidelman *et al.*, "Review of particle physics," *Phys. Lett.*, vol. B592, p. 1, 2004.

[46] I. G. Aznauryan 2005, personal communication.

[47] C. S. Armstrong *et al.*, "Electroproduction of the $S_{11}(1535)$ resonance at high momentum transfer," *Phys. Rev.*, vol. D60, p. 052004, 1999, nucl-ex/9811001.

[48] D. Allasia *et al.*, "Investigation of exclusive channels in neutrino / anti- neutrino deuteron charged current interactions," *Nucl. Phys.*, vol. B343, pp. 285–309, 1990.

[49] S. J. Barish *et al.*, "Study of Neutrino Interactions in Hydrogen and Deuterium: Inelastic Charged Current Reactions," *Phys. Rev.*, vol. D19, p. 2521, 1979.

[50] G. M. Radecky *et al.*, "Study of single pion production by weak charged currents in low-energy neutrino d interactions," *Phys. Rev.*, vol. D25, pp. 1161–1173, 1982.

[51] H. J. Grabosch *et al.*, "Cross-section Measurements of Single Pion Production in Charged Current Neutrino and Anti-Neutrino Interactions," *Z. Phys.*, vol. C41, p. 527, 1989.

[52] T. Kitagaki *et al.*, "Charged current exclusive pion production in neutrino deuterium interactions," *Phys. Rev.*, vol. D34, pp. 2554–2565, 1986.

[53] K. Abe *et al.*, "Measurement of the differential q**2 spectrum and forward-backward asymmetry for $B \to K^{(*)} l^+ l^-$," 2004, hep-ex/0410006.

[54] A. Ishikawa *et al.*, "Measurement of forward-backward asymmetry and Wilson coefficients in $B \to K^* l^+ l^-$," *Phys. Rev. Lett.*, vol. 96, p. 251801, 2006, hep-ex/0603018.

[55] B. Aubert *et al.*, "Measurements of branching fractions, rate asymmetries, and angular distributions in the rare decays $B \to K l^+ l^-$ and $B \to K^* l^+ l^-$," *Phys. Rev.*, vol. D73, p. 092001, 2006, hep-ex/0604007.

[56] F. Scuri, "Measurements of B rare decays at the Tevatron," 2007, arXiv:0705.3004 [hep-ex].

[57] A. Ali, P. Ball, L. T. Handoko, and G. Hiller, "A comparative study of the decays $B \to (K, K^*) l^+ l^-$ in standard model and supersymmetric theories," *Phys. Rev.*, vol. D61, p. 074024, 2000, hep-ph/9910221.

[58] C. Bobeth, T. Ewerth, F. Kruger, and J. Urban, "Analysis of neutral Higgs-boson contributions to the decays $\bar{B}_s \to l^+ l^-$ and $\bar{B} \to K l^+ l^-$," *Phys. Rev.*, vol. D64, p. 074014, 2001, hep-ph/0104284.

[59] F. Kruger, L. M. Sehgal, N. Sinha, and R. Sinha, "Angular distribution and CP asymmetries in the decays $\bar{B} \to K^- \pi^+ e^- e^+$ and $\bar{B} \to \pi^- \pi^+ e^- e^+$," *Phys. Rev.*, vol. D61, p. 114028, 2000, hep-ph/9907386.

[60] D. Melikhov, N. Nikitin, and S. Simula, "Probing right-handed currents in $B \to K^* l^+ l^-$ transitions," *Phys. Lett.*, vol. B442, pp. 381–389, 1998, hep-ph/9807464.

[61] C. S. Kim, Y. G. Kim, C.-D. Lu, and T. Morozumi, "Azimuthal angle distribution in $B \to K^*(\to K\pi) l^+ l^-$ at low invariant $m(l^+ l^-)$ region," *Phys. Rev.*, vol. D62, p. 034013, 2000, hep-ph/0001151.

[62] C. S. Kim, Y. G. Kim, and C.-D. Lu, "Possible supersymmetric effects on angular distributions in $B \to K^*(\to K\pi) l^+ l^-$ decays," *Phys. Rev.*, vol. D64, p. 094014, 2001, hep-ph/0102168.

[63] F. Kruger and J. Matias, "Probing new physics via the transverse amplitudes of $B^0 \to K^{*0}(\to K^-\pi^+)l^+l^-$ at large recoil," *Phys. Rev.*, vol. D71, p. 094009, 2005, hep-ph/0502060.

[64] E. Lunghi and J. Matias, "Huge right-handed current effects in $B \to K^*(K\pi)l^+l^-$ in supersymmetry," *JHEP*, vol. 04, p. 058, 2007, hep-ph/0612166.

[65] C. Bobeth, M. Misiak, and J. Urban, "Photonic penguins at two loops and m(t)-dependence of $BR(B \to X(s)l^+l^-)$," *Nucl. Phys.*, vol. B574, pp. 291–330, 2000, hep-ph/9910220.

[66] C. Bobeth, P. Gambino, M. Gorbahn, and U. Haisch, "Complete NNLO QCD analysis of $B \to X_s l^+ l^-$ and higher order electroweak effects," *JHEP*, vol. 04, p. 071, 2004, hep-ph/0312090.

[67] T. Huber, E. Lunghi, M. Misiak, and D. Wyler, "Electromagnetic logarithms in $\bar{B} \to X_s l^+ l^-$," *Nucl. Phys.*, vol. B740, pp. 105–137, 2006, hep-ph/0512066.

[68] G. Hiller and F. Kruger, "More model-independent analysis of $b \to s$ processes," *Phys. Rev.*, vol. D69, p. 074020, 2004, hep-ph/0310219.

[69] F. Borzumati, C. Greub, T. Hurth, and D. Wyler, "Gluino contribution to radiative B decays: Organization of QCD corrections and leading order results," *Phys. Rev.*, vol. D62, p. 075005, 2000, hep-ph/9911245.

[70] H. E. Haber and G. L. Kane, "The Search for Supersymmetry: Probing Physics Beyond the Standard Model," *Phys. Rept.*, vol. 117, pp. 75–263, 1985.

[71] S. P. Martin, "A supersymmetry primer," 1997, hep-ph/9709356.

[72] Y. Grossman, Z. Ligeti, and E. Nardi, "$B \to \tau^+\tau^-(X)$ decays: First constraints and phenomenological implications," *Phys. Rev.*, vol. D55, pp. 2768–2773, 1997, hep-ph/9607473.

[73] S. Davidson, D. C. Bailey, and B. A. Campbell, "Model independent constraints on leptoquarks from rare processes," *Z. Phys.*, vol. C61, pp. 613–644, 1994, hep-ph/9309310.

[74] M. Hirsch, H. V. Klapdor-Kleingrothaus, and S. G. Kovalenko, "New low-energy leptoquark interactions," *Phys. Lett.*, vol. B378, pp. 17–22, 1996, hep-ph/9602305.

[75] E. Eichten and B. R. Hill, "An Effective Field Theory for the Calculation of Matrix Elements Involving Heavy Quarks," *Phys. Lett.*, vol. B234, p. 511, 1990.

[76] B. Grinstein, "The Static Quark Effective Theory," *Nucl. Phys.*, vol. B339, pp. 253–268, 1990.

[77] H. Georgi, "An Effective Field Theory for Heavy Quarks at Low- Energies," *Phys. Lett.*, vol. B240, pp. 447–450, 1990.

[78] M. Neubert, "Heavy quark symmetry," *Phys. Rept.*, vol. 245, pp. 259–396, 1994, hep-ph/9306320.

[79] M. Beneke, A. P. Chapovsky, M. Diehl, and T. Feldmann, "Soft-collinear effective theory and heavy-to-light currents beyond leading power," *Nucl. Phys.*, vol. B643, pp. 431–476, 2002, hep-ph/0206152.

[80] P. Ball and R. Zwicky, "New results on $B \to \pi, K, \eta$ decay formfactors from light-cone sum rules," *Phys. Rev.*, vol. D71, p. 014015, 2005, hep-ph/0406232.

[81] P. Ball and R. Zwicky, "$B_{d,s} \to \rho, \omega, K^*, \Phi$ decay form factors from light-cone sum rules revisited," *Phys. Rev.*, vol. D71, p. 014029, 2005, hep-ph/0412079.

[82] T. Onogi, "Heavy flavor physics from lattice QCD," *PoS*, vol. LAT2006, p. 017, 2006, hep-lat/0610115.

[83] "A Combination of CDF and D0 results on the mass of the top quark," 2007, hep-ex/0703034.

[84] V. M. Braun, D. Y. Ivanov, and G. P. Korchemsky, "The B-meson distribution amplitude in QCD," *Phys. Rev.*, vol. D69, p. 034014, 2004, hep-ph/0309330.

[85] P. Ball and R. Zwicky, "$SU(3)$ breaking of leading-twist K and K^* distribution amplitudes: A reprise," *Phys. Lett.*, vol. B633, pp. 289–297, 2006, hep-ph/0510338.

[86] P. Ball, V. M. Braun, and A. Lenz, "Higher-twist distribution amplitudes of the K meson in QCD," *JHEP*, vol. 05, p. 004, 2006, hep-ph/0603063.

[87] H. Lacker, "CKM matrix fits including constraints on New Physics," 2007, arXiv:0708.2731 [hep-ph].

[88] H. H. Asatrian, H. M. Asatrian, C. Greub, and M. Walker, "Two-loop virtual corrections to $B \to X_s l^+ l^-$ in the standard model," *Phys. Lett.*, vol. B507, pp. 162–172, 2001, hep-ph/0103087.

[89] H. H. Asatryan, H. M. Asatrian, C. Greub, and M. Walker, "Calculation of two loop virtual corrections to $b \to s l^+ l^-$ in the standard model," *Phys. Rev.*, vol. D65, p. 074004, 2002, hep-ph/0109140.

[90] A. Ghinculov, T. Hurth, G. Isidori, and Y. P. Yao, "The rare decay $B \to X_s l^+ l^-$ to NNLL precision for arbitrary dilepton invariant mass," *Nucl. Phys.*, vol. B685, pp. 351–392, 2004, hep-ph/0312128.

[91] G. Burdman and G. Hiller, "Semileptonic form-factors from $B \to K^* \gamma$ decays in the large energy limit," *Phys. Rev.*, vol. D63, p. 113008, 2001, hep-ph/0011266.

[92] A. Ali, E. Lunghi, C. Greub, and G. Hiller, "Improved model-independent analysis of semileptonic and radiative rare B decays," *Phys. Rev.*, vol. D66, p. 034002, 2002, hep-ph/0112300.

[93] E. . Hewett, Joanne L. *et al.*, "The discovery potential of a Super B Factory. Proceedings, SLAC Workshops, Stanford, USA, 2003," 2004, hep-ph/0503261.

[94] M. Acciarri *et al.*, "Search for neutral B meson decays to two charged leptons," *Phys. Lett.*, vol. B391, pp. 474–480, 1997.

[95] M. Misiak *et al.*, "The first estimate of $B(\bar{B} \to X_s \gamma)$ at $\mathcal{O}(\alpha_s^2)$," *Phys. Rev. Lett.*, vol. 98, p. 022002, 2007, hep-ph/0609232.

[96] E. Barberio *et al.*, "Averages of b-hadron properties at the end of 2005," 2006, hep-ex/0603003.

[97] Y. Ushiroda *et al.*, "Time-dependent CP asymmetries in $B^0 \to K^0(S)\pi^0\gamma$ transitions," *Phys. Rev.*, vol. D74, p. 111104, 2006, hep-ex/0608017.

[98] B. Aubert *et al.*, "Measurement of The Time-Dependent CP Asymmetry in $B^0 \to K^{*0}\gamma$ Decays," 2007, 0708.1614.

[99] B. Aubert *et al.*, "Measurement of the $B \to X_s \ell^+ \ell^-$ branching fraction with a sum over exclusive modes," *Phys. Rev. Lett.*, vol. 93, p. 081802, 2004, hep-ex/0404006.

[100] T. Aaltonen *et al.*, "Search for $B_s \to \mu^+\mu^-$ and $B_d \to \mu^+\mu^-$ Decays with 2fb-1 of ppbar Collisions," *Phys. Rev. Lett.*, vol. 100, p. 101802, 2008, 0712.1708.

[101] W. Skiba and J. Kalinowski, "$B_s \to \tau^+\tau^-$ decay in a two Higgs doublet model," *Nucl. Phys.*, vol. B404, pp. 3–19, 1993.

[102] A. Maciel, "Rare B_s and D decays with the DØ detector, talk given at HEP 2007, July 20, 2007, Parallel Session "Flavour physics and CP violation" ,"

[103] T. Huber, T. Hurth, and E. Lunghi, "Logarithmically Enhanced Corrections to the Decay Rate and Forward Backward Asymmetry in $\bar{B} \to X_s l^+ l^-$," 2007, 0712.3009.

[104] Z. Ligeti and F. J. Tackmann, "Precise predictions for $B \to X_s l^+ l^-$ in the large q^2 region," *Phys. Lett.*, vol. B653, pp. 404–410, 2007, 0707.1694.

[105] S. Fukae, C. S. Kim, T. Morozumi, and T. Yoshikawa, "A model independent analysis of the rare B decay $B \to X_s l^+ l^-$," *Phys. Rev.*, vol. D59, p. 074013, 1999, hep-ph/9807254.

[106] K. Abe *et al.*, "Improved measurement of the electroweak penguin process $B \to X_s l^+ l^-$," 2004, hep-ex/0408119.

[107] M. Iwasaki *et al.*, "Improved measurement of the electroweak penguin process $B \to X_s l^+ l^-$," *Phys. Rev.*, vol. D72, p. 092005, 2005, hep-ex/0503044.

[108] Y. Nir, "The Mass Ratio m(c) / m(b) in Semileptonic B Decays," *Phys. Lett.*, vol. B221, p. 184, 1989.

[109] B. Grinstein and D. Pirjol, "Precise $|V_{ub}|$ determination from exclusive B decays: Controlling the long-distance effects," *Phys. Rev.*, vol. D70, p. 114005, 2004, hep-ph/0404250.

[110] D. Seidel, "Analytic two-loop virtual corrections to $b \to d l^+ l^-$," *Phys. Rev.*, vol. D70, p. 094038, 2004, hep-ph/0403185.

[111] D. Atwood, M. Gronau, and A. Soni, "Mixing-induced CP asymmetries in radiative B decays in and beyond the standard model," *Phys. Rev. Lett.*, vol. 79, pp. 185–188, 1997, hep-ph/9704272.

[112] B. Grinstein, Y. Grossman, Z. Ligeti, and D. Pirjol, "The photon polarization in $B \to X\gamma$ in the standard model," *Phys. Rev.*, vol. D71, p. 011504, 2005, hep-ph/0412019.

[113] P. H. Chankowski and L. Slawianowska, "Effects of the scalar FCNC in $b \to s l^+ l^-$ transitions and supersymmetry," *Eur. Phys. J.*, vol. C33, pp. 123–136, 2004, hep-ph/0308032.

[114] D. A. Demir, K. A. Olive, and M. B. Voloshin, "The forward-backward asymmetry of $B \to (\pi, K) l^+ l^-$: Supersymmetry at work," *Phys. Rev.*, vol. D66, p. 034015, 2002, hep-ph/0204119.

[115] G. Buchalla, G. Hiller, and G. Isidori, "Phenomenology of non-standard Z couplings in exclusive semileptonic $b \to s$ transitions," *Phys. Rev.*, vol. D63, p. 014015, 2001, hep-ph/0006136.

[116] O. Lalakulich, N. Jachowicz, C. Praet, and J. Ryckebusch, "Quark–hadron duality in lepton scattering off nuclei," 2008, 0808.0085.

[117] W. Melnitchouk, R. Ent, and C. Keppel, "Quark-hadron duality in electron scattering," *Phys. Rept.*, vol. 406, pp. 127–301, 2005, hep-ph/0501217.

Acknowledgments

First of all I would like to thank my supervisor, Prof. Gudrun Hiller, for the opportunity to work in the exiting field of B-physics. I appreciate deeply her patient guidance and personal support over the last years. The collaboration with her was very pleasant and fruitful. I am also thankful to her for the careful checking of the manuscript.

I am no less grateful to my second advisor, Prof. Emmanuel Paschos, for the chance to begin my Ph.D. studies in Dortmund. His introduction into the subject of neutrino scattering and pleasant collaboration were fruitfully benefitted.

I would like to thank my first teacher Prof. Juansher Chkareuli for the personal and pedagogical support. Thanks to him i have impressed by the amazing filed of particle physics.

I am thankful to my collaborators Dr. Christoph Bobeth and Dr. Olga Lalakulich for the numerous discussions which enrich my knowledge of particle physics. My special thanks to Christoph for the helpful collaboration and pedagogical discussions about physics. I appreciated his very carefully reading and correcting of this thesis.

I would like to thank my roommates Dr. Christoph Bobeth, Dr. Jari Laamanen and Dr. Nina Kevlishvili for the warm atmosphere accompanying our friendship. My warm thanks go to Henning Sedello and Stefan Schacht for carefully checking of this manuscript. I would like to thank all present and former members of Lehrstüle TIII and TIV for the pleasant atmosphere and enjoyable discussions about non physics topics. I am also grateful to our secretary Susanne Laurent for her help in any administrative works.

Finally, I wish to thank the Graduiertenkolleg 841 of DFG and G.I.F., the German-Israeli-Foundation for Scientific Research and Development, for financial support.